DEVELOPING RISK MODELS TO MITIGATE FUSARIUM HEAD BLIGHT IN WESTERN CANADIAN CEREAL PRODUCTION

by

Taurai Trust Matengu

A Thesis

Submitted to the Faculty of Graduate Studies of

The University of Manitoba in partial fulfilment of the requirements of the degree of

MASTER OF SCIENCE

Department of Soil Science

University of Manitoba

Winnipeg, Manitoba

ABSTRACT

Taurai T. Matengu, M.Sc., The University of Manitoba, May 2022. Developing risk models to mitigate Fusarium Head Blight in western Canadian cereal production. Advisors: Dr. Paul Bullock and Dr. Manasah Mkhabela

Producers in western Canada can mitigate the risk of Fusarium Head Blight (FHB) infection and damage to their cereal crops by growing resistant varieties and applying fungicides during the critical flowering period. However, fungicide application should not be based only on the conventional calendar since FHB occurrence and severity is sporadic and is primarily influenced by weather conditions. Weather-based decision-making tools can improve FHB management while also providing significant financial and environmental benefits. Several models have been developed worldwide, with some predicting Fusarium damaged kernels (FDK) or deoxynivalenol (DON) indirectly based on visual estimates of FHB incidence/severity/index (FHBi). This study analyzed FHB over two growing seasons and revealed no significant correlation between the FHBi and FDK and FHBi and DON in all crop types except durum (Chapter 2). The correlation between FDK and DON, on the other hand, was significant across all crop types; though, it varied between the two years. Weather-based risk models were developed for predicting FHBi, FDK, and DON in spring wheat, winter wheat, barley, and durum across three Canadian prairie provinces. The number of models developed ranged from 5 to 9 for each disease indicator and crop type, but only the two best models (based on their simplicity, fit, and accuracy) for each disease indicator and crop type were chosen for further evaluation. The prediction accuracy of the selected models ranged between 75 and 81, 77 and 84, 78 and 79% for FHBi, FDK, and DON, respectively, across crop types. The most highly correlated and frequently selected weather variable in all FDK and DON models was relative humidity. Variables with more extended weather duration summaries

(10 and 14 days before mid-anthesis) had better prediction accuracy than variables with shorter weather duration summaries (4 days before mid-anthesis). The selected models were validated using producer field data collected in western Canada. The prediction accuracy of the models across crop types ranged between 70 and 100, 66 and 89, 75 and 82% for FHBi, FDK, and DON, respectively. The accuracy of models was greatest when the distance between the fields and the nearest weather stations was less than 40 km. Additionally, this study validated FHBi models currently used in western Canada, which were originally developed in the USA. Although the De Wolf I model predicted winter wheat FHBi with high accuracy (80%), it predicted spring wheat with low accuracy (59%). Errors associated with these models were mostly false positives. The data used in this study were limited to two growing seasons and may not represent all disease-weather conditions that could favor FHB epidemics. For example, the sensitivity of the models in the validation study was low or infinite as there were few or no epidemic cases to predict. Therefore, additional data from years of high disease pressure is required to refine and validate these models. The models developed in this study will serve as the basis for an interactive FHB risk assessment tool that is currently being developed in western Canada. This risk assessment tool will assist producers in optimizing fungicide application by minimizing unnecessary fungicide application and FHB epidemic-related losses.

ACKNOWLEDGMENTS

I would like to express my gratitude to Dr. Paul Bullock, my advisor. I am indebted to you for providing me with invaluable knowledge, guidance, and support. Your encouragement and belief in my ability to succeed aided me in persevering throughout my graduate studies. I would also like to express my gratitude to my co-advisor, Dr. Manasah Mkhabela, for his assistance, support, and advice throughout this project. Dr. Francis Zvomuya and Dr. Maria Antonia Henriquez, both members of my advisory committee, deserve special recognition for their invaluable contributions during progress report meetings and for reviewing my work. Additionally, I would like to thank Dr. Timi Ojo for his assistance in sourcing weather data and mapping. I am also indebted to Dr. Dilantha Fernando and his team, including Sachithrani K. Kannangara, Dr. Abbot Oghenekaro, and Sierra Walker, for their assistance with sample threshing and FHB spore counting.

I would also like to acknowledge that this research was funded under the Integrated Crop Agronomy Cluster by Western Grain Research Foundation, Agriculture and Agri-Food Canada, Manitoba Crop Alliance, Saskatchewan Wheat Development Commission, Alberta Wheat Commission, Brewing and Malting Barley Research Institute, Canadian Agricultural Partnership, and Prairie Oat Growers Association. I also want to express my gratitude to all wheat and barley producers who contributed to this project for their unwavering support throughout the sampling years. Thank you also to the Department of Soil Science technicians, Rob Ellis and Trevor Fraser for their assistance and continued willingness to assist with my numerous requests. I am also grateful to the other technicians and summer students who contributed to this project.

I am also grateful to my fellow graduate students for their encouragement and support, particularly Takudzwa Nawu, Clemence Muitire, Kody Olson, and Keshav Mahadevan.

Finally, I would like to thank my parents and siblings Talent, Tatenda, and Tariro, for their unwavering support and prayers, not forgetting, Plaxedes (late) and Irene (late). I could not have done it without your encouragement!

FOREWORD

This thesis was prepared in the manuscript format following the thesis guidelines of the Department of Soil Science, University of Manitoba. The thesis consists of five chapters. Chapter 1 is the literature review of weather-based models for Fusarium Head Blight risk assessment in wheat and barley. Chapter 2 assessed the effect of cultivar resistance on Fusarium Head Blight index, Fusarium damaged kernels, and deoxynivalenol (disease indicators) in wheat and barley. It also assessed the correlation between disease indicators plus spore concentration. Chapter 3 documents the development of Fusarium Head Blight index, Fusarium damaged kernels, and deoxynivalenol weather-based models for winter wheat, spring wheat, barley, and durum grown in western Canada. In Chapter 4, the weather-based models developed in Chapter 3 and the existing weather-based USA FHBi models utilized in Canada were validated. Chapter 5 is the overall synthesis.

TABLE OF CONTENTS

Contents

LIST OF TABLES

LIST OF FIGURES

1. INTRODUCTION

1.1 General Background

Epidemics of Fusarium Head Blight (FHB) in small cereal crops such as wheat and barley are frequently triggered when favorable weather conditions for *Fusarium* species infection coincide with flowering and early kernel filling (De Wolf et al., 2003; McMullen et al., 2012). Numerous studies and surveys have established that temperature and moisture (rainfall and humidity) are the primary determinants of FHB development (Hooker et al., 2002; Del Ponte et al., 2009; Shah et al., 2019a). If FHB is left uncontrolled, wheat and barley heads are blighted, and severe yield reduction occurs due to flower abortion, which reduces the number of kernels formed (Bai and Shaner, 2004). Grain filling is also impacted, leading to Fusarium damaged kernels (FDK), often light in weight (Góral et al., 2018). These yield losses are exacerbated by the production of mycotoxins such as deoxynivalenol (DON) by the *Fusarium* species, which are toxic to humans and livestock (Tamburic-Ilincic et al., 2015). DON-contaminated grains may be unfit for human consumption or the production of products such as bread, beer, and animal feed and are thus frequently downgraded during marketing (Dahl and Wilson, 2018).

Due to the high cost of FHB damage to a crop, some producers do preventative fungicide applications to protect the crop from disease without knowing if FHB will cause significant damage (Nita, 2013). Fungicide overuse can be detrimental to the environment, and the marginal cost/revenue ratio of wheat makes it critical to use inputs cost-effectively, including fungicides (Wallhead and Zhu, 2017). Fungicide spray for FHB suppression in wheat and barley production can be reduced if the risk of a disease epidemic can be accurately predicted. This could result in more sustainable and environmentally friendly wheat and barley cultivation. Forecasting models

are appropriate for FHB due to the disease's sporadic manifestation, reliance on weather factors, limited periods of pathogen sporulation, inoculum dispersal, and host infection (De Wolf et al., 2003; Góral et al., 2018). Researchers worldwide have created, validated, and adapted weather-based models to predict the likelihood of the presence and severity of FHB and DON toxin levels so that informed in-season decisions can be made and post-season marketing decisions can be anticipated (Rossi et al., 2003; Del Ponte et al., 2005; Birr et al., 2019). These models are primarily based on meteorological data such as temperature, relative humidity, and precipitation, which are sometimes combined with agronomic variables such as crop residues, tillage, crop rotation, and crop variety. Some of these models are specific to where they are developed, so researchers have tested these models in different climatic zones to determine how well they work. After a few modifications, some of these models worked well in other locations and crop types (Schaafsma and Hooker, 2007; Giroux et al., 2016). Therefore, this chapter discusses the various weather-based FHB models developed around the world for assessing the real-time risk of FHB epidemics and their application and adoption in different regions/countries. It also discusses the modelling approach that is suggested for western Canada. When the model developers did not specify a name for a model, the author's name(s) was utilized.

1.2 Wheat, Durum, Barley as FHB Hosts

Wheat, durum, and barley are major small grain cereal crops grown in western Canada (Klinck, 2007). In 2019, wheat production in Manitoba, Saskatchewan, and Alberta was 5.0, 15.1, and 10.3 million metric tonnes, respectively (Statistics Canada, 2019). Wheat grain is a significant energy source for the humans and is richer in protein than most cereals (McMullen et al., 2012). Flour made from wheat is used to make bread, pasta, biscuits, cakes, pastries, sauces, and confectionery. Although durum wheat is used similarly to winter and spring wheat, its high protein content and

amber color, which is ideal for dough structure properties, make it an ideal choice for pasta production. Barley is grown primarily as a fodder crop but is also used as a source of malting in brewing (Bondalapati et al., 2012). However, wheat, barley, and durum quality and yield have been drastically reduced, mainly due to FHB in some growing seasons (Giroux et al., 2016).

1.3 The Pathogen

The predominant species that causes FHB disease in Canada, the USA, several European regions, and other temperate environments is *Fusarium graminearum* (De Wolf et al., 2003; Bernardo et al., 2007). Other species known for causing FHB include *F. avenaceum, F. poae, F. culmorum, Microdochium nivale, F. verticilloides, F. sambucinum,* and *F. sporotrichiodes* (Wolny-Koładka et al., 2015). Overwintering of *Fusarium* species in various plant debris as mycelium or macroconidia (asexual spores) and/or ascospores (asexual spores) serves as the initial inoculum for the infection process (Figure 1.1). Rain or turbulent wind currents can disperse these primary inoculums, which can travel long distances in the air. *Fusarium* species spore germination requires at least 12 hrs of precipitation or high humidity (Government of Saskatchewan, 2022) and optimal temperatures for ascospore germination at 100% RH are between 20 and 25°C (Manstretta et al., 2016). Infection occurs most frequently when *Fusarium* viable ascospores and macroconidia land on susceptible wheat/barley heads during flowering (Shah et al., 2013). Choline and betaine found in anthers promote the fungus development and serve as an initial entrance for the pathogen into the spike tissue (Bai and Shanner, 1994; Gilbert and Haber, 2013). Extended periods (48 to 72 h) of RH > 90% and temperatures between 15 and 30 °C are also beneficial for infection (Figure 1.1) (De Wolf et al., 2003; Del Ponte et al., 2005) .

The most conspicuous symptom of FHB is premature bleaching of spikelets, which occurs within three weeks of infection (Hollingsworth et al., 2006; Vogelgsang et al., 2011). Translocation of

nutrients and water is interrupted as the pathogen grows into the rachis blocking the xylem and phloem tissues (Ha et al., 2016). Grain filling is impacted, resulting in florets with shriveled or no seed (Figure 1.1) (Bernardo et al., 2007). Chalky and pinkish mycelial symptoms also appear on the surfaces of florets (Góral et al., 2018). Floret sterility, smaller shriveled, lightweight, and discolored kernels are collectively referred to as FDK. This reduces grain yield and quality, eventually downgrading grain and reducing its market value (Góral et al., 2018).

Wheat milling and secondary processing suffer from *Fusarium* damage, necessitating lower FDK limits in premium wheat milling grades than those based solely on food safety requirements (Dahl and Wilson, 2018). In addition, poor germination occurs when FDK are used for seeding (McMullen et al., 2012). The percentage of FDK in a grain sample is also directly correlated to the grade of wheat and barley in western Canada (Table 1.1) (Canadian Grain Commission, 2019).

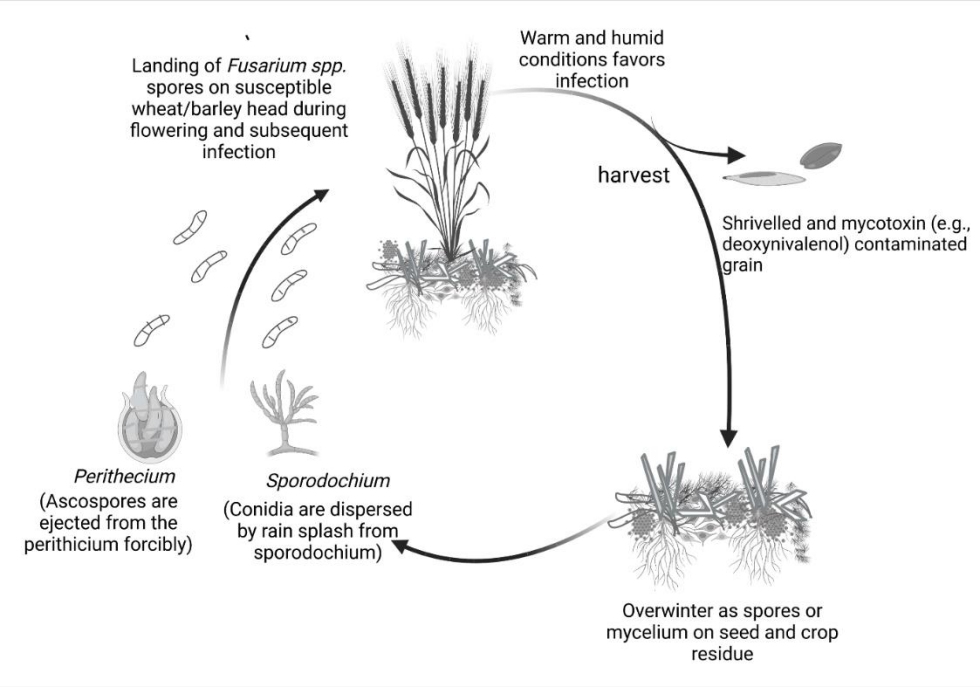

Figure 1. 1. The disease cycle of Fusarium Head Blight. *Fusarium* species overwinter as mycelium on seed or as saprophytes as spores in crop residues including maize, canola, and soybean. At flowering, both sexual (ascospores) and asexual (macroconidia) spores can be disseminated to the susceptible host, and infection occurs in warm, humid weather.

Table 1. 1. Fusarium damage % thresholds in winter wheat, spring wheat, barley, and durum in western Canada.

Crop Type	Grade Name	Fusarium damaged %
Canada Western Red Winter (CWRW) wheat	No. 1 CWRW	0.8
	No. 2 CWRW	1
	No. 3 CWRW	1.5
	CW Feed	4
	Grade if specs for CW feed not met	Wheat, sample CW account *Fusarium* damage over 10% - wheat, commercial salvage
Canada Western Red Spring (CWRS) wheat	No. 1 CWRS	0.3
	No. 2 CWRS	0.8
	No. 3 CWRS	1.5
	CW Feed	4
	Grade, if specs for CW feed not met	Wheat, sample CW account *Fusarium* damage over 10%- wheat, commercial salvage
Canada Western Amber Durum (CWAD) wheat	No. 1 CWAD	0.5
	No. 2 CWAD	0.5
	No. 3 CWAD	2
	No. 4 CWAD	2
	No. 5 CWAD	4
	Grade, if No. 5 specs not met	Wheat, sample CW account *Fusarium* damage over 10% - wheat, commercial salvage
Barley, Canada Western (CW)/Canada Eastern (CE) Malting	Select Malting CW/CE Two-row	0.2
	Select Malting CW/CE Six-row	0.2
	Select Malting CW/CE Two-row Hulless	0.2
	Select Malting CW/CE Six-row Hulless	0.2
	Grade if specs for select malting CW/CE two-row / six-row (Hulless) not met	Barley sample select malting CW/CE two-row / six-row account *Fusarium* damage

Barley that is not selected for food is graded according to "General Purpose" grades with Fusarium damage % of 0.5. https://www.grainscanada.gc.ca/en/grain-quality/official-grain-grading-guide/04-wheat/primary-grade-determinants-tables.html.

Fusarium graminearum produces trichothecene mycotoxins in addition to reducing yield. Currently, over 200 trichothecenes are identified and classified into four types (A–D) (Schmale et al., 2011). *Fusarium graminearum* is primarily responsible for producing Type B deoxynivalenol (DON) and its acetylated derivatives, 3-acetyldeoxynivalenol (3-ADON), 15-acetyldeoxynivaleol (15-ADON), and nivalenol (NIV) in Canada (Schmale et al., 2011). In the past, strains of *Fusarium graminearum* capable of producing 15-ADON were prevalent in North America, while the 3-ADON chemotype was predominant in Europe and Asia (Ward et al., 2008; van der Lee et al., 2015). However, the prevalence of 3-ADON chemotypes has recently increased in Canada's western and Atlantic regions and the upper Midwest of the USA (Ward et al., 2008; Burlakoti et al., 2017). Between 1998 and 2004, 492 *Fusarium graminearum* isolates from eastern and western Canada were 25% 3-ADON and 75% 15-ADON (Ward et al., 2008). A distinct longitudinal cline was described where 100% of 3-ADON was found in eastern Canada, and less than 10% of 3-ADON was found in western Canada (Ward et al., 2008). Variations in hosts in a region have been shown to significantly impact FHB species and trichothecenes chemotype composition (Cowger et al., 2020). Spring wheat is mainly grown in western Canada, while winter wheat is primarily grown in Ontario (Burlakoti et al., 2017; Crippin, 2019). Furthermore, 3-ADON increased 14-fold in the western provinces between 1998 and 2004. However, more recent reports indicate that 3-ADON increased 6-fold in Saskatchewan, and 2.5-fold in Manitoba, in the last 15 years (Oghenekaro et al., 2021).

The change in the chemotype from 15-ADON to 3-ADON is alarming as FHB severity, and DON levels increase (Ward et al., 2008; Gilbert et al., 2010). In vitro, 3-ADON isolates develop and produce larger and more conidia and DON than 15-ADON isolates (Ward et al., 2008). This can also reflect improved environmental fitness of the pathogen when these characteristics are

exhibited in the field (Ward et al., 2008). Although deoxynivalenol is the least toxic of the trichothecene B mycotoxins produced by *Fusarium* species, when ingested in large amounts, it can cause significant harm to humans and animals (Sobrova et al., 2010; Gaigé et al., 2013). High DON intake causes health problems, including chronic toxicity, carcinogenicity, genotoxicity, immunotoxicity, cytotoxicity, and reproductive and teratological effects in humans (Sobrova et al., 2010; Gaigé et al., 2013; Wu et al., 2014). In animals, high DON intake causes problems such as feed refusal, vomiting, retarded growth, diarrhea, and even shock or death (Gaigé et al., 2013). These effects vary depending on the gender and age of the animal but are generally more pronounced in non-ruminant animals such as swine and poultry than in ruminants (Canadian Grain Commission, 2019). As a result, Canada has imposed strict DON tolerance limits. These limits were set at 1 ppm for swine, young calves, and lactating milk animals' diets, 5 ppm for cattle and poultry diets, and 2 ppm for wheat intended for human consumption (Table 1.2) (CFIA, 2015). *Fusarium graminearum* also produces Nivalenol (NIV) and 4-acetylnivalenol (4-ANIV), which are more toxic than DON (Wang et al., 2019).

1.4 Fusarium Head Blight Control

Control of FHB outbreaks is crucial due to substantial loss in crop yield and quality and health effects of mycotoxins on consumers. Besides cereals, *Fusarium* species infect other crops grown in western Canada, causing diseases such as root rot in soybeans, peas, and beans; ear rot in corn; and Fusarium wilt in canola. As a result, FHB disease management with a single strategy such as crop rotation is challenging (Government of Saskatchewan, 2022; Harris et al., 2016). It is, therefore, essential to combine multiple control strategies to manage FHB (Bai and Shaner, 2004).

Table 1. 2. Legislated and proposed maximum tolerated levels of deoxynivalenol in certain feeds and foodstuffs in Canada.

Species/Class of Animal	Proposed Maximum Limit: Single Ingredient Feeds	Proposed Maximum Limit: Total Diet in an amount not exceeding (ppm)	Current Action Level: Complete diets, in an amount not exceeding (ppm)
	Feed[a]		
Cattle - calves (<4 months)	5	1	1
Cattle - Beef	10	5	5
Cattle - Dairy	10	5	5
Lactating Dairy Animals	5	1	1
Swine	5	1	1
Poultry: chickens, turkeys, ducks	10	5	5
Other animals including sheep, equine, and rabbits	10	5	No action levels established
	Food[b]		
Uncleaned soft wheat for human consumption	-	-	2

[a]https://inspection.canada.ca/animal-health/livestock-feeds/consultations/contaminant-standards-for-aflatoxins-deoxynivaleno/eng/1500908795245/1500908795965.

[b]Legislated maximum permissible levels of deoxynivalenol in some foodstuffs (CFIA, 2015).

1.4.1 Agronomic Control

Tillage and crop rotation with non-host crops are suitable agricultural activities that reduce the likelihood of FHB epidemics by reducing inoculum sources and eliminating wintering plant residues for the pathogen and other hosts (Bergstrom and Spolti, 2014). While reducing inoculum levels and disease epidemics with high tillage levels is significant, it is not enough to control FHB (Gilbert and Fernando, 2004). The selection of varieties with some resistance levels to FHB plays a crucial role in managing FHB. Several FHB resistance types have been identified, for example, type I (resistance to initial infection) and type II (resistance to pathogen spread throughout the spike (Ha et al., 2016, p. 1; Góral et al., 2020). The application of fungicides during flowering

greatly reduces FHB epidemics (De Wolf et al., 2003). The efficacy of chemical controls relies on predicting the best possible time for fungicide spray, as the weather plays a major role in the outbreak of FHB (Hollingsworth et al., 2006).

1.4.2 Disease Forecasting Models

FHB forecasting has gained popularity in recent decades to maximize fungicide efficiency while also minimizing its cost (Musa et al., 2007). FHB is ideal for forecasting due to environment dependency and a comparatively narrow window of pathogen sporulation, spore dispersal, and infection on the host (De Wolf et al., 2003). Disease forecasting, days or weeks before infection or major epidemic, helps producers to respond quickly and efficiently by modifying crop management practices, including fungicides application (Shah et al., 2013). FHB forecasting has adopted two strategies: i) predicting the risk of disease occurrence based on FHB incidence and severity and ii) forecasting the concentration of DON in harvested grain (Hooker et al., 2002; De Wolf et al., 2003).

1.4.2.1 The De Wolf Model in the USA

1.4.2.1.1 First-generation Models

The first generation models for FHB risk assessment in wheat in the USA were logistic regression models developed by De Wolf et al. (2003). These models utilized data gathered from four states in the USA. Field FHB severity ≥ 10% was considered an epidemic in their forecasting models. Disease forecasting depended on weather data that were observed and predicted from 7 days before to 10 days after 50% anthesis and a combination of predictor variables, which were most aligned with the disease's patterns of occurrence or severity. Predictor variables included the period (h) of $15 \leq T \leq 30$ °C in the 7 days before flowering (T15307), the period of precipitation (h) 7 days

preceding flowering (DPPT7), and the period (h) with both $15 \leq T \leq 30$ °C, and RH ≥ 90% 10 days after flowering (TRH9010) (De Wolf et al., 2003).

Three prediction models, namely model A, model B, and model I (De Wolf A, B, and I, respectively), were selected. The De Wolf A model utilized only the TRH9010 weather anthesis component (equation 1.1), while De Wolf B used T15307 and TRH9010 interaction (equation 1.2). In contrast, De Wolf I used T15307 and DPPT7 pre-anthesis weather variables (equation 1.3). The accuracy of the models (successful classification of FHB epidemics and non-epidemics) during validation was 78%, which was perceived to be good, although further improvement was needed (De Wolf et al., 2003).

$$P = 1/(1 + exp - (-3.3756 + 6.8128TRH9010)) \quad [1.1]$$

$$P = 1/(1 + exp - (-3.7251 + 10.5097INT3)) \quad [1.2]$$

$$P = 1/(1 + exp - (-8.2175 + 8.4358T15307 + 4.7319DPPT7)) \quad [1.3]$$

Where TRH9010 is the duration (h) of temperature between 15 and 30 °C, and when RH ≥ 90% 10 days pre-anthesis, T15307 is the duration (h) of temperature between 15 and 30 °C 10 days pre-anthesis, DPPT7 is the duration of precipitation (h) 7 days pre-anthesis, and INT3 is an interaction term between T15307 and TRH9010 (De Wolf et al., 2003). The probabilities (P) of FHB epidemics are defined by the chances that field severity is 10% or more. Severity corresponds to the percentage of infected spikelets, and the probability varies between 0 and 1. To use equations 1.1 to 1.3, variables must first be placed on the same scale as the data used to develop the models. This is done by dividing TRH9010, T15307, or DPPT7 by 136, 168, or 39, respectively (TRH9010/136; T15307/168; DPPT7/39) (De Wolf et al., 2003).

The models by De Wolf have been used to develop a *Fusarium* risk assessment tool, an electronic database offering FHB forecasts maps to 31 USA states across both spring and winter wheat growing regions (www.wheatscab.psu.edu). The tool provides information (risk maps) on the probability of a severe FHB outbreak (FHB ≥ 10%) based on weather data from multiple weather stations in the states covered by the prediction system (McMullen et al., 2012). The producer controls the tool, and data such as flowering date, crop type (winter wheat or spring wheat), and crop variety (very susceptible, susceptible, moderately susceptible, and moderately resistant) can be imputed to provide FHB risk at the field scale (McMullen et al., 2012; Shah et al., 2021).

Canada has also adopted the USA models for predicting FHB severity greater than 10%. In Manitoba and Alberta, FHB risk assessment maps are based on De Wolf I (equation 1.3), whereas in Saskatchewan, FHB risk assessment maps are based on the second-generation model that incorporates agronomic and climatic variables (ACIS, 2021; MARD, 2021; SWDC, 2021). However, the accuracy of these models is unknown in western Canada. In Quebec, Canada, De Wolf A, B, and I were evaluated under Quebec conditions (Giroux et al., 2016). DON levels of 1 ppm or greater were better predicted by the De Wolf A and De Wolf B models, even though these models were not designed to predict DON levels directly but rather field FHB severity or index (Giroux et al., 2016). The best of the three De Wolf models varied by region/country, possibly due to regional differences in crop type and variety, crop production practices, weather conditions, pathogen population and profile, and disease management practices, all of which have been shown to influence model adoption in various regions (Paul et al., 2005; Kelly et al., 2015; Cowger et al., 2020).

1.4.2.1.2 Second-generation Models

Recently, efforts have been made by Shah et al. (2013, 2014) to understand the role of pre-and post-anthesis weather indicators on FHB forecast utilizing an enormous dataset collected across 15 states over 27 years and an extensive number of climate-related predictors. Wheat resistance category (RESIT) was utilized as an ordinal variable, where 0, 1, 2, and 3 represented very susceptible, susceptible, moderately susceptible, and moderately resistant, respectively (Shah et al., 2013). Only 21 out of 380 total weather-based predictors through various pre- and post-anthesis periods were identified and integrated into 15 separate logistic regression models (Shah et al., 2013). These models differed in the pre or post-anthesis duration, with specific RH, temperature, or rainfall conditions (Shah et al., 2013). The pre-anthesis model with the least misclassification of FHB epidemics contained the duration (h) with a temperature between 15 and 30 °C, where RH exceeded 80% (Shah et al., 2013). The mean temperature per day was also incorporated in this model, along with the number of hours at a temperature greater than 9 °C (Shah et al., 2013). Rainfall generally was not crucial for forecasting the likelihood of epidemics in this study (Shah et al., 2013). The updated winter wheat model (equation 1.4) and spring wheat model (equation 1.5) were as follows:

$$logit\ (\mu) = -1.7954 + 0.0245\ TH2 \qquad [1.4]$$

$$logit\ (\mu) = -11.008 - 0.9578\ RESISTC + 0.1516 H1 \qquad [1.5]$$

In both equations, μ is the probability of a significant FHB epidemic (FHB index ≥ 10%), H1 is the mean hourly RH, and TH2 is the number of hours during which the following two conditions are met simultaneously within a given hour: t is 9 to 30 °C and RH ≥ 90% 7 days before anthesis. RESISTC is categorical variable of four different levels of disease resistance: very susceptible = 0; moderately susceptible = 1; moderately resistant = 2; and resistant = 3 (Shah et al., 2013).

1.4.2.1.3 Third-generation Models (Shah 2019a and 2019b)

The first and second generations of USA FHB models were based on variables that summarized temperature and moisture during short periods of not more than 15 days preceding and following anthesis (De Wolf et al., 2003; Shah et al., 2013, 2014). This was based on the idea that FHB prediction should be made in time to provide fungicide application recommendations during anthesis or no later than five days after anthesis to control the disease effectively (De Wolf et al., 2003; Shah et al., 2013). However, more early-anthesis and near-flowering signals were detected in recent years through a functional regression analysis of weather data from 120 to 30 days before and after anthesis, indicating that FHB epidemics can be detected as early as 40 to 60 days before anthesis (Shah et al., 2019a; b). The findings were utilized to construct new weather variables used to develop models that performed similarly to previously developed models for real-time disease risk, although the new models had a better fit to the data than the first- and second-generation models (Shah et al., 2019a; b).

1.4.2.2 Argentina

A site and year specific empirical model to predict the incidence of FHB (predictive index or PI%) was developed by (Moschini et al., 2001) in Argentina using cultivars of different FHB susceptibility, 2-d periods of rainfall exceeding 0.2 mm (NP2), and relative humidity > 81% and ≥ 78 % for the first and second day respectively. The empirical equations were as follows:

$$PI\ \% = 20.37 + 8.63\ X\ NP_2 - 0.49\ X\ DD_{926} \quad [1.6]$$

$$PI\ \% = 18.34 + 4.12\ X\ NP_{12} - 0.45\ X\ DD_{1026} \quad [1.7]$$

Maximum and minimum temperatures were utilized to calculate degree days between 9 and 30 °C. The observations start eight days before heading (Z51) and extend up to 530-degree days

accumulation. In the equations, DD926 and DD1026 represented 926 and 1026 accumulated extreme temperatures, respectively, and was calculated using equation 1.8 and 1.9.

$$DD_{926} = \Sigma[(Tmax) - 26) + (9 - Tmin)] \quad [1.8]$$

$$DD_{1026} = \Sigma[(Tmax) - 26) + (9 - Tmin)] \quad [1.9]$$

If the maximum daily temperature ≤ 26 °C, the accumulation of Tmax – 26 is set to zero, and if the minimum daily temperature ≥ 9 °C (or 10 °C), the 9 – Tmin (or 10 – Tmin) is set to zero. Therefore, values accumulate only on days with extreme high and low temperatures. Equations 1.8 and 1.9 lists all factors during the critical time (CPL). The CPL starts eight days before 50% heading date and ends after GDD > 0 is 530.

The specificity of the model was reduced in 2001 by adapting the model to regions from the North of Argentina (a mild oceanic climate) than for the regions from further South of Argentina (humid subtropical). The minimum and maximum daily temperatures threshold used in the equations of the 1996 model were changed from 12 to 10 °C and 26 to 30 °C, respectively. The number of degree days was also increased from 530 to 550. The model is more appropriate for cooler areas of Argentina, offering predictions closer to the observed infection (Moschini et al. 2001). However, the model does not have an action threshold (i.e., a specific level that triggers fungicides application) as it directly predicts the impact of the FHB disease on the country (Moschini et al., 2001).

1.4.2.3 Italian Model

Rossi et al. (2003) developed an epidemiological model in Italy, in which weather variables and information on wheat growth stages were used to predict the risk of FHB and DON. Model development was based on four problematic FHB pathogens in Italy (*F. culmorum*, *G. zeae*, *G.*

avenacea, and *M. nivalis)*. The model pivots on three equations related to the phases in the epidemiological cycle of FHB in wheat. In the first equation, the sporulation rate (SPO) was determined using four equations (one for each fungal species) under controlled incubation conditions (Rossi et coll. 2003). In *G. Zeae*, SPO was determined by the following equation:

$$SPO = [25.98\ x\ Teq^{8.59}\ x\ (1 - Teq)]^{0.24} / [1 + \exp(5.52 - 0.51\ x\ t\ ] \quad [1.10]$$

Where: Teq = equivalent of temperature calculated as (T- Tmin) / (Tmax - Tmin). T = temperature (Tmin = 5 °C and Tmax = 35 °C), and *t* = incubation time (days).

The second equation calculated the spore dispersal rate (DIS). Since precipitation influences the rate of spore dispersal, two regression equations were developed, one adjusted to rainy days (rain > 0.2 mm) and the other on non-rainy days (rain < 0.2 mm). The regression equations also included the rainfall intensity, daily average temperature, and RH > 80%.

$$DIS^1 = -839.7 + 410.3\ W + 4.08\ T^2 + 115.45\ RintMax\_P - 455.9\ Y95 \quad [1.11]$$

$$DIS^2 = -682.3 + 45.68\ W + 21.5\ T^2 + RH80 + 107.0\ R_{tot\_P} \quad [1.12]$$

Where DIS^1 and DIS^2 are conidia numbers (m^3 air/day) estimated in days with and without rainfall, respectively. W is an empirical weight assigned each day in a sequence of n successive rainy days, as follows: first rainy day = 1.1, second rainy day = 2.5, third rainy day = 1.2, fourth or later rainy day = 0.8. T is the average air temperature (°C). RintMax_P = maximum intensity of rain (mm h^{-1}) in the preceding day. Y95 = dummy variable for 1995, equal to zero (for the yrs 1994, 1996, and 1997) and 1 (for 1995). RH80 = number of hours with RH > 80%. Rtot_P = total rainfall (mm) on a preceding day (Rossi et al., 2003).

The third equation calculated the disease infection frequency (INF) based on leaf wetness duration and temperature combination following inoculation considering wheat growth stages (GS) (Rossi et al. 2003). The invasion rate of tissues by mycelium (INV) was calculated with equation 1.13.

$$INV = [5.33 \times (Teq) 1.55 \times (1 - Teq)]^{1.35} \quad [1.13]$$

In equation 1.13, $\text{Teq} = (\text{T} - \text{Tmin})/(\text{Tmax} - \text{Tmin})$ where Tmin = 0 and Tmax = 38.

Two risk indexes are given by the Italian model and are calculated as below:

$$FHB\_risk = \Sigma SPO \times DIS \times INF \times GS \quad [1.14]$$

$$TOX\_risk = \Sigma INF \times GS \times INV \quad [1.15]$$

The risk of FHB infection (FHB-risk) is used for the four *Fusarium* species and the risk of mycotoxin development (TOX-risk) for *F. Culmorum* and *G. Zeae*. The indices are computed daily and accumulate throughout the growing season. Data from various winter wheat crops were used to validate the model. A comparison of actual infection and mycotoxin against predicted data produced satisfactory results ($R^2 > 0.8$) (Rossi et al., 2003).

1.4.2.4 Brazil

A phenology-based FHB simulation model was developed in Brazil, accounting for host, environment, and inoculum dynamics during infection (Del Ponte et al., 2005). Firstly, the host factor calculates the groups of heads that emerged (cohort) on the same day (HNG) (equation 1.16). The daily rate in the cohort of heads as a temperature function (ANText) was then calculated (equation 1.17):

$$HNG = 1 - exp(-0.0127\, t^{2.4352}) \quad [1.16]$$

$$ANText = 1 - exp(a\, t^{b}) \quad [1.17]$$

Where t = 1 day, a = $0.225 – 0.029T + 0.0009T^2$ and b = $-5.773 + 0.966T – 0.0278T^2$ where T is daily mean temperature (°C). Equation (1.16) assumes that every part of the cohort has its first part extruded three days later. An empirical rule was determined when anthers were attached to wheat spikelets before falling on the ground (anther longevity). A rule was established based on empirical observations reporting prolongation of flowering during a series of cloudy days, indicating that flowers remained attached for longer. The rule suggested that flower longevity is a minimum of two days if the daily solar radiation on the second or next day is < 10 MJ m^{-2} day^{-1}, anther remains attached for an extra day up to a maximum of five days. Therefore, the proportion of anthers present in one day (ANT) results from the sum of extruded and attached anthers in each cohort of heads subtracted from anthers removed from the cohorts (Del Ponte et al., 2005).

Coefficients for determining the proportion of susceptible tissue (ST) were developed using ANT and coefficients for post-peak anthesis infections. ST is ANT until ANT reaches the peak and decreases to 0.25. ST = 0.25 for the next seven days after anthesis (ANT < 0.01), while ST = 0.10 for the next 8 to 14 days after anthesis. Such guidelines were developed to compensate for potential late infections from post-peak flowering to kernel filling levels (Del Ponte et al., 2005).

Secondly, the inoculum factor was derived from the night and daytime inoculum observations. Spore cloud relative density was estimated by adjusting a linear equation to the relative density of colony-forming units observed during the nighttime using equation (1.18).

$$GZ = (-0.6306 + 0.0152\,RH + 0.176\,CRD)^2 \qquad [1.18]$$

Where: RH = daily mean relative humidity (%) and CRD is a variable for the rainy-day position (> 0.3 mm) in consecutive rainy days (for four consecutive days: CRD = 1; 2; 2.5; or 0.3 for each

subsequent day). GZ is a fraction (0 < GZ < 1), which adjusts the daily index of infections by accounting for lower or higher inoculum pressure in the course of an infection event.

Thirdly, daily rainfall and mean RH combinations were used to determine head wetness duration between 30 and 48 h. Within two days, infection events were recorded, and infection happens when PREC > 0.3 mm occurs in both days with average RH > 80% for the two days or when PREC >0.3 mm with mean RH ≥ 80% followed by a non-rainy day with mean RH≥85%. An exponential to calculate *Fusarium graminearum* infection frequency (INF) under temperature effect (10 to 30 °C) for 48 h of head wetness was developed as follows:

$$INF = 0.001029\, exp(0.1957\, T) \quad [1.19]$$

In this case, T = average mean daily temperature in the two-day window of the infection event.

Finally, four models calculating the daily infection rate (GIB) were developed. The daily GIB is then added and multiplied by 100 to get the accumulated infection index (% GIB). The GIBs are calculated using equations 1.20 through 1.23.

$$GIB1 = ANT \times INF \quad [1.20]$$

$$GIB2 = ANT \times INF \times GZ \quad [1.21]$$

$$GIB3 = ST \times INF \quad [1.22]$$

$$GIB4 = ST \times INF \times GZ \quad [1.23]$$

Where ANT is the daily mean proportion of anthers during a two-day infection event (IE), ranging from 0 to 1; ST = mean daily proportion of susceptible tissue during IE; INF = Infection frequency at the second day of IE and GZ = mean spore cloud density during IE. The accumulated infection

index (GIB %) is the summation of partial infection indices by the four different models along the susceptible period (equation 1.24).

$$GIB\% = \Sigma(GIB \times 100) \quad [1.24]$$

The models were evaluated based on FHB incidence, FHB severity, and Fusarium kernel damage. Since the models estimate an infection index rather than a disease level, regression was used to validate each model using the coefficient of determination to verify the adequacy of the index to explain the observations of the disease level (Del Ponte et al., 2005). The coefficient of determination for the regression analysis between predicted and actual infection ranged from 0.73 to 0.93, 0.43 to 0.69, and 0.14 to 0.37 for FHB severity, incidence, and FDK, respectively.

1.4.2.5 The DONcast Model in Canada

Forecasting disease using the FHB incidence approach is timely, reliable, and simple, but some infected kernels are, in some instances, asymptomatic but infected with mycotoxin (Hooker et al., 2002). One limitation of the predictability of epidemics is that visual FHB intensity is not necessarily associated with DON incidence. In Ontario, Canada, a model predicting DON concentration in wheat grain was developed by Hooker et al. (2002) and consisted of three regression equations. The model was further improved through the years into a forecasting tool called DONcast (Schaafsma and Hooker, 2007). In the model, the grain DON level is dependent on three critical periods. The first critical period was 4 to 7 d before heading and calculated by equation 1.25:

$$DON = \exp[-0.30 + 1.84RAINA - 0.43(RAINA)^2 - 0.56TMIN] - 0.1 \quad [1.25]$$

Where DON concentration (mg g^{-1}) is a function of RAINA (the number of days with rain > 5 mm day^{-1}), and TMIN is the number of days of temperature < 10 °C between 4 and 7 d before heading

(Hooker et al., 2002). The second critical period was 7 d before heading to 10 d after heading and calculated as follows:

$$DON = \exp[-2.15 + 2.21\ RAINA - 0.61\ (RAINA)^2 + 0.85\ RAINB + 0.52\ RAINC - 0.30\ TMIN - 1.10\ TMAX] - 0.1 \quad [1.26]$$

Where RAINB is the number of days of rain > 3 mm day^{-1} in the period 3 to 6 days after heading, TMIN was the number of days of temperature < 10 °C between 4 and 7 days before heading, and TMAX was the number of days with temperature > 32 °C in the period 4 and 7 days before heading. The third critical period included RAINC (number of days of rain > 3 mm day^{-1} in the period 7–10 days after heading), and is given by the following equation:

$$DON = \exp[-0.84 + 0.78\ RAINA + 0.40\ RAINC - 0.42\ TMIN] - 0.1 \quad [1.27]$$

Rainfall, high humidity, and warm temperatures were favorable for disease development during all three periods, and DON concentrations in the increased set of weather variables for the three periods varied marginally. Daily rainfall > 5 mm increased the potential DON concentration in the first critical period. In contrast, DON concentration was decreased when the daily minimum temperature was < 10 °C. In the second critical period, DON levels were reduced with mean temperature > 32 °C. In both second and third critical periods, daily rainfall > 3 mm and RH > 80 % increased DON concentration in the grain, while daily average temperature < 15 °C reduced DON concentration (Schaafsma and Hooker, 2007).

The model developed by Hooker et al. (2002) explained 73% of the DON concentration variability across 5 years and 399 samples. Prediction of DON concentration lower than 1 ppm showed a high accuracy of 89% (Hooker et al., 2002). The Hooker model was further enhanced by incorporating FHB observation into the dataset and variables of crop history, tillage, and host susceptibility to

render it field-specific. The Hooker model was further developed by Weather Innovations (WIN) Consultancy LP into the world's first commercialized forecasting method, DONcast, accessible in different parts of the world (Schaafsma and Hooker, 2007). DONcast is reasonably stable across the years, continents, and cropping systems due to the robustness of the data used for its development. For example, one study found DONcast accuracy of 80 to 85% and explained 72% of DON variation in over 1000 field samples from four countries using a 1 ppm threshold level (Schaafsma and Hooker, 2007).

The DONcast model reviewed in this study considers a wide range of agronomic factors, such as varietal susceptibility to disease and the amount of crop residue on the soil surface. However, it was difficult to get accurate DON forecasts and fungicide treatment recommendations due to over-generalized agronomic factors and regional variability, which led to low system adoption (Pitblado et al., 2007). Thus, the DONcast model was refined further by including other meteorological variables such as leaf wetness and agronomic factors such as crop history, tillage, and crop FHB resistance to make it more field-specific and improve its forecasting accuracy (Schaafsma and Hooker, 2007; Pitblado et al., 2007). As a result, the DONcast has been renamed site-specific DONcast (ssDONcast) (Schaafsma and Hooker, 2007; Pitblado et al., 2007).

1.4.2.6 Germany

Birr et al. (2019) developed three multiple regression models to predict DON and ZEA concentrations in wheat grain at harvest in a maize-free crop rotation in Northern Germany. The model for the highly susceptible cultivar (model 1) was based on a 2008 to 2014 dataset. The moderately to highly susceptible cultivar (model 2) and the lowly to moderately susceptible cultivar (model 3) were based on data from 2012 to 2016. The models utilized cumulative precipitation and average temperature covariates and the interaction term of precipitation and

temperature during wheat flowering. In collaboration with the Schleswig-Holstein Plant Protection Service (SCA), the three models were adapted to farms using representative local weather stations for weather-based DON and ZEA predictions as part of the regional monitoring of leaf pathogens and FHB in wheat in Northern Germany.

Model 1: Highly susceptible ("Ritmo")

$$\text{DON } 646 - 4.50P - 31.94T + 2.70PT \quad [1.28]$$

$$\text{ZEA } -40 + 3.86P + 2.41T + 0.18PT \quad [1.29]$$

Model 2: Moderately to highly susceptible ("Inspiration")

$$\text{DON } 481 - 18.42P - 26.37T + 2.87PT \quad [1.30]$$

$$\text{ZEA } -75 + 2.17P + 5.34T + 0.14PT \quad [1.31]$$

Model 3: Lowly to moderately susceptible ("Dekan"):

$$\text{DON } 305 - 24.09P - 18.74T + 2.73PT \quad [1.32]$$

$$\text{ZEA } -39 + 1.18P + 2.87T + 0.11PT \quad [1.33]$$

Where P is the cumulative precipitation (mm) during wheat flowering (GS 61 to 69), T is the average temperature (°C) during wheat flowering (GS 61 to 69), $P \times T$ is the interaction term of precipitation and temperature. All intercepts were merged to an overall intercept *a*. *b* = fixed effect for precipitation, *c* = fixed effect for temperature, and *d* = fixed effect for the interaction of precipitation and temperature.

Model evaluation using new data sets not used in the development of the models but derived from similar sampling locations as those for the development of the models produced satisfactory results (Birr et al., 2019). The models revealed that 89, 91, and 86% of the variation for models 1, 2, and

3, respectively, in the observed DON values are accounted for by the variation in the predicted DON values. In 95.2% of the cases, model 1 correctly predicted whether DON and ZEA concentrations were lower or higher than the European limit of 1250 µg DON/kg and 100 µg ZEA/kg for both mycotoxins. The accuracy of Models 2 and 3 were 85.7 (14.3% false negative) and 100%, respectively, for DON predictions when the 2017 dataset was used (Birr et al., 2019). Models 2 and 3 accurately estimated in 100 and 85.7% (14.3% false positive) of cases, ZEA concentrations below or above the maximum level of 100 µg ZEA/kg, respectively, when the 2017 validation dataset was used (Birr et al., 2019).

In contrast to other published models (Hooker et al., 2002; Franz et al., 2009; Van Der Fels-Klerx et al., 2010), all three models produced reliable DON and ZEA concentration estimates in wheat grain without including post-anthesis weather conditions. Therefore, the models will not be used only as a tool for identifying years, regions, or fields under risk, but also to assist producers in determining whether to make a fungicide application at flowering based on weather data from local weather stations to reduce the risk of food and feed contamination with DON and ZEA (Birr et al., 2019).

1.4.2.7 Netherlands

In Netherlands, the application of the DONcast regression equations defined by Hooker et al. (2002) directly to Dutch data resulted in poor quantitative predictive performance (Franz et al., 2009). Thus, two multiple regression models specific for the Dutch conditions were developed to predict DON concentrations in mature wheat grain in Dutch-specific situations (Franz et al., 2009). These models utilize pre-, and post-heading weather data, cultivar resistance, region (REG) classified into southwest (SW), central (C), and northeast (NE), fungicide use (SPRAY) classified into Yes or No, and heading dates (HD) which include eight blocks of 6 days around the HD

(numbered 1 to 8 [as a suffix] to the weather variables as well as for the entire pre- and post-heading time blocks of 24 days) (Franz et al., 2009). The heading date was estimated by a linear relationship between the observed heading date and the pre-heading temperature sum (Tsum) when not recorded. The first model focused on average climatic variables in a 24-day pre-heading and a 24-day post-heading period. The second model focused on average climatic variables in eight-time blocks of 6 days. Model 1 and 2 explained 59% and 56% DON variation across all fields, respectively. Climate variables accounted for 30% of the overall variance in model 1.

Model 1

DON (µg/kg) = 3.771 + 0.209T (post-heading) + 0.005P_{mm} (pre-heading) + 0.004P_{mm} (post-heading) - 0.002T_{h25} (pre-heading) - 0.005T_{h25} (post-heading) + 0.001RH_{h90} (post-heading) - 0.031HD + REG + RES + SPRAY [1.34]

Where T (post-heading) is the average hourly post heading temperature, P_{mm} (pre-heading) and P_{mm} (post-heading) are the total hourly pre and post heading precipitation (mm), respectively, T_{h25} (pre-heading) and T_{h25} (post-heading) are the number of hours with a temperature greater than 250 ^{o}C and RH_{h90} is the number of post heading hours with an RH greater than 90%. Non-climatic variables included HD, which are the heading dates; REG is the wheat-producing region (factorial) with coefficients: C REG (reference level); -0.366SW REG and 0.3442NE REG. RES is the wheat resistance category with coefficients: RES 5 (reference level); -0.415RES 5.5; 0.057RES 6; 0.375RES 6.5; 0.482RES 7; 0.336RES 7.5; 0.525RES 8.5). SPRAY (factorial) is a fungicide application with coefficients: No (reference level); - 0.192Yes (Franz et al., 2009).

Model 2

DON (µg/kg) = 4.427 + 0.1320T (8) + 0.025RH (4) - 0.018T_{h25} (8) -0.034HD + REG + RES + SPRAY [1.35]

Where T (8) is the average hourly temperature 18 to 24 days after heading, RH (4) is the average hourly relative humidity 0 to 6 days before heading, and Th_{25} (8) is the number of hours with a T greater than 25 ^{o}C. The HD is the pre-and post-heading dates, the REG is the region where the wheat is produced (factorial) with coefficients as C REG, reference level; -0.385SW REG; 0.259NE REG, RES is wheat resistance (factorial) with coefficients: - 0.441RES 5.5; - 0.037RES 6; - 0.319RES 6.5; - 0.508RES 7; - 0.270RES 7.5; - 0.618RES 8.5 and SPRAY (factorial) with coefficients No, reference level; -0.211Yes (Franz et al., 2009).

Both models predict concentrations of 10 log(x+1) in DON (µg/kg). The model validation showed a strong correlation between predicted and observed DON values. Models 1 and 2 correctly predicted whether the DON concentration was lower or higher than the maximum level of 1,250 µg/kg in 92 and 88% of the cases, respectively. The estimated DON amount was increased in both models with increased average temperature, precipitation, and RH but decreased with an increased number of hours with a temperature above 25 °C (Franz et al., 2009).

There was an apparent regional effect on DON concentrations, with considerably greater levels when progressing from the SW to the NE regions of the Netherland that climatic and non-climatic variables could not explain in the models (Franz et al., 2009). Region effects were thought to be caused by differences in infection pressure in different parts of the country because of how much wheat is grown. Wheat-after-wheat rotations are more typical in the northeast, with more intensive wheat cultivation. Another possible explanation for the region effect were differences in temperature sensitivity between populations of *Fusarium* species in different locations (Franz et al., 2009). Northern populations may have adapted to lower average temperatures, resulting in

increased growth, and dividing regional impact into underlying variables could greatly increase model efficiency, making prediction models less site-specific and generally applicable to control authorities, producers, and industry (Franz et al., 2009).

1.5 Recommendation for Modelling Approach in Western Canada

The quest for a crucial period conducive to FHB epidemics is common in all models reviewed in this chapter. The timeframe for prediction of the FHB and the probability of outbreak varies from 18 days prior to the commencement of anthesis, with most models focused on 7 days prior to the beginning of the anthesis. The evidence of these models' validity is how well they link theoretical, scientific, and small-scale knowledge to knowledge on the large-scale disease, which is assessed by different measures of accuracy (R^2 and accuracy sensu stricto) (Hollingsworth et al., 2006). Of the models reviewed, only De Wolf et al. (2003) use accuracy as such (the percentage of cases accurately predicted) and is around 70% accurate when using pre-anthesis information, and 84% accurate when using additional post-anthesis information (De Wolf et al., 2003). Parsimony is the principle of modelling that means that simplicity rather than complexity is preferable (Rossi et al., 2003; Prandini et al., 2009). Models must be as efficient as possible without reduced capacity using the fewest possible variables. While complexity can increase the accuracy of a model, it can also minimize its usability and applicability. The parsimony theory ought to be used in the simulation, implying that consistency is superior to ambiguity (Rossi et al., 2003; Shah et al., 2021). Prediction of FHB days before anthesis is a valuable tool for producers to decide on fungicide spraying or not. Late-season evaluations miss the intervention window though it can be helpful to anticipate impacts on grain marketing and food systems (De Wolf et al., 2003; Rossi et al., 2003)

1.6 Objectives

The overall objective of this study was to develop and validate weather-based models for FHBi, DON, and FDK risk using weather data and FHBi, FDK, and DON levels measured in plots across 3 prairie provinces. The specific objectives were to i) assess the correlation between the FHBi, FDK, DON, and spore concentration in winter wheat, spring wheat, barley, and durum in western Canada (Chapter 2), ii) evaluate the response of winter wheat, spring wheat, and barley varieties to FHB under natural infection in the field by assessing visual symptoms (FHBi) and harvested samples for FDK and DON concentration across western Canada (Chapter 2), iii) develop FHBi, FDK and DON weather-based models to forecast the risk of FHB epidemic in wheat, barley and durum in western Canada (Chapter 3), iv) validate models that predict FHBi, FDK and DON epidemics for different spring wheat, winter wheat, barley and durum developed in western Canada (Chapter 4), v) validate and compare existing spring wheat and winter wheat FHBi in western Canada developed in the USA to FHBi models developed in western Canada using producer field data (Chapter 4), vi) determine the effect of distance between the field and the nearest weather station on the accuracy of winter wheat, spring wheat, barley and durum FHBi, FDK and DON models developed in Canada (Chapter 4).

1.7 Thesis Outline

The layout of this thesis followed the thesis guidelines of the Department of Soil Science, University of Manitoba. Chapters 2 to 4 were prepared in manuscript formats with the titles as follows:

Chapter 2: Effect of variety and correlation between FHB disease indicators in western Canadian cereal production

Chapter 3: Developing risk models to mitigate Fusarium Head Blight in western Canadian cereal production

Chapter 4: On-farm validation of Fusarium Head Blight risk models in western Canadian cereal production

1.8 References

ACIS. 2021. Alberta Climate Service -Fusarium Head Blight Map. [Online] Available at https://agriculture.alberta.ca/acis/m#!Fusarium (accessed 16 November 2021).

Bai, G., and G. Shaner. 2004. Management and resistance in wheat and barley to Fusarium Head Blight. Annu. Rev. Phytopathol **42**: 135–161.

Bai, G., and G. Shanner. 1994. Scab of Wheat: Prospects for control. Plant Dis. **78**: 760. doi: 10.1094/PD-78-0760.

Bergstrom, G.C., and P. Spolti. 2014. Triazole sensitivity in a contemporary population of *Fusarium graminearum* from New York wheat and competitiveness of a Tebuconazole-Resistant isolate. Plant Dis. **98**: 607–613. doi: 10.1094/PDis-10-13-1051-RE.

Bernardo, A., G. Bai, P. Guo, K. Xiao, A.C. Guenzi, et al. 2007. *Fusarium graminearum*-induced changes in gene expression between Fusarium Head Blight-resistant and susceptible wheat cultivars. Funct. Integr. Genomics **7:** 69–77. doi: 10.1007/s10142-006-0028-1.

Birr, T., J.-A. Verreet, and H. Klink. 2019. Prediction of deoxynivalenol and zearalenone in winter wheat grain in a maize-free crop rotation based on cultivar susceptibility and meteorological factors. J. Plant Dis. Prot. **126**: 13–27. doi: 10.1007/s41348-018-0198-9.

Bondalapati, K.D., J.M. Stein, S.M. Neate, S.H. Halley, L.E. Osborne, et al. 2012. Development of weather-based predictive models for Fusarium Head Blight and deoxynivalenol accumulation for spring malting barley. Plant Dis. **96**: 673–680. doi: 10.1094/PDis-05-11-0389.

Burlakoti, R.R., L. Tamburic-Ilincic, V. Limay-Rios, and P. Burlakoti. 2017. Comparative population structure and trichothecene mycotoxin profiling of *Fusarium graminearum* from corn and wheat in Ontario, central Canada. Plant Pathol. **66**: 14–27. doi: 10.1111/ppa.12559.

Canadian Grain Commission. 2019. Official Grain Grading Guide. [Online] Available at https://www.grainscanada.gc.ca/en/grain-quality/official-grain-grading-guide/04-wheat/grading-factors.html (accessed 24 June 2020). (accessed 24 June 2020).

CFIA. 2015. Canadian Food Inspection Agency. RG-8 Regulatory Guidance: Contaminants in Feed (formerly RG-1, Chapter 7). [Online] Available at https://inspection.canada.ca/animal-health/livestock-feeds/regulatory-guidance/rg-8/eng/1347383943203/1347384015909?chap=0 (accessed 28 December 2021).

Cowger, C., T.J. Ward, K. Nilsson, C. Arellano, S.P. McCormick, et al. 2020. Regional and field-specific differences in *Fusarium* species and mycotoxins associated with blighted North Carolina wheat. Int. J. Food Microbiol. **323**: 108594. doi: 10.1016/j.ijfoodmicro.2020.108594.

Crippin, T. 2019. Comparative analysis of *Fusarium graminearum* strain genotype and chemotype from grains sampled during the 2015-2017 Ontario Harvests. MSc Thesis, Carlton University, doi: 10.22215/etd/2019-13634.

Dahl, B., and W.W. Wilson. 2018. Risk premiums due to Fusarium Head Blight (FHB) in wheat and barley. Agric. Syst. **162**: 145–153. doi: 10.1016/j.agsy.2018.01.025.

De Wolf, E.D., L.V. Madden, and P.E. Lipps. 2003. Risk assessment models for wheat Fusarium Head Blight epidemics based on within-season weather data. Phytopathology **93**: 428–435. doi: 10.1094/Phyto.2003.93.4.428.

Del Ponte, E.M., J.M.C. Fernandes, and W. Pavan. 2005. A risk infection simulation model for Fusarium Head Blight of wheat. Fitopatol. Bras. **30**: 634–642. doi: 10.1590/S0100-41582005000600011.

Del Ponte, E.M., J.M.C. Fernandes, W. Pavan, and W.E. Baethgen. 2009. A model-based assessment of the impacts of climate variability on Fusarium Head Blight seasonal risk in Southern Brazil: Modeling impacts of climate variability on Fusarium Head Blight. J. Phytopathol. **157**:11–12: 675–681. doi: 10.1111/j.1439-0434.2009.01559.x.

Franz, E., K. Booij, and I. van der Fels-Klerx. 2009. Prediction of deoxynivalenol content in Dutch winter wheat. J. Food Prot. **72:** 2170–2177. doi: 10.4315/0362-028X-72.10.2170.

Gaigé, S., M.S. Bonnet, C. Tardivel, P. Pinton, J. Trouslard, et al. 2013. c-Fos immunoreactivity in the pig brain following deoxynivalenol intoxication: Focus on NUCB2/nesfatin-1 expressing neurons. NeuroToxicology **34**: 135–149. doi: 10.1016/j.neuro.2012.10.020.

Gilbert, J., R.M. Clear, T.J. Ward, D. Gaba, A. Tekauz, et al. 2010. Relative aggressiveness and production of 3- or 15-acetyl deoxynivalenol and deoxynivalenol by *Fusarium graminearum* in spring wheat. Can. J. Plant Pathol. **32**: 146–152. doi: 10.1080/07060661003740231.

Gilbert, J., and W.G.D. Fernando. 2004. Epidemiology and biological control of *Gibberella zeae* / *Fusarium graminearum*. Can. J. Plant Pathol. **26**: 464–472. doi: 10.1080/07060660409507166.

Gilbert, J., and S. Haber. 2013. Overview of some recent research developments in Fusarium Head Blight of wheat. Can. J. Plant Pathol. **35**: 149–174. doi: 10.1080/07060661.2013.772921.

Giroux, M.-E., G. Bourgeois, Y. Dion, S. Rioux, D. Pageau, et al. 2016. Evaluation of forecasting models for Fusarium Head Blight of wheat under growing conditions of Quebec, Canada. Plant Dis. **100**: 1192–1201. doi: 10.1094/PDis-04-15-0404-RE.

Government of Saskatchewan, 2022. Fusarium Head Blight Disease [WWW Document]. Government of Saskatchewan. [Online] Available at https://www.saskatchewan.ca/business/agriculture-natural-resources-and-industry/agribusiness-farmers-and-ranchers/crops-and-irrigation/disease/fusarium-head-blight (accessed 4.10.22).

Góral, T., H. Wiśniewska, P. Ochodzki, L. Nielsen, D. Walentyn-Góral, et al. 2018. Relationship between Fusarium Head Blight, Kernel Damage, concentration of *Fusarium* Biomass, and *Fusarium* toxins in grain of winter wheat inoculated with *Fusarium culmorum*. Toxins **11**: 2. doi: 10.3390/toxins11010002.

Góral, T., H. Wiśniewska, P. Ochodzki, A. Twardawska, and D. Walentyn-Góral. 2020. Resistance to Fusarium Head Blight, Kernel Damage and Concentration of Fusarium Mycotoxins in Grain of Winter Triticale (x Triticosecale Wittmack) Lines. Agronomy 2021, **11**, 16; https://doi.org/10.3390/agronomy11010016..

Ha, X., B. Koopmann, and A. von Tiedemann. 2016. Wheat blast and Fusarium Head Blight display contrasting interaction patterns on ears of wheat genotypes differing in resistance. Phytopathology **106**: 270–281. doi: 10.1094/Phyto-09-15-0202-R.

Harris, L.J., M. Balcerzak, A. Johnston, D. Schneiderman, and T. Ouellet. 2016. Host-preferential *Fusarium graminearum* gene expression during infection of wheat, barley, and maize. Fungal Biol. **120**: 111–123. doi: 10.1016/j.funbio.2015.10.010.

Hollingsworth, C.R., J.J. Mewes, C.D. Motteberg, and W.G. Thompson. 2006. Predictive accuracy of a Fusarium Head Blight epidemic risk forecasting system deployed in Minnesota. Plant Health Prog. **7**: 4. doi: 10.1094/PHP-2006-1031-01-RS.

Hooker, D.C., A.W. Schaafsma, and L. Tamburic-Ilincic. 2002. Using weather variables pre- and post-heading to predict deoxynivalenol content in winter wheat. Plant Dis. **86**: 611–619. doi: 10.1094/PDIS.2002.86.6.611.

Kelly, A.C., R.M. Clear, K. O'Donnell, S. McCormick, T.K. Turkington, A. Tekauz, J. Gilbert, H.C. Kistler, M. Busman and T.J. Ward. 2015. Diversity of Fusarium Head Blight populations and trichothecene toxin types reveals regional differences in pathogen

composition and temporal dynamics. Fungal Genet. Biol. **82**: 22–31. doi: 10.1016/j.fgb.2015.05.016.

Klinck, H.R. 2007. Cereal Crops | The Canadian Encyclopedia. [Online] Available at https://www.thecanadianencyclopedia.ca/en/article/cereal-crops (accessed 25 June 2020).

Manstretta, V., Morcia, C., Terzi, V., Rossi, V., 2016. Germination of *Fusarium graminearum* ascospores and wheat infection are affected by dry periods and by temperature and humidity during dry periods. Phytopathology **106**, 262–269. https:sdoi.org/10.1094/Phyto-05-15-0118-R.

MARD. 2021. Fusarium Head Blight Report-Manitoba Agriculture and Resource Development. Prov. Manit. - Agric. [Online] Available at https://www.gov.mb.ca/agriculture/ (accessed 16 November 2021).

McMullen, M., G. Bergstrom, E. De Wolf, R. Dill-Macky, D. Hershman, et al. 2012. A unified effort to fight an enemy of wheat and barley: Fusarium Head Blight. Plant Dis. **96**: 1712–1728.

Moschini, R.C., R. Pioli, M. Carmona, and O. Sacchi. 2001. Empirical predictions of wheat head blight in the Northern Argentinean Pampas region. Crop Sci. **41:** 1541–1545. doi: 10.2135/cropsci2001.4151541x.

Musa, T., A. Hecker, S. Vogelgsang, and H.R. Forrer. 2007. Forecasting of Fusarium Head Blight and deoxynivalenol content in winter wheat with FusaProg*. EPPO Bulletin. 37. 283 - 289. 10.1111/j.1365-2338.2007.01122.x..

Nita, M., editor. 2013. Fungicides - Showcases of integrated plant disease management from around the world. InTech London, 342 p. [Online] Available at https://www.intechopen.com/books/2917 doi: 10.5772/3251.

Oghenekaro, A.O., M.A. Oviedo-Ludena, M. Serajazari, X. Wang, M.A. Henrique, N.G. Wenner, G.A. Kuldau, A. Navabi, H.R. Kutcher and W.G.D. Fernando. 2021. Population genetic structure and chemotype diversity of *Fusarium graminearum* populations from wheat in Canada and North Eastern United States. Toxins 13: 180. doi:10.3390/toxins13030180.

Paul, P.A., P.E. Lipps, and L.V. Madden. 2005. Relationship between visual estimates of Fusarium Head Blight intensity and deoxynivalenol accumulation in harvested wheat grain: A Meta-Analysis. Phytopathology **95**: 1225–1236. doi: 10.1094/Phyto-95-1225.

Pitblado, R., D.C. Hooker, I. Nichols, R. Danford, and A.W. Schaafsma. 2007. DONCAST: seven years of predicting DON in wheat on a commercial scale. Proceedings of the National Fusarium Head Blight Forum; The Westin Crown Center, Kansas City, Missouri. p. 29

Prandini, A., S. Sigolo, L. Filippi, P. Battilani and G. Piva. 2009 Review of predictive models for Fusarium head blight and related mycotoxin contamination in wheat. Food Chem. Toxicol. 47(5):927-31. doi: 10.1016/j.fct.2008.06.010.

Rossi, V., S. Giosue, E. Pattori, F. Spanna, and A. Del Vecchio. 2003. A model estimating the risk of Fusarium Head Blight on wheat. EPPO Bull. **33**: 421–425. doi: 10.1111/j.1365-

Schaafsma, A.W., and D.C. Hooker. 2007. Climatic models to predict occurrence of Fusarium toxins in wheat and maize. Int. J. Food Microbiol. **119**: 116–125. doi: 10.1016/j.ijfoodmicro.2007.08.006.

Schmale, D.G., A.K. Wood-Jones, C. Cowger, G.C. Bergstrom, and C. Arellano. 2011. Trichothecene genotypes of *Gibberella zeae* from winter wheat fields in the eastern USA: Trichothecene genotypes of *G. zeae* in eastern USA. Plant Pathol. **60**: 909–917. doi: 10.1111/j.1365-3059.2011.02443.x.

Shah, D.A., E.D. De Wolf, P.A. Paul, and L.V. Madden. 2014. Predicting Fusarium Head Blight epidemics with boosted regression trees. Phytopathology **104**: 702–714. doi: 10.1094/Phyto-10-13-0273-R.

Shah, D.A., E.D. De Wolf, P.A. Paul, and L.V. Madden. 2019a. Functional data analysis of weather variables linked to Fusarium Head Blight epidemics in the United States. Phytopathology **109**: 96–110. doi: 10.1094/Phyto-11-17-0386-R.

Shah, D.A., E.D. De Wolf, P.A. Paul, and L.V. Madden. 2021. Accuracy in the prediction of disease epidemics when ensembling simple but highly correlated models (N.J. Cunniffe, editor). PLOS Comput. Biol. **17**: e1008831. doi: 10.1371/journal.pcbi.1008831.

Shah, D.A., J.E. Molineros, P.A. Paul, K.T. Willyerd, L.V. Madden and E.D. De Wolf. 2013. Predicting Fusarium Head Blight epidemics with weather-driven pre- and post-anthesis logistic regression models. Phytopathology **103**: 906–919. doi: 10.1094/Phyto-11-12-0304-R.

Shah, D.A., P.A. Paul, E.D. De Wolf, and L.V. Madden. 2019b. Predicting plant disease epidemics from functionally represented weather series. Philos. Trans. R. Soc. B Biol. Sci. **374**: 20180273. doi: 10.1098/rstb.2018.0273.

Sobrova, P., V. Adam, A. Vasatkova, M. Beklova, L. Zeman, et al. 2010. Deoxynivalenol and its toxicity. Interdiscip. Toxicol. **3**. doi: 10.2478/v10102-010-0019-x.

Statistics Canada. 2019. Production of principal field crops. [Online] Available at https://www150.statcan.gc.ca/n1/daily-quotidien/191206/dq191206b-eng.htm (accessed 24 June 2020).

SWDC. 2021. Fusarium Resources- Saskatchewan Wheat Development Commission. Sask Wheat Dev. Comm. [Online] Available at https://saskwheat.ca/Fusarium-resources (accessed 16 November 2021).

Tamburic-Ilincic, L., A. Wragg, and A. Schaafsma. 2015. Mycotoxin accumulation and *Fusarium graminearum* chemotype diversity in winter wheat grown in southwestern Ontario. Can. J. Plant Sci. **95**: 931–938. doi: 10.4141/cjps-2014-132.

Van Der Fels-Klerx, H.J., S.L.G.E. Burgers, and C.J.H. Booij. 2010. Descriptive modelling to predict deoxynivalenol in winter wheat in the Netherlands. Food Addit. Contam. Part A **27**: 636–643. doi: 10.1080/19440040903571762.

Van der Lee, T., H. Zhang, A. van Diepeningen, and C. Waalwijk. 2015. Biogeography of *Fusarium graminearum* species complex and chemotypes: a review. Food Addit. Contam. Part A **32**: 453–460. doi: 10.1080/19440049.2014.984244

Vogelgsang, S., A. Hecker, T. Musa, B. Dorn, and H.-R. Forrer. 2011. On-farm experiments over 5 years in a grain maize/winter wheat rotation: effect of maize residue treatments on Fusarium graminearum infection and deoxynivalenol contamination in wheat. Mycotoxin Res. **27**: 81–96. doi: 10.1007/s12550-010-0079-y.

Wallhead, M., and H. Zhu. 2017. Decision support systems for plant disease and insect management in commercial nurseries in the Midwest: A Perspective Review 1. J. Environ. Hortic. **35**: 84–92. doi: 10.24266/0738-2898-35.2.84.

Wang, J., Z. Zhao, X. Yang, J. Yang, A. Gong, J. Zhang, L. Chen and C. Zhou. 2019. *Fusarium graminearum* species complex and trichothecene genotype. Mycotoxins and Food Safety. IntechOpen DOI: 10.5772/intechopen.89045, [Online] Available at https://www.intechopen.com/chapters/68943

Ward, T.J., R.M. Clear, A.P. Rooney, K. O'Donnell, D. Gaba, et al. 2008. An adaptive evolutionary shift in Fusarium Head Blight pathogen populations is driving the rapid spread of more toxigenic *Fusarium graminearum* in North America. Fungal Genet. Biol. **45**: 473–484. doi: 10.1016/j.fgb.2007.10.003.

Wolny-Koładka, K., A. Lenart-Boroń, and P. Boroń. 2015. Species composition and molecular assessment of the toxigenic potential in the population of *Fusarium* spp. isolated from ears of winter wheat in southern Poland. J. Appl. Bot. Food Qual. **88**: p.139144. doi: 10.5073/jabfq.2015.088.020.

Wu, F., J.D. Groopman, and J.J. Pestka. 2014. Public Health Impacts of Foodborne Mycotoxins. Annu. Rev. Food Sci. Technol. **5**: 351–372. doi: 10.1146/annurev-food-030713-092431.

Xu, X., **L.V., M**a**dden,., S.G., Edwards, F.M., Doohan, A., Moretti, L., Hornok, P., Nicholson, and A. Ritieni.2013**. Developing logistic models to relate the accumulation of DON associated with Fusarium head blight to climatic conditions in Europe. Eur J Plant Pathol 137, 689–706. https://doi.org/10.1007/s10658-013-0280-x

2. EFFECT OF VARIETY AND CORRELATION BETWEEN FHB DISEASE INDICATORS IN WESTERN CANADIAN CEREAL PRODUCTION

2.1 Abstract

Producers of wheat and barley continue to be negatively impacted by Fusarium Head Blight (FHB) disease. The economic costs of FHB are manifested not only in yield reduction but also in the downgrading of grain as a result of Fusarium damaged kernels (FDK) and contamination with mycotoxins such as deoxynivalenol (DON). Visual FHB and FDK symptoms are frequently used as rough predictors of DON due to the high cost of DON analysis with the aim of managing FHB. Additionally, varieties with some resistance to FHB can substantially reduce the epidemic level, especially when integrated with other control strategies such as FHB forecasting and fungicide application. Field experiments were conducted in the 2019 and 2020 growing seasons to i) assess the response of winter wheat, spring wheat, barley, and durum varieties to FHB, FDK, and DON under field conditions and ii) evaluate the correlation between FHB index (FHBi), FDK, DON, and spore concentration (SC) in winter wheat, spring wheat, barley, and durum in western Canada. In contrast to other provinces, Manitoba had the highest levels of FHBi, while Saskatchewan had the highest levels of FDK. In both years, the correlation between FDK and DON was linear and significantly positive for all crop types and cultivars, with the correlation being stronger in the winter wheat crop type ($r = 0.92$). The effect of varieties on FHBi and FDK was not significant. Low disease pressure in both seasons may have obscured the impact of FHB resistance levels among crop varieties. However, the moderately resistant varieties (F. RC3) accumulated significantly less DON ($p < 0.05$) than susceptible varieties (F. RC1) in all crop types except durum, which had only one FHB category. These findings highlight the importance of incorporating the effects of resistant cultivars in developing weather-based models in western

Canada and developing independent models for FHBi, FDK, and DON, as the correlation between these disease indicators varied between the two years.

2.2 Introduction

FHB is a widespread fungal disease caused by phytopathogenic members of the *Fusarium* species (Dexter et al., 1996). *Fusarium graminearum* is regarded as one of the most damaging fungal pathogens in wheat and barley in western Canada (Fowler, 2011). *Fusarium* species infect wheat and barley heads during the flowering period, and significant yield and quality reduction occur under favorable environmental conditions (McCallum and Tekauz, 2002; De Wolf et al., 2003). *Fusarium* species have received much attention because of their ability to produce mycotoxins that can seriously contaminate the food and feed chain. Trichothecenes are the most common mycotoxins found in small grain cereals, with DON and its acetylated derivatives 3- and 15-acetyldeoxynivalenol being the most common (Clear et al., 2013). As a result, DON-contaminated grains are frequently downgraded and either fed to livestock or destroyed (Alberta Government, 2015). Economic losses in the United States of America (USA) have been estimated at $1.176 billion for wheat and $293 million for barley between 2015 and 2016 (Wilson et al., 2018). In Alberta, Canada, FHB-induced downgrading resulted in significant economic losses of about $8.7 million in 2010 and about $3 million in 2012 (Alberta Government, 2015).

FHB forecasting, fungicide applications, crop rotation, and the selection of varieties with some resistance to FHB can all be used to mitigate the negative impact of the disease (Dill-Macky, 2008). Several FHB resistance types have been identified, including resistance to the initial infection (type I), resistance to pathogen spread throughout the spike (type II), resistance to kernel infection (type III), host tolerance to FHB and DON (type IV), and resistance to DON accumulation (type V) (Kubo et al., 2014; He et al., 2015; Góral et al., 2020). The number of FHB-

resistant wheat and barley varieties available to growers in western Canada is steadily increasing (Sask Seed Guide, 2019). Continuous testing to determine a variety's resistance to FHB has the potential to avert major FHB epidemics in western Canada, given the observed shift to more aggressive *Fusarium* chemotypes. In durum, long-term control of FHB disease has been difficult because FHB resistance sources are scarce in the primary gene pool of tetraploid wheat, which complicates breeding for resistance (Haile et al., 2019).

Fungicides provide an alternative FHB management strategy to varietal resistance, especially when used with forecast models (De Wolf et al., 2003; Rossi et al., 2003; Brustolin et al., 2013). Numerous weather-based models have been developed worldwide to aid in the timing and application of fungicides, including those developed in the USA and currently used in western Canada (De Wolf et al., 2003; Shah et al., 2013). These models predict FHB epidemics with a field severity or FHBi greater than 10%, a disease severity level strongly correlated with FHB yield losses and generally associated with elevated levels of DON in harvested grain (De Wolf et al., 2003). A wide range of correlations has been found between FHB and disease indicators (FHBi, FDK, and DON), ranging from high positive correlations to low significant correlations to negative correlations to almost null correlations (Kubo et al., 2014; He et al., 2015; Miedaner et al., 2016). Understanding the relationship between disease indicators and the effect of cultivars in western Canada may aid in ongoing efforts to predict FHB. The objectives of this study were to i) evaluate the correlation between the FHBi, FDK, DON, and SC in winter wheat, spring wheat, barley, and durum in western Canada, and ii) evaluate winter wheat, spring wheat, and barley varieties response to FHB under natural infection in the field by assessing visual symptoms (FHBi) and harvested samples for FDK and DON concentration across western Canada.

2.3 Materials and Methods

2.3.1 Plot Sites

Small-plot research trials with five plot sites per province (15 sites) were conducted in Manitoba, Saskatchewan, and Alberta during the 2019 and 2020 growing seasons (Figure 2.1). The plot sites were located in fields with at least two years of FHB data collected through provincial and federal government annual FHB surveys. In addition, these 15 sites were geographically distributed across western Canada to maximize the likelihood of each site experiencing a variety of growing-season weather conditions. Each plot was approximately 4 m long and 2 m wide, with at least 8 rows.

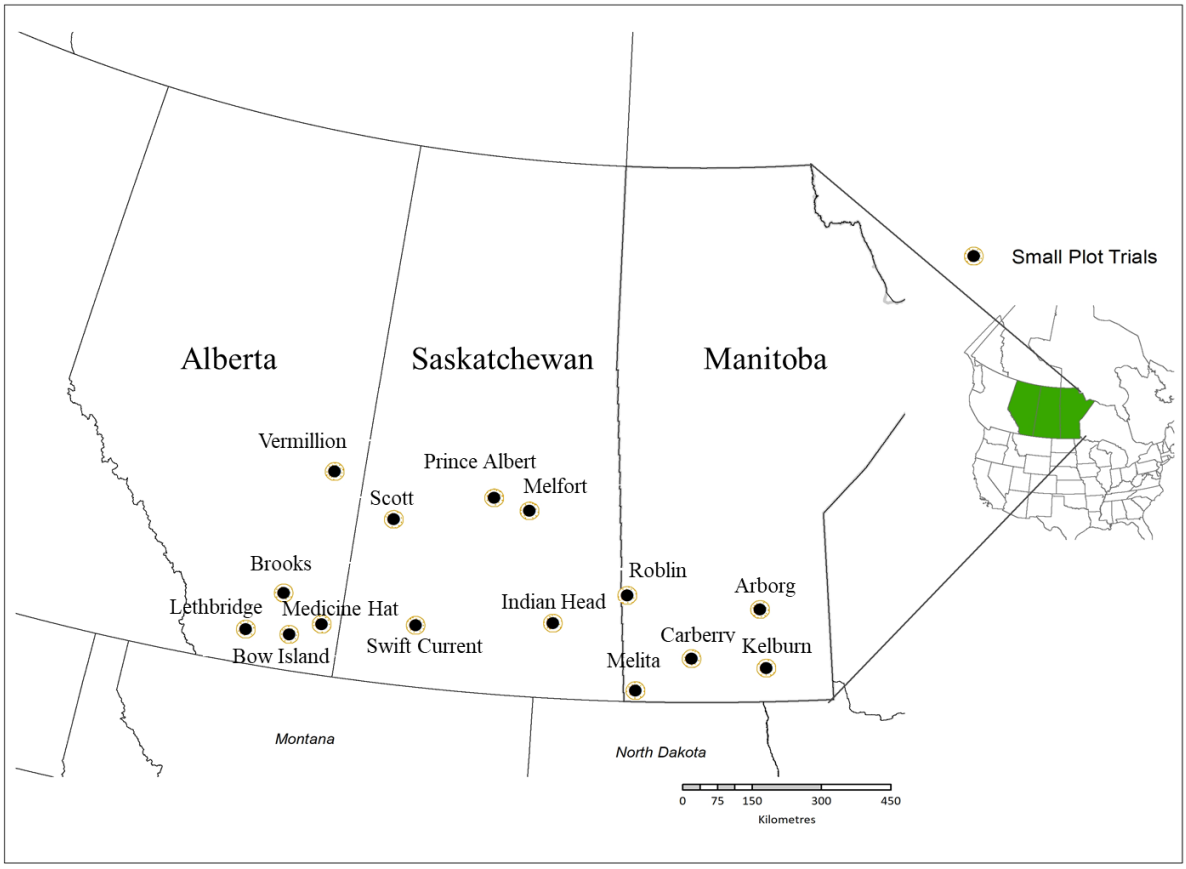

Figure 2. 1. FHB small-plot research trials in western Canada during the 2019 and 2020 growing seasons.

2.3.2 Experimental Design

The experimental design was a randomized complete block design (RCBD) with four replications (blocks) for each of the separate side by side winter wheat, spring wheat, barley, and durum experiments (Figure 2.2). Three different spring wheat, winter wheat, and barley varieties were used in the treatments, representing three different FHB resistance categories (F. RC) (Table 2.1). FHB resistance categories included F. RC1 (susceptible or moderately susceptible varieties), F. RC2 (intermediate varieties), and F. RC3 (moderately resistant or resistant varieties), depending on the crop type. Only one durum wheat variety was grown because all durum wheat varieties are FHB susceptible or moderately susceptible.

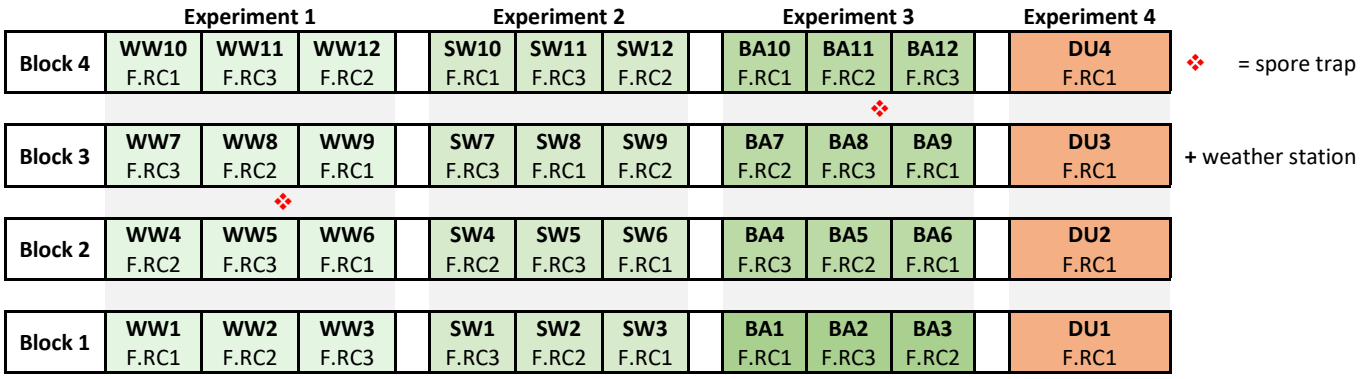

Figure 2. 2. Experimental layout at the plot sites. Winter wheat (WW), spring wheat (SW), barley (BA) and durum (DU). F.RC1, F.RC2, and F.RC3 represent susceptible or moderately susceptible, intermediate, and moderately resistant or resistant varieties depending on the crop type, respectively.

2.3.3 Planting and Crop Growth Stages

Three winter wheat varieties with three levels of FHB resistance (Table 2.1) were planted in the fall of 2018 and 2019, while spring cereals (spring wheat, barley, and durum) were planted in the spring of 2019 and 2020, based on the best management practices at each location. Standard agronomic practices such as fertilizer application, seeding depth, row spacing, and herbicide

application were implemented at each site. However, no fungicides were used. Planting, maturity, and harvesting dates for each crop were recorded. Crop growth was regularly monitored throughout the growing season, and the date when each cultivar reached BBCH stage 59 (main stem spikes completely emerged) was recorded; thereafter, BBCH growth stages were recorded weekly until BBCH 80 (Meier et al., 2009). When the 50% anthesis date in wheat and 50% heading date in barley were not observed, the planting date along with a thermal model was used to estimate these dates (Appendix 5).

Table 2. 1. Winter wheat, spring wheat, barley, and durum cultivars with their Fusarium Head Blight susceptibility category in western Canada (Sask Seed Guide, 2019).

Crop type	Variety name	FHB resistance category	Resistance category abbreviation[e]
Winter wheat (CWRW[a])	Emerson	Resistant (R)	F. RC3
	AAC[d] Gateway	Intermediate (I)	F. RC2
	Moats	Susceptible (S)	F. RC1
Spring wheat (CWRS[b])	AAC Brandon	Moderately resistant (MR)	F. RC3
	AAC Elie	Intermediate (I)	F. RC2
	Muchmore	Moderately susceptible (MS)	F. RC1
Barley	AAC Connect	Moderately resistant (MR)	F. RC3
	CDC Copeland	Intermediate (I)	F. RC2
	AAC Synergy	Moderately susceptible (MS)	F. RC1
Durum (CWAD[c])	Strongfield	Susceptible (S)	F. RC1

[a]CWRW is Canada Western Red Winter.

[b]CWRS is Canada Western Red Spring.

[c]CWAD is Canada Western Amber Durum.

[d]Acronym "AAC" denotes varieties developed by Agriculture and Agri-Food Canada.

[e]FHB resistance categories. F. RC1 (susceptible or moderately susceptible varieties), F. RC2 (intermediate varieties), and F. RC3 (moderately resistant or resistant varieties), depending on the crop type.

2.3.4 Meteorological Data

Watchdog® portable weather stations (Spectrum Technologies 2000 Series, Thayer Case, IL, USA) were used to collect data during the growing season. One weather station was mounted on

a solid post at an average height of 1.80 m within 10 m of the plots at each site. Weather data collected hourly included air temperature (°C), relative humidity (RH), rainfall (mm), solar radiation (W m^{-2}), and wind speed (km h^{-1}) and direction. The weather stations were installed following the spring crop seeding. Any meteorological data required prior to deploying the portable weather stations were obtained from a nearby weather station in the networks operated by Manitoba Agriculture Weather Program, Alberta Climate Information Service, and Environment and Climate Change Canada (ACIS, 2021; ECCC, 2021; MARD, 2021).

2.3.5 FHB Spore Traps

2.3.5.1 Spore Trap Installation and FHB Spores Identification

FHB spores were trapped using Guo's (2008) method, with minor modifications. Two adhesive spore traps were placed in two central locations within the plot area at a height of about 1 m prior to anthesis (BBCH 59). The spore traps consisted of a trap head and a supporting rod. A rectangular piece of foam with four spore collection surfaces (6 mm x 90 mm each) was used as the trap head. The spore head surfaces were covered with a base tape, followed by Melinex double-sided tape coated with a thin layer of petroleum jelly to which airborne spores adhered. The spore traps were replaced weekly for four weeks (8 spore traps in total). Following the collection of spores, a small piece measuring 5 mm x 19 mm was cut from the Melinex tape on one side of the trap head and fixed to a glass slide. *Fusarium* species spores were determined under a compound microscope (400x) to confirm the presence of the inoculum in the environment.

2.3.5.2 Determination of Spore Concentration

The volume of air passing through the area (5 mm x 19 mm) was calculated by first calculating the average daily wind speed for the period when the spore traps were in the field (i.e., from date

of installation to date of removal). The wind speed was recorded at approximately 1.8 m at the plot sites. However, the spore traps were installed at about 1 m above ground, and thus, there was a need to extrapolate the wind speed from 1.8 to 1 m. This was done using the log law wind profile formulae with roughness length set at 0.1 m (Stull, 2000). The total wind run (i.e., how much wind has passed) for the day (m) was then calculated by multiplying the average wind speed at 1 m (m/s) 86400 s (number of seconds in 24 h). The volume of air (m^3) was calculated by multiplying the wind run by sampled area (0.005 m x 0.019 m). Since the spore traps have 4 sides, the wind run (m^3) was then divided by 4, assuming that the wind run was equally divided among all 4 sides of the spore trap. The total volume of air (m^3) was calculated by multiplying the volume of air per day (m^3) by the number of days the spore traps were in the field.

2.3.6 Disease Indicators

2.3.6.1 Fusarium Head Blight Index

Fusarium Head Blight was assessed 18 to 21 days after 50% anthesis (BBCH 65). This was between the early milk stage (BBCH 73) and the soft dough stage (BBCH 85). FHB incidence (% of spikes affected) and FHB severity (mean percentage of blighted spikelets per infected head) were determined by scoring five spikes at ten random locations (total 50 spikes) within a plot. Fusarium Head Blight index (FHBi) was then determined according to Shah et al. (2014) using the following formula:

$$FHBi = (FHBincidence \times FHBseverity)/100$$

2.3.7 Fusarium Damaged Kernels and Deoxynivalenol

Grain samples (1 kg plot^{-1}) were collected for official grading, FDK and DON analysis at harvest. During combining, grain samples were collected with a level of dockage similar to that from producer fields to retain a representative amount of the lightweight Fusarium damaged kernels. Grain grading, FDK determination, and DON analysis were conducted by a commercial laboratory (Intertek, Canada) following the procedures outlined in the Canadian Grain Commission's Official Grain Grading Guide (Canadian Grain Commission, 2019). Briefly, samples were divided into a representative portion using a Boerner-type divider. The samples were then visually divided into two groups of healthy and infected kernels with different damage levels. A 10-power magnifying lens was used to confirm the presence of a chalk-like appearance or pinkish mold. FDK was then calculated as a percentage of the number of grains with FDK divided by the total number of grains in a sample. To determine DON concentration, 50 g subsamples were ground and analyzed using high sensitivity (HS) Neogen ELISA 5/5 Vomitoxin kits with a DON detection limit of 0.5 mg kg^{-1} (Neogen Corporation, 2013).

2.3.8 Statistical Analysis

Data were analyzed using SAS 9.4 (SAS Institute, 2021). Analysis of variance (ANOVA) was carried out using the generalized linear mixed model procedure (PROC GLIMMIX) to determine the effect of the cultivar (treatment) on FHBi, FDK, and DON concentration. The "DIST =" function was used in the MODEL statement of PROC GLIMMIX to specify all distributions other than Gaussian. FHBi and FDK followed a binomial distribution while DON data followed a lognormal distribution. Treatment and year were modeled as fixed effects, while block and site were random effects. Treatment means were compared using the Tukey multiple comparison procedure at $\alpha = 0.05$. The relationships between FHBi, FDK, DON and SC, and mycotoxin concentrations were investigated by Pearson correlation tests in SAS using PROC CORR.

2.4 Results

2.4.1 Prevalence of FHB in the Prairies

2.4.1.1 Weather Conditions

Weather conditions varied between the 2019 and 2020 growing seasons and plot site locations (Table 2.2). Most plot sites experienced hotter and drier than normal growing conditions in both seasons. In July, 67% of the sites were hotter in 2020 than in 2019, while 47% were wetter in 2020 than 2019 (Table 2.2). Of the 47%, 14% were sites from Manitoba, 43% from Saskatchewan, and 43% from Alberta. In 2019, monthly mean temperatures ranged from 14.2 to 24.7 °C, with monthly total rainfall ranging from 7.1 to 180 mm. In 2020, monthly mean temperatures ranged between 11.9 and 21.5 °C, while total rainfall varied between 9.3 and 197.9 mm between sites (Table 2.2). The overall highest total monthly rainfall (197.9 mm) was recorded in Kelburn in June during the 2020 growing season, while the overall lowest total monthly rainfall (7.1 mm) was recorded in Roblin in August during the 2019 growing season. Overall, the highest mean monthly air temperature (26.1 °C) was recorded in Brooks during the 2019 growing season in July, while the lowest (11.9 °C) was recorded in Melita during the 2020 growing season in June (Table 2.2).

2.4.1.2 Fusarium Head Blight Index

The occurrence of FHBi varied during the 2019 and 2020 growing seasons. FHBi levels in Alberta were slightly higher in 2019 than in 2020 across all crop types (Figure 2.3). In Saskatchewan, all crop types except barley had slightly higher FHBi levels in 2020 than 2019. In Manitoba, FHBi levels in winter wheat and spring wheat crop types were slightly higher in 2019 than 2020 (Figure 2.3). FHBi levels were highest in Manitoba, particularly Carberry and Roblin, and lowest in Alberta in both individual and combined years (Figure A2.1). The mean FHBi for both years in

Manitoba was 17.4, 14.6, 22.8, and 6.7% in winter wheat, spring wheat, barley, and durum, respectively, 7.8, 5.0, 2.5, and 12.8% in Saskatchewan, and 0.7, 0.2, 0.3, and 0.4% in Alberta (Figure 2.3).

2.4.1.3 Fusarium damaged kernels

The distribution of FDK in the prairie provinces is shown in Figure 2.4. Interestingly, the mean FDK for all crop types in Saskatchewan was higher than in other provinces, particularly in Prince Albert, Melfort, and Scott (Figure A2.2). The durum crop type had the highest DON levels in both years, while barley had the lowest. The mean FDK for both years in winter wheat, spring wheat, barley, and durum were 0.17, 0.27, 0.02, 1.69% in Manitoba, 1.23, 0.78, 0.09, 4.37% in Saskatchewan, and 0, 0.08, 0, and 1.13% in Alberta, respectively (Figure 2.4).

2.4.1.4 Deoxynivalenol

DON levels were higher in Saskatchewan than in Manitoba or Alberta in all crop types (Figure 2.5). Sites with greater DON levels included Melfort, Prince Albert, and Scott, with mean DON levels ≥ 1 mg kg^{-1} in winter wheat, spring wheat, barley, and durum (Figure A2.3). The sensitivity to DON accumulation was reduced from durum to spring wheat to winter wheat to barley in all three prairie provinces (Figure 2.5). In 2019, mean DON levels in winter wheat, spring wheat, barley, and durum ranged from 0 to 0.2, 0 to 0.93, 0 to 0.1, and 0.17 to 4.22 mg kg^{-1}, respectively. In 2020, mean DON levels in winter wheat, spring wheat, barley, and durum ranged from 0 to 0.12, 0 to 0.61, 0 to 0.19, and 0.03 to 1.9 mg kg^{-1}, respectively in the prairie (Figure 2.5).

2.4.2. Correlation between Disease Indicators

2.4.2.1 Correlation in Winter Wheat

Winter wheat correlation coefficient of FHBi versus FDK or DON was not significant in 2019 and both years combined (Table 2.3). However, in 2020, there was a significant but poor correlation between FHBi and FDK ($r = 0.2$; $p = 0.025$). The relationship between FHBi and SC in winter wheat was significantly positive in 2019 ($r = 0.3$; $p = 0.025$), but not significant ($p > 0.05$) in 2020 and both years combined. Results in 2019 ($r = 0.96$), 2020 ($r = 0.87$) and combined years ($r = 0.92$) revealed highly significant ($p < 0.0001$) positive correlation between FDK and DON. Correlation analysis in 2019 ($r = 0.21$; $p = 0.04$) and combined years ($r = 0.32$; $p < 0.0001$) indicated a highly significant but low positive correlation between FDK and SC (Table 2.3). Similarly, correlation analysis between DON and SC revealed a significant positive correlation in 2020 ($r = 0.27$; $p = 0.009$) and combined years ($r = 0.36$; $p < 0.0001$).

Table 2.4 shows the effect of winter wheat varieties on the relationship between FHB disease indicators. FHBi had no significant correlation with either FDK or DON ($p > 0.05$). However, a significant positive correlation ($p < 0.05$) between FDK and DON was observed, which varied between winter wheat varieties. The correlation coefficient for Emerson, a moderately resistant variety (F. RC3) was lower ($r = 0.84$) than for AAC Gateway, an intermediate variety (F. RC3) ($r = 0.95$) and Moats, a susceptible variety (F. RC3) ($r = 0.90$) (Table 2.4).

2.4.2.2 Correlation in Spring Wheat

There was no significant correlation ($p > 0.05$) between FHBi and FDK and FHBi and DON in both individual and combined years in spring wheat (Table 2.3). Correlation analysis revealed a significant correlation between FHBi and SC and FDK and DON in individual and combined years (Table 2.3). However, correlation between FDK and SC and DON and SC was significant ($p > 0.05$) only in 2019. The highest Pearson correlation coefficients were found between FDK and DON ($r = 0.79$) when both years were combined (Table 2.3).

Correlation analysis between spring wheat varieties is shown in (Table 2.4). There was a poor correlation ($p > 0.05$) between FHBi and FDK or DON in all spring wheat varieties. A significant ($p < 0.001$) positive correlation was found between FDK and DON, which differed between spring wheat cultivars. The correlation coefficient between FDK and DON decreased from a moderately susceptible variety Muchmore (F.RC1) ($r = 0.83$) to an intermediate variety AAC Elie (F.RC2) ($r = 0.78$) to a moderately resistant variety AAC Brandon (F.RC3) ($r = 0.68$).

2.4.2.3 Correlation in Barley

There was no significant correlation ($p > 0.05$) between FHBi and FDK, FHBi and DON, and DON and SC in both individual and combined years in barley crop type (Table 2.3). However, correlation analysis revealed a significant correlation between FHBi and SC and FDK and DON in both individual and combined years. In combined years, the highest significant correlation was found between FDK and DON ($r = 0.71$), while the lowest significant positive correlation was found between FDK and SC ($r = 0.17$; $p = 0.019$) (Table 2.3).

Results of correlation analysis between barley varieties and FHB disease indicators are presented in Table 2.4. There was no significant correlation ($p > 0.05$) between FHBi and FDK or DON in any variety. However, there was a significant positive correlation ($p < 0.001$) between FDK and DON that varied according to barley varieties (Table 2.4). Correlation coefficients between FDK and DON were found to be highest in the moderately susceptible variety (F. RC1) ($r = 0.82$). However, the correlation coefficient for the intermediate variety (F. RC2) was lower ($r = 0.5$) than for the moderately resistant variety (F. RC3) ($r = 0.7$) (Table 2.4).

2.4.2.4 Correlation in Durum

The correlation between FHBi, FDK, DON, and SC differed between the 2019 and 2020 growing seasons. The correlation between FHBi, FDK, DON, and SC was significantly higher and more positive in 2020 than 2019. However, in 2019, the correlation between FDK and SC and DON and SC were not significant ($p > 0.05$). It was interesting to note the high positive correlation between FHBi and SC in 2020 ($r = 0.72$; $p < 0.0001$). However, when both years were combined, the correlation coefficient between FHBi and SC dropped to 0.39. The strongest correlation coefficients were found between FDK and DON ($r \geq 0.65$; $p < 0.0001$) in both individual and combined years.

2.4.3 Variety Resistance

2.4.3.2 Winter Wheat Varieties

There was no significant difference ($p = 0.94$) in the mean FHBi percentage among the three winter wheat varieties with varying levels of FHB resistance (Table 2.5). However, there was a significant difference ($p < 0.0001$) in the levels of DON accumulation among the varieties. The resistant variety Emerson (F. RC3) had significantly lower DON levels (1.23 mg kg^{-1}) compared to the susceptible variety Moats (F. RC1) (1.78 mg kg^{-1}) and an intermediate variety AAC Gateway (F. RC2) (1.87 mg kg^{-1}) (Table 2.5). Across all treatments, the levels of FHBi, FDK, and DON did not differ significantly ($p > 0.05$) between 2019 and 2020 in all three winter wheat varieties (Table 2.5).

2.4.3.2 Spring Wheat Varieties

FHBi and FDK mean levels did not vary significantly with spring wheat varieties ($p > 0.05$), regardless of year ($p > 0.05$ for treatment x year interaction) (Table 2.5). However, DON levels were significantly higher in a moderately susceptible variety Muchmore (F. RC1) (1.65 mg kg^{-1})

than a moderately resistance variety AAC Brandon (F. RC3) (1.28 mg kg^{-1}) and an intermediate variety AAC Elie (F. RC2) (1.2 mg kg^{-1}) (Table 2.5). Additionally, the mean concentration of DON was significantly higher ($p < 0.0001$) in 2019 (1.51 mg kg^{-1}) than in 2020 (1.23 mg kg^{-1}) (Table 2.5).

2.4.3.3 Barley Varieties

There was no significant difference ($p > 0.05$) in the variety and the treatment x year interaction for FHBi, FDK, and DON concentration (Table 2.5). However, DON levels were significantly higher in 2020 (1.09 mg kg^{-1}) compared to 2019 (1.04 mg kg^{-1}) (Table 2.5).

Table 2. 2. Growing season weather conditions at the plot sites across Manitoba, Saskatchewan, and Alberta.

Site	Year	Mean air temperature (°C)			Total rainfall (mm)		
		June	July	August	June	July	August
				Manitoba			
Melita	2019	17.5	19.8	17.5	115.1	82.5	101.2
	2020	18.3	20.4	19.6	78.6	62.8	42.2
	Normal[a]	**16.8**	**19.6**	**18.9**	**77.7**	**70.4**	**51.6**
Carberry	2019	17.3	19.9	17.4	79.1	68.7	11.7
	2020	18.5	20.4	18.9	104.3	66.7	67.3
	Normal	**16.7**	**18.8**	**18.1**	**80.3**	**83.7**	**61.9**
Arborg	2019	18.1	20.5	18.0	30.8	87.0	24.6
	2020	17.6	20.6	19.0	86.6	61.1	32
	Normal	**15.8**	**18.6**	**17.5**	**80.9**	**70.3**	**68.9**
Kelburn	2019	19.1	20.5	19.1	32.0	122.9	20.4
	2020	19.7	21.5	19.8	197.9	45.8	83.9
	Normal	**17.0**	**19.4**	**18.8**	**99.7**	**91.7**	**72.4**
Roblin	2019	15.8	17.8	15.3	68.8	44.9	7.1
	2020	15.7	18.9	17.2	114.3	80.8	47.9
	Normal	**15.7**	**17.7**	**16.8**	**82.0**	**64.0**	**66**
				Saskatchewan			
Prince Albert	2019	15.8	17.6	15.1	52.3	75.1	19.3
	2020	16.9	19.1	17.6	69.6	34.6	31.4
	Normal	**15.3**	**18.0**	**16.7**	**68.6**	**76.6**	**61.6**
Melfort	2019	15.3	17.9	14.8	87.4	68.8	36.2
	2020	11.9	16.0	18.8	20.0	81.7	48.3
	Normal	**15.9**	**17.5**	**16.8**	**54.3**	**76.7**	**52.4**
[b]Swift Current	2019	15.6	18.2	16.7	180.0	14.0	45.4

	2020	16.6	18.0	19.5	70.6	70.7	9.3
	Normal	**15.4**	**18.5**	**18.2**	**72.8**	**52.6**	**41.5**
Indian Head	2019	16.7	18.2	16.2	80.2	75.5	96.3
	2020	16.8	19.3	19.0	26.1	57.8	33.1
	Normal	**15.8**	**18.2**	**17.4**	**77.4**	**63.8**	**51.2**
[b]Scott	2019	14.9	16.4	14.5	93.9	107.8	20.3
	2020	16.3	17.3	16.2	33.6	123	33.0
	Normal	**15.3**	**17.1**	**16.5**	**61.8**	**72.1**	**45.7**
			Alberta				
Lethbridge	2019	16.2	17.8	17.3	95.6	146.0	71.4
	2020	16.9	18.2	19.2	138.1	24.2	10.3
	Normal	**15.2**	**18.2**	**17.7**	**82.0**	**42.6**	**36.4**
Medicine Hat	2019	17.2	20.3	18.9	69.6	23.9	37.3
	2020	17.9	19.6	20.6	56.0	43.6	12.4
	Normal	**16.7**	**20.0**	**19.3**	**65.4**	**36.3**	**33.8**
Bow Island	2019	16.8	18.8	18.0	38.5	80.4	36.9
	2020	17.6	18.6	19.3	87.3	17.7	10.1
	Normal	**15.8**	**18.8**	**18.7**	**73.0**	**39.7**	**39.8**
Brooks	2019	23.9	26.1	24.7	26.3	46.4	25.8
	2020	17.7	18.9	19.7	187.9	83.2	12.6
	Normal	**15.4**	**17.7**	**17.4**	**64.5**	**44.9**	**34.7**
Vermillion	2019	14.2	15.8	14.0	130.6	98.3	36.3
	2020	16.6	16.7	15.2	44.4	98.6	115.4
	Normal	**14.6**	**17.0**	**15.9**	**68.2**	**72.5**	**61.0**

[a]Long-term normal (30 years; 1981-2010 for June-August) from Environment Canada (ECCC, 2011). Long term normal for Carberry, Kelburn, Melita, Roblin, Vermillion, Brooks were derived from nearest weather station Neepawa Murray 6 Southwest, Glenlea, Pierson Langenburg, Fayban, and Vauxhall North, respectively.

[b]Rainfall data were derived from nearest Environment and Climate Change Canada weather stations.

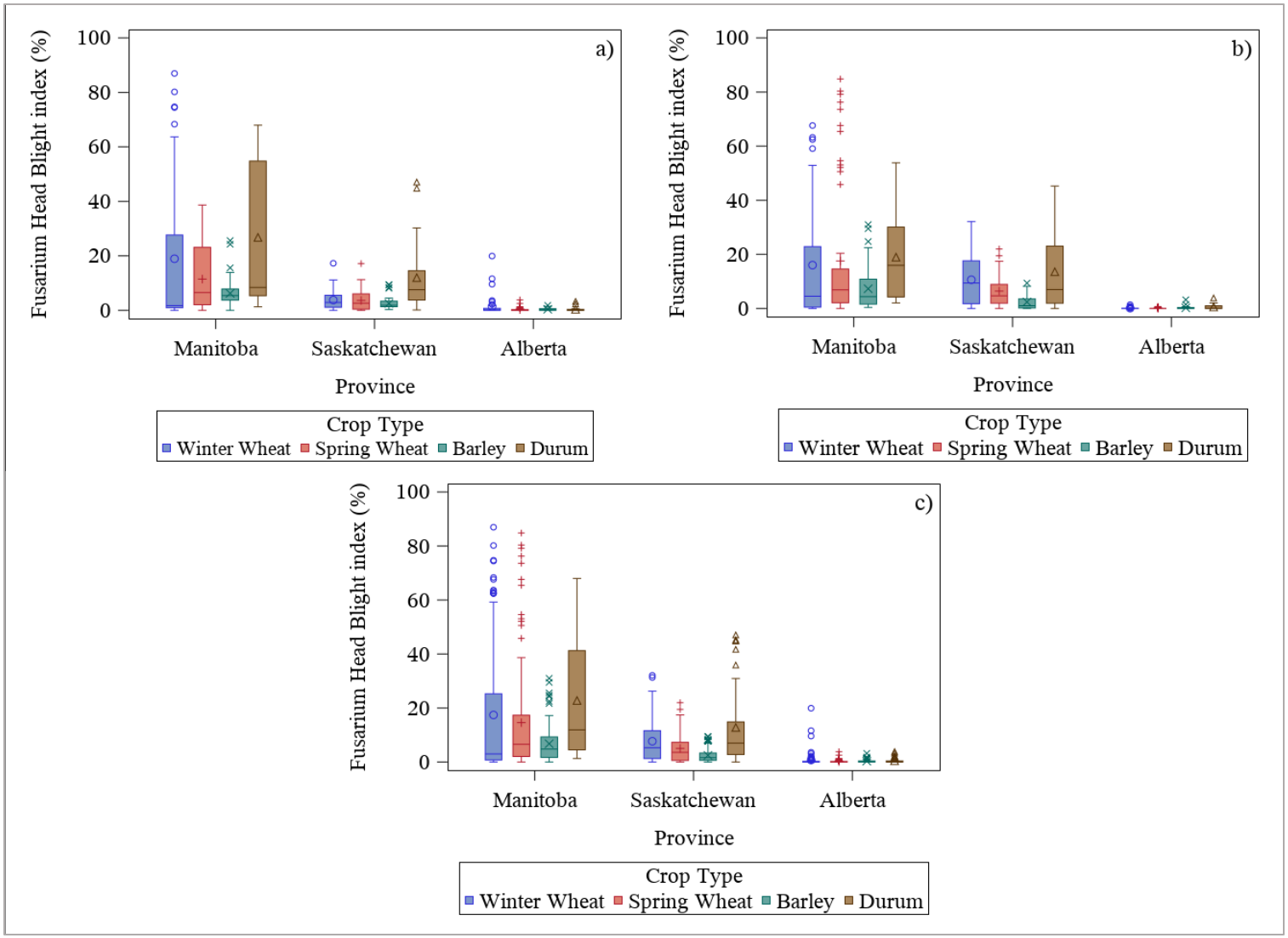

Figure 2. 3. Prevalence of Fusarium Head Blight in the prairie in winter wheat, spring wheat barley, and durum in 2019 (a), 2020 (b), and 2019 and 2020 combined (c).

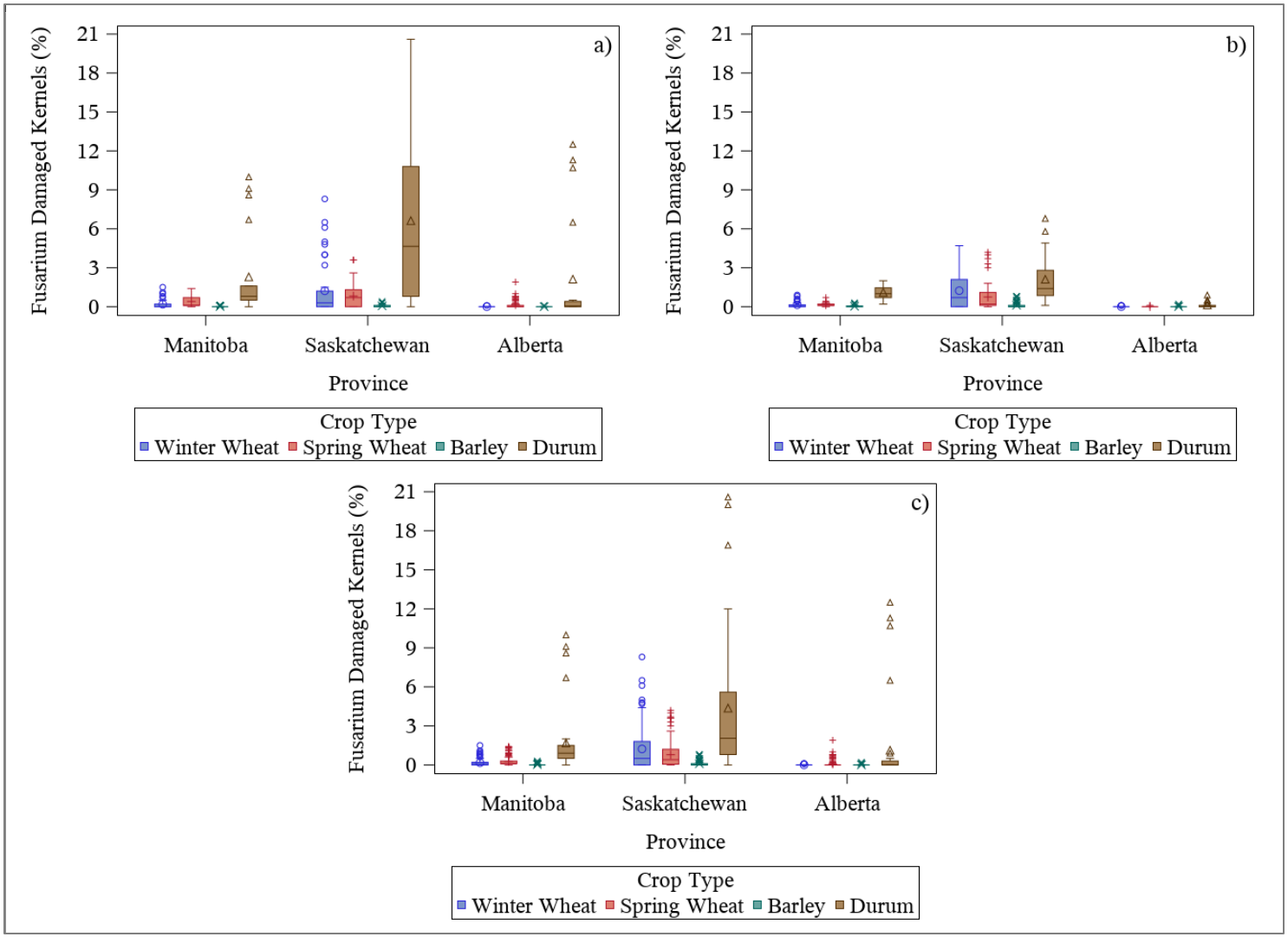

Figure 2. 4. Prevalence of Fusarium damaged kernels in the prairie in winter wheat, spring wheat barley, and durum in 2019 (a) 2020 (b) and 2019 and 2020 combined (c).

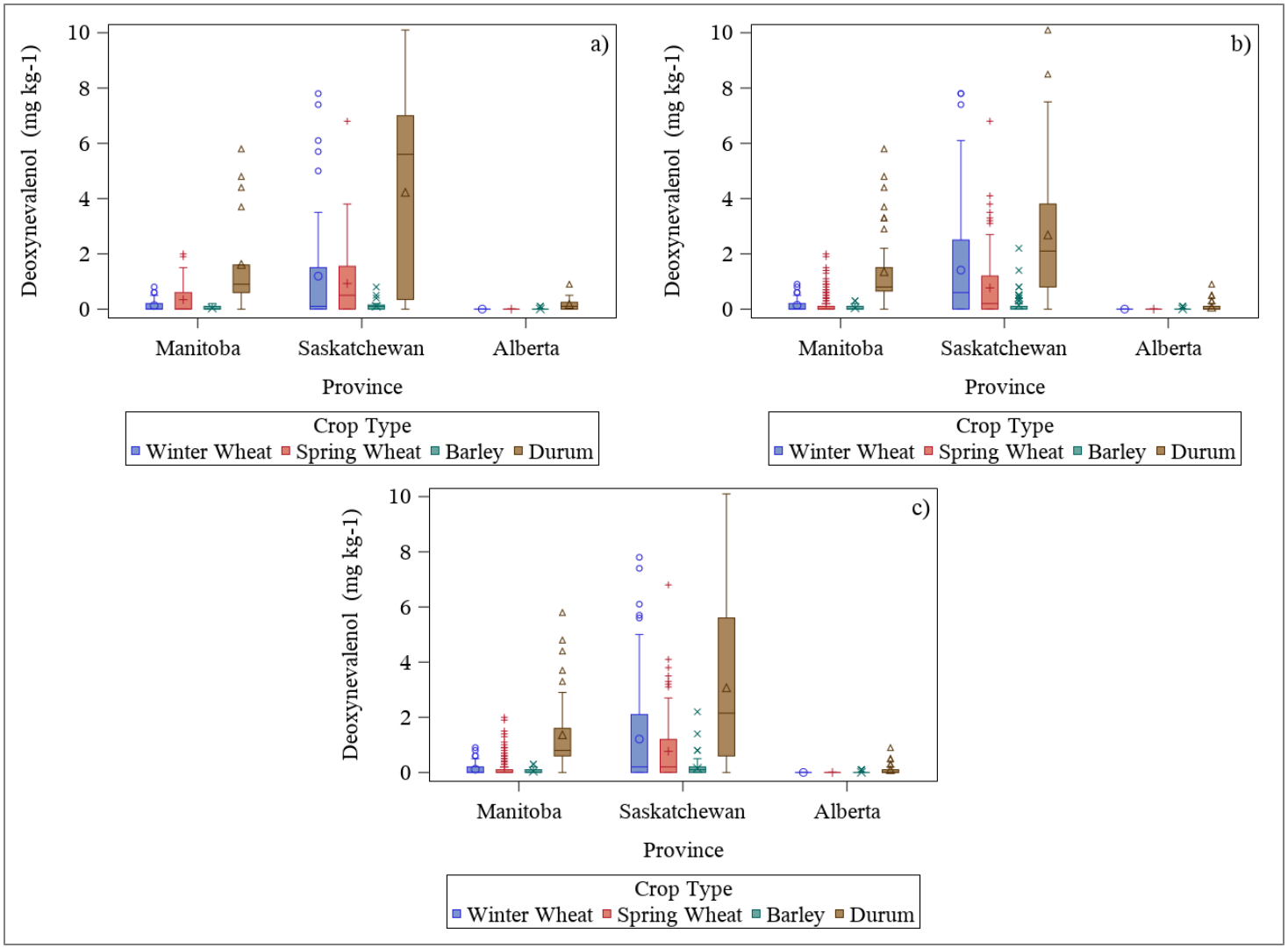

Figure 2. 5. Prevalence of deoxynivalenol in the prairie in winter wheat, spring wheat barley, and durum in 2019 (a), 2020 (b), and 2019 and 2020 combined (c).

Table 2. 3. Correlation between Fusarium Head Blight (FHBi), Fusarium damaged kernels (FDK), deoxynivalenol (DON), and spore concentration (SC) for different crop types in 2019 and 2020 growing season.

	Winter Wheat			Spring Wheat			Barley			Durum		
Variables	FHBi	FDK	DON	FHBi	FDK	DON	FHBi	FDK	DON	FHBi	FDK	DON
						2019						
FDK	-0.082	-		0.133	-		-0.008	-		0.332	-	
p-value[a]	0.352			0.077			0.923			**0.010**		
DON	-0.093	0.963	-	0.039	0.701	-	0.059	0.728	-	0.362	0.673	-
p-value	0.293	**<.0001**		0.608	**<.0001**		0.467	**<.0001**		**0.005**	**<.0001**	
SC	0.258	0.219	0.172	0.307	0.262	0.227	0.348	0.185	-0.101	0.311	0.254	0.281
p-value	**0.025**	0.059	0.139	**0.003**	**0.011**	**0.029**	**0.002**	0.097	0.371	0.09	0.168	0.126
						2020						
FDK	0.161	-		0.036	-		0.029	-		0.316	-	
p-value	**0.045**			0.629			0.703			**0.014**		
DON	0.188	0.868	-	0.015	0.93	-	0.008	0.698	-	0.464	0.862	-
p-value	**0.019**	**<.0001**		0.842	**<.0001**		0.912	**<.0001**		**0.0002**	**<.0001**	
SC	0.156	0.21	0.266	0.583	0.024	-0.02	0.521	0.089	-0.02	0.715	0.597	0.523
p-value	0.128	**0.04**	**0.009**	**<0.0001**	0.808	0.84	**<0.0001**	0.358	0.834	**<.0001**	**0.0001**	**0.0011**
						2019 and 2020						
FDK	0.026	-		0.051	-		0.019	-		0.303	-	
p-value	0.659			0.341			0.729			**0.001**		
DON	0.025	0.919	-	0.007	0.787	-	0.019	0.705	-	0.373	0.705	-
p-value	0.671	**<.0001**		0.901	**<.0001**		0.727	**<.0001**		**<.0001**	**<.0001**	
SC	0.004	0.32	0.356	0.251	0.09	0.075	0.205	0.17	0.095	0.388	0.081	0.189
p-value	0.957	**<.0001**	**<.0001**	**0.003**	0.204	0.29	**0.005**	**0.019**	0.191	**0.001**	0.513	0.125

[a]p-values in bold-face are significant ($p < 0.05$).

Table 2. 4. Correlation between Fusarium Head Blight (FHBi), Fusarium damaged kernels (FDK), and deoxynivalenol (DON) in different crop types and varieties in 2019 and 2020 growing seasons combined.

Variables	FHBi			FDK		
	F. RC1	F. RC2	F. RC3	F. RC1	F. RC2	F. RC3
			Winter Wheat			
FDK	0.05	-0.02	0.13	-	-	-
p-value [a]	0.612	0.827	0.205			
DON	0.02	-0.01	0.14	0.90	0.95	0.84
p-value	0.82	0.89	0.17	**<.0001**	**<.0001**	**<.0001**
			Spring Wheat			
FDK	0.06	0.01	0.07	-	-	-
p-value	0.505	0.892	0.444			
DON	0.03	-0.03	-0.02	0.83	0.78	0.68
p-value	0.762	0.717	0.862	**.0001**	**<.0001**	**<.0001**
			Barley			
FDK	0.03	0.10	-0.06	-	-	-
p-value	0.758	0.275	0.551			
DON	0.04	-0.02	0.02	0.82	0.59	0.66
p-value	0.680	0.852	0.861	**<.0001**	**.0001**	**.0001**

[a] p-values in bold-face are significant ($p < 0.05$).

Table 2. 5. Effect of winter wheat, spring wheat, and barley varietal resistance on Fusarium Head Blight index (FHBi), Fusarium damaged kernels (FDK), and deoxynivalenol (DON).

Treatment	FHBi (%)	FDK (%)	DON (mg kg^{-1})
		Winter Wheat	
FHB Category 1	8.54	0.55	1.78a
FHB Category 2	7.58	0.64	1.87a
FHB Category 3	8.94	0.19	1.23b
Year			
2019	7.93	0.33	1.61
2020	8.76	0.50	1.58
		p-value [a]	
Treatment	0.94	0.91	**<0.0001**
Year	0.80	0.85	0.86
Treatment × Year	0.97	0.99	0.81
		Spring Wheat	
FHB Category 1	6.64	0.52	1.65a
FHB Category 2	5.59	0.31	1.2b
FHB Category 3	6.64	0.29	1.28b
Year			
2019	4.93	0.44	1.51b
2020	7.94	0.29	1.23a
		p-value	
Treatment	0.93	0.95	**<0.0001**
Year	0.25	0.81	**<0.0001**
Treatment × Year	0.99	1.00	0.25
		Barley	
FHB Category 1	3.11	0.04	1.07
FHB Category 2	3.09	0.04	1.04
FHB Category 3	3.75	0.03	1.07
Year			
2019	3.29	0.03	1.04b
2020	3.32	0.05	1.09a
		p-value	
Treatment	0.95	0.99	0.2
Year	0.99	0.92	**0.01**
Treatment × Year	0.97	1.00	0.24

[a]p-values in bold-face are significant ($p < 0.05$). Means within a column followed by different letters are significantly different at $\alpha = 0.05$ according to Tukey's multiple comparison procedure.

2.5 Discussion

2.5.1 Prevalence of FHB

FHBi, FDK, and DON levels reflect weather conditions at the plot sites during the 2019 and 2020 growing seasons. Warm, dry weather during the optimum time for FHB infection was most likely unfavorable at most sites during the two growing seasons. There were observed differences in the occurrence of FHB across crop types. Sensitivity to FHB was higher for durum than barley. Durum wheat is infamous for its high susceptibility to FHB, and breeding for resistance is difficult. Winter wheat was less susceptible to FHB infection than spring wheat, most likely because it flowered early, before most *Fusarium* spores were present in the environment. As demonstrated in this study, the correlation between FHBi and spore concentration was significantly higher in spring wheat in both years than in winter wheat. Barley was the least susceptible, which may be because barley, typically flowers inside the boot before the spike emerges, which protects the flowers from infection with FHB (Alberta Government, 2021). FHB expressed as FHBi was found to be higher in Manitoba than in Saskatchewan and Alberta, confirming previous reports that FHB is moving east to west. However, it was interesting to note that Saskatchewan had higher FDK and DON levels than Manitoba. The causes of this disparity are unknown. Nonetheless, the relationship between FHBi, FDK, and DON has been known to be influenced by different FHB species, management practices, and weather conditions (Dill-Macky and Jones, 2000; Xu et al., 2007; Czembor et al., 2015).

2.5.2 Correlation between Disease Indicators

Winter wheat. DON is the more concerning disease indicator for food and feed safety than FHBi or FDK (Miller et al., 2014). However, it is more expensive to analyze than FHBi and FDK (Zhao

et al., 2016). As a result, producers, modellers, and breeders attempt to use visual estimates of FHBi and FDK to model DON concentration (Shah et al., 2013; Miedaner et al., 2016; Haile et al., 2019). The present study established a positive linear relationship between FDK and DON accumulation, implying that DON accumulation in grain increases as FDK percentage increases. This correlation was true across all crop types and resistance classes. These results are consistent with previous findings. Cowger et al. (2009) found a higher FDK–DON correlation in winter wheat when inoculations were done at 0 and 10 days post anthesis and misting was done at 0 to 20 days post anthesis than when inoculations were done later or longer misting was used.

Spring wheat, durum, and barley. Tittlemier et al. (2020) studied the relationships between FDK and DON in Canada Western Red Spring (CWRS) wheat and Canada Western Amber Durum (CWAD) wheat using 2016 harvest survey samples collected in western Canada. For CWAD and the majority of CWRS, they observed a positive linear relationship between FDK and DON. He et al. (2015) evaluated 402 barley advanced breeding lines from Alberta, Canada, using five cultivars released in Alberta with known FHB resistance as controls under Mexican conditions. They found a significant correlation between FDK and DON, with correlation coefficients ranging between 0.37 and 0.45 (He et al., 2015). However, correlation coefficients between FHBi and DON were greater than those between FHBi and FDK and FDK and DON (He et al., 2015). This contrasted with our finding where no significant correlation between FHBi and DON or FHBi and FDK was found. The discrepancy between these results could be explained by the fact that they inoculated barley with FHB several times after heading, whereas no inoculation was performed in our study. Previous studies have also found no correlation between FHBi and DON concentrations under field conditions (Brunner et al., 2009; Landschoot et al., 2012; Góral et al., 2018). A variety of reasons may explain the poor correlation between FHBi and DON, including i) blowing off heavily

infected FDK during harvesting, which may lower DON concentrations by reducing the proportion of contaminated FDK that contains DON, ii) unintentional bias in the field assessment of FHB because the visual symptoms of FHB were scored in this study by a variety of individuals, and iii) although less aggressive *Fusarium* strains such as *Fusarium avenaceum*, *Fusarium culmorum*, *Fusarium poae*, and *Microdochium nivale* have been known to cause the same symptoms as *Fusarium graminearum*, they do not produce the same toxin levels (Tan et al., 2020).

2.5.3 Cultivar Effect on Disease Indicators

Several studies have shown that a cultivar's ability to resist FHB depends on its environment (Dill-Macky and Jones, 2000; Xu et al., 2007; Czembor et al., 2015). In general, FHB intensity was very low in 2019 and 2020, and cultivars performed similarly across all crop types. Other studies have found no significant differences between cultivars under low FHB disease pressure (Ye et al., 2017). Our results, however, indicate that the moderately resistant wheat and barley varieties accumulated significantly less DON than the susceptible and intermediate varieties. The significant DON reductions observed in the grains of moderately resistant varieties in this study concur with previous findings. Generally, cultivars with type II resistance have been found to have lower DON concentrations in the grain, suggesting that cultivars with moderate resistance often reduce mycotoxin concentrations (Tamburic-Ilincic et al., 2007; Liu et al., 2013; Tucker et al., 2019). Previous research has established that wheat cultivars susceptible to FHB accumulate more DON than resistant cultivars. For example, Cowger et al. (2009) examined the effects of post-anthesis moisture (mist) on DON accumulation in winter wheat grown in North Carolina, USA. USG 3592, a susceptible cultivar, accumulated more DON than cultivars with moderate resistance. Similarly, Ye et al. (2017) conducted field trials at seven locations across the Canadian prairies to determine the genetic and management effects of FHB in wheat. Carberry and Emerson (spring

wheat and winter wheat, respectively) were superior to susceptible cultivars Harvest and CDC Falcon (spring wheat and winter wheat, respectively) in reducing FDK and DON concentration under conditions of high *Fusarium* pressure.

2.6 Conclusion

The correlation between FHB disease indicators and SC in wheat and barley under natural field conditions was evaluated in this study. The lack of correlation between FHB and DON in this study under field conditions in western Canada is concerning. In western Canada, existing weather-based models developed in the USA many years ago predict FHB epidemics with a field severity or FHBi greater than 10%, which is a disease severity level strongly linked to FHB yield losses and generally linked to high levels of DON in harvested grain (De Wolf et al., 2003). However, findings from this study indicate a poor relationship between FHBi and DON. In such cases, it is recommended that FHB modelling be based solely on a single and specific disease indicator (FHBi, FDK, or DON model). The Canadian Grain Commission employs FDK as a grading factor and to estimate DON levels in the grain. It is therefore suggested that the FDK-DON relationship be continuously monitored. This study found no differences in FHBi and FDK levels between the varieties under low disease pressure in all crop types. However, there were varietal differences in DON concentrations. These results emphasize the importance of selecting resistant varieties to reduce the costs associated with the downgrading of grain due to high DON levels during marketing. Additionally, breeders can use this information to enhance FHB resistance in commercial cultivars. The data in this study were limited to two growing seasons and thus may not reflect all disease-weather conditions that could influence variety performance and correlation between FHB disease indicators. Additional data from high disease pressure years may be required

to understand further the relationship between cultivar reaction and FHB disease indicators in western Canada.

2.7 References

ACIS. 2021. Alberta Climate Service -Weather and climate resources. [Online] Available at https://www.alberta.ca/acis-find-current-weather-data.aspx (accessed 16 November 2021).

Alberta Government. 2015. Economic cost of *Fusarium*: farm-level and regional economic impact of *Fusarium* in Alberta [2015]- Open Government. [Online] Available at https://open.alberta.ca/dataset/economic-cost-of-*Fusarium* -farm-level-and-regional-economic-impact-of-*Fusarium*-in-alberta/resource/03905e0b-2c3c-447a-9d5e-383492afcc68 (accessed 5 January 2022).

Alberta Government. 2021. Fusarium Head Blight – Best management practices. [Online] Available at https://www.alberta.ca/Fusarium-head-blight-best-management-practices.aspx (accessed 16 January 2022).

Brunner, K., M.P. Kovalsky Paris, G. Paolino, H. Bürstmayr, M. Lemmens, et al. 2009. A reference-gene-based quantitative PCR method as a tool to determine *Fusarium* resistance in wheat. Anal. Bioanal. Chem. **395**: 1385–1394. doi: 10.1007/s00216-009-3083-3.

Brustolin, R., S.M. Zoldan, E.M. Reis, T. Zanatta, and M. Carmona. 2013. Weather requirements and rain forecast to time fungicide application for Fusarium Head Blight control in wheat. Summa Phytopathol. **39**: 248–251. doi: 10.1590/S0100-54052013000400003.

Canadian Grain Commission. 2019. Official Grain Grading Guide. [Online] Available at https://www.grainscanada.gc.ca/en/grain-quality/official-grain-grading-guide/04-wheat/grading-factors.html (accessed 24 June 2020). (accessed 24 June 2020).

Clear, R.M., J.R. Tucker, D. Gaba, S.K. Patrick, S.-J. Lee, et al. 2013. Deoxynivalenol levels and chemotype frequency in barley cultivars inoculated with two chemotypes of *Fusarium graminearum*. Can. J. Plant Pathol. **35**: 37–45. doi: 10.1080/07060661.2012.751622.

Cowger, C., J. Patton-Özkurt, G. Brown-Guedira, and L. Perugini. 2009. Post-anthesis moisture increased Fusarium Head Blight and deoxynivalenol levels in North Carolina winter wheat. Phytopathology **99**: 320–327. doi: 10.1094/Phyto-99-4-0320.

Czembor, E., Ł. Stępień, and A. Waśkiewicz. 2015. Effect of environmental factors on *Fusarium* species and associated mycotoxins in maize grain grown in Poland (K.-H. Han, editor). PLOS ONE **10**: e0133644. doi: 10.1371/journal.pone.0133644.

De Wolf, E.D., L.V. Madden, and P.E. Lipps. 2003. Risk assessment models for wheat Fusarium Head Blight epidemics based on within-season weather data. Phytopathology **93**: 428–435. doi: 10.1094/Phyto.2003.93.4.428.

Dexter, J.E., R.M. Clear, and K.R. Preston. 1996. Fusarium Head Blight: Effect on the milling and baking of some Canadian wheats. Cereal Chem. **73:** 695–701.

Dill-Macky, R. 2008. Cultural control practices for Fusarium Head Blight: Problems and solutions. Cereal Res. Commun. **36**: 653–657. doi: 10.1556/CRC.36.2008.Suppl. B.55.

Dill-Macky, R., and R.K. Jones. 2000. The effect of previous crop residues and tillage on Fusarium Head Blight of wheat. Plant Dis. **84**: 71–76. doi: 10.1094/PDIS.2000.84.1.71.

ECCC. 2021. Canadian Climate Normals - Climate - Environment and Climate Change Canada. [Online] Available at https://climate.weather.gc.ca/climate_normals/index_e.html#1981 (accessed 1 December 2021).

Fowler, D.B. 2011. Winter wheat production in western Canada - Opportunities and obstacles. Proc. 2011 Soils Crops Workshop Mar 15-16, 2011, University of Saskatchewan, Saskatoon, [Online] Available at https://www.researchgate.net/publication/320933736_Winter_Wheat_Production_in_Western_Canada-Opportunities_and_Obstacles.

Góral, T., H. Wiśniewska, P. Ochodzki, L. Nielsen, D. Walentyn-Góral, et al. 2018. Relationship between Fusarium Head Blight, Kernel Damage, concentration of *Fusarium* biomass, and *Fusarium* toxins in grain of winter wheat inoculated with *Fusarium culmorum*. Toxins **11**: 2. doi: 10.3390/toxins11010002.

Góral, T., H. Wiśniewska, P. Ochodzki, A. Twardawska, and D. Walentyn-Góral. 2020. Resistance to Fusarium Head Blight, Kernel Damage and concentration of *Fusarium* mycotoxins in grain of winter triticale (x Triticosecale Wittmack) Lines. Agronomy 2021, 11(1), 16; https://doi.org/10.3390/agronomy11010016.

Guo, X. 2008. Development of models to predict Fusarium Head Blight disease and deoxynivalenol in wheat, and genetic causes for chemotype diversity and shifting of *Fusarium graminearum* in Manitoba. PhD Thesis, University of Manitoba [Online] Available at https://mspace.lib.umanitoba.ca/xmlui/handle/1993/21115 (accessed 16 January 2022).

Haile, J.K., A. N'Diaye, S. Walkowiak, K.T. Nilsen, J.M. Clarke, et al. 2019. Fusarium Head Blight in durum wheat: Recent status, breeding directions, and future research prospects. Phytopathology **109**: 1664–1675. doi: 10.1094/Phyto-03-19-0095-RVW.

He, X., M. Osman, J. Helm, F. Capettini, and P.K. Singh. 2015. Evaluation of Canadian barley breeding lines for Fusarium Head Blight resistance. Can. J. Plant Sci. **95:** 923–929. doi: 10.4141/cjps-2015-062.

Kubo, K., N. Kawada, T. Nakajima, K. Hirayae, and M. Fujita. 2014. Field evaluation of resistance to kernel infection and mycotoxin accumulation caused by Fusarium Head

Blight in western Japanese wheat (Triticum aestivum L.) cultivars. Euphytica **200**: 81–93. doi: 10.1007/s10681-014-1148-7.

Landschoot, S., W. Waegeman, K. Audenaert, J. Vandepitte, J.M. Baetens, et al. 2012. An empirical analysis of explanatory variables affecting Fusarium Head Blight infection and deoxynivalenol content in wheat. J. Plant Pathol. **94**: 135–147.

Liu, S., C.A. Griffey, M.D. Hall, A.L. McKendry, J. Chen, et al. 2013. Molecular characterization of field resistance to Fusarium Head Blight in two US soft red winter wheat cultivars. TAG Theor. Appl. Genet. Theor. Angew. Genet. **126**: 2485–2498. doi: 10.1007/s00122-013-2149-y.

MARD. 2021. Manitoba Ag Weather Program- Manitoba Agriculture and Resource Development. Prov. Manit. - Agric. [Online] Available at https://www.gov.mb.ca/agriculture/ (accessed 17 November 2021).

McCallum, B., and A. Tekauz. 2002. Influence of inoculation method and growth stage on Fusarium Head Blight in barley. J. Plant Path. **24:** 77-80 doi: 10.1080/07060660109506976.

Meier, U., H. Bleiholder, L. Buhr, C. Feller, H. Hack, et al. 2009. The BBCH system to coding the phenological growth stages of plants – history and publications –. J. Für Kult. **61**: 41–52. doi: 10.5073/JfK.2009.02.01.

Miedaner, T., R. Kalih, M.S. Großmann, and H.P. Maurer. 2016. Correlation between Fusarium Head Blight severity and DON content in triticale as revealed by phenotypic and molecular data (H. Bürstmayr, editor). Plant Breed. **135:** 31–37. doi: 10.1111/pbr.12327.

Miller, J.D., A.W. Schaafsma, D. Bhatnagar, G. Bondy, I. Carbone, et al. 2014. Mycotoxins that affect the North American agri-food sector: state of the art and directions for the future. World Mycotoxin J. **7**: 63–82. doi: 10.3920/WMJ2013.1624.

Rossi, V., S. Giosuè, E. Pattori, F. Spanna, and A. Del Vecchio. 2003. A model estimating the risk of Fusarium Head Blight on wheat. EPPO Bull. **33**: 421–425. doi: 10.1111/j.1365-2338.2003.00667. x.

Sask Seed Guide. 2019. Varieties of Grain Crops. [Online] Available at https%3A%2F%2Fpublications.saskatchewan.ca%2Fapi%2Fv1%2Fproducts%2F83696%2Fformats%2F96889%2Fdownload&usg=AOvVaw39lg7v2hNJWnmm_oSgJAVX (accessed 20 June 2020).

Shah, D.A., J.E. Molineros, P.A. Paul, K.T. Willyerd, L.V. Madden and E.D. De Wolf. 2013. Predicting Fusarium Head Blight epidemics with weather-driven pre- and post-anthesis logistic regression models. Phytopathology **103**: 906–919. doi: 10.1094/Phyto-11-12-0304-R.

Shah, D.A., E.D. De Wolf, P.A. Paul, and L. V. Madden. 2014. Predicting Fusarium Head Blight epidemics with boosted regression trees. Phytopathology **104**: 702–714. doi: 10.1094/Phyto-10-13-0273-R.

Stull, R.B. 2000. Meteorology for Scientists and Engineers. 2nd Edition, Brooks/Cole Thomson Learning, Pacific Grove.

Tamburic-Ilincic, L., A.W. Schaafsma, and D.E. Falk. 2007. Indirect selection for lower deoxynivalenol (DON) content in grain in a winter wheat population. Can. J. Plant Sci. **87**: 931–936. doi: 10.4141/P06-024.

Tan, J., M. Ameye, S. Landschoot, N. De Zutter, S. De Saeger, et al. 2020. At the scene of the crime: New insights into the role of weakly pathogenic members of the Fusarium Head Blight disease complex. Mol. Plant Pathol. **21**: 1559–1572. doi: 10.1111/mpp.12996.

Tittlemier, S.A., J. Arsiuta, U. Mohammad, C. Hainrich, K. Bowler, et al. 2020. Variable relationships between *Fusarium* damage and deoxynivalenol concentrations in wheat in western Canada in 2016. Can. J. Plant Pathol. **42**: 41–51. doi: 10.1080/07060661.2019.1620861.

Tucker, J.R., A. Badea, R. Blagden, K. Pleskach, S.A. Tittlemier, et al. 2019. Deoxynivalenol-3-glucoside content is highly associated with deoxynivalenol levels in two-row barley genotypes of importance to Canadian barley breeding programs. Toxins **11**: 319. doi: 10.3390/toxins11060319.

Wilson, W., B. Dahl, and W. Nganje. 2018. Economic costs of Fusarium Head Blight, scab and deoxynivalenol. World Mycotoxin J. **11**: 291–302. doi: 10.3920/WMJ2017.2204.

Xu, X., P. Nicholson, and A. Ritieni. 2007. Effects of fungal interactions among Fusarium Head Blight pathogens on disease development and mycotoxin accumulation. Int. J. Food Microbiol. **119**: 67–71. doi: 10.1016/j.ijfoodmicro.2007.07.027.

Ye, Z., A.L. Brûlé-Babel, R.J. Graf, R. Mohr, and B.L. Beres. 2017. The role of genetics, growth habit, and cultural practices in the mitigation of Fusarium Head Blight. Can. J. Plant Sci. doi: 10.1139/cjps-2016-0336.

Zhao, X., R. Li, C. Zhou, J. Zhang, C. He, et al. 2016. Separation and purification of deoxynivalenol (DON) mycotoxin from wheat culture using a simple two-step silica gel column chromatography. J. Integr. Agric. **15**: 694–701. doi: 10.1016/S2095-3119(15)61098-X.

3. DEVELOPING RISK MODELS TO MITIGATE FUSARIUM HEAD BLIGHT IN WESTERN CANADIAN CEREAL PRODUCTION

3.1 Abstract

Predicting the occurrence of Fusarium Head Blight (FHB) disease in cereal crops before flowering is critical for determining the need for and timing of fungicide sprays. Existing models for predicting FHB risk that were developed many years ago may no longer be applicable to the current *Fusarium* species complex that has evolved in Canada. Therefore, the objective of this study was to develop weather-based risk models for predicting FHB index (FHBi), Fusarium damaged kernels (FDK), and deoxynivalenol (DON) in spring wheat, winter wheat, barley, and durum across three Canadian prairie provinces. Agronomic and weather data collected from 15 small-plot research sites in western Canada in 2019 and 2020 were used to develop weather-based models for forecasting *Fusarium* epidemics. The same data were used to classify epidemic at 5% FHBi (all crops), 1 mg kg^{-1} DON (all crops), or 0.2, 0.3, 0.8, and 2% FDK thresholds for barley, spring wheat, winter wheat, and durum, respectively. Kendall correlation and stepwise logistic regression analyses identified suitable combinations of temperature, relative humidity (RH), rainfall, and solar radiation at 4, 7, 10, 14 days pre-anthesis, and 3 days pre-anthesis to 3 days post-anthesis for predicting FHB risk. The FHBi models used combinations of RH, temperature, and rainfall weather variables across crop types, while RH alone was frequently chosen in both FDK and DON models. The prediction accuracy of the models ranged from 72 to 82, 58 to 88, and 77 to 83% for FHBi, FDK, and DON, respectively. FHB pressure was low in both 2019 and 2020, most likely due to drier than normal weather conditions unfavorable for the disease. The models will be used to power an interactive, online digital viewer that will provide early warning of potential FHBi, FDK, and DON epidemics in prairie cereal crops.

3.2 Introduction

Wheat and barley are two of the most economically important hosts affected by FHB worldwide (Fowler, 2011). *Fusarium graminearum, Fusarium culmorum, Fusarium poacea*, and *Fusarium avenaceum* are among the species that cause FHB infection (Birr et al., 2020). However, *Fusarium graminearum* is the present major species of concern in western Canada (Fowler, 2011). Cool and moist conditions favor the development of FHB, and if left uncontrolled, it can result in partially or entirely bleached spikelets, which are often not viable (Gilbert and Tekauz, 2011). Bleached spikelets also contain shrivelled kernels that appear chalky white or pink discoloration and are classified as FDK (Jin et al., 2013). Since FDK grains are smaller and have less weight than healthy kernels, some are blown through the combine, resulting in yield loss (Góral et al., 2021). In addition to reduced yield, FHB infection often contributes to DON contamination, a mycotoxin toxic to humans and animals (Xu et al., 2013). Mycotoxin regulations have been established in many countries to ensure food and feed safety. In Canada, a DON limit of 2 mg kg^{-1} for domestic soft wheat and 1 mg kg^{-1} for uncleaned soft wheat for children has been set (CFIA, 2017). Livestock grain should not exceed 5 mg kg^{-1} DON for animal feed, while grain for swine, calves, and dairy cattle should not surpass 1 mg kg^{-1} DON (CFIA, 2017).

The occurrence of FHB epidemics has increased in recent decades, possibly due to the widespread use of conservation tillage and no-till farming practices (Haile et al., 2019). These practices aim to prevent topsoil erosion by retaining crop residues from previous seasons (Dill-Macky and Jones, 2000). However, retaining infected residues increases inoculum availability for *Fusarium graminearum* (Dill-Macky and Jones, 2000). The incidence and severity of FHB have also increased due to monoculture and the effects of climate variation, thus forcing growers to use excessive fungicides (Del Ponte et al., 2005). As a result, grain revenue is drastically impacted

with lower yields, lower quality, and DON presence (McCallum and DePauw, 2008). To illustrate the magnitude of the problem, approximately 65% of common spring wheat and 36% of durum were downgraded due to FHB in 2016 in Saskatchewan, Canada, costing producers an estimated $1 billion in lost revenue (Canadian Grain Commission, 2019; Haile et al., 2019).

Reducing FHB damage is desirable to maintain producer profitability, food and feed safety, and export integrity (Haile et al., 2019; Hooker et al., 2002). Breeding for FHB resistance has the potential to provide adequate control (He et al., 2015), and it is also an ecological and economical technique for successfully managing an epidemic (Chen, 2019). Enhanced cultivar resistance has become one of the world's most important goals for wheat breeding. However, the quantitative complexity of resistance and technical difficulty in screening cultivars in inoculated experiments make breeding against FHB challenging (McMullen et al., 2012). In FHB epidemic years, fungicide application dramatically reduces the severity of the disease (Musa et al., 2007). However, when weather is not favorable for FHB occurrence, producers could use FHB forecasts models to reduce unnecessary fungicide applications, thereby decreasing the financial and environmental costs associated with traditional calendar-based spray programs. Several FHB and DON forecasting models for wheat and barley have been developed around the world, including in eastern Canada (Hooker et al., 2002; Schaafsma and Hooker, 2007), the United States (De Wolf et al., 2003; Shah et al., 2013), Argentina (Moschini et al., 2001) and Brazil (Del Ponte et al., 2005). FHB is suitable for modelling due to its narrow window of infection during flowering and environmental dependence; thus, all these models use different statistical approaches to relate the biology of the fungus to environmental conditions (Rossi et al., 2003).

FHB prediction models are typically location-specific due to differences in wheat varieties and regions in fungal populations, resulting in differences in aggressiveness and mycotoxin production and thus require adjustment when used outside of the region or country in which they are used or they were developed (Cowger et al., 2020). Different FHB index models have been adopted from the USA in the prairies and use different risk assessment factors. This can be concerning, especially for producers near provincial borders, when the FHB risk model forecasts high risk near their location in one province but low FHB risk near their location in the other province. A standardized risk model across all three provinces can provide more meaningful information for producers and the agriculture industry. Furthermore, in recent years, changes in the *Fusarium* species complex have been reported in Canada, with the more toxic 3-acetyldeoxynivalenol (3-ADON) chemotypes replacing the traditional 15-acetyldeoxynivaleol (15-ADON) (Schmale et al., 2011; Crippin, 2019; Cowger et al., 2020). This suggests that current FHBi models are likely no longer representative of FHB in the prairies. Currently, western Canada has no system for estimating the risk of FDK and mycotoxins from FHB in wheat and barley. This research project aimed to develop weather-based prediction models for forecasting FHBi, FDK, and DON risk in winter wheat, spring wheat, barley, and durum with different FHB resistant categories in western Canada.

3.3 Materials and Methods

3.3.1 Site

The site description for this study is given in Chapter 2. In brief, small-plot research trials with five plot sites per province (15 sites) were conducted in the 2019 and 2020 growing seasons in Manitoba, Saskatchewan, and Alberta (Figure 2.1). The plot sites were located in fields with at least two years of FHB data collected through provincial and federal government annual FHB

surveys. These 15 sites were geographically distributed across western Canada to maximize the likelihood of each site experiencing various growing-season weather conditions and FHB occurrence. Each plot measured approximately 4 m in length and 2 m in width with at least 8 rows.

3.3.2 Experimental Design

The experimental design was a randomized complete block design (RCBD) with four replications (blocks) for separate side by side winter wheat, spring wheat, barley, and durum experiments (Figure 2.2). Treatments included three different varieties of spring wheat, winter wheat, and barley representing three types of FHB resistance categories (F. RC) (Table 2.1). FHB resistance categories included F. RC1 (susceptible or moderately susceptible varieties), F. RC2 (intermediate varieties), and F. RC3 (moderately resistant or resistant varieties), depending on the crop type. As all durum wheat varieties are FHB susceptible or moderately susceptible, only one durum variety was grown.

3.3.3 Planting and Crop Growth Stages

Three winter wheat varieties representing 3 levels of FHB resistance (Table 3.1) were planted in the fall of 2018 and 2019, while spring cereals (spring wheat, barley, and durum) were sown in spring 2019 and 2020 according to the best management practices at each location. Standard agronomic practices such as fertilizer application, seeding depth, row spacing, and herbicide application were followed at each site. However, no fungicides were applied. Planting, maturity, and harvesting dates for each crop were recorded. Crop growth was regularly monitored during the growing season, and the date when each cultivar reached BBCH stage 59 (main stem spikes completely emerged) was noted; thereafter, BBCH growth stages were recorded weekly until BBCH 80 (Shah et al., 2013). In cases where the 50% anthesis and heading date in wheat and

barley, respectively, were not directly observed, these dates were estimated using thermal models described in Appendix 5.

3.3.4 Meteorological Data

Watchdog® portable weather stations (Spectrum Technologies 2000 Series, Thayer Case, IL, USA) were used to record growing-season weather data. At each site, one weather station was mounted on a solid post at an average height of 1.82 m within 10 m of the plots. Weather data collected included air temperature (°C), relative humidity (RH), rainfall (mm), solar radiation (W m^{-2}), and wind speed (km h^{-1}) on an hourly basis. The weather stations were installed about a month after spring crop seeding. Before deploying the weather stations, pre-season calibration was conducted by running the weather stations side by side. The weather stations were calibrated in cases where the rain sensor, under a standardized sensor test, recorded rainfall values outside those recommended by Watchdog®, 2010. Briefly, 84 ml of water (equivalent to 10 tips of the tipping spoon) was slowly poured into the bucket. When the readings were lower than expected, tipping bucket adjustment screws were raised by a quarter turn, and 84 ml of water was poured through the bucket to determine if further adjustment was required. The opposite was true when rainfall measurements were overestimated.

3.3.5 Spore Traps

For FHB disease to occur, a susceptible host plant, favorable weather conditions, and the presence of *Fusarium* spores are required. To confirm the presence of *Fusarium* spores at each site, *Fusarium* spores were collected using Guo's (2008) method with minor modifications. Two adhesive spore traps were placed at two central locations inside the plot area just before the beginning of the anthesis (BBCH 59) to capture the FHB spores. The spore traps consisted of a

trap head and a supporting rod. A rectangular plastic foam with four spore collection surfaces (6 mm x 90 mm each) was used as the trap head. The spore head surfaces were covered with a base tape, followed by Melinex double-sided tape coated with a thin layer of petroleum jelly to adhere spores. The spore traps were replaced weekly for four weeks (8 spore traps in total). Following the collection of spores, a small piece measuring 5 mm x 19 mm was cut from the Melinex tape on one side of the trap head and fixed to a glass slide. *Fusarium* spores were determined under a compound microscope (400x) to confirm the presence of the inoculum in the environment.

3.3.6 Disease Indicators

3.3.6.1 Fusarium Head Blight Index

Fusarium Head Blight incidence (percentage of infected heads) was assessed 18 to 21 days after 50% anthesis (BBCH 65); between the early milk stage (BBCH 73) and the soft dough stage (BBCH 85). FHB incidence and FHB severity (mean percentage of blighted spikelets per infected head) were determined by scoring five spikes at ten random locations (total 50 spikes) within a plot. The FHB index (FHBi) was then determined according to Shah et al. (2014) using the following formula:

$$FHBi = (FHBincidence \times FHBseverity)/100$$

Observations of FHBi were further classified into two groups of either epidemic (=1) or non-epidemic (=0) using 5 and 10% FHBi thresholds to define an epidemic. Thus, for example, in the latter case, observations of FHBi ≥ 10% were regarded as an epidemic and FHBi < 10% as non-epidemics. Using the 5 and 10% FHBi disease severity thresholds is in line with previous regression models developed in the USA (De Wolf et al., 2003; Shah et al., 2013) and eastern Canada (Giroux et al., 2016).

3.3.6.2 Fusarium damaged kernels and Deoxynivalenol

Grain samples (1 kg plot^{-1}) were collected at harvest for official grading and DON analysis. During combining, grain samples were collected with a level of dockage that would be similar to that from producer fields in order to retain lightweight FDK. Grain grading, FDK determination, and DON analysis were conducted by a commercial laboratory (Intertek, Canada) following the procedures outlined in the Canadian Grain Commission's Official Grain Grading Guide (Canadian Grain Commission, 2019). Briefly, samples were divided into a representative portion using a Boerner-type divider. The samples were then visually divided into two groups of healthy and infected kernels with different damage levels. A 10-power magnifying lens was used to confirm the presence of a chalk-like appearance or pinkish mold. FDK was then calculated as a percentage of the number of grains with FDK divided by the total number of grains in a sample. For modelling purposes, samples were then classified into epidemic and non-epidemic categories using 0.2, 0.3, 0.8, and 1.5% thresholds for barley, spring wheat, winter wheat, and durum, respectively. These thresholds reflect the maximum level allowed in the number one grade for each crop and represent an economic cut-off value that would justify the application of fungicides to prevent loss of revenue as a result of downgrading. To determine DON, 50 g subsamples were ground and analyzed using high sensitivity (HS) Neogen ELISA 5/5 Vomitoxin kits with a DON detection limit of 0.5 mg kg^{-1} (Neogen Corporation, 2013). For modelling, DON thresholds of 1 and 2 mg kg^{-1} were used to distinguish between epidemic and non-epidemic cases, and these thresholds correspond to values that result in wheat downgrading during marketing as set by the Canadian grain commission (Canadian Grain Commission, 2019).

3.3.7 Logistic Regression Analysis

3.3.7.1 Selection of Predictor Variables

Predictor variables of potential value were derived using information from previous research (De Wolf et al., 2003; Hooker et al., 2002). These variables were derived from summations and averages of daily and hourly data as well as the duration (hours) of specified critical conditions during five different time periods (-4DMA, -7DMA, -10DMA, -14DMA, and ±3DMA, representing 4, 7, 10 and 14 days pre-anthesis and from 3 days pre-anthesis to 3 days post-anthesis). In total, 84 weather variables were compiled using the original hourly temperature, RH, and rainfall data (Table A3.1.1). Kendall's Tau non-parametric correlation analysis was performed to evaluate the relationship between weather variables and the binary FHB damage indicators using the PROC CORR in SAS 9.4 (SAS Institute, 2021). Only variables with a correlation coefficient greater or equal to 0.21 and ($P < 0.05$) were considered for model development. When variables providing similar information had only slight differences in correlation results, both variables were retained and tested further in model development.

Additionally, multicollinearity was determined by examining the variance inflation factor (VIF), which quantifies the inflation of parameter estimate variances due to multicollinearity possibly caused by the correlated predictors and tolerance (the inverse of VIF). Variables with VIF > 10 and tolerance < 0.2 indicated multicollinearity; therefore were discarded from the selection (Tabachnick et al., 2019).

3.3.7.2 Model Development and Evaluation

Multiple logistic regression with stepwise selection (PROC LOGISTICS; SAS Institute, 2021) was used to develop models that predict the occurrence of FHB epidemics (=1) and non-occurrence of FHB epidemics (=0) using weather predictor variables. Logistic regression is best suited for

predicting the presence or absence of an outcome based on a set of predictor variables. Similar to the more common linear regression, logistic regression aims to build the best fitting, parsimonious, and biologically rational model (Del Ponte et al., 2005). The stepwise selection was preferred over the other selection because variables must meet both the entry and retention criterion, rendering it a more stringent procedure (Hosmer et al., 2013). Thus, models were developed using entry and retention criteria probability thresholds of 0.3 and 0.5, respectively.

The accuracy and model fit of the developed models were assessed using a variety of metrics. The sensitivity (percentage of epidemic cases correctly classified) and specificity (percentage of non-epidemic cases correctly classified) of each model were determined from the analysis results. The overall accuracy of each model was calculated as (TPP+TNP)/2, where TPP is the true positive proportion, which is the proportion of correctly predicted epidemic cases with a disease response to weather variables, and TNP is the proportion of correctly classified cases with a low or no infection response to weather variables (Bondalapati et al., 2012; Giroux et al., 2016). These parameters, however, may be influenced by the proportion of cases that fall into each binary response variable category. The Youden's index (J) is a well-known receiver operating characteristic (ROC) curve measurement used to assess models' accuracy in many statistical and medical applications (Fawcett, 2006). Youden's index was calculated as J = TPP - FPP, where J is the Youden's index, TPP is the true positive proportion, and FPP is the false-positive proportion (Giroux et al., 2016). A Youden's index value of 1 indicates a perfect model (Martínez-Camblor and Pardo-Fernández, 2019). The models' optimal probability cut-off value (where sensitivity and specificity are maximized and balanced) was identified when Youden's index was at its maximum.

The area under the ROC curve helps estimate models' ability to correctly classify cases as epidemic or non-epidemic events for a number of potential posterior probability thresholds (Fawcett, 2006). Like Youden's index, a perfect model would have an area under the ROC curve (AUC) equivalent to 1. When the trapezoidal method is used to calculate the AUC, the Mann-Whitney U-statistic from which standard errors can be determined, and the AUC hypothesis that the discriminatory ability of the model is not different from 0.5 can be tested. This test compares the model's performance to random predictions. The method reported by (DeLong et al., 1988) was used to compare the AUCs of selected models in which a non-parametric approach derived from the U-statistics theory to generate an estimated covariance matrix was used. The Hosmer-Lemeshow Goodness of Fit test was used to further evaluate model's fit. The Hosmer-Lemeshow goodness-of-fit test is performed by categorizing the observations into ten groups of predicted probabilities and comparing observed and expected FHB epidemic counts in these ten categories (Hosmer et al., 2013). These three statistics (AUC, Youden's Index, and Hosmer-Lemeshow test) were used to evaluate each model's ability to predict infection events. Models that describe estimated probabilities of an event can be written as follows:

$$\pi(\mu) = e^{\alpha+\beta x} / (1 + e^{\alpha+\beta x})$$

Where $\pi(\mu)$ is the estimated probability of infection, α is the *Y*-intercept, β is the regression coefficient, and e =2.71828 is the base of the system of natural logarithms.

3.3 Results

3.3.1. Growing Season Weather Conditions

The growing season weather conditions at the plot sites are described in Chapter 2. In brief, the 2019 and 2020 growing seasons were hotter and much drier than normal at most plot sites (Table

2.2). The mean monthly temperatures ranged from 11.9 to 24.7 °C, while total monthly rainfall ranged from 7.1 to 197.9 mm across all site years (Table 2.2).

3.3.2 Disease Indicators

The prevalence of FHB in prairies during the 2019 and 2020 growing seasons is described in Chapter 2. In brief, mean FHBi levels for winter wheat, spring wheat, barley, and durum ranged from 7.9 to 9.2, 5.8 to 6.8, and 2.9 to 3.5 and 11.9%, respectively, across FHB resistance categories (Figure 2.3c). The mean FDK for winter wheat, spring wheat, barley, and durum ranged from 0.27 to 0.69, 0.29 to 0.53, 0.03 to 0.04, and 2.4%, respectively, across FHB resistance ratings (Figure 2.4c). Across FHB resistance categories, the mean DON for winter wheat, spring wheat, barley, and durum ranged from 0.21 to 0.64, 0.19 to 0.5, 0.04, and 1.5 mg kg^{-1}, respectively (Figure 2.5c).

The distribution of the samples for FHBi, FDK, and DON content is shown in Table 3.1. The percentage of epidemic cases for FHBi, FDK, and DON across crop type and crop damaged thresholds ranged from 7.3 to 45.2, 11.1 to 30.8, and 0.3 to 38.7%, respectively (Table 3.1). The optimal epidemic to non-epidemic ratio for ROC curve analyses varies according to the required model accuracy. However, to produce valid ROC analyses, the dataset used in the model development must generally contain at least 25% of both epidemic and non-epidemic samples. As a result, models with disease indicator thresholds of less than 25% of the data set, such as those predicting DON $\geq$ 2 mg kg^{-1}, were rejected (Table 3.1).

3.4.3 Variable Selection

The Kendall correlation and stepwise regression analyses identified 26, 28, 21, and 20 variables that were significantly ($p < 0.05$) related to FHBi epidemics in winter wheat, spring wheat, barley, and durum, respectively (Table A3.1.2). Kendall correlation for selected variables ranged from

0.21 to 0.5, 0.23 to 0.56, and 0.24 to 0.53 for FHBi, FDK, and DON across crop types, respectively (Table A3.1.2-A3.1.4). Many of these weather variables were highly correlated and could not be used together to develop the models. For example, mean daily temperature and duration (h) when the temperature is between 15 and 30 °C at 7-day pre-mid-anthesis (T7MA and T15307MA, respectively), for most sites, were very similar because there were few hours with temperatures above 30 °C during both growing seasons. The variance inflation factors (VIFs) obtained for the FHBi regressors in the selected models ranged from 1.3 to 9.3, 1.0 to 2, 1.0 to 1.7, and 1.0 to 1.1 for winter wheat, spring wheat, barley, and durum, respectively, allaying concerns about multicollinearity (Table A3.1.5). In addition, tolerance and VIF in all selected FDK and DON model weather predictor variables ranged between 0.28 and 1, and 1.08 and 4.41, respectively, indicating no multicollinearity (Table A3.1.6). Daily and hourly RH derivatives were the most common predictor variables with FHBi, FDK, and DON epidemics (Table A3.1.2-A3.1.4).

3.4.4 Logistic Regression Models

3.4.4.1 Fusarium Head Blight Index Models

When the weather variables selected by Kendall correlation and those selected by the stepwise procedure were used to develop logistic regression models, 5 FHBi models per crop type with prediction accuracy ranging between 55.9 and 87.7% were identified using 5% FHBi as the threshold for an epidemic (Table 3.2). Of the five winter wheat models identified, model WWFHB5 used a temperature variable that was not selected using a stepwise procedure. There was no significant difference ($p > 0.05$) in the ROC curve of this model from the no information line, indicating that it was not better than a random prediction (Table 3.3). Of the remaining four models, WWFHB3 and WWFHB4 accurately predicted > 75% of epidemic and non-epidemic

cases (Table 3.2). Their Hosmer-Lemeshow test, on the other hand, was significant ($p < 0.05$), indicating a lack of fit for these models (Table 3.3). The best-fitting winter wheat FHBi model (WWFHB2) used only RH at 14 days pre-anthesis (RH8014) and was selected for further model evaluation. This model had a sensitivity of 96.9% and a specificity of 61.3% (Table 3.2). Its Hosmer-Lemeshow test was not significant ($p > 0.05$), indicating a good fit to the dataset used for model development (Table 3.3). Another model (WWFHB1) with three variables also correctly predicted both epidemic (73%) and non-epidemic cases (76%). As a result of its accuracy and fit, this model was also considered for further model validation. Model fit, in this case, was defined as models that met the majority of test statistics rather than passing a single test.

All selected spring wheat FHBi epidemic models included RH and temperature variations (Table 3.2). These models were more accurate at predicting cases with FHBi ≥ 5% (sensitivity) than cases with FHBi < 5% (specificity). Their Youden's index ranged from 0.51 to 0.63 (Table 3.3). However, there was no significant difference ($p > 0.05$) between the AUC of models utilizing pre-anthesis variables, which means that no model clearly outperformed the others. The Hosmer-Lemeshow tests were insignificant ($p < 0.05$) for models SWFHB3,4,5. As a result, only models SWFHB1 and SWFHB2 were subjected to additional testing (Table 3.3).

Weather variables at 14 days before mid-anthesis were strongly associated with barley FHBi epidemics cases (Table 3.3). However, barley FHBi models had lower optimal predicted probability thresholds than durum models, with the exception of model BAFHB3 (Table 3.2). In comparison to other barley FHBi models, BAFHB1 model had a low sensitivity of 57% and accuracy of 73%. Model BAFHB4, which used only two weather variables (mean daily rainfall and duration (h) when temperature is between 25 and 28 ^{o}C at 14 days before anthesis), performed similarly to all barley FHBi models that used three weather variables and was thus chosen due to

its simplicity. From the remaining models, model BAFHB3 had the highest accuracy, AUC, and Youden's index, and its Hosmer-Lemeshow test was significant ($p = 0.09$), indicating no lack of fit of the model to the data used in its development (Table 3.3) Thus, model BAFHB3 was also selected for further evaluation based on these criteria.

The accuracy of durum FHBi models ranged from 74 to 82%. The AUC of these models was significantly ($p < 0.0001$) different from the no information line. However, there was no significant difference between the AUC of these models, indicating that no model outperformed the other in terms of accuracy. However, model DUFHB1 had more balanced sensitivity (70%) and (88%) specificity and a higher AUC (82%) than other models. Additionally, the Hosmer-Lemeshow test of model DUFHB1 was significant ($p = 0.06$), indicating no lack of fit of the model to the dataset on which it was developed. The remaining four models predicted epidemic cases more accurately (sensitivity) than non-epidemic cases (specificity). However, the DUFHB3 model, which uses a single variable (a combination variable of temperatures between 15 and 30 ^{o}C and RH of 80%), had the highest accuracy (81%) compared to other models. This model also had the highest Youden's index (0.62) and a non-significant Hosmer-Lemeshow test ($p = 0.2$). As a result, DUFHB1 and DUFHB3 durum FHBi models were selected for further evaluation.

3.4.4.2 Fusarium Damaged Kernels Models

Winter wheat and barley samples with FDK levels ≥ 0.8 and 0.2, respectively, were less than 25%, a minimum level required for valid ROC analyses. As a result, winter wheat and barley FDK models were not developed. Spring wheat and durum FDK models were most frequently correlated with RH as the disease risk predictor. The sensitivity and specificity for these models tended to converge between probabilities of 0.27 and 0.48 and 0.16 and 0.41 for spring wheat and durum,

respectively (Table 3.4). Models SWFDK2 and SWFDK4 for spring wheat and models DUFDK2 and DUFDK5 for durum were the most parsimonious and provided the best fit to the model development dataset. Model SWFDK2 that utilized mean daily RH at 7 days pre-anthesis correctly classified 84% of epidemic cases (sensitivity) and 73% of non-epidemic cases (specificity) (Table 3.4). Other important statistical traits associated with this model, such as Youden's index, and Hosmer-Lemeshow, are presented in Table 3.5. The ROC curves of each model are represented in Figure 3.1. The ROC curves graphically display the trade-off between the TPR (sensitivity) and FPR (one minus specificity) for the entire range of possible cut-off points (model-based probabilities). The solid diagonal line (no information line) represents a classifier with no predictive power (i.e., random guessing), AUC = 0.5. This line represents a forecasting model that is ineffective at distinguishing between epidemic and non-epidemic samples, while one with high discriminatory power will curve away from this line with TPP equal to 1 and FPP approaching 0. The SWFDK6 model had the lowest AUC (0.566) and was never different from the no information line ($p > 0.05$), indicating a low predictive power of differentiating epidemic and non-epidemic samples (Table 3.5). However, the AUC of the remaining spring wheat FDK models were significantly different from the no-information line ($p < 0.05$). The spring wheat FDK model with the highest AUC was SWFDK4 (0.882) (Figure 3.1). Other spring wheat FDK models had more or less equivalent performances, with AUC $\geq$ 0.85 (Figure 3.1), and there were no significant differences in the AUC between these models (Table 3.5). Models SWFDK2 and SWFDK4 were selected for further evaluation due to their simplicity, fit, and high prediction accuracy.

The durum model DUFDK3 also utilized mean daily RH at 7 days pre-anthesis and correctly classified 80% of epidemic cases and 91% of non-epidemic cases (Table 3.4). In addition, the AUC of the model was 86% and was significantly different ($p < 0.001$) from the no information line of

ROC curve analyses (Table 3.5). Its Youden's index was also close to 1 (0.71), showing its utility for predicting FDK epidemic and non-epidemic cases in durum.

3.4.4.3 Deoxynivalenol Model

Evaluation of logistic regression models using ROC analyses requires at least 25% of the epidemic or non-epidemic cases. As a result, no DON models for winter wheat, spring wheat, and barley were developed since epidemic cases were less than 25% (Table 3.1). Models for durum DON risk are summarized and compared in Table 3.6. Overall, 13 out of 84 predictor variables were identified as suitable input variables in the models, particularly temperature and RH. Two variable-driven models had an accuracy range of 76 to 83% but were more accurate at predicting levels of DON $\geq$ 1 mg kg^{-1} (sensitivity) than DON $\leq$ 1 mg kg^{-1} (specificity) (Table 3.6). Models with pre- and post-anthesis variables had slightly higher accuracy compared to other single variable models, but there was no significant difference ($p > 0.05$) in their AUC (Table 3.7). DUDON4 and DUDON6 models were chosen for further evaluation based on several criteria, including discriminatory ability, fit, and simplicity. These models correctly classified 75% of epidemic and non-epidemic cases based on RH 10 days before mid-anthesis (DUDON4) and RH 14 days before mid-anthesis (DUDON6). Both models misclassified six cases as false negatives, 4 of which came from the Indian Head 2020 site-year, and 11 cases as false positives, eight of which came from Vermillion site-year (Table A3.2.7).

Table 3. 1. Percentage of epidemic samples in 2019 and 2020 for different disease indicators and crop types.

Crop type	Disease indicator	Disease indicator threshold	Epidemic cases[a] (%)	Non-epidemic cases (%)
Winter wheat	FHBi	10%	25.0 (N = 288)	75.0
Spring Wheat	FHBi	10%	16.5 (N = 357)	83.5
Durum	FHBi	10%	30.7 (N =104)	69.3
Barley	FHBi	10%	7.3 (N = 357)	92.7
Winter wheat	FHBi	5%	33.7	66.3
Spring Wheat	FHBi	5%	33.3	66.7
Durum	FHBi	5%	45.2	54.8
Barley	FHBi	5%	25.0	75.0
Winter wheat	FDK	0.8%	17.9 (N =291)	82.1
Spring Wheat	FDK	0.3%	30.8 (N = 357)	69.2
Durum	FDK	2.0%	25.2 (N = 119)	74.8
Barley	FDK	0.2%	11.1 (N = 357)	88.9
Winter wheat	DON	1 mg kg^{-1}	15.2 (N = 357)	84.8
Spring Wheat	DON	1 mg kg^{-1}	11.8 (N = 289)	88.2
Durum	DON	1 mg kg^{-1}	38.7 (N = 343)	61.4
Barley	DON	1 mg kg^{-1}	0.6 (N = 357)	99.4
Winter wheat	DON	2 mg kg^{-1}	10.4	89.6
Spring Wheat	DON	2 mg kg^{-1}	5.6	94.4
Durum	DON	2 mg kg^{-1}	16.8	75.6
Barley	DON	2 mg kg^{-1}	0.3	99.7

[a]Cases are number of samples classified as an epidemic (≥ disease threshold value).

Table 3. 2. Winter wheat, spring wheat, durum, and barley Fusarium Head blight index logistic regression models, optimum predicted probability, sensitivity, specificity, and prediction accuracy.

Model	Model equation ($p = 1/1 + \exp^{-(a + bX + \ldots)}$)[a]	OPP[b]	Sensitivity[c]	Specificity[d]	Accuracy[e]
			%		
	Winter Wheat				
WWFHB1	-0.1188+0.0185RH807MA+0.7846Tmin7MA-0.6239T7MA	0.37	73.2	75.9	74.6
WWFHB2	-5.1095+0.0312RH8014MA	0.17	96.9	61.3	79.1
WWFHB3	-5.0477+0.0262RH9014MA+0.0167Tmin14MA*R14MA	0.16	96.9	61.3	79.1
WWFHB4	-10.4574+0.2506RHmin3MAPA-0.0427RH803MAPA	0.45	75.3	86.4	80.8
[f]WWFHB5	-0.9329+0.00348T15304MA	0.33	58.8	52.9	55.9
	Spring Wheat				
SWFHB1	-6.1086+0.1267RH804MA+0.2461T252804MA-0.1414TRH904MA	0.25	82.4	68.9	75.6
SWFHB2	-34.5786+0.3513RHmax14MA+0.0435T252814MA	0.39	79.8	72.7	76.3
SWFHB3	-3.77241+0.3754RHmax14MA+ 0.2146R14MA+0.0495T252814MA	0.29	89.9	66.4	78.2
SWFHB4	-2.3537+0.0980TRH903MAPA	0.32	86.6	72.3	79.4
SWFHB5	-3.0950+0.0942TRH903MAPA+0.1020R033MAPA	0.3	94.1	69.3	81.7
	Barley				
BAFHB1	-1.8438+0.4439Tmin14MH+0.2468R14MH-0.0794RH14MH	0.33	57.3	89.3	73.3
BAFHB2	-0.6985+0.0201T153014MH+0.3152R14MH-0.0890RH14MH	0.24	74.7	78.3	76.5
BAFHB3	-6.4679+0.1560RH804MH+0.2981T252804MH-0.1137TRH804MH	0.42	73.8	85.4	79.6
BAFHB4	-3.77241+0.2146R14MH+0.0495T252814MH	0.27	79.6	70.1	74.9
BAFHB5	-9.2113+0.3945T3MHPH+0.1461R3MHPH	0.19	78.7	73.7	76.2
	Durum				
DUFHB1	-8.3268+0.5906Tmin4MA+0.2714R4MA	0.59	70.2	87.7	79
DUFHB2	-16.2024+0.4175T7MA+0.1097RH7MA	0.34	95.7	52.6	74.2
DUFHB3	-2.0665+0.0326TRH8010MA	0.39	91.5	70.2	80.8
DUFHB4	-24.7498+0.2246RHmax10MA+0.0105Tmin10MA*Tmax10MA	0.34	89.4	61.4	75.4
DUFHB5	-12.0384+0.0753RHmin3MAPA+0.6378Tmin3MAPA	0.37	95.7	59.6	77.7

[a]Logistic regression models were developed using 2019 and 2020 data collected in western Canada. Variables are defined in Table A3.1.1. P = probability of an epidemic event (1), *a* and *b* are the model coefficients, and X is the predictor variable.

[b]The optimal predicted probability (OPP) is probability value where sensitivity and specificity for the full range of p-values are high.

[c]Sensitivity is the percentage of correctly classified epidemics cases (epidemic = FHBi ≥ 5%).

[d]Specificity is the percentage of correctly classified non-epidemic cases.

[e]Accuracy is the percentage of correctly classified cases of epidemic and non-epidemic (true positive proportion + true negative proposition /2).

[f] Variable utilized by the model was not selected by stepwise procedure but included in the model for comparison.

Table 3. 3. Youden's index, lack of fit, and area under receiver operator characteristic (AUC) curve of Fusarium Head Blight index models.

Crop type	Model	Youden's Index[a]	Lack Fit[b]	AUC (%)	SE[c]	p-value[d]
Winter wheat	WWFHB1	0.49	0.054	78.0	0.030b	0.0001
	WWFHB2	0.58	<.0001	82.2	0.027ab	<0.001
	WWFHB3	0.54	<.0001	84.9	0.025a	<0.001
	WWFHB4	0.62	0.085	85.0	0.027a	<0.001
	WWFHB5	0.12	<.0001	52.6	0.036c	0.392
Spring Wheat	SWFHB1	0.51	0.0003	82.3	0.041ab	<0.001
	SWFHB2	0.53	0.0268	79.2	0.013b	<0.001
	SWFHB3	0.56	0.0294	82.4	0.031ab	<0.001
	SWFHB4	0.59	<.0001	81.7	0.028ab	<0.001
	SWFHB5	0.63	<.0001	84.0	0.041a	<0.001
Barley	BAFHB1	0.47	<.0001	76.0	0.011a	<0.001
	BAFHB2	0.53	0.0001	76.9	0.011a	<0.001
	BAFHB3	0.59	0.0931	79.8	0.018a	<0.001
	BAFHB4	0.49	<.0001	77.4	0.013a	<0.001
	BAFHB5	0.52	0.0013	78.3	0.017a	<0.001
Durum	DUFHB1	0.58	0.061	82.9	0.039a	<0.001
	DUFHB2	0.48	0.050	76.7	0.020a	<0.001
	DUFHB3	0.62	0.2	78.0	0.030a	<0.001
	DUFHB4	0.51	0.059	79.5	0.029a	<0.001
	DUFHB5	0.55	0.198	79.8	0.030a	<0.001

[a]Youden's index, calculated as true positive proportion - false positive proportion.

[b]Hosmer-Lemeshow lack of fit test. A high p-value (> 0.05) indicates a good fit.

[c]Standard error (SE) of the AUC. Letters following numbers indicate differences between the AUC of the forecasting models based on ROC contrast.

[d]Statistical significance of AUC of model's difference from 0.5 or line of no-information based on the Mann-Whitney U-statistic.

Table 3. 4. Spring wheat and durum Fusarium damaged kernels logistic regression models, optimum predicted probability, sensitivity, specificity, and prediction accuracy.

Model	Model equation ($p = 1/1 + \exp^{-(a + bX + \ldots)}$)[a]	OPP[b]	Sensitivity[c]	Specificity[d]	Accuracy[e]
			%		
	Spring wheat				
SWFDK1	-20.9541+0.2683RH4MA-0.0157TRH904MA	0.48	60.9	91.5	76.2
SWFDK2	-25.27+0.3167RH7MA	0.32	83.6	72.5	78.1
SWFDK3	-25.1029+0.3309RH7MA-0.00087RH7MA*T7MA	0.27	85.5	71.7	78.6
SWFDK4	-31.6372+0.4003RH10MA	0.37	86.4	83.4	84.9
SWFDK5	-36.1580+0.4582RH3MAPA	0.44	73.6	85.8	79.7
SWFDK6[f]	-1.0397+0.0617R7MA	0.32	41.8	74.5	58.2
	Durum				
DUFDK1	-49.1961+0.5289RH4MA +0.1518T15304MA-0.2775TRH904MA	0.33	76.7	89.9	83.3
DUFDK2	-17.9341+0.2185RH4MA	0.28	80.0	83.0	81.5
DUFDK3	-25.1915+0.3119RH7MA	0.41	80.0	91.0	85.5
DUFDK4	-27.1334+0.3314RH7MA-0.0474TRH907MA+0.1818R037MA	0.16	93.3	82.0	87.7
DUFDK5	-20.7748+0.2646RH8010MA	0.57	76.1	85.9	81.0
DUFDK6	-14.9985+0.0803RH8014MA	0.23	96.7	78.7	87.7
DUFDK7	9.8192+0.1351TRH803MAPA-1.3457Tmin3MAPA	0.33	80.0	82.0	81.0

[a]Logistic regression models were developed using 2019 and 2020 data collected from various sites in Manitoba, Saskatchewan, and Alberta. Variables are defined in Table A3.1.1. P = probability of FDK ≥ 0.3, and 2% FDK thresholds for spring wheat and durum, respectively. In the equation, *a* and *b* are the model coefficients, and X is the predictor variable.

[b]The optimal predicted probability (OPP) of an epidemic case, as determined by the Youden's index maximum value (where sensitivity and specificity are maximized for the full range of p-values).

[c]Sensitivity is the percentage of correctly classified epidemics cases.

[d]Specificity is the percentage of correctly classified non-epidemic cases.

[e]Accuracy is the percentage of correctly classified cases of epidemic and non-epidemic (true positive proportion + true negative proposition).

[f]Variable utilized by the model was not selected by stepwise procedure but included in the model for comparison.

Table 3. 5. Youden's index, lack of fit, and area under receiver operator characteristic curve (AUC) of the spring wheat and durum Fusarium damaged kernels models.

Crop type	Model	Youden's Index[a]	Lack Fit[b]	AUC	SE[c]	p-value[d]
Spring wheat	SWFDK1	0.52	0.19	0.850	0.0204a	<0.001
	SWFDK2	0.56	0.05	0.854	0.0219a	<0.001
	SWFDK3	0.57	0.22	0.855	0.0213a	<0.001
	SWFDK4	0.70	0.38	0.882	0.213a	<0.001
	SWFDK5	0.59	0.02	0.881	0.0185a	<0.001
	SWFDK6	0.16	0.01	0.566	0.0232b	0.354
Durum	DUFDK1	0.67	0.002	0.887	0.0245ab	<0.001
	DUFDK2	0.62	0.05	0.828	0.0458b	<0.001
	DUFDK3	0.71	0.23	0.857	0.0453b	<0.001
	DUFDK4	0.75	0.09	0.92	0.0245a	<0.001
	DUFDK5	0.62	0.05	0.855	0.0543b	<0.001
	DUFDK6	0.75	<.0001	0.898	0.0611ab	<0.001
	DUFDK7	0.62	0.10	0.832	0.0347b	<0.001

[a]Youden's index, calculated as true positive proportion-false positive proportion.
[b]Hosmer-Lemeshow lack of fit test. A high p-value (> 0.05) indicates a good fit.
[c]Standard error (SE) of the AUC. Letters following numbers indicate differences between the AUC of the forecasting models based on ROC contrast.
[d]Statistical significance of AUC of model's difference from 0.5 or line of no-information based on the Mann-Whitney U-statistic.

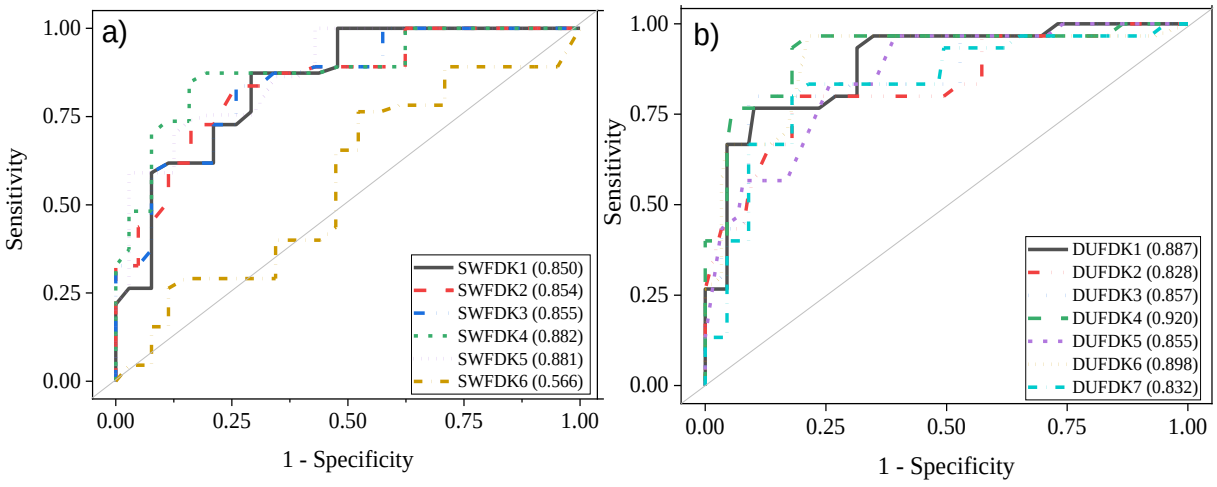

Figure 3. 1. Area under receiver operator characteristic curve for spring wheat (a) and durum (b) Fusarium Damaged Kernel models.

Table 3. 6. Durum deoxynivalenol logistic regression models, optimum predicted probability, sensitivity, specificity, and prediction accuracy.

Model	Model equation ($p = 1/1 + \exp^{-(a + bX + \ldots)}$)[a]	OPP[b]	Sensitivity (%)[c]	Specificity (%)[d]	Accuracy (%)[e]
DUDON1	-15.1371+0.3108T4MA+0.1644RHmin4MA	0.44	82.6	80.8	81.7
DUDON2	19.6034+0.2090RH7MA+0.00228RH7MA*T7MA	0.24	89.1	68.5	78.8
DUDON3	-9.3475+0.0714RH8010MA	0.38	87.0	67.1	77.0
DUDON4	-20.7748+0.2646RH10MA	0.57	71.7	84.9	78.3
DUDON5	-22.80770.2611RH10MA+0.1241T10MA	0.30	89.1	63.0	76.1
DUDON6	-24.1039+0.3114RH14MA	0.51	69.6	89.0	79.3
DUDON7	-22.2386+0.0137TRH8014MA+0.2726RH14MA	0.25	97.8	68.5	83.2
DUDON8	-13.2809+0.2360RHmin3MAPA	0.42	84.8	76.7	80.7
DUDON9	-20.5016+0.2632RH3MAPA	0.38	87.0	72.6	79.8

[a]Logistic regression models were developed using 2019 and 2020 data collected from various Manitoba, Saskatchewan, and Alberta plot sites. Variables are defined in Table A3.1.1. P = probability of DON ≥ 1mg kg^{-1}, *a* and *b* are the model coefficients, and X is the predictor variable.

[b]The optimal predicted probability (OPP) of an epidemic case, as determined by Youden's index maximum value (where sensitivity and specificity for the full range of *p* values are high).

[c]Sensitivity is the percentage of correctly classified epidemics cases (epidemic = DON ≥ 1mg kg^{-1}).

[d]Specificity is the percentage of correctly classified non-epidemic cases.

[e]Accuracy is the percentage of correctly classified cases of epidemic and non-epidemic (true positive proportion + true negative proposition/2).

Table 3. 7. Youden's index, lack of fit, and area under receiver operator characteristic (AUC) curve of the durum deoxynivalenol models.

Model	Youden's Index[a]	Lack Lit[b]	AUC	SE[c]	p-value[d]
DUDON1	0.63	0.4776	0.84	0.0443a	<0.001
DUDON2	0.58	0.1311	0.823	0.0475a	<0.001
DUDON3	0.54	0.4223	0.817	0.0359a	<0.001
DUDON4	0.57	0.148	0.825	0.0458a	<0.001
DUDON5	0.52	0.1989	0.834	0.0478a	<0.001
DUDON6	0.59	<.0001	0.822	0.0476a	<0.001
DUDON7	0.66	0.0675	0.864	0.0373a	<0.001
DUDON8	0.61	0.3179	0.848	0.0388a	<0.001
DUDON9	0.60	0.1493	0.802	0.0464a	<0.001

[a]Youden's index, calculated as true positive proportion - false positive proportion.

[b]Hosmer-Lemeshow lack of fit test. A high p-value (> 0.05) indicates a good fit.

[c]Standard error (SE) of the AUC. Letters following numbers indicate differences between the AUC of the forecasting models based on ROC contrast.

[d]Statistical significance of AUC of model's difference from 0.5 or line of no-information based on the Mann-Whitney U-statistic.

3.5 Discussion

Logistic regression has been a common technique for modelling crop fungal diseases and related mycotoxins (De Wolf et al., 2003; Hutcheson, 2011; Xu et al., 2013; Shah et al., 2014). This technique was used to model outbreaks of FHB in wheat (De Wolf et al., 2003; Xu et al., 2013; Shah et al., 2013). Similarly, logistic regression techniques were used in this study to establish weather-based models for forecasting FHBi, FDK, and DON in spring wheat and barley in western Canada. With environmental variability, the relationship between environmental conditions and biology is not always linear or easy to define (Hollingsworth et al., 2006). Therefore, weather data were divided into five critical periods (-4DMA, -7DMA, -10DMA, -14DMA, and ±3DMA). In general, FHBi models that used -4DMA appeared to be inferior in explaining epidemics compared to models that used -14DMA across crop types. This is logical as short periods might not capture any significant biological events occurring concurrently with the weather period (Nicolau and Fernandes, 2012).

All 15 models developed in this study included at least one weather predictor variable based on RH, indicating its importance in FHB epidemics. Rainfall and temperature were not significant predictors of FHB occurrence in these models when used alone. However, when used jointly, RH, temperature, and rainfall produced satisfactory models. These models have been narrowed down to two for each crop type. The models will be further evaluated for their reliability to assist producers with fungicide application decisions. For the selected spring wheat FHBi model (SWFHB2), the positive sign of estimators (RHmax14MA and T252814MA) was consistent with the biology of the pathogen, which thrives under humid conditions with optimum temperatures. This relationship is also consistent with previous observations of weather conditions associated with FHB epidemics (De Wolf et al., 2003; Del Ponte et al., 2005; Shah et al., 2013). The

development of *Fusarium* species perithecia is aided by favorable temperature and RH conditions, highlighting the importance of these variables used in the model developed by Brustolin et al., 2013. One of the selected winter wheat models (model WWFHB2) predicts FHB index events using a single variable, the duration in hours when average RH is greater than or equal to 80% for 14 days before mid-anthesis (RH8014MA). The recent winter and spring wheat risk models in the USA predict FHB index epidemics solely based on RH and FHB resistance categories (Shah et al., 2014, 2021). However, the FHB resistance category in this study was not significant; therefore, it was not incorporated into the models. The 2019 and 2020 growing seasons were characterized by low disease pressure, likely due to the hot and dry weather, which most likely masked the effect of the FHB resistance category. This low disease pressure was also confirmed by the low optimum predicted probabilities, ranging between 0.17 and 0.45, 0.25 and 0.39, and 0.19 and 0.42 for the selected winter wheat, spring wheat, and barley models.

The percentages of false positives and negatives in the models used for decision-making by producers must be carefully examined. A false-negative prediction by a model would encourage producers not to apply fungicides, resulting in fields that are FHB contaminated. In contrast, false positives can result in unnecessary fungicide sprays which can be costly to the producer and detrimental to the environment. Consequently, producers and the industry require models that can accurately predict both epidemic and non-epidemic cases, with few false negatives and positives. For example, the SWFHB1 model incorrectly classified the 2020 Roblin location-year as a low disease year. The 0.23 FHBi probability obtained using RH and temperature in this model was close to its optimal predicted probability threshold of 0.25. Persistent rainfall and high RH after anthesis, which these models did not consider, most likely contributed to the high disease levels observed that year in that location. Four durum samples from 2020 were misclassified as epidemic

by both DUFHB1 and DUFHB3. In addition, seven samples were misclassified as false positives by these models. These errors may partly be attributable to differences in disease assessment or the influence of field-scale environment and inoculum levels.

3.5.1 Fusarium Damaged Kernels (FDK)

The evaluation of two USA FHB models (De Wolf A and De Wolf B) and an Argentinean model (Moschini et al., 2001) resulted in a poor prediction of FDK levels in wheat but good prediction of DON levels under Quebec conditions (Giroux et al., 2016), although these models were not developed for predicting FDK or DON. Many studies have shown differences in the correlations between FHBi, FDK, and DON in grain (Paul et al., 2005; Miedaner et al., 2016; Schwarz, 2017; Góral et al., 2018, 2020), highlighting possible limitations in relying solely on visual FHB disease assessment. Similarly, a forecasting model developed to predict FHB would not be used to forecast FDK or DON levels. In Canada, FDK is a grading factor used by the Canadian Grain Commission's official grading guide and provides a more reliable means of estimating the cost of disease damage compared to the cost of fungicide spraying (Chapter 1: Table1.1). The models developed in this study utilize the FDK thresholds at which the cereal grains would drop their grade from No. 1 to No. 2 (Canadian Grain Commission, 2019) as a trigger for fungicide application. These percentages were relatively high to meet the minimum requirement of 25 to 75% epidemic to non-epidemic ratio for valid ROC curve analysis in winter wheat and barley due to low FDK damage in these crop types across all sites and both years. For models SWFDK2 (spring wheat) and DUFDK3 (Durum), extended periods of high RH at 7 days before mid-anthesis were associated with FDK epidemics at all 30 site-years studied. During this period, using a rainfall variable (model SWFDK6) to distinguish between epidemic and non-epidemic cases resulted in poor prediction

accuracy. Rainfall may restrict spore dispersal and wash away inoculum reservoirs counteracting the positive effect of wetness (Rossi et al., 2003).

3.5.2 Deoxynivalenol (DON)

Durum DON models with single variables representing RH at 10 and 14 days pre-anthesis (models DUDON4 and DUDON6) showed a good model fit and accuracy > 75%. Many models to predict DON risk levels have been published (Hooker et al., 2002; Musa et al., 2007; Bondalapati et al., 2012; Xu et al., 2013; Birr et al., 2019). To date, the most well-known of these is DONcast, which was developed to forecast DON risk in eastern Canada. In the DONcast model, weather variables included rainfall, temperature, and RH around the time for wheat heading, as well as post-anthesis weather conditions (Hooker et al., 2002), which were not included in our models. Additionally, the interpretation of temperature and RH differs from that of our models. In our study, models use RH compared to rainfall used in the DONcast model. Although we did not use heading and post-anthesis weather variables, our models predicted DON concentrations with great accuracy in durum wheat using only pre-anthesis weather data, indicating their potential value as management tools that producers can use to decide on fungicide application during the anthesis period. Fungicide application is justified when DON concentrations exceed 1 mg kg^{-1}, as various industries reject grain samples containing DON concentrations greater than 1 mg kg^{-1}. As a result, producers in western Canada may use maximum levels of 1 mg kg^{-1} as a trigger to apply a fungicide at anthesis for disease suppression to reduce DON concentrations in wheat grain. Producers can also use this information to make a no-spray decision if the predicted weather conditions can result in DON concentration less than 1 mg kg^{-1}.

3.6 Conclusion

Weather-based disease forecasting is a method of targeted pest management in which meteorological data such as rainfall, temperature, RH, and wind speed are used to predict the likelihood of FHB disease occurrence in wheat and barley and optimize fungicide use. The current level of model accuracy reflects significant progress in forecasting FHBi, FDK, and DON epidemics in western Canada. To the best of my knowledge, these are the first weather-driven FHBi, FDK, and DON risk-assessment models developed for wheat and barley management that are intended for use in all 3 prairie provinces. These models are intended to form the basis for a prairie-wide FHB risk forecasting system that provides estimates of disease occurrence in wheat and barley. This system could, in the future, alert producers of possible weather patterns that could lead to FHB epidemics. If the risk of infection is high, producers may take actions such as scouting their fields to assess the need to apply fungicides to protect crop yield and quality. Many of the models developed here were more than 70% accurate. However, model accuracy can be improved by incorporating more site-year data into the model development process. Data from sites where the FHB pathogen was confirmed to exist in the environment were used to develop the models in this study, and these models assume that there is enough inoculum present for infection. However, in Alberta, FHB inoculum is sometimes present at very low levels suggesting that the assumption that spores are present in sufficient quantity to cause an epidemic may not always be true. In this scenario, it is recommended that the FHB infection models be coupled with either information from the local disease scouting or inclusion of variables that provide information about inoculum sources such as previous residues and tillage method to minimize model errors.

3.7 References

Birr, T., M. Hasler, J.-A. Verreet, and H. Klink. 2020. Composition and predominance of *Fusarium* species causing Fusarium Head Blight in winter wheat grain depending on cultivar susceptibility and meteorological factors. Microorganisms **8**: 617. doi: 10.3390/microorganisms8040617.

Birr, T., J.-A. Verreet, and H. Klink. 2019. Prediction of deoxynivalenol and zearalenone in winter wheat grain in a maize-free crop rotation based on cultivar susceptibility and meteorological factors. J. Plant Dis. Prot. **126**: 13–27. doi: 10.1007/s41348-018-0198-9.

Bondalapati, K.D., J.M. Stein, S.M. Neate, S.H. Halley, L.E. Osborne, et al. 2012. Development of weather-based predictive models for Fusarium Head Blight and deoxynivalenol accumulation for spring malting barley. Plant Dis. **96:** 673–680. doi: 10.1094/Pdis-05-11-0389.

Brustolin, R., S.M. Zoldan, E.M. Reis, T. Zanatta, and M. Carmona. 2013. Weather requirements and rain forecast to time fungicide application for Fusarium Head Blight control in wheat. Summa Phytopathol. **39**: 248–251. doi: 10.1590/S0100-54052013000400003.

Canadian Grain Commission. 2019. Official Grain Grading Guide. [Online] Available at https://www.grainscanada.gc.ca/en/grain-quality/official-grain-grading-guide/04-wheat/grading-factors.html (accessed 24 June 2020). (accessed 24 June 2020).

CFIA, 2017. Section 1 - RG-8 Regulatory Guidance: Contaminants in Feed (formerly RG-1, Chapter 7) Canadian Food Inspection Agency (CFIA). [Online] Available at https://inspection.canada.ca/animal-health/livestock-feeds/regulatory-guidance/rg-8/eng/1347383943203/1347384015909?chap=1 (accessed 5.2.22).

Chen, Y., H.C. Kistler, and Z. Ma. 2019. *Fusarium graminearum* Trichothecene mycotoxins: biosynthesis, regulation, and management. Annu. Rev. Phytopathol. **57**: 15–39. doi: 10.1146/annurev-phyto-082718-100318.

Cowger, C., T.J. Ward, K. Nilsson, C. Arellano, S.P. McCormick, et al. 2020. Regional and field-specific differences in *Fusarium* species and mycotoxins associated with blighted North Carolina wheat. Int. J. Food Microbiol. **323**: 108594. doi: 10.1016/j.ijfoodmicro.2020.108594.

Crippin, T. 2019. Comparative analysis of *Fusarium graminearum* strain genotype and chemotype from grains sampled during the 2015-2017 Ontario harvests. MSc Thesis, Carlton University, doi: 10.22215/etd/2019-13634.

De Wolf, E.D., L.V. Madden, and P.E. Lipps. 2003. Risk Assessment models for wheat Fusarium Head Blight epidemics based on within-season weather data. Phytopathology **93**: 428–435. doi: 10.1094/Phyto.2003.93.4.428.

Del Ponte, E.M., J.M.C. Fernandes, and W. Pavan. 2005. A risk infection simulation model for Fusarium Head Blight of wheat. Fitopatol. Bras. **30**: 634–642. doi: 10.1590/S0100-41582005000600011.

DeLong, E.R., D.M. DeLong, and D.L. Clarke-Pearson, 1988. Comparing the areas under two or more correlated receiver operating characteristic curves: a nonparametric approach. Biometrics **44**, 837–845. PMID: 3203132.

Dill-Macky, R., and R.K. Jones. 2000. The effect of previous crop residues and tillage on Fusarium Head Blight of wheat. Plant Dis. **84**: 71–76. doi: 10.1094/PDIS.2000.84.1.71.

Fawcett, T. 2006. ROC graphs with instance-varying costs. Pattern Recognit. Lett. **27**: 882–891. doi: 10.1016/j.patrec.2005.10.012.

Fowler, D.B. 2011. Winter wheat production in Western Canada - Opportunities and obstacles. Proc. 2011 Soils Crops Workshop Mar 15-16 2011 Univ. Sask. Saskat. SK: 17.

Gilbert, J., and A. Tekauz. 2011. Strategies for management of Fusarium Head Blight (FHB) in cereals. Prairie Soils and Crops Journal 4: 97–104.

Giroux, M.E., G. Bourgeois, Y. Dion, S. Rioux, D. Pageau, et al. 2016. Evaluation of forecasting models for Fusarium Head Blight of wheat under growing conditions of Quebec, Canada. Plant Dis. **100**: 1192–1201. doi: 10.1094/PDis-04-15-0404-RE.

Góral, T., H. Wiśniewska, P. Ochodzki, L. Nielsen, D. Walentyn-Góral, et al. 2018. Relationship between Fusarium Head Blight, kernel damage, concentration of *Fusarium* biomass, and Fusarium toxins in grain of winter wheat inoculated with *Fusarium culmorum*. Toxins **11**: 2. doi: 10.3390/toxins11010002.

Góral, T., H. Wiśniewska, P. Ochodzki, A. Twardawska, and D. Walentyn-Góral. 2021. Resistance to Fusarium Head Blight, kernel damage and concentration of Fusarium mycotoxins in grain of winter triticale (x Triticosecale Wittmack) Lines. Agronomy 2021, 11(1), 16; https://doi.org/10.3390/agronomy11010016.

Guo, X. 2008. Development of models to predict Fusarium Head Blight disease and deoxynivalenol in wheat, and genetic causes for chemotype diversity and shifting of *Fusarium graminearum* in Manitoba. PhD Thesis, [Online] Available at https://mspace.lib.umanitoba.ca/xmlui/handle/1993/21115 (accessed 16 Jan 2022).

Haile, J.K., A. N'Diaye, S. Walkowiak, K.T. Nilsen, J.M. Clarke, et al. 2019. Fusarium Head Blight in durum wheat: Recent status, breeding directions, and future research prospects. Phytopathology **109**: 1664–1675. doi: 10.1094/Phyto-03-19-0095-RVW.

He, X., M. Osman, J. Helm, F. Capettini, and P.K. Singh. 2015. Evaluation of Canadian barley breeding lines for Fusarium Head Blight resistance. Can. J. Plant Sci. **95**: 923–929. doi: 10.4141/cjps-2015-062.

Hollingsworth, C.R., J.J. Mewes, C.D. Motteberg, and W.G. Thompson. 2006. Predictive accuracy of a Fusarium Head Blight epidemic risk forecasting system Deployed in Minnesota. Plant Health Prog. **7**: 4. doi: 10.1094/php-2006-1031-01-rs.

Hooker, D.C., A.W. Schaafsma, and L. Tamburic-Ilincic. 2002. Using weather variables pre- and post-heading to predict deoxynivalenol content in winter wheat. Plant Dis. **86**: 611–619. doi: 10.1094/PDIS.2002.86.6.611.

Hosmer, D.W., S. Lemeshow, and R.X. Sturdivant. 2013. Applied logistic regression. Third edition. Wiley, Hoboken, New Jersey.

Hutcheson, G. D. 2011. Logistic Regression. In L. Moutinho and G. D. Hutcheson, The sage dictionary of quantitative management research. Pages 173-175. Logist. Regres.: 3–5.

Jin, F., G. Bai, D. Zhang, Y. Dong, L. Ma, et al. 2013. Fusarium -Damaged Kernels and deoxynivalenol in *Fusarium* -Infected U.S . Winter Wheat. **9**: 472–478.

Martínez-Camblor, P., and J.C. Pardo-Fernández. 2019. The Youden's index in the generalized receiver operating characteristic curve context. Int. J. Biostat. **15.** doi: 10.1515/ijb-2018-0060.

McCallum, B.D., and R.M. DePauw. 2008. A review of wheat cultivars grown in the Canadian prairies. Can. J. Plant Sci. **88:** 649–677. doi: 10.4141/CJPS07159.

McMullen, M., G. Bergstrom, E. De Wolf, R. Dill-Macky, D. Hershman, et al. 2012. Fusarium Head Blight disease cycle, symptoms , and impact on grain yield and quality frequency and magnitude of epidemics Since 1997. Plant Dis. **96**: 1712–1728.

Miedaner, T., R. Kalih, M.S. Großmann, and H.P. Maurer. 2016. Correlation between Fusarium Head Blight severity and DON content in triticale as revealed by phenotypic and molecular data (H. Bürstmayr, editor). Plant Breed. **135**: 31–37. doi: 10.1111/pbr.12327.

Moschini, R.C., R. Pioli, M. Carmona, and O. Sacchi. 2001. Empirical predictions of wheat head blight in the Northern Argentinean pampas region. Crop Sci. **41**: 1541–1545. doi: 10.2135/cropsci2001.4151541x.

Musa, T., A. Hecker, S. Vogelgsang, and H.R. Forrer. 2007. Forecasting of Fusarium Head Blight and deoxynivalenol content in winter wheat with FusaProg. EPPO Bull. **37**: 283–289. doi: 10.1111/j.1365-2338.2007.01122.x.

Nicolau, M., and J.M.C. Fernandes. 2012. A predictive model for daily inoculum levels of G*ibberella zeae* in Passo Fundo, Brazil. Int. J. Agron. 2012: 1–7. doi: 10.1155/2012/795162.

Paul, P.A., P.E. Lipps, and L.V. Madden. 2005. Relationship between visual estimates of Fusarium Head Blight intensity and deoxynivalenol accumulation in harvested wheat grain: A Meta-Analysis. Phytopathology **95**: 1225–1236. doi: 10.1094/Phyto-95-1225.

Rossi, V., S. Giosuè, E. Pattori, F. Spanna, and A. Del Vecchio. 2003. A model estimating the risk of Fusarium Head Blight on wheat. EPPO Bull. **33**: 421–425. doi: 10.1111/j.1365-2338.2003.00667.x.

Schaafsma, A.W., and D.C. Hooker. 2007. Climatic models to predict occurrence of *Fusarium* toxins in wheat and maize. Int. J. Food Microbiol. **119**: 116–125. doi: 10.1016/j.ijfoodmicro.2007.08.006.

Schmale, D.G., A.K. Wood-Jones, C. Cowger, G.C. Bergstrom, and C. Arellano. 2011. Trichothecene genotypes of *Gibberella zeae* from winter wheat fields in the eastern USA: Plant Pathol. **60**: 909–917. doi: 10.1111/j.1365-3059.2011.02443. x.

Schwarz, P.B. 2017. Fusarium Head Blight and deoxynivalenol in malting and brewing: successes and future challenges. Trop. Plant Pathol. **42**: 153–164. doi: 10.1007/s40858-017-0146-4.

Shah, D.A., E.D. De Wolf, P.A. Paul, and L.V. Madden. 2014. Predicting Fusarium Head Blight epidemics with boosted regression trees. Phytopathology **104**: 702–714. doi: 10.1094/Phyto-10-13-0273-R.

Shah, D.A., E.D. De Wolf, P.A. Paul, and L.V. Madden. 2021. Accuracy in the prediction of disease epidemics when ensembling simple but highly correlated models (N.J. Cunniffe, editor). PLOS Comput. Biol. **17**: e1008831. doi: 10.1371/journal.pcbi.1008831.

Shah, D.A., J.E. Molineros, P.A. Paul, K.T. Willyerd, L.V. Madden and E.D. De Wolf. 2013. Predicting Fusarium Head Blight epidemics with weather-driven pre- and post-anthesis logistic regression models. Phytopathology **103**: 906–919. doi: 10.1094/Phyto-11-12-0304-R.

Tabachnick, B.G., L.S. Fidell, and J.B. Ullman. 2019. Using multivariate statistics. Seventh edition. Pearson, NY.

Xu, X., L.V. Madden, S.G. Edwards, F.M. Doohan, A. Moretti, et al. 2013. Developing logistic models to relate the accumulation of DON associated with Fusarium Head Blight to climatic conditions in Europe. Eur. J. Plant Pathol. **137**: 689–706. doi: 10.1007/s10658-013-0280-x.

4. ON-FARM VALIDATION OF FUSARIUM HEAD BLIGHT RISK MODELS IN WESTERN CANADIAN CEREAL PRODUCTION

4.1 Abstract

Fusarium Head Blight prediction models are increasingly being developed to complement fungicides decision-making to prevent disease loss and introduction of mycotoxins into the food and feed chain. While prediction models may demonstrate exceptional predictive accuracy using the development dataset, their predictive accuracy may decline significantly when applied to a different dataset. Thus, models must be tested in validation datasets to ensure their accuracy before being used for management purposes. Therefore, the objectives of this study were to validate weather-based FHBi (FHB index), Fusarium damaged kernels (FDK), and deoxynivalenol (DON) models developed in western Canada and to compare the performance of existing USA models used in western Canada to those developed in this study. Weather and disease data were collected in western Canada during the 2019 and 2020 growing seasons to validate FHB models. PROC LOGISTIC in SAS was used to score the validation data using previously fitted models. The scores were summarized in a 2 x 2 matrix to determine the models' sensitivity, specificity, accuracy, and errors. The models exhibited high accuracy ranges of 80 to 100% for FHBi, 66 to 89% for FDK, and 75 to 82% for DON. However, the models' sensitivity was infinite or low, owing to a small number or absence of epidemic fields. FHB pressure was low in both years, most likely due to drier than normal weather conditions, which were unfavorable for disease development. Based on model performance and error analysis, seven models, each tailored to a specific crop type and disease indicator, were identified as the most suitable for forecasting FHBi, FDK, and DON levels in western Canada. These models will power an online FHB risk tool that will use real-time

weather data to provide early warning of potential FHBi, FDK, and DON epidemics in the Canadian prairie's cereal crops.

4.2 Introduction

Fusarium Head Blight (FHB) is a devastating disease that affects small cereal crops worldwide, including wheat and barley. Since the early 1990s, enormous crop losses ranging from $50 million to $300 million per year in Canada have been attributed to FHB (Government of Alberta, 2021). Losses occur due to floret bleaching, grain filling disruption, and, most importantly, grain contamination with trichothecene mycotoxins, primarily DON (Dexter et al., 1996; Gilbert et al., 2014). The consensus is that moist and warm conditions during the anthesis period favor FHB development (Hooker et al., 2002; De Wolf et al., 2003; Bondalapati et al., 2012; Brustolin et al., 2013; Shah et al., 2019; Kochiieru et al., 2020; Moreno-Amores et al., 2020). The severity of FHB varies from year to year, and this is due to the disease's need for favorable weather conditions during critical stages of wheat development (McMullen et al., 1997; Brustolin et al., 2013). FHB is currently managed through agronomic practices that limit in-field inoculum, such as crop rotation, tillage, and fungicide application during flowering (Gilbert and Tekauz, 2011; Wegulo et al., 2015). The need for FHB control varies by location and year, depending on weather conditions during the period when the plant is most vulnerable to infection. Given the sporadic occurrence of FHB and the dependency of FHB on weather conditions, forecasting models that predict the likelihood of FHB outbreaks can provide important information through an early warning system for wheat and barley producers in western Canada, allowing producers to implement more effective disease management plans.

Fungicide use is beneficial during *Fusarium*-epidemic years because it reduces losses due to FHB damage. When the weather is not favorable for FHB development, growers can use the forecasts

to reduce unnecessary fungicide applications, lowering the monetary and environmental costs associated with conventional calendar-based spray programs. Forecasting systems for FHB are mainly based on disease development (incidence and/or severity) or DON contamination directly or indirectly via FHB severity (Hooker et al., 2002; De Wolf et al., 2003; Rossi et al., 2003; Del Ponte et al., 2005). A site-specific DON forecasting system called DONcast, commercialized in Ontario, is an example of a DON contamination forecasting system (Hooker et al., 2002; Schaafsma and Hooker, 2007). It is driven by a model composed of three regression equations that predict DON in wheat grain based on temperature and rainfall during three critical periods (Schaafsma and Hooker, 2007).

Disease risk models described by De Wolf et al. (2003) and Shah et al. (2013) are currently being used to forecast FHB risk in western Canada. These models predict the risk of FHB field severity greater than 10% based on weather conditions observed 7 days prior to flowering (De Wolf et al., 2003; Shah et al., 2013). To be valuable, the models used must be tested across the prairies to ensure that they provide reliable information about FHB risk. However, there is no information on the performance of the existing FHB models in western Canada. In addition, there is variation in the distance from the wheat and barley fields to the nearest weather station that provides weather data to these models. The effects of distance between the nearest weather station and the field on the accuracy of these models are unknown.

The current FHB maps are primarily for spring wheat, but the risks are also used for barley (ACIS, 2021a; MARD, 2021a; SWDC, 2021). The models are based on a field severity of more than 10%, a disease severity level strongly correlated with FHB yield losses and is generally associated with high levels of deoxynivalenol (DON) in harvested grain (De Wolf et al., 2003; Shah et al., 2013). However, disease symptoms in the field do not always accurately reflect the amount of FDK and

DON, and recent research has revealed complex relationships between disease symptoms and DON accumulation (Miedaner et al., 2016). The reasons stated above prompted the development of standardized FHBi, FDK, and DON risk models for spring wheat, winter wheat, barley, and durum in western Canada. These models had a high prediction accuracy of more than 75% (Chapter 3). While the regression model results on the development data were encouraging, using statistical techniques without subsequent performance analysis of the obtained models can result in poorly fitting results that incorrectly predict outcomes on new subjects. Evaluating the model's predictive performance in datasets that were not used to develop the model (external validation) is necessary before implementing prediction models to make management decisions (Van der Fels-Klerx, 2014; Giroux et al., 2016). This evaluation is necessary because it will help quantify optimism due to model overfitting or deficiencies in statistical modelling during model development (Giroux et al., 2016; Hooker et al., 2002). The ability of a model to perform well across multiple validations is a good indication of how well it will perform once implemented. Thus, the objectives of this study were to i) validate FHBi, FDK, and DON models for spring wheat, winter wheat, barley, and durum developed in western Canada; ii) determine the effect of distance between the field and the nearest weather station on model accuracy; and iii) compare the performance of existing USA models to those developed in western Canada. The models that perform the best in the validation dataset will be used in the new online FHB risk management tool currently under development in western Canada.

4.3 Materials and Methods

4.3.1 Sites Location

Research trials were conducted in the 2019 and 2020 growing seasons in Manitoba, Saskatchewan, and Alberta producer fields (Figure 4.1). The plot sites were located in fields with at least two years of FHB data collected through provincial and federal government annual FHB surveys. These fields were geographically distributed across western Canada to maximize the expected variation in weather conditions and disease occurrence.

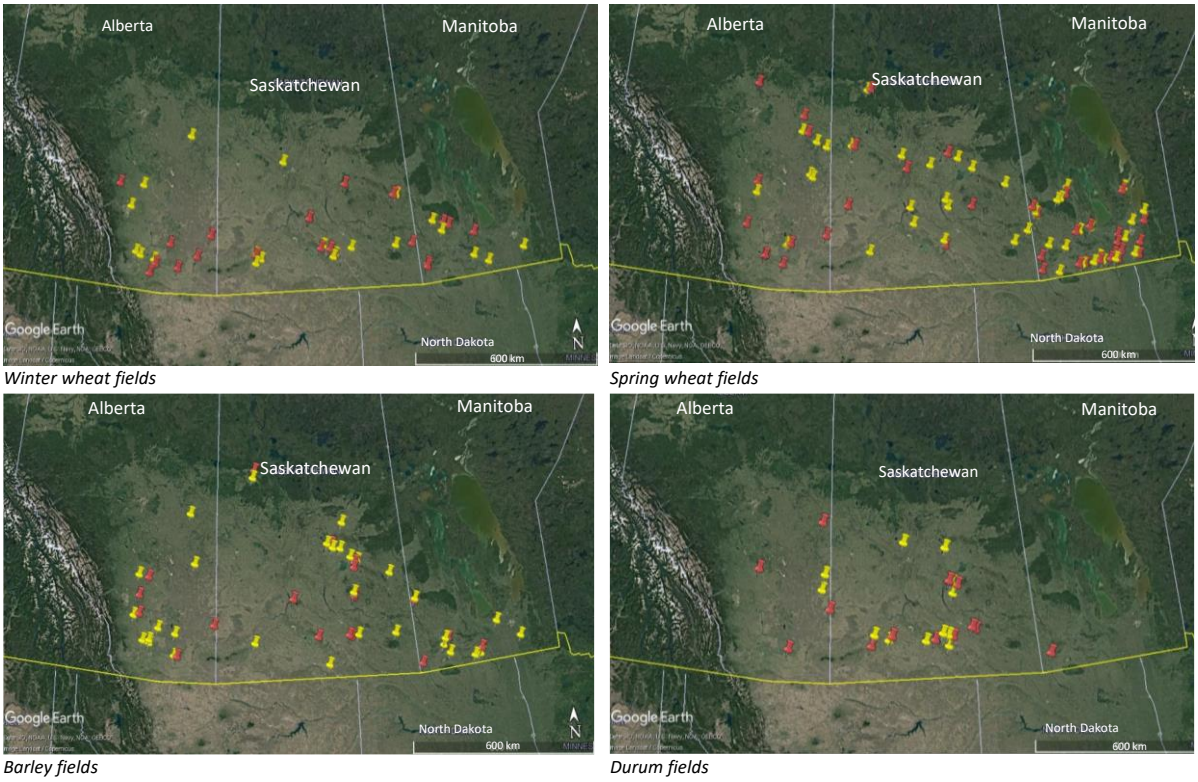

Figure 4. 1. Winter wheat (upper left), spring wheat (upper right), barley (bottom left), and durum fields (bottom right) in western Canada for the 2019 (yellow) and 2020 (red) growing seasons.

4.3.2 Agronomy Data

A small area measuring about 30 m x 30 m (check area) was left unsprayed with a fungicide at each producer field site. Producers followed their own agronomic practices such as fertilizer application, seeding depth, and row spacing on their fields. However, no fungicides were used in

the check area. Information about each field, including crop rotation history, seeding date, crop variety, anthesis date, and pest and stubble management, were collected. Crop growth stages were regularly monitored during the growing season. The planting date, along with heat unit accumulation was utilized to determine the date of mid-anthesis for each wheat field and mid-boot for each barley field (Appendix 5). Just prior to harvest, approximately two square meters of crop plants were harvested and bagged from within each check area and later threshed for grain.

4.3.3 Meteorological Data

Meteorological data were sourced from over 500 provincially (Manitoba Agriculture Weather Program and Alberta Climate Information Service) and federally (Environment Canada weather stations) monitored weather stations (ACIS, 2021b; ECCC, 2021; MARD, 2021b). Most of the stations transmit hourly and daily observations for various weather elements, including rainfall (mm), air temperature (^{o}C), relative humidity (RH) (%), wind speed (km h^{-1}), and wind direction. Missing data were filled using data from the second or in some cases third nearest weather stations. Latitude and longitude coordinates associated with each producer field were used to identify the closest reporting weather station with hourly and daily air temperature, RH, and rainfall data. Weather data during each growing season (May to August) were downloaded and used to calculate the variables of the selected models (Table 4.18).

4.3.4 Spore Traps

FHB spore trapping was done according to Guo (2008), with slight modifications. In brief, spore traps, consisting of a trap head and a supporting rod, were designed to simulate the deposition of spores on wheat heads. Two adhesive spore traps were placed at two locations along the edge of the check area at the beginning of anthesis (BBCH 61) to capture FHB spores. The traps were

retrieved near the soft dough stage (BBCH 85). A rectangular plastic foam prism with four spore collection surfaces (6 mm x 90 mm each) was used as the trap head. The spore head surfaces were covered with base tape and Melinex tape coated with a thin layer of petroleum jelly to which spores adhere. Following the collection of spores, a small piece measuring 5 mm x 19 mm was cut from the Melinex tape on one side of the trap head and fixed to a glass slide. *Fusarium* spores were determined under a compound microscope (400x) to confirm the presence of the inoculum in the environment.

4.3.5 Disease Indicators

4.3.5.1 Fusarium Head Blight Index (FHBi)

From 18 to 21 days after 50% anthesis (BBCH 65) between the early milk stage (BBCH 73) and the soft dough stage (BBCH 85), disease incidence and severity assessments were performed within the unsprayed check area. Five randomly selected spikes at 10 different locations within the check area were assessed for FHB infection (a total of 50 heads per field). Each spike was rated as infected or not infected to calculate the proportion of infected spikes per plot (disease incidence). The percentage of the spikelets infected was determined for each infected head based on the proportion of infected spikelets in each spike (disease severity). FHBi was calculated for each producer field using the disease incidence and severity as shown in equation 4.1.

$$FHB\ Index\ (\%) = (\%\ of\ spikes\ af\ infected\ x\ mean\ \%\ of\ kernels\ infected)/100 \quad [4.1]$$

Observations of FHBi were further classified into two groups of epidemics (=1) and non-epidemics (=0) using 5 and 10% FHBi thresholds. Thus, for example, observations of FHBi ≥ 10% were regarded as an epidemic and FHBi < 10% as non-epidemics. Choosing 5 and 10% FHBi disease severity thresholds correspond with previous FHB models developed in the USA (De Wolf et al.,

2003; Shah et al., 2013; Giroux et al., 2016) and western Canada, which are being validated in this study.

4.3.5.2 Fusarium Damaged Kernels (FDK) and Deoxynivalenol (DON)

Eight quarter square meter samples were selected randomly from within the unsprayed check area and hand-harvested by cutting all the plants within the quarter square meter. The plants were placed in mesh bags and taken to a drying facility as soon as possible. Each sample was threshed to determine the mass of grain per quarter square meter (Appendix 4). However, harvested grain samples were not allowed to pass through a cleaner so that lightweight FDK were retained during threshing. All threshing equipment was sterilized after each sample to avoid contamination of subsequent samples. Threshed grain was sent to a commercial lab (Intertek Lab) for official grading and to assess FDK and DON concentration following procedures outlined in the Canadian Grain Commission's Official Grain Grading Guide (Canadian Grain Commission, 2019). In brief, samples were divided into a representative portion using a Boerner-type divider. The samples were then visually divided into two groups of healthy and infected kernels with different damage levels. A 10-power magnifying lens was used to confirm the presence of a chalk-like appearance or pinkish mold. Fusarium damaged kernels were then calculated as a percentage of the number of grains with FDK divided by the total number of grains in each sample. Samples were then classified into epidemic or non-epidemic categories using the 0.2, 0.3, 0.8, and 2% number one grade thresholds for barley, spring wheat, winter wheat, and durum, respectively, as was done for the development of the FDK models in western Canada (Chapter 3).

DON concentration (mg kg^{-1}) in all crop types was determined by firstly grinding 50 g of grain samples with a laboratory grinder. High sensitivity (HS) and 5/5 Vomitoxin kits from the Neogen

ELISA test method were then used with a DON detection limit of 0.5 mg kg^{-1} (Neogen Corporation, 2013). DON thresholds of 1 mg kg^{-1} were used to distinguish between epidemic and non-epidemic cases, and this threshold correspond to DON level that is toxic to several domestic animals and humans (Table1.2) (CFIA, 2015).

4.3.6 Model Validation and Evaluation

PROC LOGISTIC using SAS 9.4 (SAS Institute, 2021) was used to fit the logistic regression models to the producer field samples (scoring technique). The prediction output scores obtained from the models were then categorized into epidemic or non-epidemic groups based on the optimum predicted probability thresholds of the models. The predicted binary model outcomes were compared with actual observations of FHBi, FDK, and DON. All possible combinations of predicted outcomes versus observed outcomes were organized in a 2 × 2 contingency table, with the following categories: (1) true positives (TP), when the model predicted an epidemic case in agreement with observed case; (2) false positives (FP), when the model predicted epidemic case, whereas the observed case was non-epidemic; (3) false negatives (FN), when the model predicted non-epidemic case, whereas the observed case was epidemic; and (4) true negatives (TN), when the model predicted a non-epidemic event in agreement with an observed case (Fienberg, 2005).

Model sensitivity, specificity, and accuracy were determined based on the contingency matrix table. The ability of models to correctly classify epidemic cases (sensitivity) was calculated using equation 4.2 (Fienberg, 2005).

$$Sensitivity = TP / (TP + FN) \quad [4.2]$$

Specificity refers to the ability of the model to correctly classify non-epidemic cases and was calculated using equation 4.3 (Fienberg, 2005).

$$Specificity = TN / (TN + FP) \quad [4.3]$$

Model accuracy was calculated as the percentage of correctly classified epidemic and non-epidemic cases using equation 4.4 (Fienberg, 2005).

$$Accuracy = (TP + TN) / (TP + TN + FP + FN) \quad [4.4]$$

False positives (overprediction) or false negatives (underprediction) errors were also recorded for each model failure.

4.3.6.1 Evaluation of the Existing USA Models

Another objective of the present study was to evaluate the performance of USA models under western Canadian conditions. In the USA, De Wolf et al. (2003) developed several empirical models for forecasting probabilities of FHB outbreak in wheat (De Wolf et al. 2003). Of the three selected models (A, B, and I), the De Wolf I model (equation 4.6) had the highest accuracy of 70% (De Wolf et al., 2003; Shah et al., 2013) and was adopted for use in Manitoba and Alberta. This model was fitted to wheat fields surveyed in the present study using published regression equation coefficients and weather data 7 days prior to flowering.

$$P = 1/ (1 + exp - (-8.2175 + (8.4358T15307)/168 + (4.7319DPPT7)/39)) \quad [4.6]$$

Where T15307 is the duration (h) of temperature between 15 and 30 °C, and DPPT7 is the duration of precipitation (h) at 7 days before anthesis (De Wolf et al., 2003). The probabilities (P) of FHB epidemics are defined by the chances that field severity reaches 10% or more. The severity corresponds to the percentage of infected spikelets, and the probability varies between 0 and 1. To use equation 4.6, variables must first be placed on the same scale as the data used to develop the models. This is done by dividing T15307 and DPPT7 by 168 and 39, respectively (TRH9010/136;

T15307/168) (De Wolf et al., 2003). The critical predicted probability for this forecasting model is 0.5 (De Wolf et al., 2003). The performance of the De Wolf I model was evaluated according to the criteria described in section 4.3.6.

The spring wheat FHB model currently being used in Saskatchewan (equation 4.8) was derived from the USA. It utilizes an agronomic variable (crop resistant category) and a weather variable (relative humidity) 7 days before anthesis and was also validated (Shah et al., 2013). The updated winter wheat model equation (4.7) was also evaluated in this study.

$$logit\ (\mu) = -1.7954 + 0.0245\ TH2 \quad (4.7)$$

$$logit\ (\mu) = -11.008 - 0.9578\ RESISTC + 0.1516 H1 \quad (4.8)$$

In both equations, μ is the probability of an FHB epidemic ≥ 10%, H1 is the mean hourly RH 7 days before anthesis, and TH2 is the number of hours during which the following two conditions are met simultaneously within a given hour: t is 9 to 30 °C and RH ≥ 90% 7 days before anthesis. RESISTC is categorical variable of four different levels of disease resistance: very susceptible = 0; moderately susceptible = 1; moderately resistant = 2; and resistant = 3. The critical predicted probability is 0.37 for the spring wheat model (equation 4.8) and 0.23 for the winter wheat model (equation 4.7) (Shah et al., 2013). The performance of the models was evaluated according to the criteria described in the model evaluation section.

4.4 Results

4.4.1 Descriptive Analyses

The mean FHBi values for barley, spring wheat, winter wheat, and durum for the 2019 and 2020 growing seasons ranged from 0 to 0.8, 0 to 4, 0 to 0.1, and 0.3%, respectively, across the three

resistance categories (Figure 4.2). Although FHB was detected most frequently in wheat fields, only one spring wheat field had FHBi levels greater than the 5% threshold utilized by our models (6.8%) (Figure 4.2). While disease pressure was low, it was interesting that the barley crop had significantly higher FHBi levels than other crops. The mean FDK percentage was nearly zero except for the spring wheat varieties with intermediate resistance (F. RC2) (0.4%) and the durum (2.9%), which are all susceptible (F. RC1). Durum fields had the highest DON concentration (11.4 mg kg^{-1}) (Figure 4.2). Several fields, however, contained DON levels less than 0.5 mg kg^{-1} (Figure 4.2). Correlation analyses revealed a non-significant ($p > 0.05$) relationship between the FHBi and the FDK or the DON for all crop types. However, there was a significant ($p < 0.05$) positive correlation between FDK and DON for all crop types except durum (Table 4.1).

4.4.2 Fusarium Head Blight Index Models

Table 4.3 summarizes the validation results for the FHBi, FDK, and DON models. Validation of the WWFHB2 model, which uses only RH, achieved an accuracy of 70%. The remaining 30% were fields with FHBi less than 5% but predicted to have FHBi ≥ 5% (false positives) (Table 4.11). However, model WWFHB1, which utilizes RHmax and a temperature variable, correctly predicted all cases (100% accuracy) (Table 4.3). It is important to note that the sensitivity of winter wheat FHBi models was infinite because there were no winter wheat fields that exceeded the epidemic threshold of ≥ 5% FHBi (epidemics) in both 2019 and 2020 growing seasons (Table 4.3). Furthermore, accuracy for winter wheat FHBi model WWFHB1 was not compromised when meteorological data were supplied from weather stations more than 40 km away from the field (Table 4.4).

Model SWFHB1 was more accurate (84%) than model SWFHB2 (80%) in discriminating between epidemic and non-epidemic spring wheat fields (Table 4.3). The latter model correctly predicted 1 of 1 epidemic spring wheat field (100% sensitivity) and 67 of 84 non-epidemic spring wheat fields (80% specificity) (Table 4.3). However, both models incorrectly classified two fields in Alberta as having FHBi ≥ 5% (Table 4.17). Accuracy for the SWFHB1 model was highest when the distance between the fields and the nearest weather stations was 10 km or less (88%) and dropped to 84% when fields utilizing weather data from weather stations 40 km or greater were included in the validation (Table 4.5).

There were no barley fields classified as FHBi epidemic in both the 2019 and 2020 growing seasons, implying that no field exceeded the FHBi threshold of 5% (Table 4.2). Model BAFHB1 correctly predicted 94% of the barley fields as non-epidemic (Table 4.3). The remaining 6% were fields with FHBi < 5% but predicted to have FHBi > 5%. These false positives were 2019 fields in Alberta. However, model BAFHB2 predicted all fields correctly (100% accuracy) using mean daily rainfall (R14MH) and duration in hours when the temperature is between 25 and 28 ^{o}C at 14 days pre-mid-heading (T252814MH) (Table 4.3). Weather data supplied by weather stations more than 40 km away from the fields did not affect the accuracy of the barley FHBi models (Table 4.6).

4.4.2.1 Comparison with USA Models

Table 4.17 shows comparisons of spring wheat (SWFHB1 and SWFHB2) and winter wheat (WWFHB1, WWFHB2, $WWFHB_{10}$ 6, and $WWFHB_{10}$ 7) models developed in western Canada with USA models. The overall dataset of 86 and 45 for spring wheat and winter wheat fields, respectively, were used to compare the models (Table 4.2). The accuracy of models utilizing a 5% spring wheat FHBi epidemic threshold ranged from 59 to 87% (Table 4.17). However, only 1 of 84 epidemic fields could be predicted, so the models' sensitivity was either 0 or 100%. The

SWFHB1 model had the highest accuracy (87%), while the De Wolf I model had the lowest (59%). SWFHB2 and Shah et al. (2013) models both had an accuracy of 80%. However, SWFHB2 had a sensitivity of 100%, while Shah et al. (2013) had a sensitivity of 0% (Table 4.17). When a 10% threshold was used, the De Wolf Model I had lower accuracy (77%) than the Shah et al. (2013) model (81%). However, the De Wolf model predicted 1 of 1 epidemic spring wheat case (100% sensitivity), whereas Shah et al. (2013) had 0% sensitivity (Table 4.17).

The De Wolf I model is also used to forecast FHB risk in winter wheat in Alberta and Manitoba and was compared to the winter wheat models developed in western Canada (Table 4.17). Using a 5% epidemic threshold, the most accurate winter model, WWFHB1, accurately predicted all winter wheat fields (100% accuracy). It should also be noted that the sensitivity of winter wheat models was also infinite because there were no epidemic cases to predict (Table 4.17). The Shah et al. 2013 model correctly predicted 87% of the fields using 5 and 10% FHBi epidemic thresholds (Table 4.17). It was also interesting that the De Wolf I model correctly predicted 77% of the winter wheat fields using both 5 and 10% FHBi epidemic thresholds (Table 4.17). However, models WWFHB2, De Wolf I, and Shah et al. 2013 misclassified 6 2019 Alberta similar fields using either a 5 or 10% FHBi epidemic threshold. When models with a 10% epidemic threshold were compared, the most accurate winter wheat model, $WWFHB_{10}$ 6, correctly predicted 92% of winter wheat fields, whereas the De Wolf I had the lowest prediction accuracy of 77% (Table 4.17).

4.4.3 Fusarium Damaged Kernel (FDK) Models

The validation results of the best-selected spring wheat and durum FDK models are presented in Table 4.3. The SWFDK1 model had an accuracy of 84%, while the SWFDK2 model had an accuracy of 66%. However, these models had very low sensitivity due to the scarcity of epidemic cases to predict. When compared to SWFDK2, SWFDK1 had higher specificity. Figure 4.2 is the

graphical representation of spring wheat models and describes the classification of cases for spring wheat SWFDK1 (a) and SWFDK2 (b) models. SWFDK1 model uses a probability threshold of 0.37 to split between fields with FDK ≥ 0.3% (above the line) and fields with FDK < 0.3% (below the line), while SWFDK2 uses a probability threshold of 0.32. The figure classifies fields into four categories: true positives (TP in blue); true negatives (TN in green); false positives (FP in red); and false negatives (FN in black). True positive cases are correctly predicted fields with FDK ≥ 0.3%; true negatives are correctly predicted fields with FDK < 0.3%; false negatives are fields with FDK ≥ 0.3% being predicted to have FDK < 0.3%, and false positives are fields with FDK < 0.3% being predicted to have FDK ≥ 0.3%. Model SWFDK1 had fewer errors (false positives and negatives) compared to SWFDK2. This difference in errors between the models prompted further error analysis (Figure 4.3).

Figure 4.3 shows relative humidity on the y axis and cultivar susceptibility on the horizontal axis. The split between FP and FN indicates a different RH threshold required to have an epidemic case. This value can be solved by using logistic regression, replacing the desired probability of an epidemic case, and solving RH. The RH thresholds were 80 and 74% for SWFDK1 and SWFDK2 models, respectively. Most of the overpredicted cases had higher RH than the model's RH threshold, while underpredicted cases had lower RH. Most false positives were from a moderately resistant variety, while most FN cases were from the intermediate variety.

The means of model error in the validation dataset are compared to the errors in the model development dataset (Table 4.14). While the mean RH10MA (model SWFDK1) and RH7MA (model SWFDK2) values for TP cases were consistently higher than those for TN cases, they remained within one standard deviation of the development dataset's non-epidemics. In contrast, in both SWFDK1 and SWFDK2 models, FN cases were consistently lower than TP cases.

However, the mean of RH10MA FN cases in the validation dataset was within two standard deviations of the mean of TP cases in the model development dataset.

The DUFDK2 model demonstrated sensitivity, specificity, and accuracy of 50, 94, and 89%, respectively (Table 4.3). This model is based on the mean RH four days before anthesis. The model incorrectly classified only two fields, one in Saskatchewan being underestimated and the other being overestimated to have FDK of 2%. The total accuracy of the DUFDK1 model was 78%.

4.4.4 Deoxynivalenol Models

Model DUDON1 correctly classified all durum fields as having DON below 1 mg kg^{-1} when the nearest weather stations were 25 km or less from the fields. The accuracy of this model was 100% using a 0.57 optimum predicted threshold (Table 4.10). However, when all data were used, the accuracy dropped to 82%. The model failed to predict any of the three durum fields with DON levels ≥ 1 mg kg^{-1} (0% sensitivity) but correctly predicted all durum fields with DON levels < 1 mg kg^{-1} (100% specificity) (Table 4.3). The DUDON2 model had an overall accuracy of 75% (Table 4.3). Both models incorrectly classified three 2019 Saskatchewan fields as having DON levels below 1 mg kg^{-1}, yet DON levels were above 1 mg kg^{-1} (false negative) (Table 4.16). These fields used weather data gathered from stations located 30 km away from the fields. However, the specificity of these models was greater than 80% (Table 4.3). Only one field in Alberta, 2019 growing season was underestimated by DUDON2 (Table 4.16).

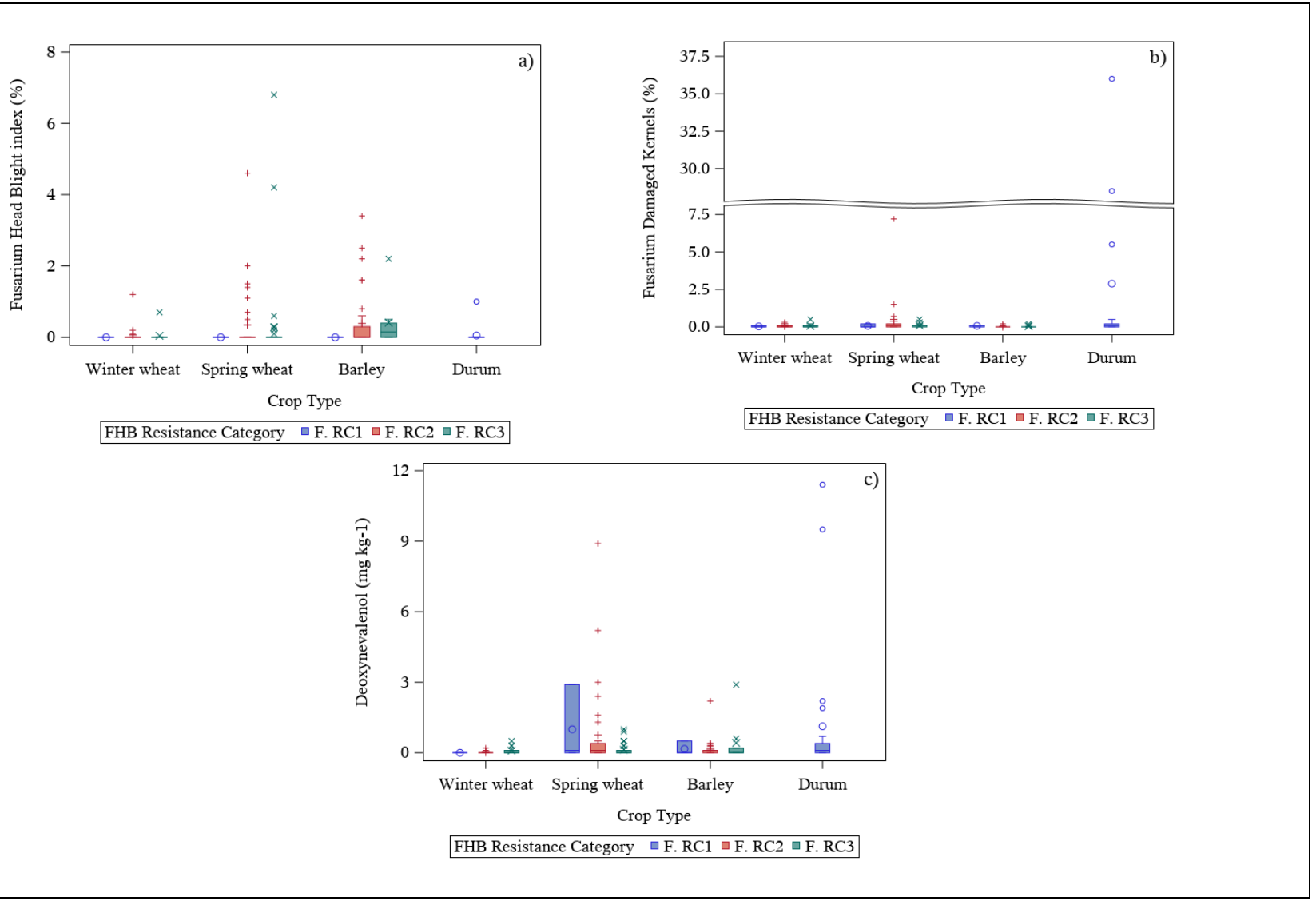

Figure 4. 2. Prevalence of Fusarium Head Blight (a), Fusarium damaged kernels (b), and deoxynivalenol (c) in susceptible/moderately susceptible varieties (F. RC1), intermediate varieties (F. RC2), and resistant/moderately resistant varieties (F. RC3) in wheat and barley in western Canada during the 2019 and 2020 growing seasons.

Table 4. 1. Correlations between Fusarium Head Blight index (FHBi), Fusarium damaged kernels (FDK), and deoxynivalenol (DON) in winter wheat, spring wheat, barley, and durum grain samples.

Crop Type	N	Variables	FHBi	FDK
Winter Wheat	45	FDK	0.080	
		p-value	0.603	
		DON	0.218	0.909
		p-value	0.150	**<.0001**
Spring Wheat	84	FDK	-0.043	
		p-value	0.699	
		DON	-0.009	0.936
		p-value	0.934	**<.0001**
Barley	49	FDK	-0.090	
		p-value	0.537	
		DON	-0.101	0.416
		p-value	0.492	**0.003**
Durum	19	FDK	0.064	
		p-value	0.796	
		DON	-0.074	0.221
		p-value	0.764	0.363

Table 4. 2. Percentage of epidemic wheat and barley fields during the 2019 and 2020 growing season in western Canada.

Crop Type	Disease Indicator	Epidemic Threshold	N[a]	Epidemic samples (%)	Non-Epidemic samples (%)
Winter Wheat	FHB index	5%	47	0	100
Spring Wheat	FHB index	5%	85	1	99
Durum	FHB index	5%	19	0	100
Barley	FHB index	5%	48	0	100
Spring Wheat	FDK	0.3%	84	10	90
Durum	FDK	2%	19	10	90
Durum	DON	1 mg kg^{-1}	18	15	85

[a]N is the number of fields

Table 4. 3. Validation results of selected Fusarium Head Blight index, Fusarium damaged kernel, and deoxynivalenol models for spring wheat, winter wheat, barley, and durum developed in western Canada.

Crop Type	Model	Model equation ($p = 1/1 + \exp^{-(a + bX + \ldots)}$)[a]	OPP[b]	Sens[c]	Spec[d]	Acc[e]
Winter Wheat	WWFHB1	-0.1188+0.0185RH807MA+0.7846Tmin7MA-0.6239T7MA	0.37	*[f]	100	100
	WWFHB2	-5.1095+0.0312RH8014MA	0.17	*	70	70
Spring Wheat	SWFHB1	-6.1086+0.1267RH804MA+0.2461T252804MA-0.1414TRH904MA	0.25	0	88	87
	SWFHB2	-34.5786+0.3513RHmax14MA+0.0435T252814MA	0.39	100	80	80
Barley	BAFHB1	-6.4679+0.1560RH804MH+0.2981T252804MH-0.1137TRH804MH	0.42	*	94	94
	BAFHB2	-3.77241+0.2146R14MH+0.0495T252814MH	0.27	*	100	100
Durum	DUFHB1	-2.0665+0.0326TRH8010MA	0.39	*	94	94
	DUFHB2	-8.3268+0.5906Tmin4MA+0.2714R4MA	0.58	*	84	84
Spring Wheat	SWFDK1	-31.6372+ 0.40037RH10MA	0.37	22	84	84
	SWFDK2	-25.27+0.3167RH7MA	0.32	11	72	66
Durum	DUFDK1	-11.9932+0.0847RH8010MA	0.29	0	88	78
	DUFDK2	-17.9341+0.2185RH4MA	0.28	50	94	89
Durum	DUDON1	-20.7748+0.2646RH10MA	0.57	0	100	82
	DUDON2	-24.1039+0.3114RH14MA	0.51	0	92	75

[a]Logistic regression models were developed using 2019 and 2020 data collected in Manitoba, Saskatchewan, and Alberta. Variables are defined in Table 3.1.1. P = probability of an epidemic event (1), *a* and *b* are the model coefficients, and X is the predictor variable(s).

[b]The optimal predicted probability of an epidemic case is determined by Youden's index max (where sensitivity and specificity for the full range of *p* values are high).

[c]Sensitivity (Sens) is the percentage of correctly classified epidemics cases.

[d]Specificity (Spec) is the percentage of correctly classified non-epidemic cases.

[e]Accuracy (Acc) is the percentage of correctly classified cases of epidemic and non-epidemic.

[f]No fields with FHBi ≥ 5%.

Table 4. 4. The effect of the distance between the field and the nearest weather station on the accuracy of winter wheat Fusarium Head Blight index (FHBi) models.

		Winter wheat WWFHB1 Model			Winter wheat WWFHB2 Model		
Distance (km)[a]	N[b]	Sensitivity (%)	Specificity (%)	Accuracy (%)	Sensitivity (%)	Specificity (%)	Accuracy (%)
10	14	*[d]	57	57	*	100	100
15	20	*	50	50	*	100	100
20	27	*	52	52	*	100	100
25	27	*	52	52	*	100	100
30	32	*	56	56	*	100	100
35	35	*	60	60	*	100	100
40	37	*	62	62	*	100	100
All data[c]	**47**	*****	**70**	**70**	*****	**100**	**100**

[a]Cumulative distance from producer field to nearest weather station.

[b]Number of winter wheat fields.

[c]All fields, including those with weather stations located more than 40 km away.

[d]No fields with FHBi ≥ 5%.

Table 4. 5. The effect of the distance between the field and the nearest weather station on the accuracy of spring wheat Fusarium Head Blight index (FHBi) models.

		Spring wheat SWFHB1 Model			Spring wheat SWFHB2 Model		
Distance (km)[a]	N[b]	Sensitivity (%)	Specificity (%)	Accuracy (%)	Sensitivity (%)	Specificity (%)	Accuracy (%)
10	40	0	89.7	88	100	76.9	78
15	59	0	87.9	86	100	75.9	76
20	65	0	85.9	85	100	75.0	75
25	68	0	85.1	84	100	74.6	75
30	72	0	85.1	84	100	74.6	75
35	75	0	84.5	83	100	76.1	76
40	79	0	84.7	84	100	76.4	77
All data[c]	**86**	**0**	**84.5**	**84**	**100**	**79.8**	**80**

[a]Cumulative distance from producer field to nearest weather station.

[b]Number of spring wheat fields.

[c]All fields, including those with weather stations located more than 40 km away.

Table 4. 6. The effect of the distance between the field and the nearest weather station on the accuracy of barley Fusarium Head Blight index (FHBi) models.

		Barley BAFHB1 Model			Barley BAFHB2 Model		
Distance (km)[a]	N[b]	Sensitivity (%)	Specificity (%)	Accuracy (%)	Sensitivity (%)	Specificity (%)	Accuracy (%)
10	17	*[d]	94.1	94	*	100	100
15	21	*	95.2	95	*	100	100
20	28	*	96.4	96	*	100	100
25	32	*	90.6	91	*	100	100
30	34	*	91.9	92	*	100	100
35	37	*	92.3	92	*	100	100
40	39	*	93.8	94	*	100	100
All data[c]	**48**	*	**93.8**	**94**	*	**100**	**100**

[a]Cumulative distance from producer field to nearest weather station.

[b]Number of barley fields.

[c]All fields, including those with weather stations located more than 40 km away.

[d]No fields with FHBi ≥ 5%.

Table 4. 7. The effect of the distance between the field and the nearest weather station on the accuracy of durum Fusarium Head Blight index models.

		Durum DUFHB1 Model			Durum DUFHB2 Model		
Distance (km)[a]	N[b]	Sensitivity (%)	Specificity (%)	Accuracy (%)	Sensitivity (%)	Specificity (%)	Accuracy (%)
10	3	*[d]	66.7	67	*	100	100
15	4	*	75.0	75	*	100	100
20	5	*	80.0	80	*	100	100
25	7	*	85.7	86	*	100	100
30	9	*	77.8	78	*	100	100
35	11	*	81.8	82	*	100	100
40	14	*	83.3	83	*	91.7	91.7
All data[c]	**19**	*	**84.2**	**84**	*	**94.4**	**94.4**

[a]Cumulative distance from producer field to nearest weather station.

[b]Number of durum fields.

[c]All fields, including those with weather stations located more than 40 km away.

[d]No fields with FHBi ≥ 5%.

Table 4. 8. Influence of distance between field and nearest weather station on the accuracy of durum Fusarium damaged kernels (FDK) models.

		Durum DUFDK1 Model			Durum DUFDK2 Model		
Distance (km)[a]	N[b]	Sensitivity (%)	Specificity (%)	Accuracy (%)	Sensitivity (%)	Specificity (%)	Accuracy (%)
10	4	*[d]	100	100	*	100	100
15	5	*	80.0	80	*	100	100
20	6	*	83.3	83	*	100	100
25	7	*	71.4	71	*	100	100
30	8	0	71.4	63	100	100	100
35	11	0	80.0	73	100	90.0	91
40	12	0	83.3	77	100	91.7	92
All data[c]	**18**	**0**	**87.5**	**78**	**50**	**93.8**	**89**

[a]Cumulative distance from producer field to nearest weather station.

[b]Number of durum fields.

[c]All fields, including those with weather stations located more than 40 km away.

[d]No fields with FDK ≥ 2%.

Table 4. 9. Influence of distance between field and nearest weather station on the accuracy of spring wheat Fusarium damaged kernels (FDK) models.

		Spring wheat SWFDK1 Model			Spring Wheat SWFDK2 Model		
Distance (km)[a]	N[b]	Sensitivity (%)	Specificity (%)	Accuracy (%)	Sensitivity (%)	Specificity (%)	Accuracy (%)
10	40	25	86	80	25	72	68
15	59	25	84	80	25	67	64
20	65	25	84	80	25	69	66
25	68	25	83	79	25	69	66
30	71	25	83	79	25	69	66
35	73	20	82	78	20	71	67
40	76	20	82	78	20	71	67
All data[c]	**84**	**22**	**84**	**84**	**11**	**72**	**66**

[a]Cumulative distance from producer field to nearest weather station.

[b]Number of spring wheat fields.

[c]All fields, including those with weather stations located more than 40 km away.

Table 4. 10. The effect of distance between the field and the nearest weather station on the accuracy of durum deoxynivalenol (DON) models.

		Durum DUDON1 Model			Durum DUDON2 Model		
Distance (km)[a]	N[b]	Sensitivity (%)	Specificity (%)	Accuracy (%)	Sensitivity (%)	Specificity (%)	Accuracy (%)
10	3	*[d]	100	100	*	100	100
15	4	*	100	100	*	100	100
20	5	*	100	100	*	100	100
25	7	*	100	100	*	83	71
30	9	0	100	89	0	88	78
35	10	0	100	91	0	90	82
40	12	0	100	92	0	91	77
All data[c]	18	0	100	82	0	92	75

[a]Cumulative distance from producer field to nearest weather station.

[b] No fields with DON ≥ 1 mg kg^{-1}.

[c] All fields, including those with weather stations located more than 40 km away.

[d]No fields with DON ≥ 1 mg kg^{-1}.

Table 4. 11. Winter wheat WWFHB2 Fusarium Head Blight index model errors in the winter wheat validation dataset.

Field Code	Province	Year	FHB Rating[a]	Latitude	Longitude	False Positive	False Negative
MBWW36	Manitoba	2020	I	50.6115	-100.6964	x[b]	-[c]
MBWW34	Manitoba	2020	I	50.1530	-98.9000	x	-
MBWW33	Manitoba	2020	R	49.5199	-101.0567	x	-
MBWW32	Manitoba	2019	I	50.3174	-100.2972	x	-
MBWW33	Manitoba	2019	R	50.3163	-100.2973	x	-
MBWW32	Manitoba	2020	MR	49.4558	-101.0563	x	-
MBWW35	Manitoba	2020	I	50.4348	-99.9812	x	-
SKWW07	Saskatchewan	2020	I	50.1641	-105.5408	x	-
ABWW01	Alberta	2019	S	53.0196	-111.1825	x	-
ABWW01	Alberta	2020	I	49.7529	-112.6171	x	-
ABWW03	Alberta	2020	MR	50.2772	-111.9921	x	-
ABWW09	Alberta	2020	MR	49.5123	-112.8687	x	-
ABWW12	Alberta	2020	MR	51.7499	-114.3519	x	-
ABWW05	Alberta	2020	MR	50.5175	-110.2283	x	-

[a]Winter wheat varieties that are Susceptible (S), Intermediate (I), Moderately Resistant (MR), and Resistant (R) to Fusarium Head Blight.

[b]Presence of a false positive or false negative case.

[c]Absence of a false positive or false negative case.

Table 4. 12. Spring wheat Fusarium Head Blight index model errors in the validation dataset.

Field Code	Province	Year	FHB Rating[a]	Latitude	Longitude	False Positive	False Negative
			SWFHB1 Model				
MBSW21	Manitoba	2019	MR	49.287	-98.547	-[b]	x[c]
MBSW24	Manitoba	2019	MR	50.697	-101.164	x	-
MBSW25	Manitoba	2019	I	50.778	-101.233	x	-
MBSW26	Manitoba	2019	MR	50.874	-101.302	x	-
SKSW01	Manitoba	2019	MR	50.040	-108.297	x	-
SKSW04	Saskatchewan	2019		52.460	-106.850	x	-
SKSW09	Saskatchewan	2019	I	54.155	-108.321	x	-
SKSW11	Saskatchewan	2019	MS	52.737	-109.046	x	-
SKSW01	Saskatchewan	2020	MR	50.140	-105.121	x	-
ABSW04	Alberta	2019	I	51.499	-113.210	x	-
ABSW05	Alberta	2019	S	52.833	-110.604	x	-
ABSW07	Alberta	2019	MR	52.703	-110.167	x	-
ABSW11	Alberta	2019	I	53.488	-111.225	x	-
ABSW04	Alberta	2020	I	53.474	-111.209	x	-
							-
			SWFHB2 Model				
MBSW10	Manitoba	2019	MR	50.364	-96.471	x	-
MBSW12	Manitoba	2019	I	49.036	-98.969	x	-
MBSW19	Manitoba	2019	I	49.044	-99.609	x	-
MBSW20	Manitoba	2019	MR	49.903	-100.773	x	-
MBSW27	Manitoba	2019	MR	49.411	-98.692	x	-
MBSW10	Manitoba	2020	I	49.029	-98.767	x	-
MBSW17	Manitoba	2020	I	49.268	-101.141	x	-
MBSW18	Manitoba	2020	MR	49.421	-98.682	x	-
MBSW19	Manitoba	2020	I	49.079	-99.619	x	-
MBSW20	Manitoba	2020	MR	49.800	-100.046	x	-
MBSW29	Manitoba	2020	MR	49.167	-99.304	x	-
ABSW01	Alberta	2019	MR	50.183	-111.830	x	-
ABSW04	Alberta	2019	I	51.499	-113.210	x	-
ABSW02	Alberta	2020	I	53.056	-111.002	x	-
ABSW04	Alberta	2020	I	53.474	-111.209	x	-
ABSW09	Alberta	2020	I	50.448	-110.125	x	-
ABSW11	Alberta	2020	I	54.295	-113.385	x	-

[a]Spring wheat varieties that are Susceptible (S), Moderately Susceptible (MS), Intermediate(I), and Moderately Resistant (MR), to Fusarium Head Blight.

[b]Absence of a false positive or false negative case.

[c]Presence of a false positive or false negative case.

Table 4. 13. Durum DUFHB1 Fusarium Head Blight index model errors in the validation dataset.

Field Code	Province	Year	Latitude	Longitude	False Positive	False Negative
MBDU08	Manitoba	2020	49.296	-101.071	x[a]	-[b]
SKDU02	Saskatchewan	2019	50.145	-105.129	x	-
SKDU03	Saskatchewan	2019	49.715	-105.225	x	-

[a]Presence of a false positive or false negative case.

[b]Absence of a false positive or false negative case.

Table 4. 14. Means of variables during spring wheat Fusarium damaged kernels error analysis during model validation and development. Standard deviations are presented in parenthesis.

Model	Modelling Stage	Variable	False Negative	False Positive	True Negative	True Positive
SWFDK1	Validation	RH10MA	72.8 (2.7)	79.4 (0.9)	70.8 (6.0)	81.1 (2.4)
SWFDK1	Development	RH10MA	71.1 (5.4)	79.6 (1.2)	71.6 (10.0)	80.6 (3.6)
SWFDK2	Validation	RH7MA	73.9 (1.4)	79.8 (1.6)	68.9 (6.2)	82.0 (3.0)
SWFDK2	Development	RH7MA	72.0 (5.6)	78.0 (2.2)	70.9 (10.7)	83.1 (0.0)

Table 4. 15. Durum Fusarium damaged kernels model errors in the validation dataset.

Model	Field Code	Province	Year	Latitude	Longitude	False Positive	False Negative
DUFDK1	ABDU02	Alberta	2019	51.1943	-110.4642	x[a]	-[b]
	ABDU01	Alberta	2019	51.5870	-110.3386	x	-
	SKDU04	Saskatchewan	2019	52.3876	-106.9698	-	x
	SKDU09	Saskatchewan	2019	51.0485	-104.9671	-	x
DUFDK2	SKDU09	Saskatchewan	2019	51.0485	-104.9671	-	x
	SKDU05	Saskatchewan	2020	50.1499	-104.2346	x	-

[a]Presence of a false positive or false negative case.

[b]Absence of a false positive or false negative case.

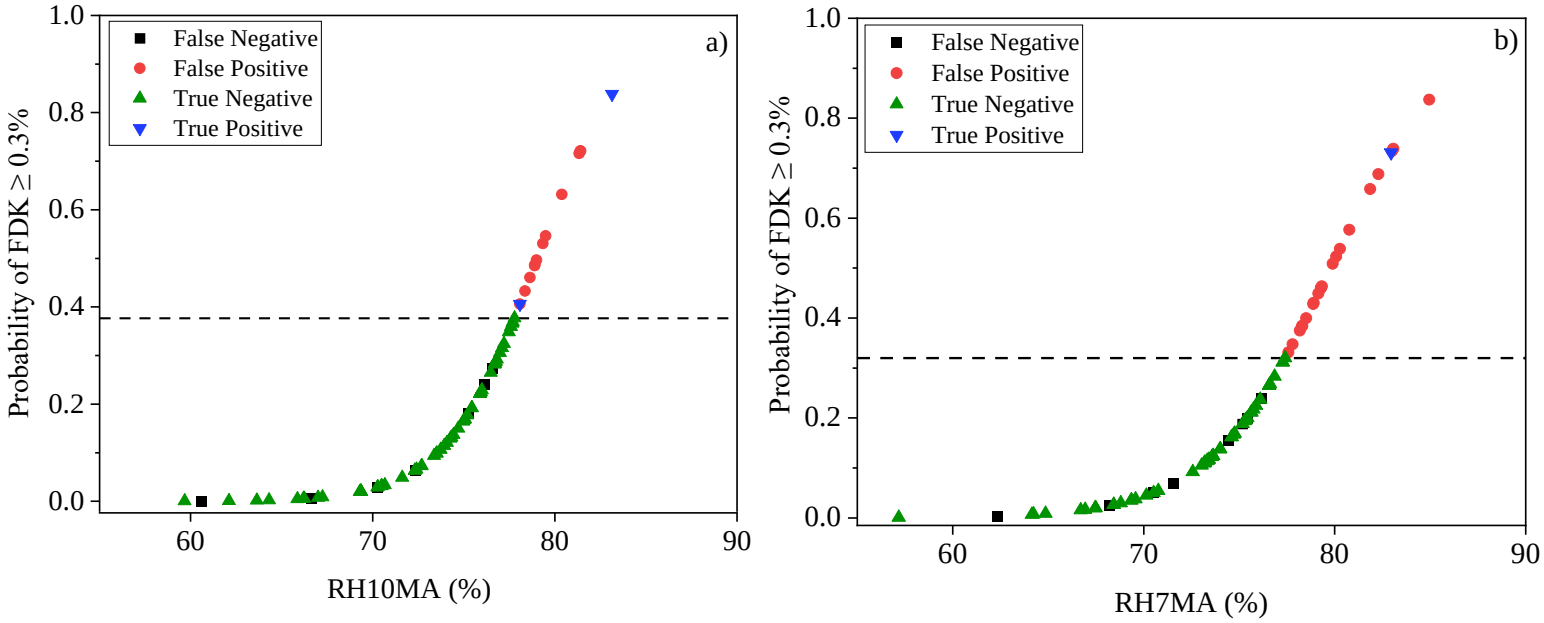

Figure 4. 3. Probability of FDK ≥ 0.3% against relative humidity for SWFDK1 (a), and SWFDK2 (b) models. The dashed line shows the optimum probability threshold for discriminating fields with FDK ≥ 0.3% (above the line) from FDK < 0.3% (below the line). RH10MA and RH7MA are mean daily relative humidity 10 and 7 days prior to middle anthesis, respectively.

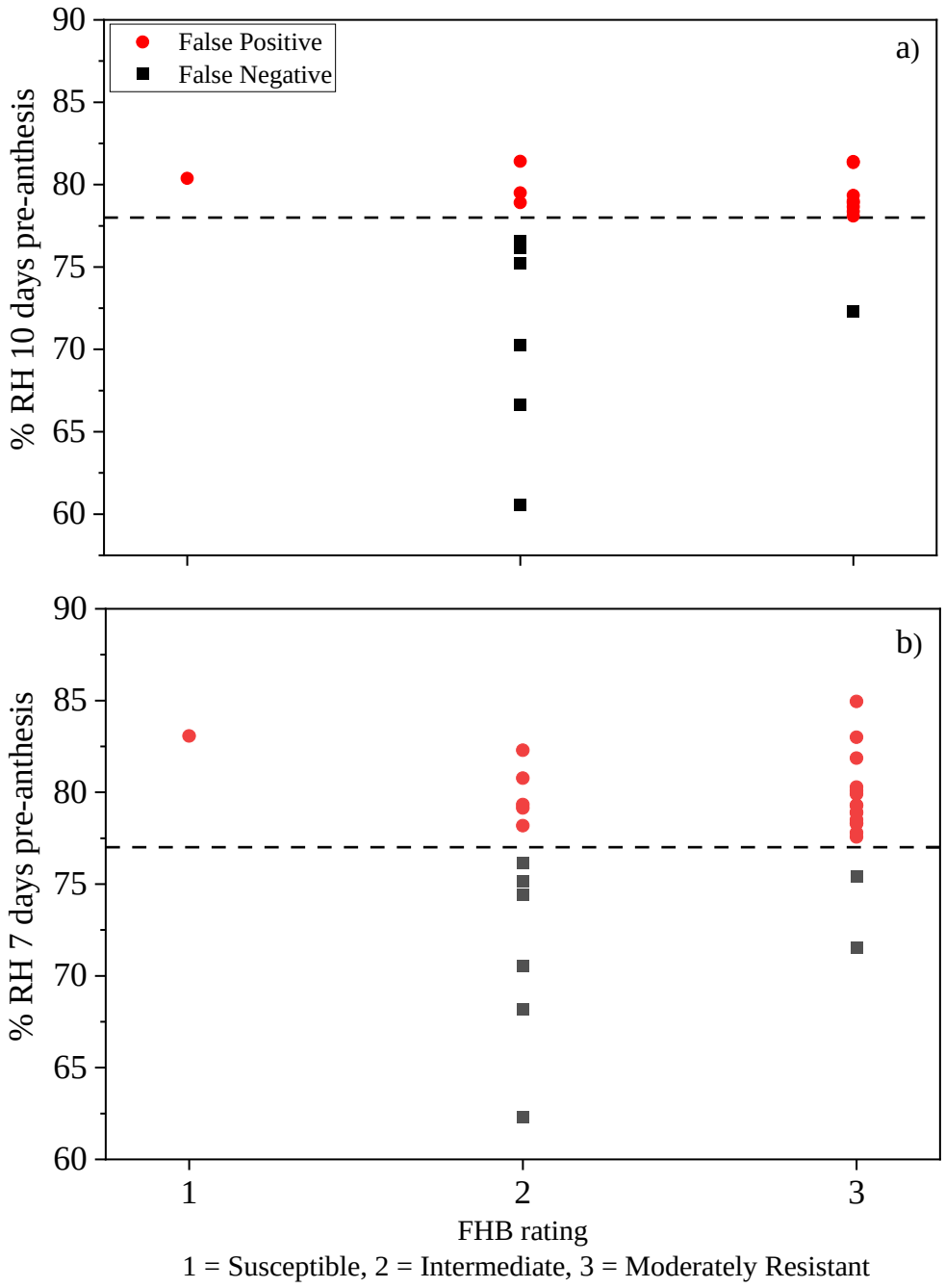

Figure 4. 4. Fusarium Head Blight (FHB) rating for spring wheat varieties vs. relative humidity (RH) at 10 and 7 days before anthesis for SWFDK1 and SWFDK2 models, respectively.

Table 4. 16. Durum deoxynivalenol model errors in the validation dataset.

Model	Field Code	Province	Year	Latitude	Longitude	False Positive	False Negative
DUDON1	SKDU04	Saskatchewan	2019	52.388	-106.970	-	x[a]
	SKDU08	Saskatchewan	2019	51.304	-105.095	-	x
	SKDU09	Saskatchewan	2019	51.049	-104.967	-	x
DUDON2	SKDU04	Saskatchewan	2019	52.388	-106.970	-	x
	SKDU08	Saskatchewan	2019	51.304	-105.095	-	x
	SKDU09	Saskatchewan	2019	51.049	-104.967	-	x
	ABDU01	Alberta	2019	51.587	-110.339	x	-[b]

[a]Presence of a false positive or false negative case.

[b]Absence of a false positive or false negative case.

Table 4. 17. Performance of Fusarium Head Blight index models developed in the USA (De Wolf I and Shah et al. 2013) and models developed in western Canada using spring wheat (N=86) and winter wheat (N=45) validation dataset collected in western Canada.

Model	Epidemic Threshold	OPP[a]	FN[b]	FP[c]	Sensitivity (%)	Specificity (%)	Accuracy (%)
			Spring Wheat				
SWFHB1	5	0.25	1	10	0	88	87
SWFHB2	5	0.3	0	17	100	80	80
De Wolf I	5	0.5	0	32	100	58	59
De Wolf I	10	0.5	0	33	0	58	58
Shah et al. 2013	5	0.37	1	16	0	81	80
Shah et al. 2013	10	0.37	0	16	0	81	81
			WinterWheat				
WWFHB1	5	0.37	0	0	*[e]	100	100
WWFHB2	5	0.17	0	14	*	70	70
$WWFHB_{10}$ 6[d]	10	0.34	0	4	*	88	92
$WWFHB_{10}$ 7	10	0.37	0	6	*	81	87
De Wolf I	5	0.5	0	10	*	77	77
De Wolf I	10	0.5	0	10	*	77	77
Shah et al. 2013	5	0.5	0	6	*	87	87
Shah et al. 2013	10	0.5	0	6	*	87	87

[a]Optimum predicted probability of the model determined during model development.

[b]FN is false negative cases.

[c]FP is false positive cases.

[d]Winter wheat models with FHBi epidemic threshold of ≥ 10% (Table A3.11).

[e]No fields with FHBi ≥ 5%.

Table 4. 18. Description of selected weather predator variables.

Variable	Variable Description	Days Prior to Mid-Anthesis
RH4MA	Mean daily relative humidity (%)	4
RH804MA	Duration (h) RH ≥ 80 %	4
T252804MA	Duration (h) air temperature 25 ≤ T ≤ 28 ^{o}C	4
Tmin4MA	Mean daily minimum temperature (%)	4
TRH804MA	Duration (h) air temperature 15 ≤ T ≤ 30 ^{o}C, and RH ≥ 80 %	4
TRH904MA	Duration (h) air temperature 15 ≤ T ≤ 30 ^{o}C, and RH ≥ 90 %	4
R4MA	Mean daily rainfall (mm)	4
RH7MA	Mean daily relative humidity (%)	7
RH807MA	Duration (h) RH ≥ 80 %	7
T7MA	Mean daily temperature (^{o}C)	7
Tmin7MA	Mean daily minimum temperature (%)	7
RH10MA	Mean daily relative humidity (%)	10
RH8010MA	Duration (h) RH ≥ 80 %	10
TRH8010MA	Duration (h) air temperature 15 ≤ T ≤ 30 ^{o}C, and RH ≥ 80 %	10
RH8014MA	Duration (h) RH ≥ 80 %	14
T252814MA	Duration (h) air temperature 25 ≤ T ≤ 28 ^{o}C	14
R14MA	Mean daily rainfall (mm)	14
RHmax14MA	Mean daily maximum relative humidity (%)	14

4.5 Discussion

In general, the occurrence of FHBi, FDK, and DON reflects weather conditions that occurred at producer fields during the 2019 and 2020 growing seasons. Warm, dry weather was most likely unfavorable for FHB epidemics at most fields during the two growing seasons. The low correlation between FHBi and FDK and DON in this study suggests that FHBi models can only be rough predictors of FDK and DON levels in wheat and barley. Several studies have also found a poor association between FHBi, FDK, and DON, which changes year to year (Paul et al., 2005; Miedaner et al., 2016; Góral et al., 2018). This poor relationship may be due to less aggressive *Fusarium* strains such as *Fusarium poae* and *Microdochium nivale*, which have been reported to cause the same FDK symptoms as *Fusarium graminearum* but do not produce the same amount

of mycotoxin (Góral et al., 2018). Furthermore, due to late-season infections, grains with low amounts of FDK might nonetheless contain high levels of DON (Cowger et al., 2009; Andersen et al., 2015).

Fusarium Head Blight index models. The overall accuracy of the FHBi model varied between 70 and 100% across crop types. The high predictive ability of the FHBi models is partly due to the diverse weather conditions and disease occurrence on plot sites in the data set used to develop the models, which can be extended to many areas of western Canada not included in the model development. The temperature and moisture variables used by the FHBi wheat and barley models represent field conditions that should be optimal for *Fusarium* species infection and subsequent symptom development that are ≥ 5% FHBi. For example, the RH9014MA weather variable for model WWFHB2 measures prolonged periods of high humidity ≥ 80%, 14 days pre-mid-anthesis, a condition associated with the development of FHB symptoms in wheat (De Wolf et al., 2003; Froment et al., 2011; Shipe et al., 2019).

In this study, when RH was used alone in the WWFHB2 model, prediction accuracy of 70% was obtained using the validation dataset. However, when RH and temperature were used together in model WWFHB1, prediction accuracy increased to 100%. It is also critical to take note of the sign of the coefficients in the models. For example, the positive sign of daily minimum temperature (Tmin) for winter wheat model WWFHB1 indicates that *Fusarium* species prefer cooler than warmer temperatures. This finding can be explained by the humid conditions that often accompany low temperatures and provide an ideal environment for fungal infection during the pre-anthesis period.

The models for spring wheat, barley, and durum likely discriminate epidemic cases less well due to the small number of fields with FHB ≥ 5% in the model validation data set. However, this validation dataset is typical of the situations the model would experience in the real world and indicates how well the model will perform after deployment. Given the low disease pressure in both the 2019 and 2020 growing seasons, which was most likely caused by dry conditions, producers could largely avoid costly application of fungicides. Furthermore, the fact that the models had few errors under diverse conditions demonstrates their general applicability within western Canada, as the samples used in the development of these models came from various locations in western Canada that were not included in the development of these models. The error analysis of the spring wheat FHBi models revealed that both models misclassified two similar Alberta fields. These errors could be explained by low FHB spore levels detected in these fields near flowering. Even though the weather conditions were favorable for infection, low FHB spore levels may have resulted in fewer spores landing on the flowers, thereby reducing disease incidence and severity. A lack of epidemic cases in the validation dataset may have resulted in no effect of distance between the farm and the nearest weather station.

Comparison of FHBi Models. The models developed in this study for spring and winter wheat were compared to those currently being used in western Canada to predict FHB risk. When applied to the western Canadian spring wheat field data, the De Wolf I model performed poorly. The differences in prediction performance between the models developed in the current study and the USA models may partially be attributed to differences in weather conditions, cultivars, and FHB species. The De Wolf I model, when evaluated under Quebec conditions to predict DON levels greater than 1 mg kg^{-1} resulted in a sensitivity of 6.7%, specificity of 64.9%, and prediction accuracy less than 50% (Giroux et al., 2016). It is interesting to note that the De Wolf I model

performed better in predicting FHB risk in winter wheat. The data set used to develop the De Wolf models included more winter wheat site-years (30 of 50) than spring wheat site-years, which may account for why winter wheat predictions were better than spring wheat predictions (De Wolf et al., 2003).

Fusarium damaged kernels. Spring wheat models SWFDK1 and SWFDK2 used mean RH averaged 10 and 7 days before mid-anthesis, respectively. The accuracy of SWFDK1 was 18% greater than SWFDK2, and this difference may have been due to more extended periods of favorable humidity captured by SWFDK1 but missed by SWFDK2. The sensitivity of spring wheat FDK models during validation decreased dramatically compared to model development because there were very few or no epidemic cases to predict. Model sensitivity can only be improved with more data collection that balances the dry conditions and low FHB disease levels observed over the two growing seasons. Nonetheless, the models correctly predicted most site-years, achieving accuracy up to 84%. Therefore, these models can be used as a starting point to identify weather conditions that may result in wheat being downgraded during marketing if FDK is greater than 0.3% in spring wheat.

While the sensitivity of the two durum FDK models was also low due to a lack of epidemic cases to predict, the higher specificity and accuracy of the models indicate that fungicide application would not be recommended because conditions in durum were not conducive for FDK. This will reduce the use of unnecessary fungicides, lowering the producer's production costs and potential environmental damage. However, the accuracy of these models also relies on the distance between the field and the nearest weather station. Model DUFDK2, for example, showed reduced accuracy when the distance between the field and the nearest weather station was greater than 40 km. The error analysis of durum FDK models revealed that model DUFDK1 which uses duration (h) when

relative humidity is 80% at 10 days before mid-anthesis had fewer errors (4 errors) than DUFDK2 which uses mean RH at 4 days before anthesis (2 errors). The differences in errors could be due to a combination of factors including the duration of weather conditions considered by the predictor variables and the distance between the field and the nearest weather station. Thus, the shorter the duration and distance to the nearest weather station, the more accurate the estimate of weather conditions in the specific environment/field.

Deoxynivalenol models. The DON durum models correctly classified a high percentage of fields as having less than 1 mg kg^{-1} DON concentration. The accuracy of DONDU1 was 82%, and the remaining 18% were fields classified as having DON levels less than 1 mg kg^{-1}. Post-anthesis conditions that favor DON accumulation, but which our models did not consider, may be the cause of these false-negative errors. False positives may not be surprising for several reasons. First, DON is water-soluble, and delayed rains that occurred during the end of the 2019 growing season could have washed down some of the DON contamination in the grain resulting in DON concentration less than 1 mg kg^{-1} not predicted by our models (Nita, 2013; Crippin, 2019). Secondly, mycotoxin production is affected by several other factors not considered by our models, including competition with other pathogens (Xu et al., 2007).

In contrast to the DUDON1 model, cross-validation results of durum DON models in the study conducted by Gourdain and Rosengarten (2011) showed that their model predicted more false positives (52%) than false negatives (8%) when the DON threshold was > 1,750 µg kg^{-1}. However, their model correctly predicted DON content below or above 1,750 µg kg^{-1}in 85% of cases. This level of accuracy is comparable to what our models achieved (82% accuracy). Validation of DONcast in Ontario, Canada, also resulted in 80 to 85% prediction accuracy using a 1 mg kg^{-1} threshold (Schaafsma and Hooker, 2007). However, the sensitivity and specificity of the models

are unknown. Furthermore, the DONcast model utilizes weather conditions that extend from 7 days before heading to 10 days after wheat heading. Compared to previous modelling studies (Del Ponte et al., 2005; Schaafsma and Hooker, 2007; Franz et al., 2009), the current study demonstrated that DON epidemics in wheat could be accurately predicted using a narrow time window around wheat flowering.

The quality of the data used in the development of predictive models for mycotoxins in wheat impacts their prediction performance. For example, the DUDON1 model's accuracy was 100% when weather data were sourced from weather stations within 25 km from the field. However, accuracy dropped to 89% when data were sourced from weather stations that were 40 km or more from the field. Although various factors can affect the model's sensitivity, specificity, and overall accuracy, some of the model errors are due to variation in the response variable (DON levels) as well as the explanatory (meteorological) variables. Improving model performance may thus be achieved with higher-quality data, such as data acquired from weather stations as close as possible to the fields.

4.6 Conclusion

The FHBi, FDK, and DON models for wheat and barley were successfully validated using weather and disease data collected from producer fields in western Canada during the 2019 and 2020 growing seasons. The best models for predicting the occurrence of FHBi $\geq$ 5% in western Canada are WWFHB1, SWFHB1, BAFHB1 and DUFHB1 for winter wheat, spring wheat, barley, and durum, respectively; SWFDK1 and DUFDK1 for spring wheat, and durum FDK models, respectively, and DUDON2 for DON $\geq$1 mg kg^{-1} in durum. The models were able to predict mostly non-epidemic fields (specificity) correctly. However, it is unclear how accurately the models predict high FHBi, FDK, and DON levels because most fields were below epidemic thresholds.

Data from years with favorable conditions for FHB occurrence will be required to further evaluate these models. For the majority of the models, it was observed that the closer the distance between the weather station and the field, the more accurate the prediction, so this will be an important factor to consider when selecting weather stations that feed weather data to these models. However, it should be noted that there was a lack of data points to fully determine the accuracy of the models in the categorized distances between producer fields and nearest weather stations. More data is needed to determine the accuracy of the models based on the distance between producer fields and nearest weather stations. Spraying fungicides only when necessary and minimizing any adverse effects on the environment while maintaining yield and quality can maximize fungicide use. By using the newly developed forecasting models, producers in western Canada can better predict the need for spraying against FHB. Control agencies and industry could also use the models to help predict DON levels and identify high-risk fields, regions, or years to reduce mycotoxins levels in the food and feed supply chain.

4.7 References

ACIS. 2021a. Alberta Climate Service -Fusarium Head Blight Map. [Online] Available at https://agriculture.alberta.ca/acis/m#!Fusarium (accessed 16 November 2021).

ACIS. 2021b. Alberta Climate Service -Weather and climate resources. [Online] Available at https://www.alberta.ca/acis-find-current-weather-data.aspx (accessed 16 November 2021).

Andersen, K.F., L.V. Madden, and P.A. Paul. 2015. Fusarium Head Blight development and deoxynivalenol accumulation in wheat as influenced by post-anthesis moisture patterns. Phytopathology **105**: 210–219. doi: 10.1094/Phyto-04-14-0104-R.

Bondalapati, K.D., J.M. Stein, S.M. Neate, S.H. Halley, L.E. Osborne, et al. 2012. Development of weather-based predictive models for Fusarium Head Blight and deoxynivalenol accumulation for spring malting barley. Plant Dis. **96**: 673–680. doi: 10.1094/PDIS-05-11-0389.

Brustolin, R., S.M. Zoldan, E.M. Reis, T. Zanatta, and M. Carmona. 2013. Weather requirements and rain forecast to time fungicide application for Fusarium Head Blight control in wheat. Summa Phytopathol. **39**: 248–251. doi: 10.1590/S0100-54052013000400003.

Canadian Grain Commission. 2019. Official Grain Grading Guide. [Online] Available at https://www.grainscanada.gc.ca/en/grain-quality/official-grain-grading-guide/04-wheat/grading-factors.html (accessed 24 June 2020). (accessed 24 June 2020).

CFIA. 2015. Canadian Food Inspection Agency. RG-8 Regulatory Guidance: Contaminants in Feed (formerly RG-1, Chapter 7) [WWW Document]. URL https://inspection.canada.ca/animal-health/livestock-feeds/regulatory-guidance/rg-8/eng/1347383943203/1347384015909?chap=0 (accessed 12.28.21).

Cowger, C., J. Patton-Özkurt, G. Brown-Guedira, and L. Perugini. 2009. Post-anthesis moisture increased Fusarium Head Blight and deoxynivalenol levels in North Carolina winter wheat. Phytopathology **99**: 320–327. doi: 10.1094/Phyto-99-4-0320.

Crippin, T. 2019. Comparative analysis of *Fusarium Graminearum* strain genotype and chemotype from grains sampled during the 2015-2017 Ontario harvests. MSc Thesis, Carlton University, doi: 10.22215/etd/2019-13634.

De Wolf, E.D., L.V. Madden, and P.E. Lipps. 2003. Risk assessment models for wheat Fusarium Head Blight epidemics based on within-season weather data. Phytopathology **93**: 428–435. doi: 10.1094/Phyto.2003.93.4.428.

Del Ponte, E.M., J.M.C. Fernandes, and W. Pavan. 2005. A risk infection simulation model for Fusarium Head Blight of wheat. Fitopatol. Bras. **30**: 634–642. doi: 10.1590/S0100-41582005000600011.

Dexter, J.E., R.M. Clear, and K.R. Preston. 1996. Fusarium Head Blight: Effect on the milling and baking of some Canadian wheats. Is **6:** 695–701.

ECCC. 2021. Historical Data - Climate - Environment and Climate Change Canada. [Online] Available at https://climate.weather.gc.ca/historical_data/search_historic_data_e.html (accessed 16 November 2021).

Van der Fels-Klerx, H.J. 2014. Evaluation of performance of predictive models for deoxynivalenol in wheat: Models for deoxynivalenol in wheat. Risk Anal. **34**: 380–390. doi: 10.1111/risa.12103.

Fienberg, S.E. 2005. Contingency tables and log-linear models. In: Kempf-Leonard, K., editor, Encyclopedia of Social Measurement. Elsevier, New York. p. 499–506

Franz, E., K. Booij, and I. Van der Fels-Klerx. 2009. Prediction of deoxynivalenol content in Dutch winter wheat. J. Food Prot. **72**: 2170–2177. doi: 10.4315/0362-028X-72.10.2170.

Froment, A., P. Gautier, A. Nussbaumer, and A. Griffiths. 2011. Forecast of mycotoxins levels in soft wheat, durum wheat and maize before harvesting with Qualimètre®. J. Für Verbraucherschutz Leb. **6**: 277–281. doi: 10.1007/s00003-010-0655-2.

Gilbert, J., A. Brûlé-Babel, A.T. Guerrieri, R.M. Clear, S. Patrick, et al. 2014. Ratio of 3-ADON and 15-ADON isolates of *Fusarium graminearum* recovered from wheat kernels in Manitoba from 2008 to 2012. Can. J. Plant Pathol. **36**: 54–63. doi: 10.1080/07060661.2014.887033.

Gilbert, J., and A. Tekauz. 2011. Strategies for management of Fusarium Head Blight (FHB) in cereals. Prairie Soils and Crops J. **4**: 97–104.

Giroux, M.-E., G. Bourgeois, Y. Dion, S. Rioux, D. Pageau, et al. 2016. Evaluation of forecasting models for Fusarium Head Blight of wheat under growing conditions of Quebec, Canada. Plant Dis. **100**: 1192–1201. doi: 10.1094/PDIS-04-15-0404-RE.

Góral, T., H. Wiśniewska, P. Ochodzki, L. Nielsen, D. Walentyn-Góral, et al. 2018. Relationship between Fusarium Head Blight, Kernel Damage, concentration of *Fusarium* biomass, and *Fusarium* toxins in grain of winter wheat inoculated with *Fusarium culmorum*. Toxins **11**: 2. doi: 10.3390/toxins11010002.

Gourdain, E., and P. Rosengarten. 2011. Effects of infection time by *Fusarium graminearum* on ear blight, deoxynivalenol and zearalenone production in wheat. Plant Breed. Seed Sci. **63**. doi: 10.2478/v10129-011-0017-y.

Government of Alberta. 2021. Alberta *Fusarium graminearum* management plan. [Online] Available at https://www.alberta.ca/alberta-Fusarium-graminearum-management-plan.aspx (accessed 16 November 2021).

Guo, X. 2008. Development of models to predict Fusarium Head Blight disease and deoxynivalenol in wheat, and genetic causes for chemotype diversity and shifting of *Fusarium graminearum* in Manitoba. PhD Thesis, [Online] Available at https://mspace.lib.umanitoba.ca/xmlui/handle/1993/21115 (accessed 16 Jan 2022).

Hooker, D.C., A.W. Schaafsma, and L. Tamburic-Ilincic. 2002. Using Weather variables pre- and post-heading to predict deoxynivalenol content in winter wheat. Plant Dis. **86**: 611–619. doi: 10.1094/PDIS.2002.86.6.611.

Kochiieru, Y., A. Mankevičienė, J. Cesevičienė, R. Semaškienė, Z. Dabkevičius, et al. 2020. The influence of harvesting time and meteorological conditions on the occurrence of *Fusarium* species and mycotoxin contamination of spring cereals. J. Sci. Food Agric. **100**: 2999–3006. doi: 10.1002/jsfa.10330.

MARD. 2021a. Fusarium Head Blight Report-Manitoba Agriculture and Resource Development. Prov. Manit. - Agric. [Online] Available at https://www.gov.mb.ca/agriculture/ (accessed 16 November 2021).

MARD. 2021b. Manitoba Ag Weather Program- Manitoba Agriculture and Resource Development. Prov. Manit. - Agric. [Online] Available at https://www.gov.mb.ca/agriculture/ (accessed 17 November 2021).

McMullen, M., R. Jones, and D. Gallenberg. 1997. Scab of Wheat and Barley: A re-emerging disease of devastating impact. Plant Dis. **81**: 1340–1348. doi: 10.1094/PDIS.1997.81.12.1340.

Miedaner, T., R. Kalih, M.S. Großmann, and H.P. Maurer. 2016. Correlation between Fusarium Head Blight severity and DON content in triticale as revealed by phenotypic and molecular data (H. Bürstmayr, editor). Plant Breed. **135**: 31–37. doi: 10.1111/pbr.12327.

Moreno-Amores, J., S. Michel, F. Löschenberger, and H. Buerstmayr. 2020. Dissecting the contribution of environmental influences, plant phenology, and disease resistance to improving genomic predictions for Fusarium Head Blight resistance in wheat. Agronomy **10**: 2008. doi: 10.3390/agronomy10122008.

Nita, M., editor. 2013. Fungicides - Showcases of integrated plant disease management from around the world. Intech, London, 342 p. [Online] Available at https://www.intechopen.com/books/2917 doi: 10.5772/3251.

Paul, P.A., P.E. Lipps, and L.V. Madden. 2005. Relationship between visual estimates of Fusarium Head Blight intensity and deoxynivalenol accumulation in harvested wheat grain: a meta-analysis. Phytopathology **95**: 1225–1236. doi: 10.1094/Phyto-95-1225.

Rossi, V., S. Giosuè, E. Pattori, F. Spanna, and A. Del Vecchio. 2003. A model estimating the risk of Fusarium Head Blight on wheat. EPPO Bull. **33**: 421–425. doi: 10.1111/j.1365-2338.2003.00667. x.

Schaafsma, A.W., and D.C. Hooker. 2007. Climatic models to predict occurrence of *Fusarium* toxins in wheat and maize. Int. J. Food Microbiol. **119**: 116–125. doi: 10.1016/j.ijfoodmicro.2007.08.006.

Shah, D.A., E.D. De Wolf, P.A. Paul, and L.V. Madden. 2019. Functional data analysis of weather variables linked to Fusarium Head Blight epidemics in the United States. Phytopathology **109**: 96–110. doi: 10.1094/Phyto-11-17-0386-R.

Shah, D.A., J.E. Molineros, P.A. Paul, K.T. Willyerd, L.V. Madden and E.D. De Wolf. 2013. Predicting Fusarium Head Blight Epidemics with weather-driven pre- and post-anthesis logistic regression models. Phytopathology **103**: 906–919. doi: 10.1094/Phyto-11-12-0304-R.

Shipe, M.E., S.A. Deppen, F. Farjah, and E.L. Grogan. 2019. Developing prediction models for clinical use using logistic regression: an overview. J. Thorac. Dis. **11**: S574–S584. doi: 10.21037/jtd.2019.01.25.

SWDC. 2021. Fusarium Resources- Saskatchewan Wheat Development Commission. Sask Wheat Dev. Comm. [Online] Available at https://saskwheat.ca/Fusarium-resources (accessed 16 November 2021).

Wegulo, S.N., P.S. Baenziger, J. Hernandez Nopsa, W.W. Bockus, and H. Hallen-Adams. 2015. Management of Fusarium Head Blight of wheat and barley. Crop Prot. **73**: 100–107. doi: 10.1016/j.cropro.2015.02.025.

Xu, X., P. Nicholson, and A. Ritieni. 2007. Effects of fungal interactions among Fusarium Head Blight pathogens on disease development and mycotoxin accumulation. Int. J. Food Microbiol. **119**: 67–71. doi: 10.1016/j.ijfoodmicro.2007.07.027.

5. OVERALL SYNTHESIS

5.1 Conclusion and Recommendations

Fusarium Head Blight (FHB) disease is a major wheat and barley disease that reduces yield and quality, posing a major threat to global food and feed security. FHB epidemics can be managed more effectively with the help of decision-support tools based on disease monitoring models and weather variables, which can reduce harmful side effects of excessive fungicide applications and ensure economic benefits to the producer. The overall goal of this project was to develop and validate weather-based FHB risk models in western Canadian cereal production. In Chapter 2, the relationship between disease indicators (FHBi, FDK, and DON) was examined, and the effect of cultivars on disease indicators used in the development of the FHB models was also evaluated. The results of Chapter 2 showed that there was no correlation between FHBi and FDK or FHBi and DON in all crop types except durum. Visual estimation-based disease evaluation may have limitations due to the variability of estimates from different evaluators. This may also result in ineffective disease forecasting and prevention strategies due to the subjectivity of the estimation. As a result of the findings in Chapter 2 and the supporting literature, it was recommended that FHB modelling not rely exclusively on FHBi. Disease-damage factors such as FDK and DON may be more informative because they are currently used by the Canadian grain commission for grading (FDK) or cause downgrading or rejection of grain during marketing by some buyers (DON). The effect of different levels of FHB resistance by variety was not significant for FHBi and FDK. The effect could have been masked by the low disease pressure, likely due to the dry and hot weather conditions experienced at most sites during the study period. In the long term, with continuous data collection, the cultivar effect on FHB disease resistance will likely become more apparent and play a significant role in FHB prediction.

The objectives of Chapter 3 were to develop FHBi, FDK, and DON weather-based models for wheat and barley in western Canada. The prediction accuracy of the models for FHBi in wheat and barley was greater than 70%. Rainfall, relative humidity, and temperature were not significant in any FHBi model when used alone but produced satisfactory results when used in combination. However, FDK models for spring wheat and durum performed best when relative humidity was used as the sole predictor variable. A critical factor to consider was the number of variables included in the models and the need to balance simplicity and disease risk prediction accuracy. Models with few variables were preferred over models with many variables. The accuracy of FDK models varied between 77 and 89%. Similarly, DON models for durum used relative humidity values from 10 and 14 days prior to mid-anthesis and had a prediction accuracy of between 75% and 82%. In Chapter 4, these selected models were validated using an independent dataset collected in the same years as those for model development but from more than 200 producer fields in western Canada. These models produced satisfactory results, with prediction accuracy ranging from 70 to 100% for the FHBi, 66 to 89% for the FDK, and 75 to 82% for the DON. However, the sensitivity of the models was infinite or low because there were no or few epidemic cases to predict. More data from high disease pressure years is required to test these models for their sensitivity.

The FHB models developed in this study will be used as a starting point in the customized online viewer (FHB risk tool) that is currently under development. This tool will allow producers to select crop type, variety, field location, and assessment date that corresponds to 50% anthesis and local weather data. Following the selection of these inputs, the FHB risk tool will provide users with the probability of FHB epidemic using the models developed in this study and real-time weather data from more than 500 weather stations across western Canada. When the probability of FHB

epidemic is high (at or above the epidemic threshold), producers can take steps such as field scouting to determine the need for a fungicide application to avoid yield or downgrading losses. Thus, the FHB epidemic warning system will assist producers to increase wheat and barley production, sustainability and profitability by spraying only when needed and avoiding unnecessary fungicide expenditures when yield and quality loss are unlikely.

Several factors may be considered to improve the prediction accuracy of the models and delivery of the FHB risk tool. First, accounting for FHB species could improve the model's prediction accuracy. Climate variation currently being experienced may impact the distribution and intensity of FHB epidemics. Climate variation can affect pathogen biology directly or indirectly via host development and phenology (Hooker et al., 2002; Shah et al., 2019a). The prediction models for FHBi and DON in this study did not account for the effect of FHB species or chemotypes, which may affect prediction results, particularly for DON levels, due to the difference in DON production between the 3-ADON and I5-ADON chemotypes. Additional research may be required to ascertain the distribution of *Fusarium* species within and between provinces, given the observed shift in chemotypes in the prairies (Oghenekaro et al., 2021), and to incorporate this information into FHB modelling.

Second, another critical factor in FHB modelling is the date of 50% anthesis, as FHB infects wheat and barley mainly during anthesis. Although we are confident that the actual anthesis date that was estimated for each field was within a day or two of the actual mid-anthesis date, the model could be improved with a more accurate estimate of mid-anthesis date for each field. Several agronomic factors influence the timing and duration of the mid-anthesis date within and between fields, including cultivar, tillage, planting date, and weather. For this reason, producers need to estimate the heading date as accurately as possible to improve FHB prediction and the timing of fungicide

application. Additionally, the FHB weather-based prediction tool should incorporate crop growth models (thermal models), which will aid producers in estimating heading or anthesis dates based on planting date in cases where direct observations are difficult. However, it should be noted that the most accurate method for determining 50% anthesis and heading dates is through direct observation.

Thirdly, the defined epidemic thresholds used in this study correspond to the FDK levels that downgrades grain from No. 1 grade for each crop or DON thresholds, which result in buyer downgrading or rejection during marketing. Using this approach, fungicide treatments should be applied only when weather conditions are favorable to exceed these thresholds, which will result in loss of revenue for producers. Thus, the FHB risk models have been designed so that when they indicate high risk of an epidemic, significant economic losses can be minimized by applying fungicide, but when the risk of an epidemic is low, unnecessary costs for fungicide treatment can be avoided. In Chapter 4, the De Wolf models utilizing an FHBi ≥ 10% threshold were validated using producer field samples collected in western Canada. The De Wolf I model in spring wheat had the lowest accuracy of 57%. Errors associated with these models were mainly false positives, which may result in the unnecessary application of fungicides. Fungicides are an additional cost to growers, and in areas and years with low disease pressure, growers may not derive an increase in yields or an economic benefit from fungicide use. The developed FHBi models in this study used a 5% FHBi threshold, which has been used by other researchers. The FHBi thresholds are linked to yield and DON levels, resulting in economic loss, but this study found no correlation between these disease indicators. Therefore, FHBi thresholds need to be used with caution. Further studies are required to quantify the percentage of disease damage (yield, FDK, or DON) when FHBi is either ≥ 10 or 5%.

Fourth, the type of weather variables and the quality of measured data from different weather stations are important considerations for these FHB weather-based prediction models. Weather station networks in western Canada are diverse, with over 500 stations monitored by ECCC, MARD, and ACIS. Temperature, rainfall, and RH are measured at multiple weather stations in real-time throughout western Canada and will be utilized in models developed in this study to provide a warning system for users. The distance between the producer field and the weather station was a related factor influencing the accuracy of the FHB models developed in this study in some crop types, notably when the distance exceeded 40 km. Estimation errors for temperature are lower than for moisture variables like relative humidity and rainfall, which are more challenging to estimate accurately from a long-distance away. Therefore, the distance between fields and weather stations should be considered when using weather-based models to estimate FHB risk. In conclusion, the models developed and validated in this study are critical to improve the management of FHB in western Canada. These models will reduce unnecessary fungicide applications and FHB disease-related losses in western Canada.

5.2 References

Hooker, D.C., A.W. Schaafsma, and L. Tamburic-Ilincic. 2002. Using weather variables pre- and post-heading to predict deoxynivalenol content in winter wheat. Plant Dis. **86**: 611–619. doi: 10.1094/PDIS.2002.86.6.611.

Oghenekaro, A.O., M.A. Oviedo-Ludena, M. Serajazari, X. Wang, M.A. Henriquez, N.G. Wenner, G.A. Kuldau, A. Navabi, H.R. Kutcher and W.G.D. Fernando. 2021. Population genetic structure and chemotype diversity of *Fusarium graminearum* populations from wheat in Canada and North Eastern United States. Toxins **13**: 180. doi: 10.3390/toxins13030180.

Shah, D.A., E.D. De Wolf, P.A. Paul, and L.V. Madden. 2019. Functional data analysis of weather variables linked to Fusarium Head Blight epidemics in the United States. Phytopathology **109**: 96–110. doi: 10.1094/Phyto-11-17-0386-R.

APPENDICES

Appendix 2. FHB occurrences in winter wheat, spring wheat barley, and durum in various locations throughout western Canada in 2019 and 2020 (Chapter 2).

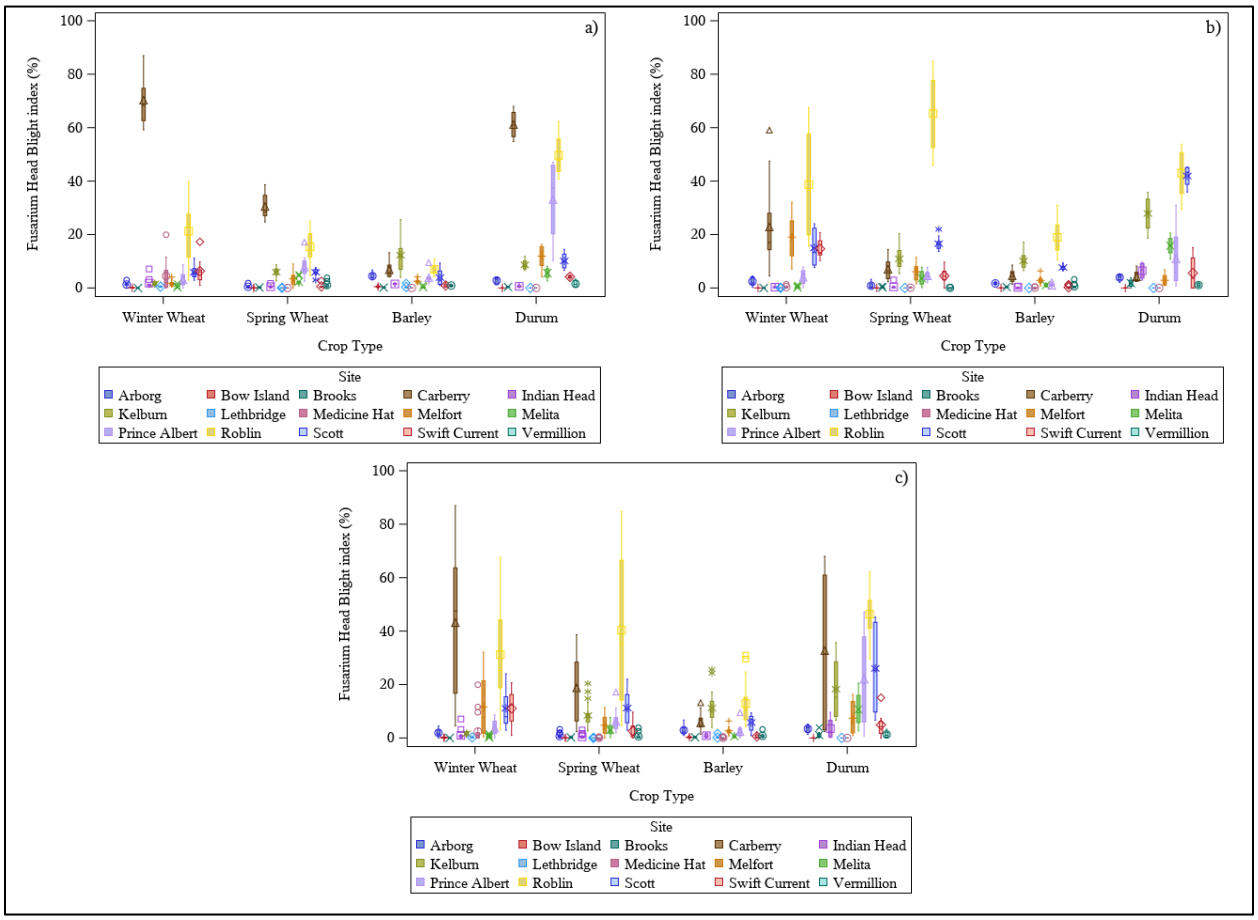

Figure A2. 1. Occurrence of Fusarium Head Blight at small-plot research sites for winter wheat, spring wheat, barley, and durum in 2019 (a), 2020 (b), and 2019 and 2020 combined (c). Location of research sites is shown in Figure 2.1.

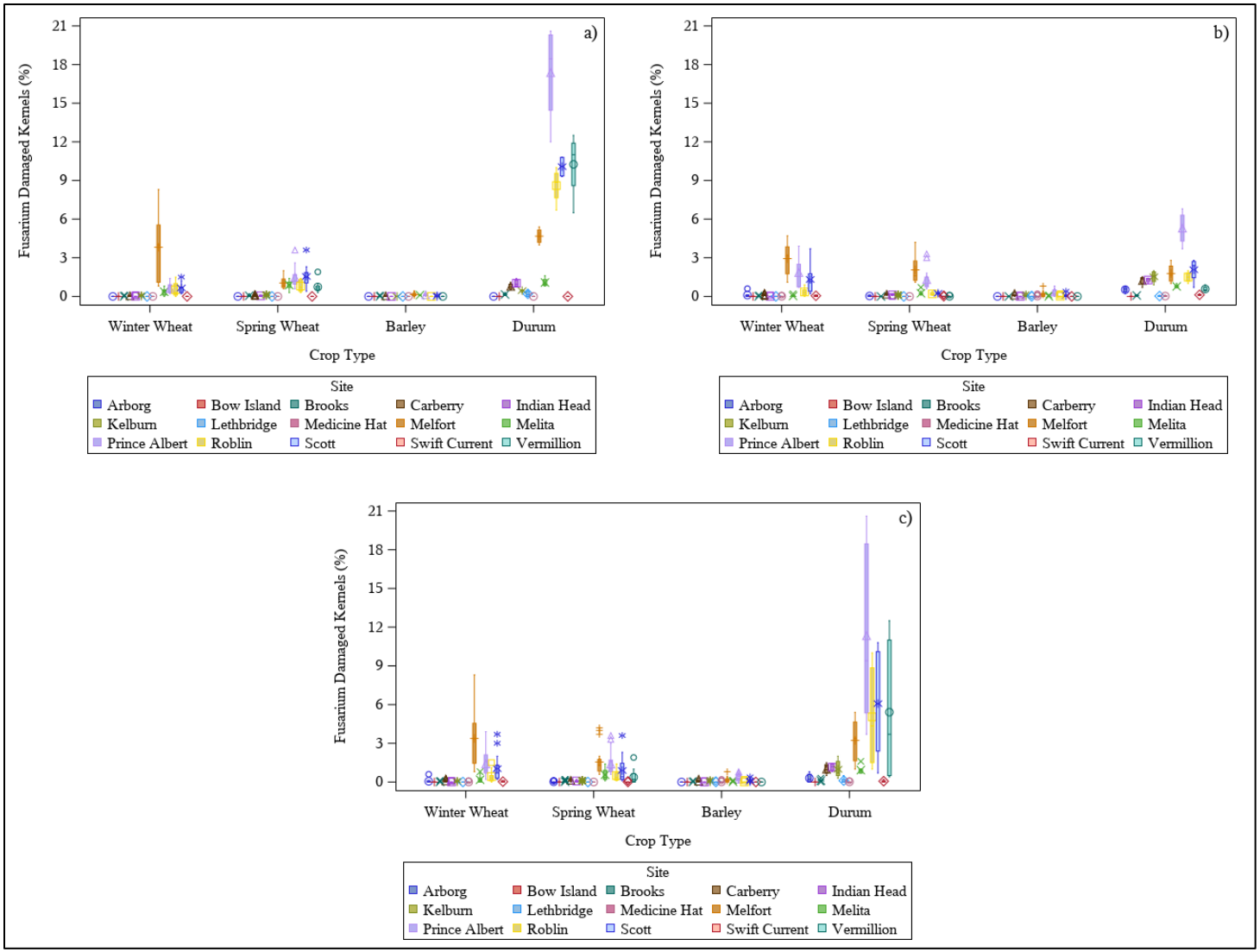

Figure A2. 2. Occurrence of Fusarium damaged kernels at small-plot research sites for winter wheat, spring wheat, barley, and durum in 2019 (a) 2020 (b) and 2019 and 2020 combined (c). Location of research sites is shown in Figure 2.1.

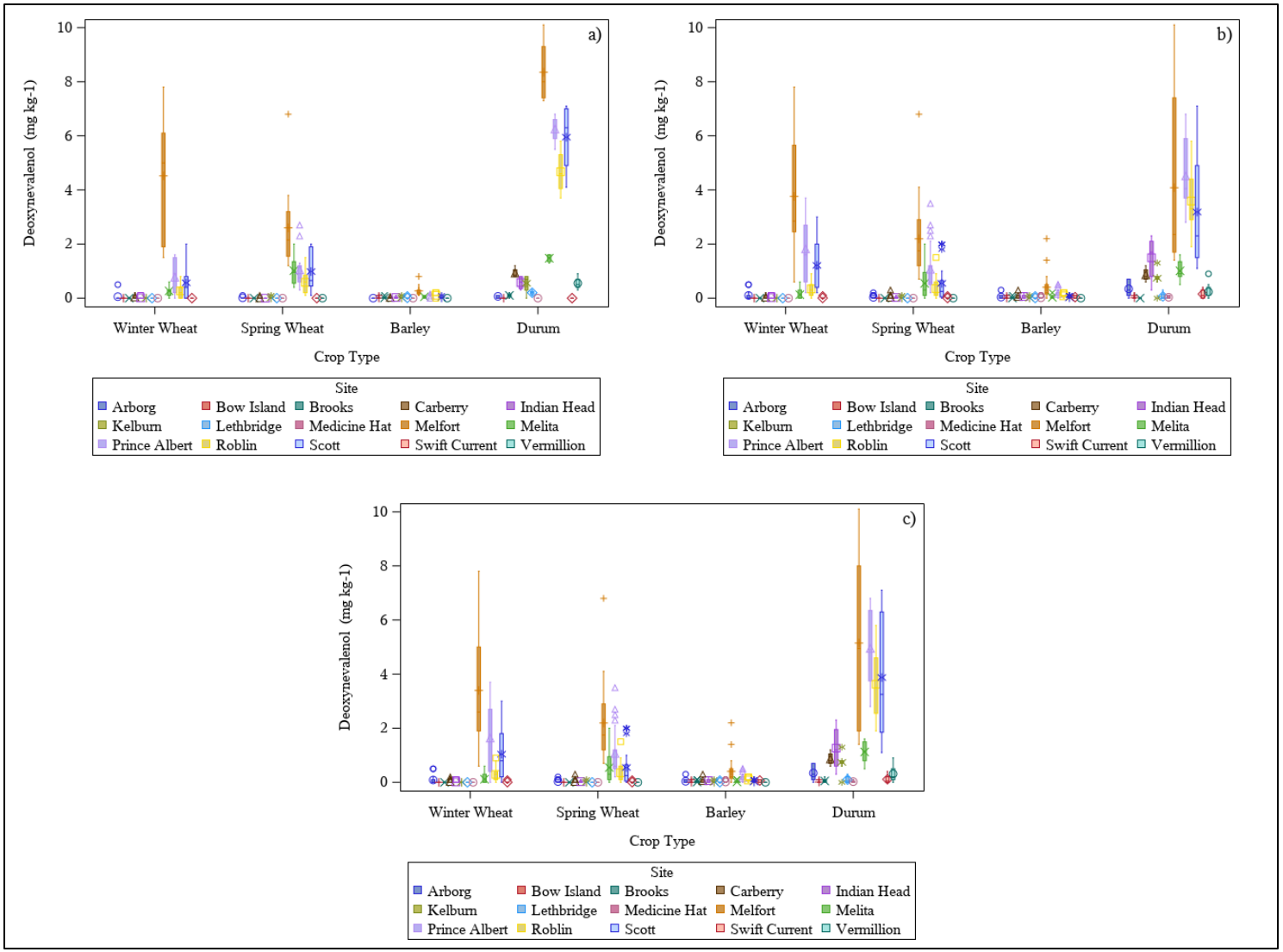

Figure A2. 3. Occurrence of deoxynivalenol at small-plot research sites for winter wheat, spring wheat, barley, and durum in 2019 (a) 2020 (b) and 2019 and 2020 combined (c) in the prairie. Location of research sites is shown in Figure 2.1.

Appendix 3. 1. Description and Selection of Weather Predictors Variables (Chapter 3)

Table A3.1. 1. Weather variables of potential importance for FHB infection in different wheat and barley crop types.

4 days pre-anthesis	7 days pre-anthesis	10 days pre-anthesis	14 days pre-anthesis	3 days pre & post-anthesis	Description
R4MA[a]	R57MA	R10MA	R14MA	R3MAPA[b]	Mean daily rainfall (mm)
R034MA	R037MA	R0310MA	R0314MA	R033MAPA	Duration (h) rainfall ≥ 0.3mm
R54MA	R7MA	R510MA	R514MA	R53MAPA	Duration (h) rainfall ≥ 5mm
RH4MA	RH7MA	RH10MA	RH14MA	RH3MAPA	Mean daily relative humidity (%)
RH804MA	RH807MA	RH8010MA	RH8014MA	RH803MAPA	Duration (h) RH ≥ 80 %
RH904MA	RH907MA	RH9010MA	RH9014MA	RH903MAPA	Duration (h) RH ≥ 90 %
RHmax4MA	RHmax7MA	RHmax10MA	RHmax14MA	RHmax3MAPA	Mean daily maximum relative humidity (%)
RHmin4MA	RHmin7MA	RHmin10MA	RHmin14MA	RHmin3MAPA	Mean daily minimum relative humidity (%)
SR4MA	SR7MA	SR10MA	SR14MA	SR3MAPA	Mean daily Solar Radiation (Wm^2)
T15304MA	T15307MA	T10MA	T14MA	T3MAPA	Duration (h) air temperature 15 ≤ T ≤ 30 ^oC
T252804MA	T252807MA	T153010MA	T153014MA	T153003MAPA	Duration (h) air temperature 25 ≤ T ≤ 28 ^oC
T4MA	T7MA	T252810MA	T252814MA	T252803MAPA	Mean daily temperature (^{o} C)
Tmax4MA	Tmax7MA	Tmax10MA	Tmax14MA	Tmax3MAPA	Mean daily maximum temperature (%)
Tmin4MA	Tmin7MA	Tmin10MA	Tmin14MA	Tmin3MAPA	Mean daily minimum temperature (%)
TRH804MA	TRH807MA	TRH8010MA	TRH8014MA	TRH803MAPA	Duration (h) air temperature 15 ≤ T ≤ 30^{o}C, and RH ≥ 80 %
TRH904MA	TRH907MA	TRH9010MA	TRH9014MA	TRH903MAPA	Duration (h) air temperature 15 ≤ T ≤ 30^{o}C, and RH ≥ 90 %

[a]Mean daily rainfall 4 days before mid-anthesis (MA). Mid-anthesis is when 50% of the flowers are extruded on the head.

[b]Mean daily rainfall between 3 days before mid-anthesis and 3 days post mid-anthesis (MAPA). Variables for barley were calculated at intervals around mid-heading (MH) and pre-, and post-mid-heading (MHPH).

Table A3.1. 2. Potential weather variables for Fusarium Head Blight index models. Only variables with Kendall values in boldface were selected by stepwise regression procedure.

	Winter wheat		Spring wheat		Barley		Durum	
	Kendall	p-value	Kendall	p-value	Kendall	p-value	Kendall	p-value
RH4MA	**0.29**	<.0001	0.32	<.0001	-[a]	-	-	-
RH804MA	**0.25**	<.0001	**0.31**	<.0001	-	-	-	-
RH904MA	0.25	<.0001	0.31	<.0001	-	-	-	-
RHmax4MA	-	-	**0.3**	<.0001	-	-	-	-
RHmin4MA	**0.3**	<.0001	0.27	<.0001	-	-	-	-
R034MA	-	-	**0.25**	<.0001	-	-	-	-
R4MA	-	-		-	**0.21**	0.0006	-	-
RH804MA	-	-	**0.21**	<.0001	-	-	-	-
R14MA	**0.23**	<.0001	**0.21**	<.0001	-	-	**0.21**	0.0096
T15304MA	-	-	-	-	0.34	<.0001	-	-
T252804MA	-	-	**0.26**	<.0001	-	-	**0.3**	<.0001
T4MA	-	-	-	-	**0.33**	<.0001	0.28	<.0001
Tmin4MA	**0.32**	<.0001	0.27	<.0001	0.33	<.0001	**0.33**	<.0001
TRH804MA	**0.34**	<.0001	0.34	<.0001	-	-	**0.28**	<.0001
TRH904MA	0.36	<.0001	**0.28**	<.0001	-	-	**0.36**	<.0001
Tmin4MA	-	-	-	-	**0.33**	<.0001	-	-
Tmin14MA	**0.33**	<.0001	-	-	-	-	-	-
RH807MA	**0.28**	<.0001	-	-	-	-	-	-
RH907MA	0.28	<.0001	-	-	-	-	-	-
RHmax7MA	-	-	**0.3**	<.0001	-	-	0.25	<.0001
RH7MA	0.36	<.0001	**0.23**	<.0001	-	-	**0.25**	0.0002
RH807MA	**0.28**	<.0001	-	-	-	-	-	-
T15307MA	**0.31**	<.0001	**0.3**	<.0001	0.33	<.0001	0.33	<.0001
T252807MA	**0.39**	<.0001	**0.25**	<.0001	-	-	0.3	<.0001
TRH807MA	-	-	0.4	<.0001	0.34	<.0001	**0.4**	<.0001
TRH907MA	**0.42**	<.0001	**0.33**	<.0001	**0.35**	<.0001	-	-
Tmax7MA	-	-	-	-	**0.26**	<.0001	**0.3**	<.0001
Tmin7MA	**0.36**	<.0001	**0.34**	<.0001	**0.28**	<.0001	**0.39**	<.0001
T7MA	**0.24**	<.0001	**0.26**	<.0001	**0.31**	<.0001	**0.36**	<.0001
T7MA	**0.24**	<.0001	-	-	**0.31**	<.0001	-	-
RHmax10MA	-	-	-	-	**0.21**	<.0001	-	-
Tmin10MA	**0.3**	<.0001	**0.4**	<.0001	**0.27**	<.0001	-	-
T10MA	**0.26**	<.0001	**0.3**	<.0001	0.25	<.0001	-	-
TRH8010MA	-	-	-	-	**0.33**	<.0001	-	-
Tmax10MA	-	-	-	-	**0.28**	<.0001	-	-
Tmin10MA	-	-	-	-	**0.27**	<.0001	-	-
R14MA	**0.23**	<.0001	-	-	-	-	-	-
RH8014MA	**0.42**	<.0001	0.32	<.0001	-	-	-	-
RH9014MA	0.42	<.0001	**0.32**	<.0001	-	-	-	-
R0314MA	0.33	<.0001	-	-	-	-	-	-
RHmax14MA	-	-	**0.31**	<.0001	-	-	-	-
RH14MA	-	-	-	-	-	-	**0.22**	0.0015

T153014MA	**0.26**	<.0001	**0.32**	<.0001	**0.3**	<.0001	**0.4**	<.0001
TRH8014MA	**0.43**	<.0001	**0.42**	<.0001	**0.32**	<.0001	**0.42**	<.0001
TRH9014MA	**0.44**	<.0001	**0.41**	<.0001	**0.34**	<.0001	0.45	<.0001
T252814MA	-	-	**0.24**	0.0003	-	-	**0.23**	0.0067
RH3MAPA	**0.38**	<.0001	**0.36**	<.0001	-	-	**0.24**	0.0006
RH803MAPA	**0.31**	<.0001	0.29	<.0001	-	-	-	-
RH903MAPA	0.31	<.0001	0.29	<.0001	-	-	-	-
RHmax3MAPA	**0.29**	<.0001	0.36	<.0001	**0.38**	<.0001	0.24	0.0005
RHmin3MAPA	**0.41**	<.0001	**0.33**	<.0001	-	-	**0.24**	0.0004
RHmin3MAPA	-	-	-	-	**0.23**	0.0005	-	-
R033MAPA	-	-	**0.21**	<.0001	-	-	-	-
R3MAPA	-	-	-	-	-	-	**0.21**	0.0051
T153003MAPA	-	-	0.39	<.0001	0.35	<.0001	0.35	<.0001
Tmin3MAPA	-	-	**0.43**	<.0001	**0.28**	<.0001	**0.4**	<.0001
TRH803MAPA	0.32	<.0001	0.49	<.0001	**0.36**	<.0001	0.35	<.0001
TRH903MAPA	0.34	<.0001	**0.5**	<.0001	**0.39**	<.0001	**0.31**	<.0001
T3MAPA	-	-	-	-	-	-	**0.31**	-
TRH903MAPA	-	-	**0.50**	<.0001	-	-	-	-

[a]Variables with Kendall correlation less than 0.21.

Table A3.1. 3. Weather variables of potential value for Fusarium damaged kernels models for spring wheat and durum crop types. Only variables with Kendall values in boldface were selected by stepwise regression procedure.

	SWFDK		DUFDK	
Variable	Kendall	p-value	Kendall	p-value
RH804MA	**0.49**	<.0001	0.28	<.0001
RH904MA	0.49	<.0001	0.28	<.0001
TRH804MA	**0.34**	<.0001	**0.31**	<.0001
TRH904MA	0.30	<.0001	**0.31**	<.0001
R034MA	0.29	<.0001	-	<.0001
Tmin4MA	-[a]	-	**0.28**	<.0001
RHmax4MA	0.41	<.0001	0.35	<.0001
RHmin4MA	0.41	<.0001	0.44	<.0001
RH4MA	0.49	<.0001	**0.43**	<.0001
RH807MA	0.43	<.0001	**0.45**	<.0001
RH907MA	0.43	<.0001	**0.45**	<.0001
TRH807MA	**0.42**	<.0001	0.30	<.0001
TRH907MA	0.39	<.0001	0.28	<.0001
RHmax7MA	0.47	<.0001	0.39	<.0001
RHmin7MA	**0.43**	<.0001	0.52	<.0001
RH7MA	**0.46**	<.0001	**0.53**	<.0001
RHmax10MA	0.45	<.0001	**0.51**	<.0001
RHmin10MA	0.41	<.0001	**0.43**	<.0001
RH10MA	**0.46**	<.0001	0.51	<.0001
RH8010MA	**0.37**	<.0001	**0.50**	<.0001
RH9010MA	0.37	<.0001	0.50	<.0001
TRH8010MA	**0.43**	<.0001	0.36	<.0001
TRH9010MA	0.39	<.0001	**0.28**	<.0001
RHmax14MA	**0.48**	<.0001	0.51	<.0001
RHmin14MA	**0.40**	<.0001	**0.44**	<.0001
RH14MA	**0.47**	<.0001	0.51	<.0001
RH8014MA	**0.51**	<.0001	**0.49**	<.0001
RH9014MA	**0.51**	<.0001	0.49	<.0001
TRH8014MA	**0.45**	<.0001	**0.38**	<.0001
TRH9014MA	0.40	<.0001	**0.31**	<.0001
Tmin3MAPA	0.29	<.0001	**0.28**	<.0001
RHmax3MAPA	**0.38**	<.0001	**0.38**	<.0001
RHmin3MAPA	**0.51**	<.0001	**0.56**	<.0001
RH3MAPA	**0.46**	<.0001	0.53	<.0001
RH803MAPA	**0.34**	<.0001	**0.47**	<.0001
RH903MAPA	0.34	<.0001	0.47	<.0001
T153003MAPA	-	-	0.23	<.0001
TRH803MAPA	**0.37**	<.0001	**0.38**	<.0001
TRH903MAPA	**0.43**	<.0001	0.34	<.0001

[a]Variables with Kendall correlation less than 0.21.

Table A3.1. 4. Weather variables of potential value for deoxynivalenol in durum. Only variables with Kendall values in boldface were selected by stepwise regression procedure.

Variable	Kendall	p-value
RH804MA	**0.30**	<.0001
RH904MA	0.30	<.0001
T15304MA	**0.24**	<.0001
TRH804MA	**0.39**	<.0001
TRH904MA	**0.37**	<.0001
Tmin4MA	**0.26**	<.0001
RHmax4MA	0.32	<.0001
RHmin4MA	**0.44**	<.0001
RH4MA	**0.44**	<.0001
T4MA	**0.27**	<.0001
RH807MA	0.41	<.0001
RH907MA	0.41	<.0001
TRH807MA	0.37	<.0001
TRH907MA	**0.35**	<.0001
RHmax7MA	**0.37**	<.0001
RHmin7MA	**0.52**	<.0001
RH7MA	**0.51**	<.0001
RHmax10MA	0.43	<.0001
RHmin10MA	**0.43**	<.0001
RH10MA	0.49	<.0001
RH8010MA	0.48	<.0001
RH9010MA	0.48	<.0001
TRH8010MA	**0.45**	<.0001
TRH9010MA	0.35	<.0001
RHmax14MA	0.43	<.0001
RHmin14MA	**0.45**	<.0001
RH14MA	0.45	<.0001
RH8014MA	**0.44**	<.0001
RH9014MA	0.44	<.0001
T153014MA	**0.24**	<.0001
TRH9014MA	**0.38**	<.0001
Tmin3MAPA	**0.35**	<.0001
RHmax3MAPA	**0.37**	<.0001
RHmin3MAPA	**0.53**	<.0001
RH3MAPA	**0.49**	<.0001
RH803MAPA	**0.46**	<.0001
RH903MAPA	0.46	<.0001
T153003MAPA	**0.29**	<.0001
TRH803MAPA	0.49	<.0001
TRH903MAPA	**0.42**	<.0001

Table A3.1. 5 Multicollinearity diagnosis indexes for predictor variables used in the winter wheat, spring wheat, barley, and durum Fusarium Head Blight index models.

Model	Variable	Tolerance	Variance Inflation	Eigen value
	winter wheat			
WWFHB1	RH807MA	0.55	1.8	0.08
	Tmin7MA	0.21	9.3	0.02
	T7MA	0.31	7.0	0.00
WWFHB3	RH9014MA	0.78	1.3	0.24
	Tmin14MAR14MA	0.78	1.3	0.07
WWFHB4	RHmin3MAPA	0.26	6.4	0.05
	RH803MAPA	0.26	6.4	0.00
	Spring wheat			
SWFHB1	RH804MA	0.49	2.0	0.59
	T252804MA	0.57	1.8	0.26
	TRH904MA	0.38	2.6	0.03
SWFHB2	RHmax14MA	0.98	1.0	0.53
	T252814MA	0.98	1.0	0.00
SWFHB3	RHmax14MA	0.98	1.0	0.62
	R14MA	0.99	1.0	0.23
	T252814MA	0.97	1.0	0.00
SWFHB5	TRH903MAPA	0.95	1.1	0.32
	R033MAPA	0.95	1.1	0.18
	Barley			
BAFHB1	Tmin14MA	0.99	1.0	0.20
	R14MA	0.92	1.1	0.02
	RH14MA	0.91	1.1	0.00
BAFHB2	T153014MA	0.95	1.0	0.21
	R14MA	0.88	1.1	0.03
	RH14MA	0.92	1.1	0.00
BAFHB3	RH804MA	0.59	1.7	0.79
	T252804MA	0.68	1.5	0.23
	TRH804MA	0.72	1.4	0.03
BAFHB4	R14MA	0.95	1.1	0.64
	T252814MA	0.95	1.1	0.11
BAFHB5	T3MAPA	0.98	1.0	0.44
	R3MAPA	0.98	1.0	0.01
	Durum			
DUFHB1	Tmin4MA	0.96	1.0	0.44
	R4MA	0.96	1.0	0.01
DUFHB2	T7MA	1.00	1.0	0.01
	RH7MA	1.00	1.0	0.00
DUFHB4	RHmax10MA	0.94	1.1	0.05
	Tmin10MATmax10MA	0.94	1.1	0.00
DUFHB5	RHmin3MAPA	0.89	1.1	0.02
	Tmin3MAPA	0.89	1.1	0.01

Table A3.1. 6. Multicollinearity diagnosis indexes for predictor variables used in the spring wheat and durum, Fusarium damaged kernels, and deoxynivalenol models.

Crop type	Model	Variable	Tolerance	Variance Inflation	Eigen value
		Fusarium damaged kernels			
Spring Wheat	SWFDK2	RH4MA	0.71	1.41	0.35
		TRH904MA	0.71	1.41	0.00
	SWFDK4	RH7MA	0.66	1.51	0.01
		RH7MAT7MA	0.66	1.51	0.00
Durum	DUFDK1	RH4MA	0.56	1.80	0.34
		T15304MA	0.29	3.49	0.02
		TRH904MA	0.23	4.42	0.00
	DUFDK4	RH7MA	0.72	1.39	0.39
		TRH907MA	0.76	1.32	0.17
		R037MA	0.93	1.08	0.00
	DUFDK7	TRH803MAPA	0.28	3.51	0.16
		Tmin3MAPA	0.28	3.51	0.00
		Deoxynivalenol			
Durum	DUDON1	T4MA	0.98	1.02	0.03
		RHmin4MA	0.98	1.02	0.01
	DUDON2	RH7MA	0.66	1.51	0.01
		RH7MAT7MA	0.66	1.51	0.00
	DUDON5	RH10MA	1.00	1.00	0.01
		T10MA	1.00	1.00	0.00
	DUDON7	TRH8014MA	0.78	1.28	0.19
		RH14MA	0.78	1.28	0.00

Appendix 3.2. Error Analysis of the Models

Table A3.2. 1. Errors in winter wheat Fusarium Head Blight index (FHBi) models' development dataset.

Model	Province	Site	Year	False Negatives[a]			False Negatives[b]		
				R	I	S	R	I	S
WWFHB1	Alberta	Medicine Hat	2019	1	1	1	-[c]	-	-
	Manitoba	Carberry	2019	3	3	3	-	-	-
	Manitoba	Roblin	2019	3	2	3	-	-	-
	Saskatchewan	Indian Head	2019	-	-	-	3	3	2
	Saskatchewan	Prince Albert	2019	1	1	1	-	-	-
	Saskatchewan	Scott	2019	1	1	3	-	-	-
	Saskatchewan	Swift Current	2019	-	-	-	2	1	1
	Manitoba	Arborg	2020	-	-	-	4	4	4
	Saskatchewan	Indian Head	2020	-	-	-	4	4	4
	Saskatchewan	Prince Albert	2020	-	-	-	3	4	2
WWFHB2	Alberta	Medicine Hat	2019	1	1	1	-	-	-
	Manitoba	Melita	2019	-	-	-	3	3	3
	Manitoba	Roblin	2019	-	-	-	-	1	-
	Saskatchewan	Indian Head	2019	-	-	-	3	3	2
	Saskatchewan	Melfort	2019	-	-	-	3	3	3
	Saskatchewan	Prince Albert	2019	-	-	-	2	2	2
	Saskatchewan	Scott	2019	-	-	-	2	2	-
	Saskatchewan	Swift Current	2019	-	-	-	2	1	1
	Manitoba	Arborg	2020	-	-	-	4	4	4
	Saskatchewan	Indian Head	2020	-	-	-	4	4	4
	Saskatchewan	Prince Albert	2020	-	-	-	4	2	2

[a]Number of samples incorrectly classified as non-epidemic yet epidemic in resistant (R), intermediate (I), and susceptible (S) FHB winter wheat varieties.

[b]Number of samples incorrectly classified as epidemic yet non-epidemic in resistant, intermediate, and susceptible FHB winter wheat varieties.

[c]No false positive or negative case.

Table A3.2. 2. Errors in spring wheat Fusarium Head Blight index models' development dataset.

Model	Province	Site	Year	False Negatives[a]			False Negatives[b]		
				MR	I	MS	MR	I	MS
SWFHB1	Alberta	Vermillion	2019	-[c]	-	-	4	4	4
	Manitoba	Kelburn	2019	-	-	-	-	-	3
	Manitoba	Melita	2019			1	-	-	-
	Manitoba	Roblin	2019	-	-	-	-	-	1
	Saskatchewan	Melfort	2019	-	-	-	2	4	4
	Saskatchewan	Prince Albert	2019	-	-	-	1	2	-
	Saskatchewan	Scott	2019	-	-	-	1	1	-
	Saskatchewan	Swift Current	2019	-	-	-	4	4	4
	Manitoba	Carberry	2020	3	2	3	-	-	-
	Manitoba	Melita	2020	-	-	-	4	3	1
	Manitoba	Roblin	2020	4	4	4	-	-	-
	Saskatchewan	Indian Head	2020	-	-	-	4	4	4
	Saskatchewan	Melfort	2020	-	-	-	1	2	2
	Saskatchewan	Prince Albert	2020	-	-	-	3	3	-
	Saskatchewan	Swift Current	2020	1	2	1	-	-	-
SWFHB2	Manitoba	Kelburn	2019	-	-	-	-	-	3
	Manitoba	Melita	2019	-	-	-	4	4	3
	Manitoba	Roblin	2019	-	-	-	-	-	1
	Saskatchewan	Melfort	2019	2	-	-	-	-	-
	Saskatchewan	Prince Albert	2019	-	-	-	1	2	-
	Saskatchewan	Scott	2019	-	-	-	1	1	-
	Alberta	Vermillion	2019	-	-	-	4	4	4
	Manitoba	Arborg	2020	-	-	-	4	4	4
	Manitoba	Carberry	2020	-	-	-	1	2	1
	Manitoba	Melita	2020	-	-	-	3	3	1
	Saskatchewan	Melfort	2020	-	-	-	-	-	-
	Saskatchewan	Prince Albert	2020	1	1	4	-	-	-
	Saskatchewan	Scott	2020	4	4	4	-	-	-
	Saskatchewan	Swift Current	2020	1	2	1	-	-	-

[a]Number of samples incorrectly classified as non-epidemic yet epidemic in moderately resistant (MR), intermediate (I), and moderately susceptible (MS) FHB spring wheat varieties.

[b]Number of samples incorrectly classified as epidemic yet non-epidemic in MR, I, and MS FHB spring wheat varieties.

[c]No false positive or negative case.

Table A3.2. 3. Barley Errors in barley Fusarium Head Blight index models' development dataset.

Model	Province	Site	Year	False Negatives[a]				False Negatives[b]		
				MR	I	MS		MR	I	MS
BAFHB3	Manitoba	Arborg	2019	-[a]	-	-	-	3	1	1
	Manitoba	Carberry	2019	-	-	-	-	1	2	2
	Saskatchewan	Indian Head	2019	-	-	-	-	4	4	4
	Manitoba	Kelburn	2019	-	-	-	-		1	1
	Manitoba	Melita	2019	-	-	-	-	4	4	4
	Saskatchewan	Prince Albert	2019	-	-	1	-	-	-	-
	Manitoba	Roblin	2019	3	4	3	-	-	-	-
	Saskatchewan	Scott	2019	3	-	-	-	-	-	-
	Manitoba	Arborg	2020	-	-	-	-	4	4	4
	Manitoba	Carberry	2020	-	-	-	-	1	3	4
	Saskatchewan	Melfort	2020	1	-	-	-	-	-	-
	Manitoba	Melita	2020	-	-	-	-	4	4	4
BAFHB4	Manitoba	Arborg	2019	-	-	-	-	3	2	1
	Manitoba	Carberry	2019	-	-	-	-	1	2	2
	Manitoba	Kelburn	2019	-	-	-	-		1	1
	Manitoba	Melita	2019	-	-	-	-	4	4	4
	Saskatchewan	Prince Albert	2019	-		1	-	-	-	-
	Manitoba	Roblin	2019	3	3	4	-	-	-	-
	Manitoba	Arborg	2020	-	-	-	-	4	4	4
	Alberta	Brooks	2020	-	-	-	-	4	4	4
	Manitoba	Carberry	2020	-	-	-	-	1	4	3

[a]No false positive or negative case.

Table A3.2. 4. Errors in durum Fusarium Head Blight index models' development dataset.

Model	Province	Site	Year	False Negative	False Positive
DUFHB1	Manitoba	Melita	2019	3	-
	Saskatchewan	Melfort	2019	-[a]	1
	Saskatchewan	Prince Albert	2019	4	-
	Manitoba	Arborg	2020	-	3
	Manitoba	Carberry	2020	1	-
	Saskatchewan	Indian Head	2020	2	-
	Saskatchewan	Melfort	2020	-	3
	Saskatchewan	Prince Albert	2020	2	-
	Saskatchewan	Swift Current	2020	2	-
DUFHB3	Manitoba	Melita	2019	-	3
	Saskatchewan	Indian Head	2019	-	4
	Saskatchewan	Melfort	2019	-	1
	Manitoba	Arborg	2020	-	3
	Manitoba	Carberry	2020	-	3
	Saskatchewan	Indian Head	2020	2	-
	Saskatchewan	Melfort	2020	-	3
	Saskatchewan	Prince Albert	2020	-	2
	Saskatchewan	Swift Current	2020	2	-

[a]No false positive or negative case.

Table A3.2. 5. Errors in spring wheat Fusarium damaged kernels models' development dataset.

Model	Province	Site	Year	False Negatives[a]			False Negatives[b]		
				MR	I	MS	MR	I	MS
SWFDK2	Manitoba	Carberry	2019	-[c]	-	-	4	4	4
	Saskatchewan	Indian Head	2019	-	-	-	4	4	4
	Saskatchewan	Melfort	2019	4	4	4	-	-	-
	Manitoba	Carberry	2020	-	-	2	-	-	-
	Saskatchewan	Indian Head	2020	-	-	-	4	4	4
	Alberta	Vermillion	2020	-	-	-	4	4	4
	Manitoba	Melita	2020	-	-	-	4	3	2
	Manitoba	Roblin	2020	1	1	2	-	-	-
	Saskatchewan	Scott	2020	-	-	-	4	2	1
SWFDK4	Saskatchewan	Melfort	2019	4	4	4	-	-	-
	Manitoba	Arborg	2020	-	-	-	4	4	4
	Manitoba	Carberry	2020	-	-	2	-	-	-
	Manitoba	Melita	2020	-	1	2	-	-	-
	Manitoba	Roblin	2020	-	-	-	3	3	2
	Saskatchewan	Scott	2020	-	-	-	4	2	1
	Alberta	Vermillion	2020	-	-	-	4	4	4

[a]Number of samples incorrectly classified as non-epidemic yet epidemic in moderately resistant (MR), intermediate (I), and moderately susceptible (MS) FHB spring wheat varieties.

[b]Number of samples incorrectly classified as epidemic yet non-epidemic in MR, I, and MS FHB spring wheat varieties.

[c]No false positive or negative case.

Table A3.2. 6. Errors in durum Fusarium damaged kernels models' development dataset.

Model	Province	Site	Year	False Negative	False Positive
DUFDK3	Saskatchewan	Melfort	2019	4	-[a]
	Manitoba	Kelburn	2020	1	-
	Manitoba	Roblin	2020	1	-
	Saskatchewan	Melfort	2020	-	3
	Saskatchewan	Scott	2020	-	1
	Alberta	Vermillion	2020	-	4
DUFDK5	Saskatchewan	Melfort	2019	4	-
	Manitoba	Carberry	2019	-	4
	Manitoba	Kelburn	2020	1	-
	Manitoba	Roblin	2020	-	3
	Manitoba	Melita	2020	-	4
	Saskatchewan	Swift Current	2020	-	4
	Saskatchewan	Melfort	2020	-	3
	Saskatchewan	Scott	2020	-	1
	Alberta	Vermillion	2020	-	4

[a]No false positive or negative case.

Table A3.2. 7. Errors in Durum deoxynivalenol models' development dataset.

Model	Province	Site	Year	False Negative	False Positive
DUFDK3	Manitoba	Carberry	2019	-[a]	3
	Saskatchewan	Indian Head	2019	-	4
	Alberta	Vermillion	2019	-	4
	Manitoba	Arborg	2020	-	4
	Manitoba	Carberry	2020	1	-
	Manitoba	Kelburn	2020	1	-
	Manitoba	Melita	2020	-	4
	Saskatchewan	Indian Head	2020	4	-
	Saskatchewan	Swift Head	2020	-	4
	Alberta	Vermillion	2020	-	4
DUFDK5	Manitoba	Carberry	2019	-	3
	Saskatchewan	Melfort	2019	4	-
	Alberta	Vermillion	2019	-	4
	Alberta	Vermillion	2020	-	4
	Manitoba	Kelburn	2020	1	-
	Manitoba	Carberry	2020	1	-
	Saskatchewan	Indian Head	2020	4	-

[a]No false positive or negative case.

Appendix 3.3. Additional Winter Wheat and Durum Models with a 10% FHBi Epidemic Threshold

Table A3.3. 1. Winter wheat and durum Fusarium Head Blight index logistic regression models, optimum predicted probability, sensitivity, specificity, and prediction accuracy.

Model	Equation $(1/(1 + \exp^{-(a + bx + \ldots)}))$[a]	Optimum predicted probability[b]	Sensitivity (%)[c]	Specificity (%)[d]	Accuracy (%)[e]
	Winter wheat				
$WWFHB_{10}$ 1	-5.3434+0.3548Tmin7MA	0.31	61.1	85.6	73.4
$WWFHB_{10}$ 2	-2.0925+0.0294TRH807MA	0.18	93.1	62.5	77.8
$WWFHB_{10}$ 3	-5.7739+0.3315Tmin7MA+0.1700R7MA	0.23	72.2	78.2	75.2
$WWFHB_{10}$ 4	-2.0704+0.0233TRH8010MA	0.19	93.1	67.1	80.1
$WWFHB_{10}$ 5	-8.6829+0.0881RHmin10MA+0.0195T153010MA	0.21	94.4	67.6	81.0
$WWFHB_{10}$ 6	-8.4018+0.1474RHmin14MA	0.34	83.3	75.9	79.6
$WWFHB_{10}$ 7	-3.9244+0.0249TRH8014+ 0.0893R0314MA	0.37	73.6	82.9	78.2
$WWFHB_{10}$ 8	-3.4392+0.0442TRH9014MA+0.0828R0314MA	0.28	73.6	77.3	75.5
$WWFHB_{10}$ 9	-2.2097+0.0494TRH803MAPA-0.1167T252803MAPA	0.20	95.8	62.5	79.2
	Durum				
$DUFHB_{10}$ 1	-2.1791+0.0349TRH807MA	0.26	96.9	54.2	75.5
$DUFHB_{10}$ 2	-7.9013+0.5056Tmin7MA+0.3143R7MA	0.37	71.9	81.9	76.9
$DUFHB_{10}$ 3	-12.6912+0.5362T7MA+0.2382R037MA	0.50	59.4	93.1	76.2
$DUFHB_{10}$ 4	-15.6859+0.6537Tmin7MA+.0661RH7MA+0.2259R037MA	0.42	71.9	81.9	76.9
$DUFHB_{10}$ 5	-2.6328+0.0291TRH8010MA	0.24	93.8	63.9	78.8
$DUFHB_{10}$ 6	-4.3451+0.3593R10MA+TRH8010MA	0.27	93.8	80.6	87.2

[a]Logistic regression models were developed using 2019 and 2020 data collected in western Canada. Variables are defined in Table A3.1.1. P = probability of FHBi ≥ 10%. In the equation, *a* and *b* are the model coefficients, and X is the predictor variable(s).

[b]The optimal predicted probability of an epidemic case, as determined by Youden's index maximum value (where sensitivity and specificity for the full range of *p* values are high).

[c]Sensitivity is the percentage of correctly classified epidemics cases.

[d]Specificity is the percentage of correctly classified non-epidemic cases.

[d]Accuracy is the percentage of correctly classified cases of epidemic and non-epidemic (true positive proportion+ true negative proposition).

Table A3.3. 2. Youden's index, lack of fit, and area under receiver operator characteristic (AUC) curve of the spring wheat and durum Fusarium Head Blight index models.

Model	Youden's index	Lack of fit	AUC[c]
	Winter wheat		
$WWFHB_{10}$ 1	0.47	<.0001	0.78b
$WWFHB_{10}$ 2	0.56	<.0001	0.76b
$WWFHB_{10}$ 3	0.50	<.0001	0.79ab
$WWFHB_{10}$ 4	0.61	<.0001	0.76b
$WWFHB_{10}$ 5	0.62	<.0001	0.79ab
$WWFHB_{10}$ 6	0.59	<.0001	0.81a
$WWFHB_{10}$ 7	0.56	<.0001	0.81a
$WWFHB_{10}$ 8	0.51	<.0001	0.79ab
$WWFHB_{10}$ 9	0.58	<.0001	0.77b
	Durum		
$DUFHB_{10}$ 1	0.51	0.00	0.73c
$DUFHB_{10}$ 2	0.54	0.01	0.79b
$DUFHB_{10}$ 3	0.52	0.02	0.79b
$DUFHB_{10}$ 4	0.54	0.01	0.83ab
$DUFHB_{10}$ 5	0.58	0.00	0.77b
$DUFHB_{10}$ 6	0.74	<.0001	0.87a

[a]Youden's index, calculated as true positive proportion - false positive proportion.

[b]Hosmer-Lemeshow lack of fit test. A high p-value (> 0.05) indicates a good fit.

[c]Letters following numbers indicate differences between the AUC of the forecasting models based on ROC contrast.

Appendix 4. Wheat and Barley Threshing Procedure (Chapter 4)

To begin, a 2.5 cm diameter hole was cut in the middle of the bucket lid (Figure A4.1a). Following that, two rubber straps measuring 15 cm each were attached at 90^{o} to the bottom of a threshing shaft measuring 0.5 cm in diameter. Next, the threshing rod (with paddle head diameter of 12.07 cm; chuck size of 1.11 cm, shaft length of 58 cm) was threaded with a bucket lid, and the drill (Makita® 8450) was securely attached to the threshing shaft (Figure 4.4a). A bucket measuring 22.7 l was half-filled with dried wheat or barley samples, and the samples were threshed until no more kernels remained on the stalks (Figure A4.1b-c). Next, the threshed sample was transferred from the bucket to an open rectangular container (36 x 24 x 14 cm) with a small rectangular hole (20 x 8 cm) cut on one side (Figure A4.1c). The container was allowed to rest on a trapezium pipe stand with the uncut open container at the bottom to collect grain (Figure A4.1d). The threshed wheat/barley samples were then winnowed by slowly pouring them from the top bucket to the bottom in front of a low-speed electric fan (Figure A4.1e). The samples were passed two to three times until there was less chaff in the grain (Figure A4.1f). After each wheat/barley sample, aseptic techniques such as disinfecting surfaces and equipment using spray nine were employed.

Figure A4. 1. Wheat and barley threshing procedures. Assembling the thresher rod (a), sample loaded in the bucket (b), threshing the sample (c), transferring the sample to the winnowing container (d), winnowing the sample (e), collected grain (f).

Appendix 5. Assessments of Methods for Determining the Anthesis Dates of Wheat and Barley for the western Canadian FHB Risk Tool

A5.1 Introduction

Cereal crops are most susceptible to Fusarium Head Blight (FHB) infection during anthesis when the anthers are protruding, and the fungus can penetrate the developing spikelet. If weather conditions near anthesis are favorable for fungal growth, FHB can significantly affect cereal plants. Pre-heading inoculation may be critical in barley because the crop flowers, while still in the boot stage and therefore, is highly susceptible even before the heads are exposed (McCallum and Tekauz, 2002). If the inoculum comes into contact with host tissues late in the grain's development, infection and major visual symptoms may not manifest to the same extent as in early anthesis infections. Thus, the stage of growth at which barley is most susceptible to *Fusarium* infection is considered to be when half of the head has emerged, as barley is normally flowering at this stage.

Applying fungicide during anthesis is one way to suppress the level of FHB infection (Gilbert and Tekauz, 2011). A weather-based model for FHB risk can aid in determining whether to apply fungicide based on the expected severity of the disease. FHB risk models make estimates of FHB severity based on weather conditions near anthesis. Thus, the anthesis date is a critical variable in FHB risk models. Although direct observation is considered the most accurate method for determining the anthesis date, it is not possible to guarantee the daily observations required to witness the date when 50% of the spikes flower. Thus, direct observation is not a practical means for widespread anthesis date determination.

Several different thermal models have been developed and tested for spring wheat phenological development in western Canada (e.g., Saiyed et al., 2009; Mkhabela et al., 2016), but none are available for winter wheat and durum. However, the linear response of spring wheat phenology using the Haun scale compared to accumulated heat reported by Mkhabela et al. (2016) is a useful concept that can assist with developing estimates of the date of 50% anthesis in durum. The modelled accuracy of anthesis date determination compared to the observed date for spring wheat varies, but for the period between planting date and anthesis, phenological model errors are 4 to 6 days. Hence, the use of daily temperature data and planting date to model the date of anthesis for spring wheat at a specific location could exhibit 4 to 6 days difference to an observed date. Therefore, the linear response of spring wheat phenology using the Haun scale compared to

accumulated heat reported by Mkhabela et al. (2016) can be used to estimate the date of 50% anthesis when it is not directly observed. For winter wheat, this approach is complicated because the crop is planted in late fall, enters a period of dormancy during the winter, and requires sufficiently cold temperature duration for vernalization. In spring, the plants break dormancy and resume active growth, usually much earlier than the spring-sown crops. Therefore, using planting dates for phenological modelling using thermal time is not straightforward. Instead, the growing season start (GSS) date in the spring is a more useful benchmark for estimating the anthesis date using thermal time.

In barley, two previously developed thermal models were available to estimate the date of 50% anthesis (or 50% head emergence). Juskiw et al. (2001) developed a barley phenology model using GDD_0 (base 0 °C) based on phenology observations across 12 site-years in Alberta. The North Dakota Agricultural Weather Network (NDAWN, 2005) developed a model for barley development using a special formula for GDD (base 32 °F) and observations in North Dakota. In addition, the linear response of spring wheat phenology using the Haun scale in comparison to accumulated heat reported by Mkhabela et al. (2016) is a useful concept that can facilitate estimation of the date of 50% head emergence in situations with observations of other growth stages and air temperature data.

The FHB risk modelling in the present study uses direct observations of wheat and barley phenological development to determine the date of 50% anthesis and head emergence, respectively. However, this specific stage may not be observed directly at all study locations due to the fact that observations were taken once a week. Therefore, an estimate of the date of 50% anthesis and head emergence is required at the locations where it is not directly observed. The objective of this study was to assess thermal time models using daily temperature and several methods for determining the date of 50% anthesis and head emergence. This assessment will help minimize potential errors in anthesis date estimation at locations where it was not observed by revealing the most accurate methods.

A5.2 Materials and Methods

A5.2.1 Site

The description of sites for this study is given in Chapter 2. In brief, small-plot research trials with five plot sites per province (15 sites) were conducted in the 2019 and 2020 growing seasons in

Manitoba, Saskatchewan, and Alberta (Figure 2.1). These 15 sites were geographically distributed across western Canada to maximize the likelihood of each site experiencing various growing-season weather conditions. Each plot measured approximately 4 m in length and 2 m in width with at least 8 rows.

A5.2.2 Experimental Design

The experimental design of this study is described in Chapter 2. In brief, the experimental design was a randomized complete block design (RCBD) with four replications (blocks) for each of the separate side by side winter wheat, spring wheat, barley, and durum experiments (Figure 2.2). Three different spring wheat, winter wheat, and barley varieties were used in the treatments, representing three different FHB resistance categories (F. RC) (Table 2.1). FHB resistance categories included F. RC1 (susceptible or moderately susceptible varieties), F. RC2 (intermediate varieties), and F. RC3 (moderately resistant or resistant varieties), depending on the crop type. Only one durum wheat variety was grown because all durum wheat varieties are FHB susceptible.

A5.2.3 Meteorological Data

Watchdog® portable weather stations (Spectrum Technologies 2000 Series, Thayer Case, IL, USA) were used to record growing-season weather data. At each site, one weather station was mounted on a solid post at an average height of 1.80 m within 10 m of the plots. Weather data collected hourly included air temperature (°C), relative humidity (RH), rainfall (mm), solar radiation (W m^{-2}), and wind speed (km h^{-1}). The weather stations were installed about a month after spring crop seeding. Meteorological data before deployment of the weather stations were sourced from Manitoba Agriculture Weather Program and Alberta Climate Information Service, and Environment and Climate Change Canada weather stations monitored weather stations (ACIS, 2021b; ECCC, 2021; MARD, 2021b).

A5.2.4 Agronomy and Phenology Observations

Three winter wheat varieties representing 3 levels of FHB resistance (Table 2.1) were planted in the fall of 2018 and 2019, while spring cereals (spring wheat, barley, and durum) were sown in spring 2019 and 2020 according to the best management practices at each location. At each site, standard agronomic practices such as fertilizer application, seeding depth, row spacing, and herbicide application were followed. Planting, maturity, and harvesting dates for each crop were

recorded. Phenology observations were collected multiple times at all 15 plot locations using the BBCH scale (Meier, 2001), then converted to the Haun scale (Haun 1973) to facilitate the use of the thermal models described by Mkhabela et al. (2016). The Haun scale conversion was based on equivalent values between the Haun scale and the Zadoks scale (Zadoks et al., 1974) reported by Fowler (2018). The BBCH scale is similar to the Zadoks scale, and the Fowler (2018) comparison facilitated a conversion. The equivalent values reported in Fowler (2018) are highlighted in Table A5.1. Fractional Haun scale values were interpolated between the equivalent values to provide a complete conversion for all observed BBCH values from 45 (boot just swollen) to 71 (kernel is watery). The purpose of the conversion was to exploit the linearity of heat unit accumulation (quantitative) in relation to the Haun scale (ordinal) in the period preceding and following the anthesis stage as reported by Mkhabela et al. (2016).

Table A5. 1. BBCH Scale to Haun Scale Conversion (bold values are from Fowler, 2018).

BBCH	Haun		BBCH	Haun	
45	**9.2**	(boot just swollen)	**59**	**11**	(emergence of head complete)
46	9.425		**60**	**11.4**	(beginning of flowering)
47	9.65		61	11.42	
48	9.875		62	11.44	
49	**10.1**	(first awns visible)	63	11.46	
50	**10.2**	(first spikelet visible)	64	11.48	
51	10.26		**65**	**11.5**	(flowering half complete)
52	10.32		66	11.525	
53	10.38		67	11.55	
54	10.44		68	11.575	
55	**10.5**	(1/2 of head emerged)	**69**	**11.6**	(flowering complete)
56	10.6		70	11.85	
57	**10.7**	(3/4 of head emerged)	**71**	**12.1**	(kernel is watery)
58	10.85				

For each observation date at each plot location, a set of 18 to 24 phenology observations were made. The BBCH stage for each observation was converted to the Haun scale using Table A5.1. Only observation dates for which at least 90% of the observations were between BBCH 45 and 71 were included in the analysis. The median Haun scale value on each observation date at each plot site was used to determine the stage of crop development on the specific date for all varieties.

A5.2.5 Spring Wheat Thermal Models

For each plot location, on-site daily temperature data were used to determine three different cumulative thermal model measures of heat units, including GDD (base 0 °C), GDD (base 5 °C) and the North Dakota GDD (base 32°F) as described by Mkhabela et al. (2016). These heat units were the ones with the closest linear relationship to wheat phenological development in the

Mkhabela et al. (2016) study. The values were accumulated daily throughout the growing season, starting the day after planting. Tables AA5.1 and AA5.2 list the Haun scale phenological stage and the accumulated values of the three thermal models on the dates of the observations at all plot site locations in 2019 and 2020, respectively.

Figure A5.1 shows the observed Haun scale development for all sites and observation dates compared to the three different accumulated thermal models and the regression line reported by Mkhabela et al. (2016) for each specific heat unit model. The range of accumulated values near the time of 50% anthesis was, in both years, similar to that reported for the same three models by Mkhabela et al. (2016), as can be seen by comparing the values in Figure A5.1 to those in Figure A5.2. Statistical comparison of the 3 models showed the RMSE in modelled Haun scale varied by nearly 2 Haun scale units with a small negative bias and low regression coefficient for all three models in both years (Table A5.2).

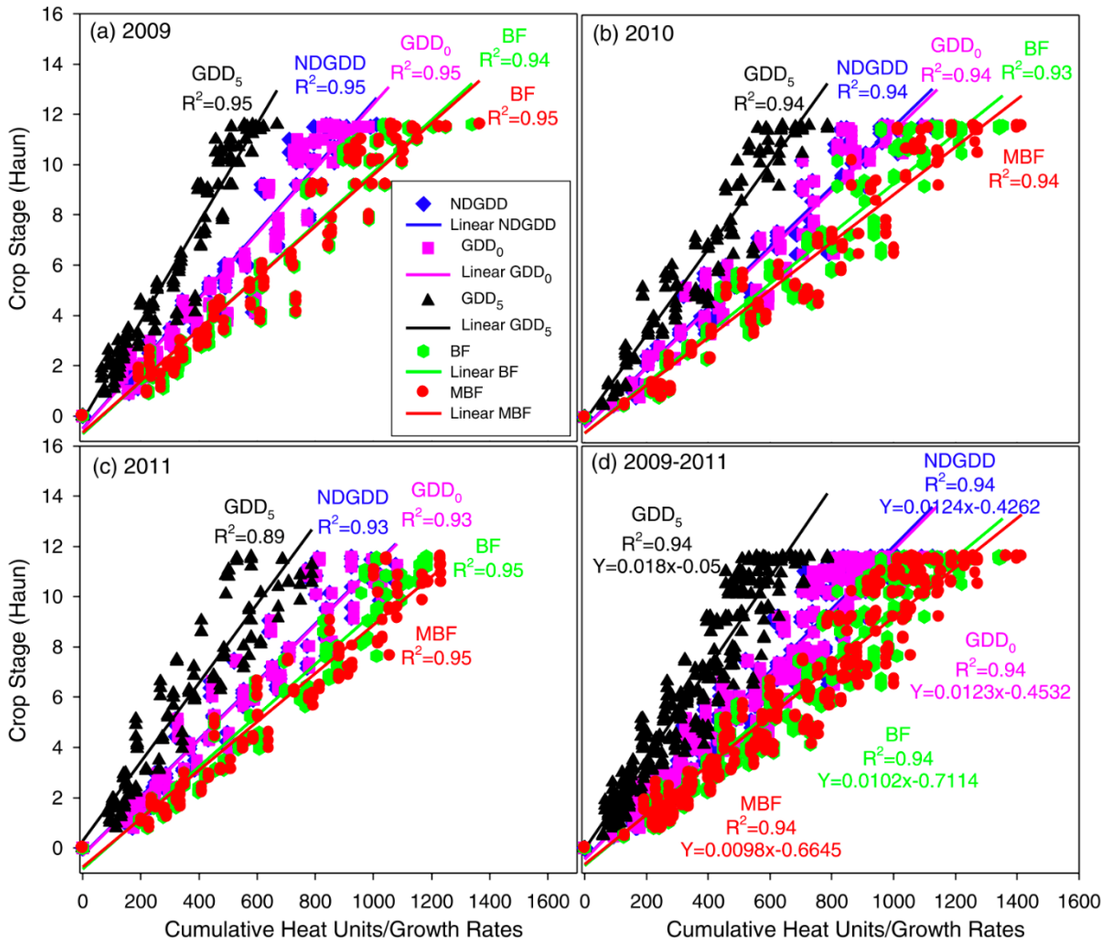

Figure A5. 1. Linear relationship between wheat growth stage (planting to anthesis) for three spring wheat cultivars and accumulated heat units/growth rates calculated using five different thermal time models in (a) 2009, (b) 2010, (c) 2011, and (d) 2009-2011 combined. Note that the accumulated growth rate values for the BF and MBF models were multiplied by 100 to be plotted on the same graph as the other models. (Mkhabela et al. 2016).

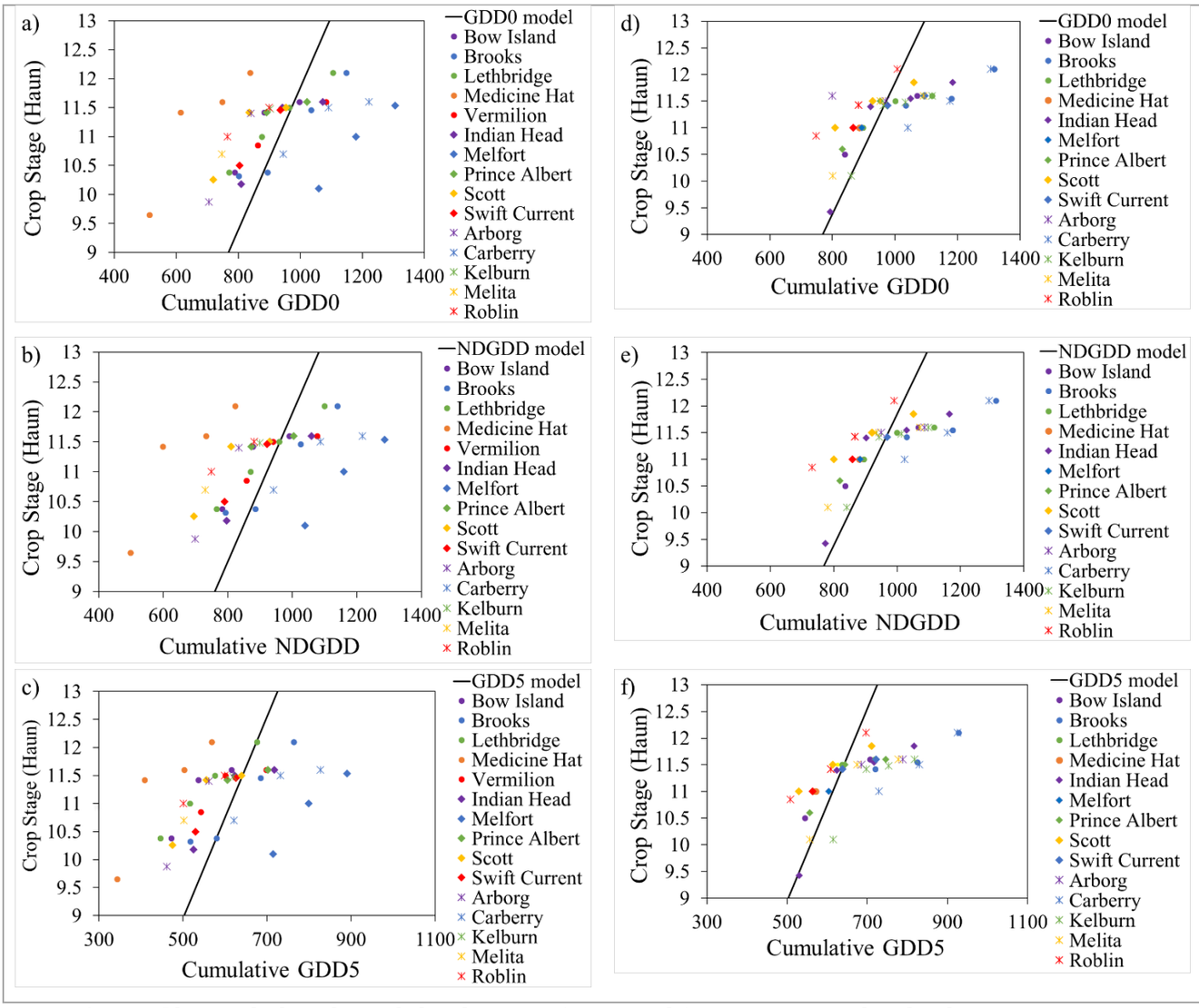

Figure A5. 2**.** Observed phenological development (Haun scale) versus accumulated values of (a) and (d) Growing Degree Day base 0 ºC (GDD0), (b) and (e) North Dakota growing degree day (NDGDD) base 32F, and (c) and (f) Growing Degree Day base 5 ºC (GDD5) by plot location for each observation date in the 2019 (a, b, c) and 2020 (d, e, f) growing seasons respectively.

Table A5. 2. Performance of the three GDD thermal models described by Mkhabela et al. (2016) for the 2019 and 2020 FHB plot study. RMSE and MBE values are Haun scale units.

	Year	Base 0°C	Base 32°F	Base 5°C
R^2	2019	0.301	0.30	0.292
RMSE		1.776	1.811	1.858
MBE		-0.352	-0.38	-0.435
R^2	2020	0.574	0.579	0.508
RMSE		1.384	1.406	1.814
MBE		-0.505	-0.474	-0.907

The values illustrated in Figure A5.2 and the statistics in Table A5.2 show variation in the amount of accumulated heat to reach a specific growth stage between sites. For example, in 2019, the wheat at Medicine Hat reached specific stages of development with fewer heat units than the other sites, especially compared to Melfort, but there is no way to know the amount of variation between sites based solely on modelled values. Therefore, comparing observed values is the only way to discern the differences between sites. It is also important to note that this was not an issue with a particular model since all three heat unit models display the same pattern. Therefore, the remainder of the analysis used the GDD (base 0 °C) method of Mkhabela et al. (2016) because it provided a slightly better statistical comparison to observed phenological development than the other two models (Table A5.2). However, it should be noted that the differences were slight, and any of the three models could have been selected.

A5.2.6. Anthesis Estimation Method: Interpolation in Spring Wheat

The best method of estimating the date of 50% anthesis for spring wheat is an interpolation, which can be used in cases such as the Medicine Hat and Melfort 2019 locations, with observations both immediately prior to and after the date of anthesis. The date of 50% anthesis (i.e., Haun scale 11.5) can be calculated using the rate of Haun scale increase per day between the two dates, as shown in equation A5.1.

x days to anthesis = ((date following 50% anthesis - date preceding 50% anthesis) / (Haun value following 50% anthesis - Haun value preceding 50% anthesis)) * (11.5 - Haun value preceding) [A5.1]

An example of the calculation for 2019 Medicine Hat plot site is shown below:

June 26 – Haun scale 11.42, July 4 – Haun scale 11.6,

x days to anthesis = [(July 4 – June 26) / (11.6 – 11.42)] * (11.5 – 11.42) = 3 days

June 26 plus 3 days = June 29

A5.2.7. Anthesis Estimation Method: Extrapolation in Spring Wheat

Other methods must be employed for locations where the 50% anthesis date was not directly observed, and there are no observations that facilitate interpolation of the date. One approach is to use a phenological observation on a given date and extrapolate to the anthesis date by selecting a representative slope value for the rate of Haun scale change per heat unit. This analysis tested three different representative slope values by comparing their estimated date of 50% anthesis with the observed values. The slope values selected were:

i) the slope of the Haun scale-GDD (base 0 °C) relationship from observations at the local site,

ii) the mean slope of the Haun scale-GDD (base 0 °C) relationship from observations at several sites with multiple observations and

iii) the slope of the Haun scale-GDD (base 0 °C) relationship from Mkhabela et al. (2016).

Figure A5.3 shows examples of the Haun scale-GDD (base 0 °C) relationship at two individual plot locations. The slope of the linear regression line at each site was utilized for analysis (i) above. Table A5.3 shows the linear regression equations for all 2019 and 2020 plot sites with at least 3 phenological observation dates. The mean slope of all the lines in Table A5.3 was utilized for analysis (ii) above. The slope of the Haun scale-GDD (base 0 °C) relationship from Mkhabela et al. (2016) is 0.0123, which was utilized for analysis (iii) above.

a) 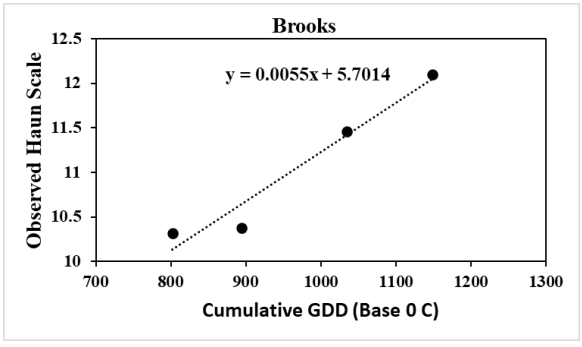

b) 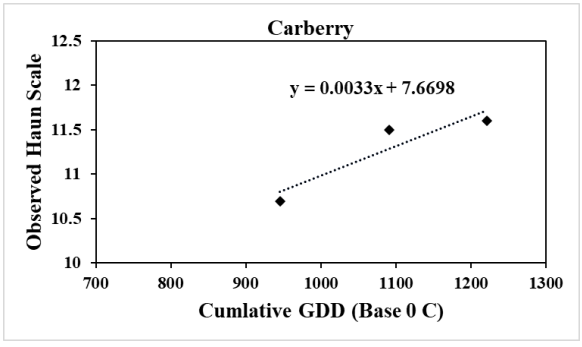

Figure A5. 3. Haun scale-GDD (base 0 °C) relationship for phenological observations at (a) Brooks, Alberta and (b) Carberry, Manitoba, showing the linear regression lines and equations.

Table A5. 3. Haun scale-GDD (base 0 °C) linear regression equations for all 2019 and 2020 plot sites with at least 3 spring wheat phenology observations.

Plot Site	2019	2020
Bow Island	y = 0.0057x + 6.043	
Brooks	y = 0.0055x + 5.7014	y = 0.0026x +7.7807
Carberry	y = 0.0033x + 7.6698	
Indian Head	y = 0.0054x + 5.9875	y = 0.0017x+9.7909
Kelburn		y = 0.0012x+10.286
Lethbridge	y = 0.0051x + 6.4739	
Medicine Hat	y = 0.0067x + 6.6461	
Melfort	y = 0.0058x + 4.0019	
Roblin		y = 0.0048x+7.2227
Scott	y = 0.0053x + 6.6589	
Swift Current		y = 0.0026x+8.7816
Vermilion	y = 0.0031x + 8.289	
Mean slope	**0.0051**	**0.00258**

The slope values can be used to extrapolate the accumulated GDD (base 0 °C) at 50% anthesis from an observation of the Haun scale and its accompanying GDD (base 0°C) accumulation from the date of planting. The accumulated heat unit value expected for the 50% anthesis stage (Haun scale 11.5) can be compared to the daily GDD (base 0 °C) accumulation measured for the site to find the date closest to when the accumulated value occurred.

Finally, any of the Mkhabela et al. (2016) models along with planting date can be utilized to estimate the date of 50% anthesis in spring wheat at a specific location by using the measured accumulated heat units at the location. For this analysis, the accumulated value of 971.8 GDD (base 0 °C) model was utilized. The date closest to when the accumulated value occurred was selected as the modelled value.

The plot sites that had the date of 50% anthesis (Haun scale 11.5) specifically observed are shown in Tables AA5.1 (2019) and Table AA5.2 (2020). An estimate of 50% anthesis date was generated using extrapolation from the other phenology observations at these plot sites and compared to the

observed date. The extrapolation estimates were calculated using the 3 different slope values described previously. In addition, the GDD (base 0 °C) model from Mkhabela et al. (2016) was compared to the observed value at each of the six locations.

A5.2.8. Anthesis Estimation Method: Extrapolation in Durum

The best method of estimating the date of 50% anthesis for durum is interpolation, which can be determined by using equation A5.1. An alternate method is required in locations with insufficient phenology observations to provide either direct observation or an interpolated date of 50% anthesis. Previous assessment of various thermal heat units for spring wheat showed that the GDD (base 0 °C) model was the most accurate (Mkhabela et al., 2016). Therefore, the simplest approach for durum would be to utilize the spring wheat model as a proxy for durum phenological development estimation. However, simultaneous observations of spring wheat and durum development at the same locations showed that durum tended to develop slightly slower than spring wheat (Figure A5.4) and that the model would require adjustment.

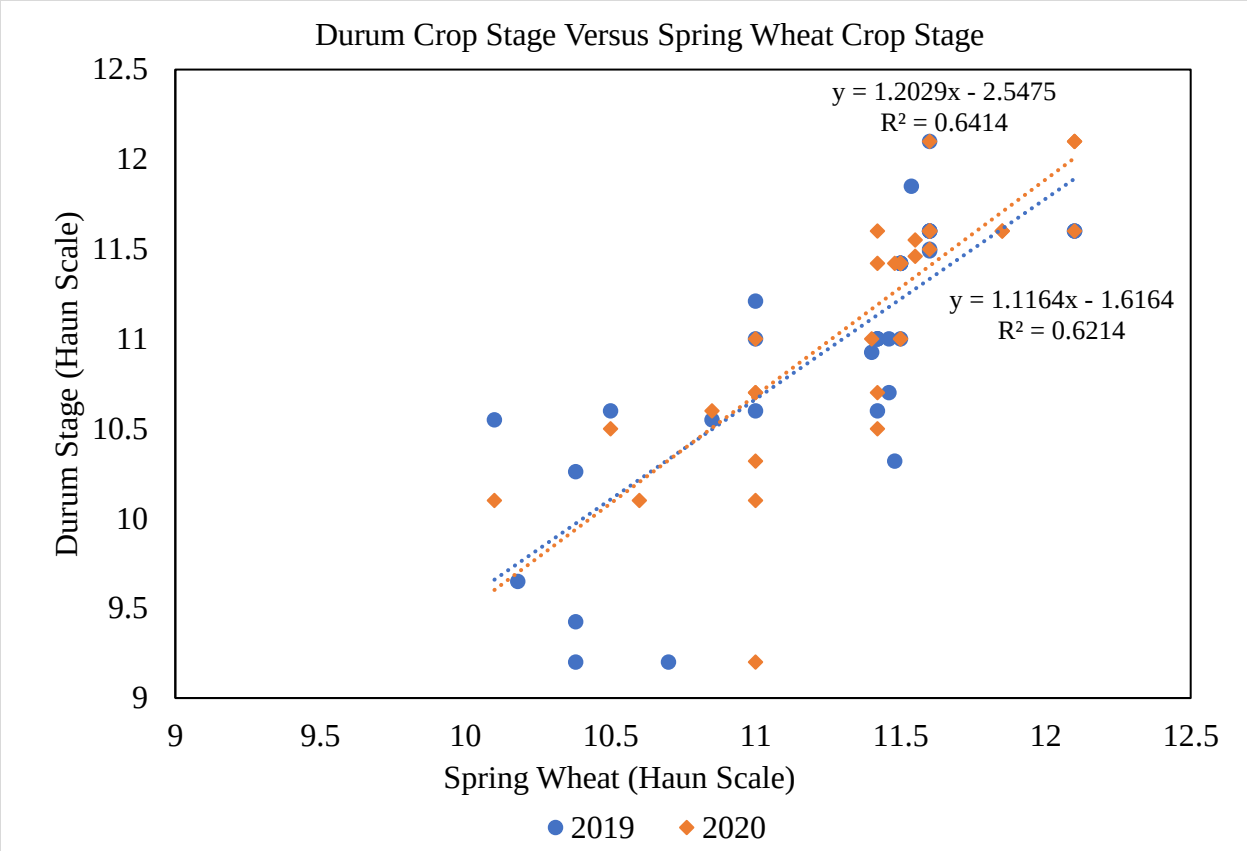

Figure A5. 4**.** Comparison of durum and spring wheat observed stage of development made on the same date and locations in 2019 and 2020 growing seasons.

The regression equations in Figure A5.4 were used to determine a comparable Haun stage of spring wheat on the date that durum reached 50% anthesis at the same location with the same planting date. The calculation was done by inserting a value of 11.5 for y in the regression equation and solving for x, which yielded an estimated Haun stage of 11.75 for spring wheat in 2019. This implied that, on average, the stage of spring wheat at the time of 50% anthesis for durum was Haun stage 11.75. This slightly more advanced stage for spring wheat compared to durum was justifiable based on observations of phenological development for both crops at multiple locations.

A5.2.9. Anthesis estimation method: Extrapolation in Winter Wheat

The best method of estimating the date of 50% anthesis for winter wheat is interpolation, which can be determined by using equation A5.1. For locations where neither direct observation nor interpolation of 50% anthesis are possible because of limited observed phenology data, an alternative method is required. For winter wheat, the method needs to consider the date when the crop breaks dormancy to start active growth in the spring plus the rate of phenological development after that date. Therefore, the first step for estimating the date of 50% anthesis is to estimate the growing season start (GSS) date. Three different methods were investigated. Selirio and Brown (1979) described the commencement of forage growth in the spring as the day following a period after March 15 when the daily mean temperature exceeded 5 °C for 5 days. Bootsma, (1994) described a method for calculating GSS for a perennial grass crop as the day the weighted mean air temperature (WT) reached 5.5 °C for 5 consecutive days (equation A5.2)

$$WT_{(n)} = [T_{(n-2)} + 4T_{(n-1)} + 6T_{(n)} + 4T_{(n+1)} + T_{(n+2)}] / 16 \qquad [A5.2]$$

Where $WT_{(n)}$ is the weighted mean temperature for day n, and $T_{(n)}$ is the temperature on day n. Qian et al. (2010) described the same weighted mean temperature approach for determining GSS for overwintering crops as shown in equation A5.2, except that the date was defined when WT reached 5.0 °C for 5 consecutive days. Air temperature data were compiled for each location starting on March 1. The mean temperature for each date was used to determine GSS using each of the 3 methods above. The methods of Bootsma, (1994) and Qian et al. (2010) yielded exactly the same dates for GSS at all plot sites in both years (Table A5.4). Therefore, the method of Qian et al. (2010) was retained, and the method of Bootsma (1994) was not utilized in further analysis.

Table A5. 4. Estimated dates of Growing Season Start (GSS) for winter wheat in 2019 and 2020 plot sites using the methods of Selirio and Brown (1979), Bootsma (1994), and Qian et al. (2010).

	2019 Growing Season Start			2020 Growing Season Start		
Start Methods	5 days 5.0°C[a]	5 days > Wt Mean 5.5°C[b]	5 days > Wt Mean 5.0°C[c]	5 days 5.0°C[a]	5 days > Wt Mean 5.5°C[b]	5 days > Wt Mean 5.0°C[c]
Bow Island	7-Apr	24-Mar	24-Mar	23-Apr	21-Apr	21-Apr
Brooks	23-Mar	23-Mar	23-Mar	23-Apr	23-Apr	23-Apr
Lethbridge	23-Mar	23-Mar	23-Mar	23-Apr	21-Apr	21-Apr
Medicine Hat	7-Apr	24-Mar	24-Mar	23-Apr	22-Apr	22-Apr
Indian Head	22-Apr	21-Apr	21-Apr	25-Apr	25-Apr	25-Apr
Melfort	17-Apr	18-Apr	18-Apr	7-May	27-Apr	27-Apr
Prince Albert	22-Apr	19-Apr	19-Apr	26-Apr	26-Apr	26-Apr
Scott	11-May	17-Apr	17-Apr	25-Apr	25-Apr	25-Apr
Swift Current	21-Apr	8-Apr	8-Apr	24-Apr	24-Apr	24-Apr
Arborg	22-Apr	19-Apr	19-Apr	27-Apr	27-Apr	27-Apr
Carberry	19-Apr	19-Apr	19-Apr	26-Apr	26-Apr	26-Apr
Kelburn	19-Apr	19-Apr	19-Apr	-	-	-
Melita	19-Apr	18-Apr	18-Apr	25-Apr	25-Apr	25-Apr
Roblin	22-Apr	19-Apr	19-Apr	27-Apr	27-Apr	27-Apr

[a]Selirio and Brown (1979)

[b]Bootsma (1994)

[c]Qian et al. (2010)

The cumulative heat unit values were plotted against Haun scale observations for all dates, excluding the dates with a Haun value of 11.5 (Figure A5.5). The latter dates were used for model testing. Linear regression equations were used to create 6 models of Haun scale value from cumulative heat units generated by the 3 thermal time measures for each of the 2 GSS methods. The modelled values of cumulative heat for Haun stage 11.5 were then used to estimate the date of 50% anthesis for each of the 6 locations with an observed Haun scale of 11.5. The regression coefficients, RMSE and MBE, were calculated for each linear regression approach to determine which one provided the most accurate 50% anthesis date estimate.

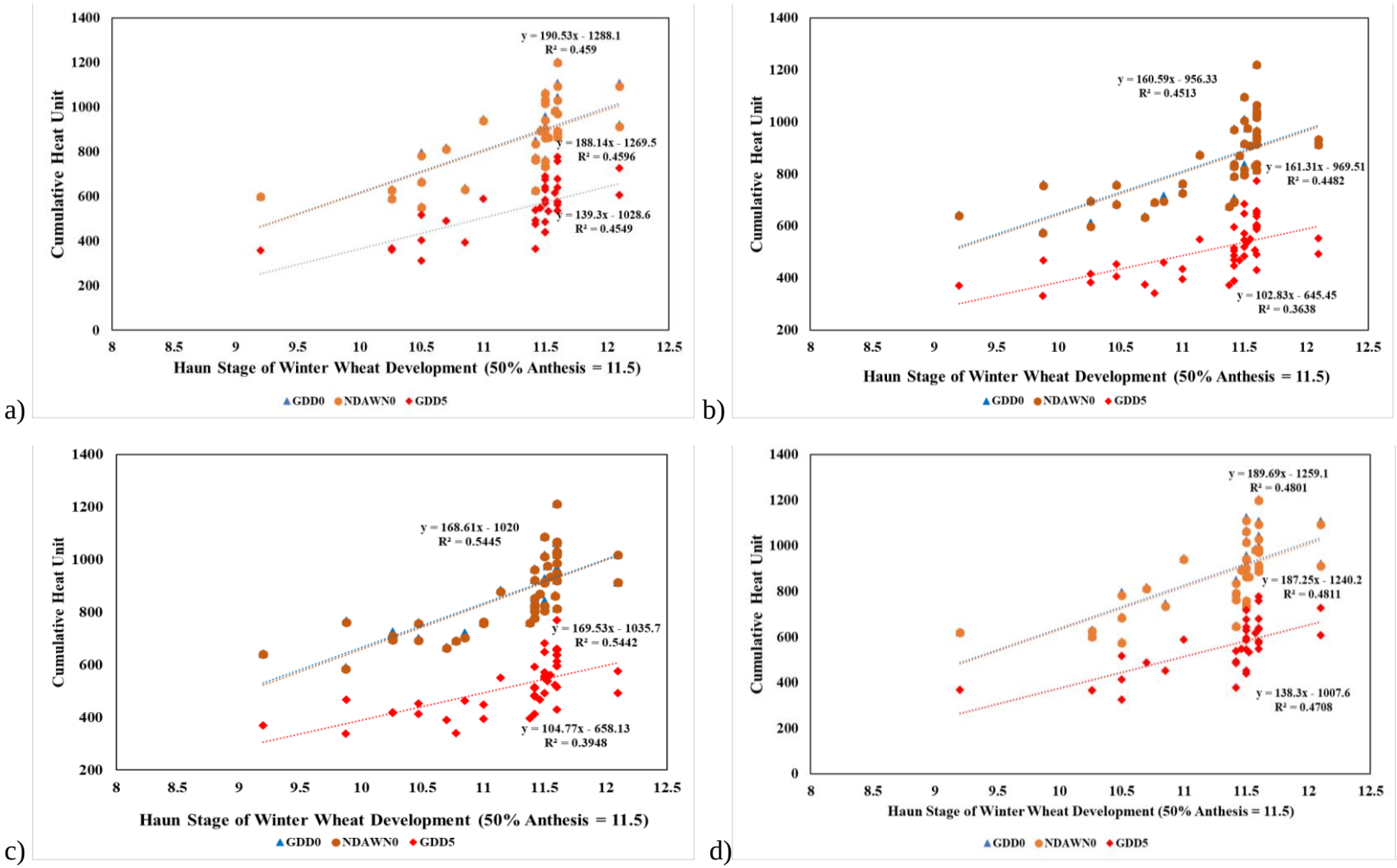

Figure A5. 5. Linear regression models of cumulative heat units versus observed Haun scale at plot sites using growing season start defined by 5 consecutive days with daily mean temperature > 5.0 °C (a and c in 2019 and 2020, respectively) and growing season start defined by 5 consecutive days with weighted mean temperature (see equation A5.2) > 5.0 °C (b and d in 2019 and 2020, respectively). Note that observation dates with Haun scale = 11.5 were not included but used for model testing.

A5.2.10. Anthesis Estimation Method: Extrapolation in Barley

The best method of estimating the date of 50% anthesis for barley is interpolation, which can be determined by using equation A5.1. However, other methods must be employed for locations where the 50% anthesis date was not directly observed, and there are no observations that facilitate interpolation of the date. One approach uses the regression equation for the relationship between the observations and accumulated heat units at each location. Another method is to use a phenological observation on a given date and extrapolate to the anthesis date by selecting a representative slope value for the rate of Haun scale change per heat unit. In this analysis, two different representative slope values were tested by comparing their estimated date of 50% anthesis with the observed and interpolated values from seven of the 2019 plot sites:

i) the slope of the Haun scale-GDD (base 0 °C) relationship from observations at the local site and,

ii) the mean slope of the Haun scale-GDD (base 0 °C) relationship from observations at several sites with multiple observations.

Figure A5.6 shows examples of the Haun scale-GDD (base 0 °C) relationship at two individual barley plot locations. The slope of the linear regression line at each site was utilized for analysis (i) above.

a) 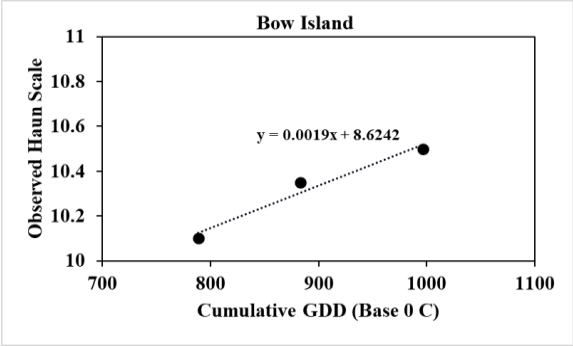

b) 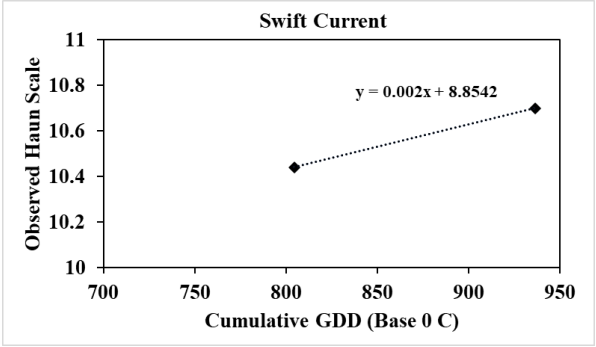

Figure A5. 6**.** Haun scale-GDD (base 0ºC) relationship for 2019 phenological observations at (a) Bow Island, AB and (b) Swift Current, SK showing the linear regression lines and equations.

The slope values were used to extrapolate the accumulated GDD (base 0 °C) at 50% head emergence from an observation of the Haun scale and its accompanying GDD (base 0 °C) accumulation from the date of planting. As for the local regression approach, the accumulated heat unit value expected for the 50% head emergence stage (Haun scale 10.5) can be compared to the daily GDD (base 0 °C) accumulation measured for the site to find the date closest to when the accumulated value occurred.

Another method for 50% head emergence estimation is to solve the local regression equation for a specific site to return an accumulated GDD (base 0 °C) at Haun scale 10.5. Then, the accumulated heat unit value expected for the 50% head emergence stage (Haun scale 10.5) can be compared to the daily GDD (base 0 °C) accumulation measured for the site to find the date closest to when the accumulated value occurred.

In addition, the accumulated GDD (base 0 °C) and the GDD (base 32 °F) can be used to estimate the date of 50% head emergence with the models developed by Juskiw et al. (2001) and NDAWN (2005), respectively, then compared to observed/interpolated values. This analysis tested the accuracy of the date of “anthesis” and “heading” as described by Juskiw et al. (2001) as well as

the date of “mid-boot” and “head emerged” as described by NDAWN (2005). Further, the dates for each of these stages were determined with 2 slightly different approaches. The first approach selected the first date on which the cumulative heat unit value was equal to or greater than that specified for the phenological stage. The second approach selected the date on which the cumulative heat unit value was numerically closest to that specified for the phenological stage. An additional model using a target GDD (base 0 °C) cumulative threshold of 905 units was also tested. In total, there were 9 different modelled growth stage estimates generated for each site (2 models x 2 phenological stages x 2 methods of date selection plus 1 target model).

A5.3. Results

A5.3.1. Spring Wheat

Table A5.5 shows the estimated dates for 50% anthesis using all three extrapolation methods. In the 2019 and 2020 growing seasons, the deviation of the estimated dates varied from 7 days and 9 prior to the observed date to 8 and 7 days following the observed date, respectively. More than 40% of the estimated dates were more than 2 days earlier or later than the observed date in both years.

Table A5. 5. Extrapolated estimates of spring wheat 50% anthesis date using three different Haun scale-GDD (base 0 °C) slopes.

		Extrapolated Estimates of 50% Anthesis Date		
Plot Site	Observation date used to Extrapolate	Local Slope Method	Mean Slope Method	Mkhabela et al. (2016) slope
Lethbridge	21-Jun-19	6-Jul-19	6-Jul-19	27-Jun-19
Lethbridge	28-Jun-19	5-Jul-19	5-Jul-19	1-Jul-19
Lethbridge	12-Jul-19	6-Jul-19	6-Jul-19	10-Jul-19
Vermilion	11-Jul-19	23-Jul-19	19-Jul-19	14-Jul-19
Vermilion	24-Jul-19	22-Jul-19	23-Jul-19	24-Jul-19
Indian Head	5-Jul-19	18-Jul-19	19-Jul-19	11-Jul-19
Indian Head	19-Jul-19	18-Jul-19	18-Jul-19	18-Jul-19
Scott	9-Jul-19	23-Jul-19	23-Jul-19	15-Jul-19
Scott	16-Jul-19	17-Jul-19	17-Jul-19	16-Jul-19
Carberry	8-Jul-19	20-Jul-19	16-Jul-19	11-Jul-19
Carberry	22-Jul-19	20-Jul-19	21-Jul-19	21-Jul-19
Roblin	9-Jul-19	16-Jul-19	14-Jul-19	11-Jul-19
Bow Island	29-Jun-20	11-Jul-20	11-Jul-20	4-Jul-20
Bow Island	13-Jul-20	12-Jul-20	12-Jul-20	12-Jul-20
Lethbridge	29-Jun-20	10-Jul-20	3-Jul-20	3-Jul-20
Lethbridge	13-Jul-20	12-Jul-20	12-Jul-20	6-Jul-20
Prince Albert	9-Jul-20	19-Jul-20	19-Jul-20	13-Jul-20
Prince Albert	23-Jul-20	22-Jul-20	22-Jul-20	22-Jul-20
Scott	15-Jul-20	20-Jul-20	20-Jul-20	17-Jul-20
Scott	29-Jul-20	26-Jul-20	26-Jul-20	27-Jul-20
Arborg	16-Jul-20	15-Jul-20	15-Jul-20	16-Jul-20
Carberry	9-Jul-20	14-Jul-20	14-Jul-20	11-Jul-20
Carberry	23-Jul-20	13-Jul-20	17-Jul-20	16-Jul-20
Melita	29-Jun-20	12-Jul-20	12-Jul-20	4-Jul-20
Melita	13-Jul-20	12-Jul-20	13-Jul-20	13-Jul-20

The Mkhabela et al. (2016) modelled dates using GDD (base 0 °C) are shown in Table A5.6. The deviation of the estimated dates varied from 6 days prior to the observed date to 4 days following the observed date. Half of the estimated dates were more than 2 days earlier or later than the observed date in both years.

Table A5. 6. Modelled dates of spring wheat 50% anthesis in 2019 and 2020 growing seasons using the Mkhabela et al. (2016) GDD (base 0 °C) model.

Plot Site	Observed Date of 50% Anthesis	Modeled Date of 50% Anthesis
Lethbridge	4-Jul-19	5-Jul-19
Vermilion	16-Jul-19	18-Jul-19
Indian Head	12-Jul-19	12-Jul-19
Scott	23-Jul-19	23-Jul-19
Carberry	15-Jul-19	9-Jul-19
Roblin	16-Jul-19	20-Jul-19
Bow Island	6-Jul-20	7-Jul-20
Lethbridge	6-Jul-20	4-Jul-20
Prince Albert	16-Jul-20	17-Jul-20
Scott	22-Jul-20	24-Jul-20
Arborg	9-Jul-20	9-Jul-20
Carberry	16-Jul-20	6-Jul-20
Melita	13-Jul-20	8-Jul-20

A statistical comparison of the different methods for estimating 50% anthesis date is shown in Table A5.7. The Mkhabela et al. (2016) GDD (base 0 °C) model returned the highest regression coefficient and the lowest RMSE and MBE values in both 2019 and 2020; therefore, it was the most accurate method for estimating 50% anthesis date at a location where it was not directly observed and could not be interpolated.

Table A5. 7. Performance of the three extrapolation methods and the GDD (base 0 °C) model from Mkhabela et al. (2016) for estimation of spring wheat 50% anthesis date in comparison to the observed date in 2019 and 2020 growing seasons. RMSE and MBE values are in units of days.

	Local slope Method	Mean Slope Method	Mkhabela et al (2016) Slope Method	Mkhabela et al (2016) GDD (Base 0°C)
			2019	
R^2	0.706	0.676	0.447	0.765
RMSE	4.583	4.368	5.694	3.082
MBE	2.833	2.250	-0.917	0.167
			2020	
R^2	0.594	0.674	0.574	0.681
RMSE	4.780	4.076	4.624	4.071
MBE	2.692	2.154	-0.462	-1.714

A5.3.2. Durum

The Haun value of 11.75 was inserted into the regression equation between Haun scale and GDD (base 0 °C) developed by Mkhabela et al. (2016, Figure A5.1d). This yielded a cumulative heat unit value of 992 units of GDD (base 0 °C) from the day after planting. Using this value, an estimated date of 50% anthesis was generated for each location where the date was either observed or interpolated (Table A5.8). The deviation of the estimated dates varied from 13 days prior to the observed date to 17 days following the observed date. The accuracy of this method for 50% anthesis date of durum was poorer than those for the other spring crops (Table A5.9).

Table A5. 8. Estimated dates of durum 50% Anthesis using 992 cumulative GDD (base 0 °C) in 2019, compared to observed dates.

Plot Site	Observed Date of 50% Anthesis	Modeled Date of 50% Anthesis
Bow Island	4-Jul	3-Jul
Brooks	21-Jul	13-Jul
Lethbridge	7-Jul	6-Jul
Medicine Hat	29-Jun	16-Jul
Vermilion	24-Jul	19-Jul
Indian Head	15-Jul	14-Jul
Melfort	3-Aug	21-Jul
Prince Albert	23-Jul	23-Jul
Scott	23-Jul	25-Jul
Swift Current	22-Jul	18-Jul
Carberry	18-Jul	10-Jul
Kelburn	10-Jul	8-Jul
Roblin	19-Jul	22-Jul

Table A5. 9. Performance of the durum 50% anthesis date method. RMSE and MBE values are in units of days.

R^2	0.447
RMSE	7.055
MBE	-1.615

A5.3.3. Winter Wheat

Winter wheat phenology observations were sufficient at all 14 sites to provide either an observed or interpolated date of 50% anthesis in 2019. (Table A5.10). However, only one site (Arborg) did not have enough phenology observations in 2020 to provide either an observed, interpolated, or extrapolated date of 50% anthesis.

Table A5. 10. Observed, interpolated, and modelled dates of winter wheat 50% anthesis in 2019 and 2020 growing seasons.

	2019 growing season		2020 growing season	
	Date of 50% Anthesis	Method of Determination	Date of 50% Anthesis	Method of Determination
Bow Island	21-Jun	Interpolation	22-Jun	Observed
Brooks	16-Jun	Interpolation	22-Jun	Observed
Lethbridge	25-Jun	Interpolation	25-Jun	Interpolation
Medicine Hat	14-Jun	Interpolation	24-Jun	Interpolation
Indian Head	12-Jul	Observed	03-Jul	Observed
Melfort	17-Jul	Observed	20-Jul	Observed
Prince Albert	11-Jul	Observed	16-Jul	Observed
Scott	09-Jul	Observed	15-Jul	Observed
Swift Current	30-Jun	Interpolation	30-Jun	Observed
Arborg	05-Jul	Interpolation	04-Jul	Modelled
Carberry	02-Jul	Observed	02-Jul	Observed
Kelburn	29-Jun	Interpolation	-	-
Melita	25-Jun	Observed	22-Jun	Interpolation
Roblin	06-Jul	Interpolation	05-Jul	Interpolation

Figure A5.5 show linear regression equations that were used to provide estimated cumulative heat value for Haun scale 11.5 (Table A5.11) in 2019 and 2020, respectively. The modelled cumulative heat values for Haun scale 11.5 were used to determine the date of 50% anthesis for the locations where the date had been directly observed (Table A5.12). Estimated dates of 50% anthesis ranged from 13 days prior to the observed date in both years to 5 and 11 days following the observed date in 2019 and 2020, respectively. Comparisons of observed versus modelled dates for 50% anthesis

showed that the GSS method of Qian et al. (2010 (equation A5.2) 2019 and 2020 yielded higher R^2 values and lower error than the GSS method of Selirio and Brown (1979) (Table A5.13).

For the cumulative heat unit methods using the Qian et al. (2010) GSS, the GDD (base 5 °C) had the highest R^2, the GDD (base 0 °C) had the lowest RMSE, and the NDAWN (base 32 °F) had the lowest MBE in 2019. Thus, the method of choice is not completely the best for all 3 statistics. However, the GDD (base 0 °C), with the lowest RMSE, only slightly higher MBE than NDAWN (base 32 °F) and a higher R^2 than NDAWN (base 32 °F) was the recommended procedure since it was shown to produce the lowest absolute error in the estimated anthesis date in 2019. In 2020, the GDD (base 0 °C) had the highest R^2 and the lowest RMSE compared to NDAWN (base 32 °F) and GDD (base 5 °C). However, the MBE of the NDAWN (base 32 °F) was the lowest. As a result, the GDD (base 0 °C) was also recommended in estimating the anthesis date in 2020.

Table A5. 11. Cumulative heat values at winter wheat Haun scale 11.5 for each of 3 thermal time units and 2 different GSS methods.

	Thermal Time Accumulations					
	GSS-5 days > 5ºC Mean Temp (Selirio and Brown 1997)			GSS-5 days > 5ºC > W Mn 5.0ºC (Qin et al. 2010)		
year	GDD (0ºC)	NDAWN (32ºC)	GDD (5ºC)	GDD (0ºC)	NDAWN (32ºC)	GDD (5ºC)
2019	885.93	881.67	529.58	915.77	911.36	539.54
2020	898.20	894.80	573.25	916.60	908.18	580.89

Table A5. 12. Modelled dates of winter wheat 50% anthesis for 6 sites in 2019 and 2020 where Haun scale 11.5 was directly observed.

		Modeled date of 50% anthesis					
		GSS-5 days > 5°C Mean Temp (Selirio and Brown 1997)			GSS-5 days > 5°C > W Mn 5.0°C (Qian et al. 2010)		
Plot Site	Observed Date 50% Anthesis	GDD (0°C)	NDAWN (32°C)	GDD (5°C)	GDD (0°C)	NDAWN (32°C)	GDD (5°C)
			2019				
Indian Head	12-Jul-19	6-Jul-19	6-Jul-19	3-Jul-19	7-Jul-19	7-Jul-19	4-Jul-19
Melfort	17-Jul-19	5-Jul-19	5-Jul-19	4-Jul-19	7-Jul-19	7-Jul-19	6-Jul-19
Prince Albert	11-Jul-19	14-Jul-19	14-Jul-19	10-Jul-19	15-Jul-19	16-Jul-19	10-Jul-19
Scott	9-Jul-19	13-Jul-19	14-Jul-19	10-Jul-19	8-Jul-19	9-Jul-19	7-Jul-19
Carberry	2-Jul-19	30-Jun-19	30-Jun-19	29-Jun-19	2-Jul-19	2-Jul-19	30-Jun-19
Melita	25-Jun-19	29-Jun-19	29-Jun-19	28-Jun-19	30-Jun-19	30-Jun-19	28-Jun-19
			2020				
Bow Island	22-Jun-20	1-Jul-20	1-Jul-20	3-Jul-20	1-Jul-20	1-Jul-20	3-Jul-20
Brooks	22-Jun-20	1-Jul-20	1-Jul-20	3-Jul-20	2-Jul-20	2-Jul-20	4-Jul-20
Indian Head	3-Jul-20	2-Jul-20	3-Jul-20	2-Jul-20	3-Jul-20	3-Jul-20	3-Jul-20
Melfort	20-Jul-20	11-Jul-20	11-Jul-20	10-Jul-20	8-Jul-20	8-Jul-20	9-Jul-20
Prince Albert	16-Jul-20	6-Jul-20	7-Jul-20	8-Jul-20	9-Jul-20	7-Jul-20	8-Jul-20
Scott	15-Jul-20	7-Jul-20	7-Jul-20	10-Jul-20	8-Jul-20	8-Jul-20	11-Jul-20
Swift Current	30-Jun-20	8-Jul-20	8-Jul-20	7-Jul-20	2-Jul-20	3-Jul-20	3-Jul-20
Carberry	2-Jul-20	29-Jun-20	30-Jun-20	29-Jun-20	1-Jul-20	30-Junl-20	30-Jun-20

Table A5. 13. Comparison of methods for estimation of 50% anthesis date to observed date.

		GSS-5 days > 5ºC Mean Temp (Selirio and Brown 1997)			GSS-5 days > 5ºC > W Mn 5.0ºC (Qian et al. 2010)		
	Year	GDD (0ºC)	NDAWN (32ºC)	GDD (5ºC)	GDD (0ºC)	NDAWN (32ºC)	GDD (5ºC)
R^2	2019	0.360	0.342	0.393	0.491	0.453	0.636
RMSE		6.124	6.245	6.708	5.276	5.401	5.817
MBE		-1.500	-1.333	-3.667	-1.167	-0.833	-3.500
R^2	2020	0.538	0.617	0.528	0.797	0.796	0.601
RMSE		7.754	7.550	7.826	7.340	7.649	7.738
MBE		-0.625	-0.250	0.250	-0.375	-1.000	-0.125

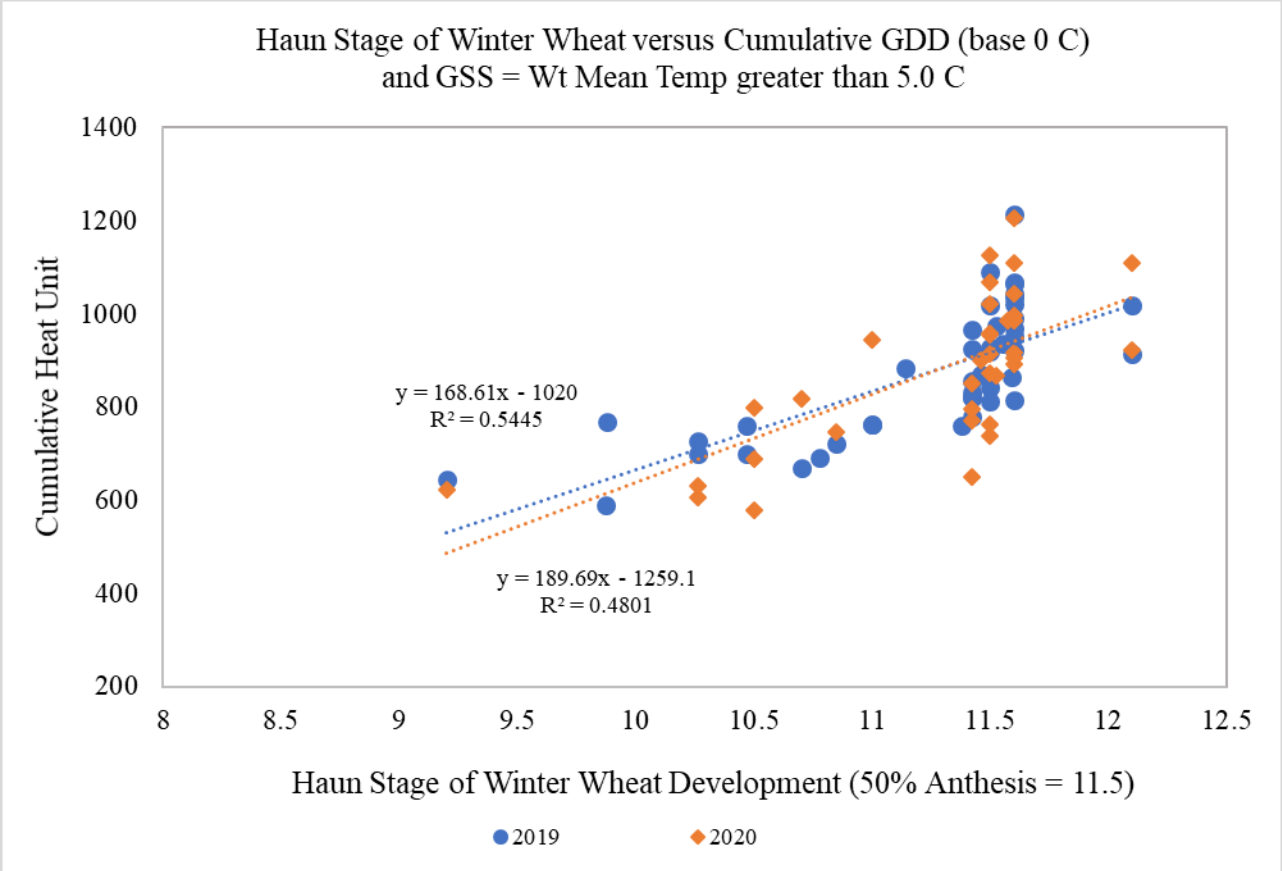

Figure A5. 7. Linear regression model of cumulative GDD (base 0 °C) using growing season start defined by 5 consecutive days with weighted mean temperature (see equation A5.2) > 5.0 °C versus observed Haun scale at plot sites for all observations in 2019 and 2020.

A5.3.4. Barley

The estimated dates for 50% head emergence using the 2 extrapolation methods are shown in Table A5.14. The deviation of the estimated dates varied from 8 days prior to the observed date to 5 days following the observed date. Less than 20% of the estimated dates were more than 2 days earlier or later than the observed date.

Table A5. 14. Extrapolated estimates of 50% head emergence (HE) date using two different Haun scale-GDD (base 0 °C) slopes.

	Observed/ Interpolated Date of 50%	Observed Date Used to	Estimated Dates of 50% Head Emergence	
			Local slope	Mean slope
Plot Site	HE	Extrapolate	Method	Method
Bow Island	04-Jul	21-Jun	04-Jul	28-Jun
Bow Island	04-Jul	27-Jun	02-Jul	29-Jun
Brooks	11-Jul	08-Jul	12-Jul	11-Jul
Brooks	11-Jul	15-Jul	10-Jul	12-Jul
Lethbridge	29-Jun	28-Jun	30-Jun	01-Jul
Lethbridge	29-Jun	04-Jul	30-Jun	26-Jun
Indian Head	13-Jul	12-Jul	14-Jul	14-Jul
Indian Head	13-Jul	19-Jul	14-Jul	14-Jul
Swift Current	09-Jul	08-Jul	10-Jul	09-Jul
Swift Current	09-Jul	15-Jul	10-Jul	14-Jul
Kelburn	05-Jul	04-Jul	05-Jul	07-Jul
Kelburn	05-Jul	11-Jul	05-Jul	27-Jun
Roblin	10-Jul	09-Jul	10-Jul	10-Jul
Roblin	10-Jul	16-Jul	10-Jul	11-Jul

The local regression estimated dates of 50% head emergence are shown in Table A5.15. The deviation of the estimated dates varied from 1 day prior to the observed date to 1 day following the observed date. Therefore, none of the estimates were more than 2 days earlier or later than the observed date.

Table A5. 15. Estimated dates of 50% head emergence (HE) using the local regression equation for Haun scale versus GDD (base 0 °C).

Plot Site	Observed/Interpolated Date of 50% HE	Modelled Date of 50% HE
Bow Island	04-Jul	03-Jul
Brooks	11-Jul	10-Jul
Lethbridge	29-Jun	30-Jun
Indian Head	13-Jul	14-Jul
Swift Current	09-Jul	09-Jul
Kelburn	05-Jul	05-Jul
Roblin	10-Jul	10-Jul

The modelled dates for anthesis and heading from Juskiw et al. (2001) and the target model using GDD (base 0 °C) are shown in Table A5.16 in comparison to the observed/interpolated 50% head emergence dates. The deviation of the modelled dates varied from 12 days prior to the observed date to 7 days following the observed date. More than 50% of the estimated dates were more than 2 days earlier or later than the observed date. However, the modelled date of heading reflected the 50% head emergence date more accurately than the modelled date of anthesis. The deviation of the former ranged from 5 days prior to the observed/interpolated date to 7 days following the observed/interpolated date. Over 40% of the modelled dates of heading were more than 2 days earlier or later than the observed/interpolated dates. The target model date of 50% head emergence varied from 6 days prior to the observed/interpolated date to 6 days following the observed/interpolated date, with over 50% of the modelled dates more than 2 days earlier or later.

Table A5. 16. Estimated dates of anthesis and heading using Juskiw et al. (2001) in comparison to observed/interpolated date of 50% head emergence.

Plot Site	Observed/ Interpolated Date of 50% HE	Juskiw-1[a] Modeled Date of Anthesis	Juskiw-1[b] Modeled Date of Heading	Juskiw-2[c] Modeled Date of Anthesis	Juskiw-2[d] Modeled Date of Heading	Target[e] Model Date of 50%HE
Bow Island	04-Jul	23-Jun	29-Jun	22-Jun	29-Jun	28-Jun
Brooks	11-Jul	03-Jul	10-Jul	03-Jul	10-Jul	09-Jul
Lethbridge	29-Jun	24-Jun	01-Jul	24-Jun	01-Jul	30-Jun
Indian Head	13-Jul	06-Jul	11-Jul	05-Jul	11-Jul	10-Jul
Swift Current	09-Jul	09-Jul	14-Jul	09-Jul	14-Jul	13-Jul
Kelburn	05-Jul	30-Jun	05-Jul	30-Jun	05-Jul	04-Jul
Roblin	10-Jul	12-Jul	17-Jul	12-Jul	17-Jul	16-Jul

[a]Date on which cumulative GDD (base 0°C) from day after planting was ≥ 813.

[b]Date on which cumulative GDD (base 0°C) from day after planting was ≥ 916.

[c]Date on which cumulative GDD (base 0°C) from day after planting was numerically closest to 813.

[d]Date on which cumulative GDD (base 0°C) from day after planting was numerically closest to 916.

[e]Date on which cumulative GDD (base 0°C) from day after planting was numerically closest to 905.

The modelled dates for mid-boot and head emerged from NDAWN (2005) are shown in Table A5.17 compared to the observed/interpolated 50% head emergence dates. The deviation of the modelled dates varied from 13 days prior to the observed date to 4 days following the observed date. Almost 80% of the estimated dates were more than 2 days earlier or later than the observed date. Therefore, neither the mid-boot nor head emerged modelled date accurately reflected the observed/interpolated date of 50% head emergence.

Table A5. 17. Estimated dates of mid-boot and head emerged using NDAWN (2005) in comparison to observed/interpolated date of 50% head emergence (HE).

Plot Site	Observed/ Interpolated Date of 50% HE	NDAWN-1[a] Modeled Date of Mid-boot	NDAWN-1[b] Modeled Date of Head Emerged	NDAWN-2[c] Modeled Date of Mid-boot	NDAWN-2[d] Modeled Date of Head Emerged
Bow Island	04-Jul	22-Jun	24-Jun	21-Jun	24-Jun
Brooks	11-Jul	02-Jul	05-Jul	02-Jul	05-Jul
Lethbridge	29-Jun	23-Jun	26-Jun	23-Jun	25-Jun
Indian Head	13-Jul	06-Jul	08-Jul	05-Jul	07-Jul
Swift Current	09-Jul	09-Jul	11-Jul	09-Jul	11-Jul
Kelburn	05-Jul	30-Jun	01-Jul	29-Jun	01-Jul
Roblin	10-Jul	12-Jul	14-Jul	12-Jul	14-Jul

[a]Date on which cumulative special GDD (Base 32 °F) from day after planting was ≥ 792.

[b]Date on which cumulative special GDD (Base 32 °F) from day after planting was ≥ 831.

[c]Date on which cumulative special GDD (Base 32 °F) from day after planting was numerically closest to 792.

[d]Date on which cumulative special GDD (Base 32 °F) from day after planting was numerically closest to 831.

A statistical comparison of the different methods for estimating 50% anthesis date is shown in Table A5.18. The local regression method was the most accurate method with the highest R^2 and lowest RMSE and MBE. The hybrid methods used either the local or average GDD (base 0 °C) versus Haun scale regressions were the next most accurate methods. Among the different modelling approaches, the Juskiw-1 heading and Juskiw-2 heading had the highest R2 and lowest RMSE and MBE for estimating 50% head emergence compared to the locations where it was directly observed or interpolated.

Table A5. 18. Performance of the local regression, extrapolation, and modelling methods for estimating 50% head emergence date compared to the observed/interpolated date. Root mean square error (RMSE) and Mean bias error (MBE) values are in units of days.

Plot Site	Observed/ Interpolated Date of 50% HE	Juskiw-1[a] Modeled Date of Anthesis	Juskiw-1[b] Modeled Date of Heading	Juskiw-2[c] Modeled Date of Anthesis	Juskiw-2[d] Modeled Date of Heading	Target[e] Model Date of 50%HE
Bow Island	04-Jul	23-Jun	29-Jun	22-Jun	29-Jun	28-Jun
Brooks	11-Jul	03-Jul	10-Jul	03-Jul	10-Jul	09-Jul
Lethbridge	29-Jun	24-Jun	01-Jul	24-Jun	01-Jul	30-Jun
Indian Head	13-Jul	06-Jul	11-Jul	05-Jul	11-Jul	10-Jul
Swift Current	09-Jul	09-Jul	14-Jul	09-Jul	14-Jul	13-Jul
Kelburn	05-Jul	30-Jun	05-Jul	30-Jun	05-Jul	04-Jul
Roblin	10-Jul	12-Jul	17-Jul	12-Jul	17-Jul	16-Jul

[a]Date on which cumulative GDD (base 0°C) from day after planting was ≥ 813.

[b]Date on which cumulative GDD (base 0°C) from day after planting was ≥ 916.

[c]Date on which cumulative GDD (base 0°C) from day after planting was numerically closest to 813.

[d]Date on which cumulative GDD (base 0°C) from day after planting was numerically closest to 916.

[e]Date on which cumulative GDD (base 0°C) from day after planting was numerically closest to 905.

A5.4. Discussion

Spring wheat. Based on the Haun scale-GDD observations in Figure A5.2, the initial expectation would be that extrapolation from a measured point would provide the most accurate estimate of 50% anthesis date because of the site-to-site variation from the Mkhabela et al. (2016) models. Essentially, this offset correction should help reflect differences in the Haun scale-GDD relationships between locations. However, it requires an estimate of the slope of the relationship to extrapolate an estimated accumulated GDD value for the Haun scale 11.5. Although several different slopes were tested, the results were not as accurate as using the Mkhabela et al. (2016) GDD (base 0 °C) model and the planting date. Extrapolation is clearly very sensitive to the

estimated slope of the Haun scale-GDD relationship. The examples in Figure A5.3 illustrate the variation in slope between different points of the observed Haun scale versus accumulated GDD. Thus, the locally-derived slopes and measured values are a less accurate method for estimating GDD than the Mkhabela et al. (2016) models using planting date. The latter were derived from many more observations than those in the 2019 and 2020 plot site study, which may account for its higher accuracy for estimation of 50% anthesis dates. It should be noted that the estimated date varied by up to 6 days from the observed date with a RMSE of 3 days in 2019. This was slightly better than the results for multiple sites reported by Mkhabela et al. (2016).

Durum. The approach for estimating 50% anthesis date in durum by relating it to the spring wheat model is a compromise. There is an error associated both with the spring wheat equivalent Haun scale 11.75 value at the time of durum reaching Haun scale 11.5 and the error associated with the spring wheat thermal time model based on GDD (base 0 °C). This is part of why there is a larger RMSE for the estimates of 50% anthesis date in durum compared to the other spring-sown crops. The fact that, on average, there is a difference of 7 days between the actual and estimated date is not encouraging.

Winter Wheat. Unlike spring-sown crops, estimation of 50% anthesis date for winter wheat cannot rely upon models that use cumulative heat units following the planting date. This is because the temperature dormancy period during the winter can vary in length, and it is the period following the commencement of active growth in spring up to the date of anthesis that is relevant.

In 2019, the date of 50% anthesis for all 14 plot sites was either directly observed or could be interpolated from phenology observations both preceding and following Haun scale 11.5. However, for all the producer fields in the FHB study, the date of 50% anthesis must be modelled. The modelling method must provide both an estimate of GSS and a target cumulative heat unit

value from the day following GSS and thus require a record of daily air temperature from March 1. Although the most accurate GSS method was determined to be the one described by Qian et al. (2010) and the most accurate cumulative heat unit was GDD (base 0 °C), the estimated dates varied between 13 days prior and 5 days following the actual observed date. In addition, the RMSE for winter wheat was larger than that for spring crops. This could impact the accuracy of FHB risk models using weather conditions based on the date of anthesis because of the very large discrepancy that could occur in defining anthesis date.

Barley. Unlike the results for spring wheat, the local regression and hybrid extrapolation methods were the most accurate for estimating the date of 50% head emergence in barley. However, these methods all require multiple phenology observations at a location or several locations. The modelling methods are more attractive because they require only the seeding date and a record of daily air temperature throughout the growing season.

The Juskiw-1 heading, Juskiw-2 heading, and target models, were the most accurate among the tested modelling approaches. The RMSE and absolute value of MBE for the 2 Juskiw models were just slightly higher than those for the average slope method of extrapolation. Likewise, the target model RMSE was just slightly higher than that for the average slope extrapolation method, and the absolute value of the MBE was half a day less for the target model. However, the Juskiw-1 anthesis and Juskiw-2 anthesis and all four of the NDAWN models had higher negative bias values indicating that their estimated date tended to be too early. Part of the reason for the NDAWN estimates being too early may be related to the fact that the models were developed in North Dakota with barley varieties that normally produced 8 leaves (NDAWN, 2005). Juskiw et al. (2001) reported that barley varieties used in their assessment in Alberta usually developed 9 leaves.

A5.5. Conclusion

The most accurate method for determining date of 50% anthesis is direct observation. However, since this requires a high frequency of observations, it is impractical for widespread use. Interpolation of the date between two observations that immediately precede and follow the 50% anthesis stage offers a reliable and simple method for its estimation. In cases where neither of the above is available:

i) The most accurate alternative method for spring wheat is to use planting date and an accumulated heat model from Mkhabela et al. (2016). The Mkhabela et al. (2016) models using planting date and accumulated heat are the best choice for estimating date of 50% anthesis at those fields, but the actual date across fields would be expected to vary from the estimate by 3 days.

ii) A conversion of the spring wheat thermal time model to adapt it for durum provides an alternative method. It requires only the seeding date and cumulative GDD (base 0 °C) to find the date on which the value is closest to 992. This is relatively simple, but it may not have satisfactory accuracy for modelling purposes.

iii) The most accurate alternative method for winter wheat is to model the date for GSS using the method of Qian et al. (2010) using equation A5.2 and a weighted mean temperature of 5.0 °C, then accumulate GDD (base 0 °C) from the day after GSS to the closest day when the total reaches 919. This analysis showed that the above method had the lowest RMSE, 2nd lowest MBE, and 2nd highest R^2. This is important for the producer fields used in the study for FHB risk model validation. This method is the best choice for estimating the date of 50% anthesis at those fields, but the actual date

across all fields would be expected to vary on average from the estimate by more than 5 days.

iv) The most accurate alternative method for barley is to use a regression equation for the relationship between multiple observations of phenology (Haun scale) and cumulative GDD (base 0 °C). Again, a lack of observations will likely preclude this method in practice. The alternative is to model the 50% head emergence date using planting date and cumulative heat units. In this analysis, the closest date at which GDD (base 0 °C) accumulated to a value of 905 gave the highest R^2 and the lowest RMSE and MBE values amongst all of the assessed modelling methods. This is important for the producer fields used in the study for FHB risk model validation. The target model using 905 accumulated GDD (base 0 °C) and planting date is the best choice for estimating the 50% head emergence date at those fields, but the actual date across all fields would be expected to vary from the estimate less than 4 days.

A5.6. References

ACIS. 2021. Alberta Climate Service -weather and climate resources. [Online] Available at https://www.alberta.ca/acis-find-current-weather-data.aspx (accessed 16 November 2021).

Bootsma, A. 1994. Long term (100 yr) climatic trends for agriculture at selected locations in Canada. Climatic Change **26**: 65-88, doi: 10.1007/BF01094009.

ECCC. 2021. Historical Data - Climate - Environment and Climate Change Canada. [Online] Available at https://climate.weather.gc.ca/historical_data/search_historic_data_e.html (accessed 16 November 2021).

Fowler, D. 2018. Growth stages of wheat, in winter wheat wroduction manual, Ch 10, Publisher: Ducks Unlimited Canada and Conservation Production Systems Ltd

Gilbert, J., and A. Tekauz. 2011. Strategies for management of Fusarium Head Blight (FHB) in cereals. Prairie soils Crop J. **4**, 97–104. [Online] Available at https://prairiesoilsandcrops.ca/articles/volume-4-11-screen.pdf.

Haun, J.R. 1973. Visual quantification of wheat development. Agron. J. **65**:116–119.

Juskiw, P., Y. Jame and L. Kryzanowski. 2001. Phenological development of spring barley in a short-season growing area. Agron. J. 93:370–379 [Online] Available at https://www.academia.edu/25168235/Phenological_Development_of_Spring_Barley_in_a_Short_Season_Growing_Area (accessed 20 December 2021).

MARD. 2021. Manitoba Ag Weather Program- Manitoba Agriculture and Resource Development. Prov. Manit. - Agric. [Online] Available at https://www.gov.mb.ca/agriculture/ (accessed 17 November 2021).

McCallum, B., and A. Tekauz. 2002. Influence of inoculation method and growth stage on Fusarium Head Blight in barley. J. Plant Path. **24**: 77-80 doi: 10.1080/07060660109506976.

Meier, U. 2001. Growth Stages of mono and dicotyledonous plants. BBCH monograph, Federal Biological Research Centre for Agriculture and Forestry, Bonn. [Online] Available at https://www.politicheagricole.it/flex/AppData/WebLive/Agrometeo/MIEPFY800/BBCHengl2001.pdf (accessed 19 December 2021).

Mkhabela, M., G. Ash, M. Grenier, and P. Bullock. 2016. Testing the suitability of thermal time models for forecasting spring wheat phenological development in western Canada. Can. J. Plant Sci. **96:** 765–775. doi: 10.1139/cjps-2015-0351.

NDAWN. 2005. Barley growing degree day information. [Online] Available at https://ndawn.ndsu.nodak.edu/help-barley-growing-degree-days.html (accessed 20 December 2021).

Qian, B., X. Zhang, K. Chen, Y. Feng, and T. O'Brien. 2010. Observed long-term trends for agroclimatic conditions in Canada. J. Appl. Meteorol. Climatol. **49**: 604–618. doi: 10.1175/2009JAMC2275.1.

Saiyed, I., P. Bullock, H. Sapirstein, G. Finlay, and C. Jarvis. 2009. Thermal time models for estimating wheat phenological development and weather-based relationships to wheat quality. Can. J. Plant Sci. **89**: 429-439 doi: 10.4141/CJPS07114.

Selirio, I.S., and D.M. Brown. 1979. Soil moisture-based simulation of forage yield. Agric. Meteorol. **20**: 99–114. doi: 10.1016/0002-1571(79)90030-X.

Zadoks, J.C., T.T. Chang, and C.F. Konzak. 1974. A decimal code for the growth stages of cereals. Weed Res. **14**: 415–421. doi: 10.1111/j.1365-3180. 1974.tb01084.x.

Table AA5. 1. Spring wheat crop stage by observation date and location with cumulative GDD (base 0 °C) in 2019.

Site	Observed Date	Haun Scale	NDGDD GDD (0°C)	(32°F)	GDD (0°C)
Bow Island	21-Jun-19	10.38	788.75	782.95	472.25
Bow Island	27-Jun-19	11.42	883.35	877.55	536.85
Bow Island	4-Jul-19	11.6	996.85	991.05	615.35
Brooks	2-Jul-19	10.32	802.05	793.05	517.05
Brooks	8-Jul-19	10.38	894.55	885.55	579.55
Brooks	15-Jul-19	11.46	1034.6	1025.6	684.6
Brooks	22-Jul-19	12.1	1148.9	1139.9	763.9
Lethbridge	21-Jun-19	10.38	770.2	765.1	446
Lethbridge	28-Jun-19	11	875.65	870.55	516.45
Lethbridge	4-Jul-19	11.5	964.85	959.75	575.65
Lethbridge	12-Jul-19	12.1	1105.25	1100.15	676.05
Medicine Hat	19-Jun-19	9.65	513.75	497.9	343.75
Medicine Hat	26-Jun-19	11.42	613.95	598.1	408.95
Medicine Hat	4-Jul-19	11.6	747.85	732	502.85
Medicine Hat	9-Jul-19	12.1	837.9	822.05	567.9
Vermilion	11-Jul-19	10.85	862.65	857.15	542.65
Vermilion	16-Jul-19	11.5	945.75	940.25	600.75
Vermilion	24-Jul-19	11.6	1082.7	1077.2	697.7
Indian Head	5-Jul-19	10.18	809.5	796.7	524.9
Indian Head	12-Jul-19	11.5	942.8	930	623.2
Indian Head	19-Jul-19	11.6	1072.4	1059.6	717.8
Melfort	24-Jul-19	10.1	1059.4	1040.1	714.4
Melfort	31-Jul-19	11	1179.5	1160.2	799.5
Melfort	7-Aug-19	11.538	1305.8	1286.5	890.8
Prince Albert	18-Jul-19	11.42	891.25	873	606.25
Prince Albert	25-Jul-19	11.6	1022.1	1003.85	702.1
Scott	9-Jul-19	10.26	720	694.4	475
Scott	16-Jul-19	11.42	835.4	809.8	555.4
Scott	23-Jul-19	11.5	954.6	929	639.6
Swift Current	8-Jul-19	10.5	804.5	790.25	529.5
Swift Current	15-Jul-19	11.46	936.4	922.15	626.4
Arborg	2-Jul-19	9.875	705.95	699.1	461.7
Arborg	9-Jul-19	11.4	840.45	833.6	561.2
Carberry	8-Jul-19	10.7	945.8	942.05	621.5
Carberry	15-Jul-19	11.5	1091.3	1087.55	732
Carberry	22-Jul-19	11.6	1221.25	1217.5	826.95
Kelburn	4-Jul-19	11.48	904.05	899.2	619.05
Melita	2-Jul-19	10.7	746.75	729.55	501.8
Roblin	9-Jul-19	11	766	748.9	501
Roblin	16-Jul-19	11.5	899.1	882	599.1

Table AA5. 2. Spring wheat crop stage by observation date and location with cumulative GDD (base 0 °C) in 2020.

			NDGDD		
Site	Observed Date	Haun Scale	GDD (0°C)	(32°F)	GDD (0°C)
Bow Island	29-Jun-20	10.5	839.4	835.4	544.6
Bow Island	06-Jul-20	11.5	956.25	952.25	626.45
Bow Island	13-Jul-20	11.6	1071.3	1067.3	706.5
Brooks	13-Jul-20	11.42	1034.95	1029.95	719.95
Brooks	20-Jul-20	11.55	1180	1175	825
Brooks	27-Jul-20	12.1	1317.4	1312.4	927.4
Lethbridge	29-Jun-20	11	897.1	895.05	567.35
Lethbridge	06-Jul-20	11.5	1001.6	999.55	636.85
Lethbridge	13-Jul-20	11.6	1118.7	1116.65	718.95
Medicine Hat	26-Jun-20	11	885.9	880.8	571.7
Indian Head	03-Jul-20	9.425	793.7	773.5	530.15
Indian Head	10-Jul-20	11.4	922.55	902.35	624
Indian Head	17-Jul-20	11.55	1049.95	1029.75	716.4
Indian Head	24-Jul-20	11.85	1185.15	1164.95	816.6
Melfort	20-Jul-20	11	893.45	883.1	603.45
Prince Albert	09-Jul-20	10.6	831.65	819.6	556.65
Prince Albert	16-Jul-20	11.5	953.9	941.85	643.9
Prince Albert	23-Jul-20	11.6	1090.9	1078.85	745.9
Scott	15-Jul-20	11	809.1	799.85	529.1
Scott	22-Jul-20	11.5	928.95	919.7	613.95
Scott	29-Jul-20	11.85	1060.3	1051.05	710.3
Swift Current	07-Jul-20	11	867.05	859.55	564.1
Swift Current	14-Jul-20	11.42	976.1	968.6	638.15
Swift Current	21-Jul-20	11.6	1095.25	1087.75	722.3
Arborg	09-Jul-20	11.5	970.55	949.05	685.75
Arborg	16-Jul-20	11.6	1107.85	1086.35	788.05
Carberry	09-Jul-20	11	1040.6	1023.8	728.95
Carberry	16-Jul-20	11.5	1176.1	1159.3	829.45
Carberry	23-Jul-20	12.1	1306.3	1289.5	924.65
Kelburn	29-Jun-20	10.1	860.3	840.45	615.3
Kelburn	03-Jul-20	11.42	963.05	943.2	698.05
Kelburn	06-Jul-20	11.48	1033.1	1013.25	753.1
Kelburn	10-Jul-20	11.6	1118.2	1098.35	818.2
Melita	29-Jun-20	10.1	800.2	780.6	556.25
Melita	06-Jul-20	11.5	953.05	933.45	674.1
Melita	13-Jul-20	11.6	1091.35	1071.75	777.4
Roblin	02-Jul-20	10.85	747.95	731.25	507.95
Roblin	09-Jul-20	11.42	884.2	867.5	609.2
Roblin	16-Jul-20	12.1	1007.05	990.35	697.05

Table AA5. 3. Durum crop stage by observation date and location with cumulative GDD (base 0 °C) in 2019.

Plot site	Date	Observed Haun	Cum GDD_0
Bow Island	21-Jun	9.425	788.75
Bow Island	27-Jun	11	883.35
Bow Island	4-Jul	11.5	996.85
Brooks	8-Jul	10.26	894.55
Brooks	15-Jul	10.7	1034.6
Brooks	22-Jul	11.6	1148.9
Lethbridge	21-Jun	9.2	770.2
Lethbridge	28-Jun	11	875.65
Lethbridge	4-Jul	11.42	964.85
Lethbridge	12-Jul	11.6	1105.25
Medicine Hat	26-Jun	11	613.95
Medicine Hat	4-Jul	12.1	747.85
Vermilion	11-Jul	10.55	862.65
Vermilion	16-Jul	11	945.75
Vermilion	24-Jul	11.49	1082.7
Indian Head	5-Jul	9.65	809.5
Indian Head	12-Jul	11.42	942.8
Indian Head	19-Jul	11.6	1072.4
Melfort	24-Jul	10.55	1059.4
Melfort	31-Jul	11.21	1179.5
Melfort	7-Aug	11.85	1305.8
Prince Albert	18-Jul	11	891.25
Prince Albert	25-Jul	11.6	1022.1
Scott	16-Jul	10.6	835.4
Scott	23-Jul	11.42	954.6
Scott	30-Jul	12.1	1074.8
Swift Current	8-Jul	10.6	804.5
Swift Current	15-Jul	11	936.4
Swift Current	22-Jul	11.5	1053.8
Arborg	9-Jul	10.925	840.45
Carberry	8-Jul	9.2	945.8
Carberry	15-Jul	11.42	1091.3
Carberry	22-Jul	11.6	1221.25
Kelburn	4-Jul	10.32	904.05
Kelburn	11-Jul	11.6	1044.95
Kelburn	17-Jul	12.1	1175.1
Roblin	9-Jul	10.6	766
Roblin	16-Jul	11.42	899.1
Roblin	23-Jul	11.6	1016.55

Table AA5. 4. Durum crop stage by observation date and location with cumulative GDD (base 0 °C) in 2020.

Location	Date	Observed Haun	Cum GDD0
Bow Island	29-Jun	10.5	839.4
Bow Island	6-Jul	11.42	956.25
Bow Island	13-Jul	11.6	1071.3
Brooks	13-Jul	10.7	1389.75
Brooks	20-Jul	11.55	1518.65
Brooks	27-Jul	12.1	1656.05
Lethbridge	29-Jun	10.7	897.1
Lethbridge	6-Jul	11.42	1001.6
Lethbridge	13-Jul	11.6	1118.7
Indian Head	10-Jul	11	513.4
Indian Head	17-Jul	11.46	640.8
Indian Head	24-Jul	11.6	776
Melfort	20-Jul	10.7	893.45
Melfort	27-Jul	11.55	1032.1
Prince Albert	9-Jul	10.1	831.65
Prince Albert	16-Jul	11	953.9
Prince Albert	23-Jul	11.6	1090.9
Scott	15-Jul	10.32	809.1
Scott	22-Jul	11	928.95
Scott	29-Jul	11.6	1060.3
Swift Current	7-Jul	11	867.05
Swift Current	14-Jul	11.42	976.1
Swift Current	21-Jul	11.6	1095.25
Arborg	9-Jul-20	11.42	970.3
Arborg	16-Jul-20	12.1	1107.6
Carberry	9-Jul	9.2	1025.15
Carberry	16-Jul	11.42	1160.65
Carberry	23-Jul	11.6	1290.85
Melita	29-Jun	10.1	800.2
Melita	6-Jul	11.42	953.05
Melita	13-Jul	11.6	1091.35

Table AA5. 5. Winter wheat crop stage by observation date and location with thermal time model accumulations in 2019.

	Thermal Time Accumulations					
	GSS–5 days > 5°C Mean Temp (Selirio and Brown 1979)			GSS–5 days > W Mn 5.0°C (Qian et al. 2010		
Observations						
Haun	GDD	NDAWN	GDD	GDD	NDAWN	GDD

Plot Site	Date	Scale	(0°C)	(32°F)	(5°C)	(0°C)	(32°F)	(5°C)
Bow Island	11-Jun	11.38	676.65	674.5	373.2	761	758.85	396.7
Bow Island	21-Jun	11.42	840.65	838.5	487.2	925	922.85	510.7
Bow Island	27-Jun	12.1	935.25	933.1	551.8	1020	1017.45	575.3
Brooks	10-Jun	10.78	692.35	690.8	341.2	692.4	690.8	341.15
Brooks	17-Jun	11.6	815.9	814.35	429.7	815.9	814.35	429.7
Brooks	24-Jun	12.1	914.75	913.2	493.6	914.8	913.2	493.55
Lethbridge	14-Jun	11	763.1	763.1	394.8	763.1	763.1	394.8
Lethbridge	21-Jun	11.46	870.55	870.55	467.3	870.6	870.55	467.25
Lethbridge	28-Jun	11.535	976	976	537.7	976	976	537.7
Lethbridge	4-Jul	11.6	1065.2	1065.2	596.9	1065	1065.2	596.9
Medicine Hat	11-Jun	11.42	696.6	695.1	389.6	779.8	778.3	413.95
Medicine Hat	19-Jun	11.6	838.65	837.15	491.6	921.9	920.35	516
Indian Head	28-Jun	9.88	761.15	755.65	467.3	767.6	762.1	468.75
Indian Head	5-Jul	11.14	877.95	872.45	549.1	884.4	878.9	550.55
Indian Head	12-Jul	11.5	1011.25	1005.75	647.4	1018	1012.2	648.85
Melfort	10-Jul	11.42	973.6	971.1	595.4	965.6	963.05	592.35
Melfort	17-Jul	11.5	1098	1095.5	684.8	1090	1087.45	681.75
Melfort	24-Jul	11.6	1221.95	1219.45	773.8	1214	1211.4	770.7
Prince Albert	4-Jul	10.85	715.1	696.25	460.1	722.9	704	462.85
Prince Albert	11-Jul	11.5	835.5	816.65	545.5	843.3	824.4	548.25
Prince Albert	18-Jul	11.6	961.45	942.6	636.5	969.2	950.35	639.2
Scott	26-Jun	10.26	613.5	597.7	383.5	726.7	710.2	420.05
Scott	2-Jul	11.42	707.75	691.95	447.8	821	804.45	484.3
Scott	9-Jul	11.5	815.15	799.35	520.2	928.4	911.85	556.7
Scott	16-Jul	11.6	930.55	914.75	600.6	1044	1027.25	637.1
Swift Current	18-Jun	10.7	637.75	633.35	375.5	668.3	663.7	391
Swift Current	25-Jun	11	731.4	727	434.2	761.9	757.35	449.65
Swift Current	1-Jul	11.59	835.05	830.65	507.8	865.6	861	523.3
Arborg	2-Jul	11.42	833.15	830.1	505.7	856.3	853.2	513.75
Arborg	9-Jul	11.6	967.65	964.6	605.2	990.8	987.7	613.25
Carberry	17-Jun	9.2	643.6	640.35	370.6	643.6	640.35	370.6
Carberry	24-Jun	10.47	761.15	757.9	453.2	761.2	757.9	453.15
Carberry	2-Jul	11.5	919.4	916.15	571.4	919.4	916.15	571.4
Carberry	8-Jul	11.6	1033.85	1030.6	655.9	1034	1030.6	655.85
Kelburn	18-Jun	10.26	699.4	695.65	416.9	699.4	695.65	416.9
Kelburn	25-Jun	11.42	832.5	828.75	515	832.5	828.75	515
Kelburn	4-Jul	11.6	1021.15	1017.4	658.7	1021	1017.4	658.65
Melita	11-Jun	9.88	577.7	572.8	331.3	590.9	583.85	339.4
Melita	18-Jun	10.47	687.25	682.35	405.8	700.4	693.4	413.95
Melita	25-Jun	11.5	800.5	795.6	484.1	813.7	806.65	492.2
Melita	2-Jul	11.6	938.25	933.35	586.8	951.4	944.4	594.95
Roblin	2-Jul	11.42	792.6	790.75	469	819.7	817.8	481.05
Roblin	9-Jul	11.55	909.2	907.35	550.6	936.3	934.4	562.65
Roblin	16-Jul	11.6	1042.3	1040.45	648.7	1069	1067.5	660.75

Table AA5. 6. Winter wheat crop stage by observation date and location with thermal time model accumulations in 2020.

			Thermal Time Accumulations					
			GSS–5 days > 5°C Mean Temp (Selirio and Brown 1979)			GSS–5 days > W Mn 5.0°C (Qian et al. 2010		
Plot Site	Date	Observed Haun Scale	GDD (0°C)	NDAWN (32°F)	GDD (5°C)	GDD (0°C)	NDAWN (32°F)	GDD (5°C)
Bow Island	11-Jun	10.5	556.1	551.85	312.05	579	574.75	324.95
Bow Island	15-Jun	11.42	628.6	624.35	364.55	651.5	647.25	377.45
Bow Island	22-Jun	11.5	738.9	734.65	439.85	761.8	757.55	452.75
Bow Island	29-Jun	11.6	869.2	864.95	535.15	892.1	887.85	548.05
Brooks	15-Jun	10.26	631.85	627.25	366.95	631.85	627.25	366.95
Brooks	22-Jun	11.5	739.25	734.65	439.35	739.25	734.65	439.35
Brooks	29-Jun	11.525	867.95	863.35	533.05	867.95	863.35	533.05
Brooks	6-Jul	11.575	986.75	982.15	616.85	986.75	982.15	616.85
Lethbridge	11-Jun	9.2	601.85	598.25	357.3	623.35	619.75	368.8
Lethbridge	15-Jun	10.5	667.75	664.15	403.2	689.25	685.65	414.7
Lethbridge	22-Jun	11.42	774.2	770.6	474.65	795.7	792.1	486.15
Lethbridge	29-Jun	11.6	896.25	892.65	561.7	917.75	914.15	573.2
Medicine Hat	9-Jun	10.26	594.25	589.15	360.05	605.25	600.15	366.05
Medicine Hat	26-Jun	11.6	895.65	890.55	576.45	906.65	901.55	582.45
Indian Head	3-Jul	11.5	915.5	901.1	585.2	915.5	901.1	585.2
Indian Head	10-Jul	11.6	1044.35	1029.95	679.05	1044.35	1029.95	679.05
Melfort	20-Jul	11.5	876.65	860.9	569.05	954.1	938.05	596.6
Melfort	27-Jul	11.5	1048.55	1032.8	690.95	1126	1109.95	718.5
Prince Albert	9-Jul	11	945.45	939.55	588.95	945.45	939.55	588.95
Prince Albert	16-Jul	11.5	1067.7	1061.8	676.2	1067.7	1061.8	676.2
Prince Albert	23-Jul	11.6	1204.7	1198.8	778.2	1204.7	1198.8	778.2
Scott	2-Jul	10.7	817.75	810.5	489.25	817.75	810.5	489.25
Scott	7-Jul	11.46	900.55	893.3	547.05	900.55	893.3	547.05
Scott	15-Jul	11.5	1022.8	1015.55	629.3	1022.8	1015.55	629.3
Swift Current	23-Jun	10.85	636.7	629.3	393.55	745.5	735	452.35
Swift Current	30-Jun	11.5	764.65	757.25	486.5	873.45	862.95	545.3
Swift Current	7-Jul	11.6	888.75	881.35	575.6	997.55	987.05	634.4
Carberry	25-Jun	10.5	797.3	781.4	517.1	797.3	781.4	517.1
Carberry	2-Jul	11.5	958.05	942.15	642.85	958.05	942.15	642.85
Carberry	9-Jul	11.6	1108.95	1093.05	758.75	1108.95	1093.05	758.75
Melita	22-Jun	11.42	771.9	762.6	492.35	771.9	762.6	492.35
Melita	29-Jun	12.1	921.8	912.5	607.25	921.8	912.5	607.25
Roblin	2-Jul	11.42	849.6	835.15	537.6	849.6	835.15	537.6
Roblin	9-Jul	11.6	985.85	971.4	638.85	985.85	971.4	638.85
Roblin	16-Jul	12.1	1108.7	1094.25	726.7	1108.7	1094.25	726.7

Table AA5. 7. Barley crop stage by observation date and location with thermal time model accumulations in 2019.

Plot Site Location	Observation Date	Haun Scale	GDD (0°C)	NDAWN (32°F)	GDD (5°C)
Bow Island	21-Jun	10.1	792.95	786.6	476.45
Bow Island	27-Jun	10.35	887.55	881.2	541.05
Bow Island	4-Jul	10.5	1001.05	994.7	619.55
Brooks	2-Jul	10.26	802.05	792.7	517.05
Brooks	8-Jul	10.32	894.55	885.2	579.55
Brooks	15-Jul	10.7	1034.6	1025.25	684.6
Lethbridge	28-Jun	10.38	875.65	870.3	516.45
Lethbridge	4-Jul	11	964.85	959.5	575.65
Medicine Hat	26-Jun	10.44	613.95	587.15	408.95
Vermilion	11-Jul	10.7	862.65	853.6	542.65
Vermilion	24-Jul	11.85	1082.7	1073.65	697.7
Indian Head	12-Jul	10.38	942.8	924.25	623.2
Indian Head	19-Jul	10.85	1072.4	1053.85	717.8
Melfort	17-Jul	10.7	935.45	912.4	625.45
Melfort	24-Jul	11	1059.4	1036.35	714.4
Melfort	31-Jul	12.1	1179.5	1156.45	799.5
Prince Albert	18-Jul	10.85	891.25	871.75	606.25
Scott	16-Jul	11.42	835.4	807.4	555.4
Scott	23-Jul	11.6	954.6	926.6	639.6
Swift Current	8-Jul	10.44	804.5	779.15	529.5
Swift Current	15-Jul	10.7	936.4	911.05	626.4
Arborg	9-Jul	10.32	840.45	832.85	561.2
Carberry	15-Jul	10.85	1091.3	1084.85	732
Carberry	22-Jul	11.6	1221.25	1214.8	826.95
Kelburn	4-Jul	10.26	904.05	893.65	619.05
Kelburn	11-Jul	11.6	1044.95	1034.55	724.95
Roblin	9-Jul	10.44	766	742.45	501
Roblin	16-Jul	10.85	899.1	875.55	599.1

Table AA5. 8. Barley crop stage by observation date and location with thermal time model accumulations in 2020.

Plot Site Location	Observation Date	Haun Scale	GDD (0°C)	NDAWN (32°F)	GDD (5°C)
Bow Island	29-Jun	10.26	839.4	835.25	544.6
Bow Island	6-Jul	10.5	956.25	952.1	626.45
Bow Island	13-Jul	12.1	1071.3	1067.15	706.5
Brooks	13-Jul	10.5	1389.75	1387.5	937
Brooks	20-Jul	11.525	1518.65	1516.4	1030.9
Lethbridge	29-Jun	10.26	897.1	893.55	567.35
Lethbridge	6-Jul	11	1001.6	998.05	636.85
Lethbridge	13-Jul	12.1	1118.7	1115.15	718.95
Medicine Hat	26-Jun	10.1	885.9	878.9	571.7
Medicine Hat	8-Jul	11.6	1088.4	1081.4	714.2
Indian Head	10-Jul	10.2	922.55	901.2	624
Indian Head	17-Jul	10.7	1049.95	1028.6	716.4
Melfort	20-Jul	10.7	893.45	882.95	603.45
Melfort	27-Jul	11.55	1032.1	1021.6	707.1
Prince Albert	9-Jul	10.26	831.65	818	556.65
Prince Albert	16-Jul	10.85	953.9	940.25	643.9
Scott	15-Jul	10.6	809.1	799.85	529.1
Scott	22-Jul	11.4	928.95	919.7	613.95
Swift Current	7-Jul	10.26	867.05	859.55	564.1
Swift Current	14-Jul	10.44	976.1	968.6	638.15
Swift Current	21-Jul	11	1095.25	1087.75	722.3
Arborg	9-Jul-20	10.1	970.3	948.6	685.75
Arborg	16-Jul-20	10.7	1107.6	1085.9	788.05
Carberry	9-Jul	9.65	1040.6	1021.55	728.95
Carberry	16-Jul	10.85	1176.1	1157.05	829.45
Carberry	23-Jul	11.6	1306.3	1287.25	924.65
Kelburn	3-Jul	9.65	860.3	838.25	615.3
Kelburn	6-Jul	10.44	963.05	941	698.05
Kelburn	10-Jul	11.42	1033.1	1011.05	753.1
Melita	29-Jun	10.1	800.2	779.8	556.25
Melita	6-Jul	10.7	953.05	932.65	674.1
Roblin	9-Jul	10.6	747.95	726.45	507.95
Roblin	16-Jul	11.6	884.2	862.7	609.2